Structural Biology of Prohibitins and Annexin B1

by

Anja Winter

PhD by Research

The University of Edinburgh

2008

Abstract

This thesis deals with the structural biology of two integral membrane proteins, prohibitin1 and prohibitin 2, and the membrane-associated protein Annexin B1. The biophysical properties of the proteins were characterised and their interaction with different ligands was investigated. Furthermore, crystallisation trials were undertaken in both projects.

Prohibitins are members of the evolutionary well-conserved SPFH (stomatin/prohibitin/flotillin/HflK/C) super-family and exert important cellular functions such as cell-cycle control, tumour suppression and regulation of protein turnover in mitochondria. *In vivo*, prohibitins consist of two proteins, prohibitin 1 and prohibitin 2, that form a transmembrane complex in the inner mitochondrial membrane. The complex of full-length prohibitins 1 and prohibitin 2 could be refolded successfully but only generation of truncation mutants enabled characterisation of the protein complex using spectroscopic methods. Homology modelling of the PHB domains of prohibitin 1 and 2 allowed insights into their three-dimensional structures, their dimer formation and the interactions with target proteins and melanogenin. Furthermore, an interaction with the inter-membrane space region of mitochondrial *m*-AAA-protease was proposed. The intermembrane space region of *m*-AAA-protease from *E. coli* was investigated using spectroscopic methods and subjected to crystallisation trials.

Annexin B1 belongs to the well-conserved family of annexins that are versatile adapter and regulator proteins in membrane-associated processes. Similar to other annexins, annexin B1 was found to bind to liposomes and heparin in a calcium-dependent fashion. Interestingly, its liposome binding behaviour is reminiscent of plant annexins suggesting the presence of a calcium-independent binding mode, whereas its lectin property is a shared feature with mammalian annexins. Annexin B1 shows Redox-dependent oligomer formation in solution.

Summary

Aim of this work was to gain insights into biochemical and structural features of the prohibitin complex, an integral membrane complex, and the membrane-associated protein annexin B1.

The full-length prohibitin complex, consisting of prohibitin 1 (BAP32) and prohibitin 2 (BAP37), was produced recombinantly and refolded from inclusion bodies. To increase solubility of the proteins, several truncation mutants were generated, refolded and subjected to CD spectroscopy. The complex consisting of N-terminally truncated prohibitins 1 and 2 was proven to be folded revealing both α-helices and β-sheets as secondary structure elements. Thermal denaturation experiments revealed a two-state transition process upon unfolding giving a melting temperature of 62ºC. This indicated that both, dissociation of the complex and unfolding of the monomers, occur in one step. Gel filtration analysis determined the apparent molecular weight of the complex to be 63kDa which is slightly higher than its theoretical molecular mass of 56kDa. This discrepancy might be due to an elongated shape of the complex. In a protein engineering approach to further increase the solubility and stability of the complex, the N-terminal hydrophobic helix of BAP32 was replaced by an artificial, self-folding soluble helix. Introduction of this helix did not lead to successful refolding of the prohibitin complex. In a modelling study, the PHB domains of BAP32 and BAP37 were generated using an NMR structure of mouse flotillin-2 as template. Dimerisation was achieved by manual rigid body movement leading to a parallel alignment of both domains with their N-termini pointing in the same direction as required by their function as an integral membrane complex. Possible interaction interfaces with target proteins were elucidated as well as possible binding to melanogenin, a precursor in melanogenesis. Furthermore, a dimerisation of their N-terminal helices in the membrane was proposed which could mask otherwise exposed charged and polar residues within the membrane. A model of the prohibitin complex in the membrane was suggested.

Interaction of the prohibitin complex with *m*-AAA-protease was elucidated, and two possible interaction interfaces proposed: interaction of the N-terminal helices of both proteins in the membrane and interaction of the PHB domains of the prohibitins with a newly identified intermembrane space (IMS) region of the *m*-AAA-protease. This

region was identified by comparing multiple sequence alignments with secondary structure predictions and indicates a conserved fold within the N-terminal domain of *m*-AAA-proteases from different species. The IMS-region of the *E.coli m*-AAA-protease FtsH was produced as recombinant protein and subjected to CD spectroscopy where it was shown to be folded revealing both α-helical and β-sheet content in its secondary structure. Analysis of the protein by gel filtration and SAXS revealed the presence of a dimer in solution. A two-state transition process was observed in thermal denaturation monitored by CD. The FtsH-IMS region was also subjected to crystallisation trials but no crystals were obtained thus far.

Annexin B1 from the tape worm larva *Cysticercus cellulosae* was produced as a recombinant protein. CD spectroscopy revealed an α-helical protein which undergoes a two-state transition process upon thermal denaturation with a melting temperature of 51ºC. Addition of both 1mM DTT and 5mM $CaCl_2$ has a stabilising effect on the protein as seen in thermal denaturation experiments. In gel filtration experiments, a mixture of monomers, dimers and trimers in solution was observed. Addition of 1mM DTT induced monomer formation indicating a Redox-dependent dimer formation. Using mass spectrometry and molecular modelling, two of the four cysteins present in the protein could be identified as likely to form inter-molecular disulfide bonds which could lead to oligomerisation. A cysteine on the concave side of the protein and the N-terminal cysteine residue are likely to form an intra-molecular disulfide bridge locking the N-terminus to the C-terminal core domain of the protein. In biochemical assays, annexin B1 showed calcium-dependent phospholipid binding with preference for acidic liposomes. The protein also exhibited calcium-independent phospholipid binding with a binding degree of about 50% for PS/PC (3:1) liposomes, a behaviour akin to bell pepper and cotton annexins, although the latter proteins have a less stringent requirement for PS in this context. In a newly developed heparin-binding assay, annexin B1 showed calcium-dependent heparin binding in a cooperative manner. Two main heparin binding sites, one on the convex side and the other on the concave side of the protein, are thought to engage in recognition or binding of heparin. This feature may be employed as an infection strategy by the parasite to attach to the extra-cellular matrix of host cells. Annexin B1 was subjected to crystallisation trials yielding in crystals that diffracted to 3.8Å.

Declaration

I hereby declare that all work submitted for assessment is my own effort (unless stated otherwise) and without falsification of any kind. It is an original work on the basis of three years postgraduate study and research.

Parts from this work were published in the following peer reviewed publications:

Winter A, Yusof AM, Gao E, Yan HL, Sun SH, Hofmann A., (2006): Biochemical characterization of annexin B1 from *Cysticercus cellulosae*. *FEBS J.* **273**(14): p. 3238-47.

Winter, A., O. Kamarainen, and A. Hofmann, (2007): Molecular modeling of prohibitin domains. *Proteins*. **68**(1): p. 353-62.

Winter, A. and A. Hofmann: Towards understanding the roles of prohibitins, multi-functional regulator proteins. *Current Chemical Biology, in press*

Acknowledgements

This thesis is the work of three years intensive study in which I mainly neglected my family and friends. I do apologise to all of you for the birthday parties I have missed and the evenings I have been working in the lab instead of going out.

First of all, I would like to thank my aunt Isolde, my mother and my siblings Sarah and Tobias for supporting me when I first decided to go to university in Berlin. My boyfriend Matt is a very important person to me, and I would like to thank him for his support and his respect for me and my work. The decision to move to Australia was very hard on our relationship. I hope that we will share more precious moments in the years to come in whatever continent or country that may be. I would also like to thank my special friends Ariana in Edinburgh and Nadine and Tanja in Berlin. They always had an open ear for my problems during those years and were a constant source of entertainment. In Berlin, I left good friends behind who knew me for years and to who I owe thanks for their support and friendship: Mücke and his wife Nadine, Matthias and Kathrin. Special thanks go to Angelika, a lab technician at Schering. She helped me to grow up and find my way in life.

I would like to thank Takashi Tatsuta and Thomas Langer who gave me great insight in the field of prohibitins and *m*-AAA-proteases, and provided me with the original BAP32 and BAP37 construct which enabled me to do the major part of the work on the prohibitin project. I would also like to thank Prof. A. Aitken who let me use his Biocad® and his collection of cross-linkers, Dr. Iain McNae who collected the annexin B1 data set for me, and Outi Kämäräinen who helped me with docking of melanogenin to prohibitin 1 and its analysis. Finally, I thank my supervisor Andreas Hofmann for teaching me not only essential things in crystallography and structural biology but also about research, researcher and the higher goals in life. He is an inspiration to me and I enjoyed working in his group over the past 3 years. I am very thankful for the great support he gave me when I moved to Australia.

Abbreviations

AA / Bis-AA	acrylamide / bisacrylamide
APS	ammonium persulfate
BAP	B-cell receptor associated proteins
CHCA	α-cyano-4-hydroxycinnamic acid
CD	circular dichroism
EDTA	Ethylenediaminetetraacetic acid tetrasodium salt dihydrate
DTT	DL-Dithiothreitol
IAA	iodoacetamide
IPTG	isopropyl-beta-D-thiogalactopyranoside
MALDI-TOF	Matrix assisted Desorption Ionisation – Time of Flight analyser
PC	1,2-dioleoyl-*sn*-glycero-3-phosphocholine
PCR	polymerade chain reaction
PMSF	phenylmethylsulfonyl fluoride
PS	1,2-dioleoyl-*sn*-glycero-3-phosphoserine
SDS-PAGE	sodium dodecyl sulphate polyacrylamide gel electrophoresis
TEMED	*N*,*N*,*N*′,*N*′-Tetramethylethylenediamine

Contents

PART A

Structural biology of Prohibitins:

Molecular mechanisms of the cell ageing process

Table of contents

PART A: Structural Biology of Prohibitins

1 Introduction to prohibitins

1.1 The super family of SPFH (PHB) domain proteins

Prohibitins were first described by Nuell and colleagues in 1991 and thought to be involved in cancer development . They belong to a larger family of proteins that share an evolutionarily conserved stomatin/prohibitin/flotillin/HflK/C (SPFH) domain with significant homology to several eukaryotic and prokaryotic proteins. Members of this protein family are membrane-associated and implicated in cellular processes concerned with protein turnover , senescence and proliferation control . However, different data mining tools describe the conserved domain as either a SPFH, PHB or band 7 domain, but it appears that regardless of the slight variation in determination of the domain boundaries, essentially the same domain is described . The core motif of the SPFH domain is partially described in the Pfam database (Pfam entry: Band_7, accession number: PF01145).

Members of the SPFH domain family can be found in divergent species. They are present in higher eukaryotes (prohibitin, stomatin and podocin), as well as in lower eukaryotes and prokaryotes (vacuolin A and vacuolin B, HflK and HflC, UNC-1, UNC-24 and MEC-2). The SPFH domain is conserved in proteins that are ubiquitously expressed like flotillin, as well as in proteins that show extremely restricted expression like the stomatin-related olfactory protein (SROP), whose expression is constrained to olfactory sensory neurons . The evolutionary significance of this domain is unclear but its prokaryotic conservation suggests that it is indeed a primordial motif as there are more than 700 non-redundant sequences containing the SPFH domain throughout all kingdoms. It is clear that this domain is likely to perform an important cellular function and worthy of further examination . Interestingly, most mutations that disrupt or alter the activities of MEC-2, UNC-1 and UNC-24 in *C. elegans* are found in conserved amino acids within the SPFH domain which suggest that this domain is crucial for function of the protein .

Classification of proteins into the SPFH superfamily is based mainly on similarities in fold and protein architecture. Rather poor matches in amino acid sequences reveal only

ambiguous relationships within this superfamily. While domain databases recognize all these protein families as members of the same superfamily, their SPFH domains are so variable that it is virtually impossible to obtain a consensus sequence (see figure 1-1). Greater sequence similarity can be found within the subfamilies such as prohibitins, flotillins, stomatins and HflC/K indicating independent origins for the individual members and convergent evolution of the SPFH domain .

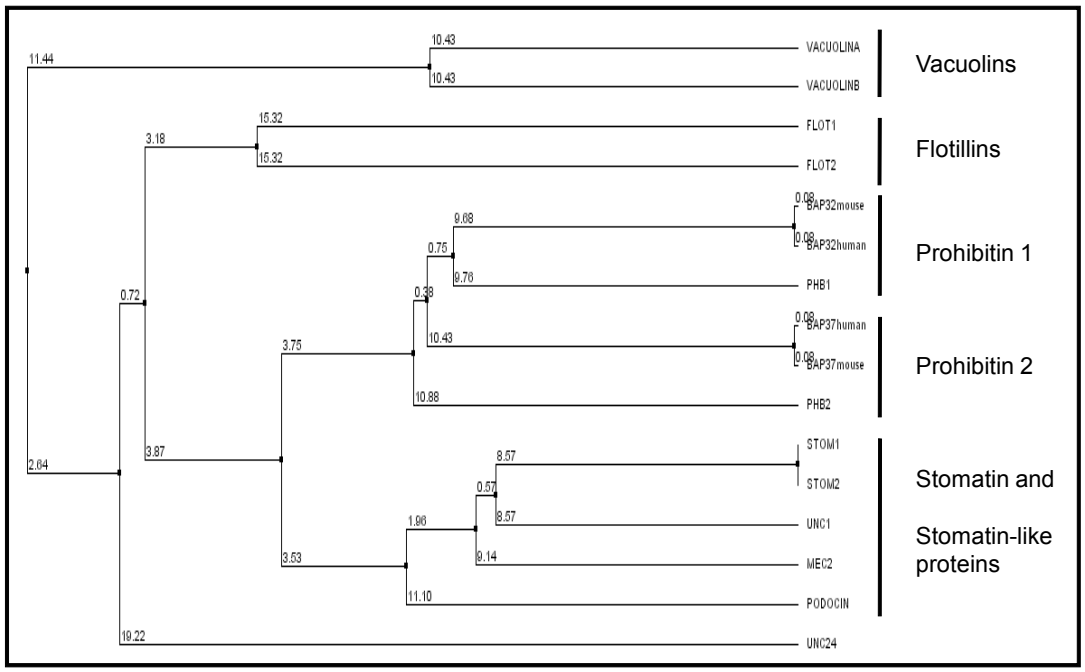

Figure -1: Phylogenetic tree of SPFH domain proteins from different species as average distance of percent identity. Indicated are subfamilies vacuolins, flotillins, prohibitins, stomatins and stomatin-like proteins. Figure prepared with Jalview .

The prohibitin proteins BAP32 and BAP37 reveal a sequence similarity of 60% and an identity of 47%, the similarity of both proteins to mouse flotillin-2 is only 4% and 7%, respectively. As found with prohibitins, flotillin paralogues also show a high degree of conservation, e.g. mouse flotillin-1 and flotillin-2 that show 47% identity and 68% similarity.

However, several hallmark features are shared among members of SPFH domain proteins. They are integral membrane proteins with the SPFH domain situated in the cytosol but close to the membrane. The proteins insert into plasma or mitochondrial membranes via their hydrophobic N–terminal domain which is often preceded by a palmitoylation site as found in flotillin-1 , flotillin-2 and podocin and mec-2 . In case

of flotillins, stomatin and podocin, the hydrophobic N-terminal domain does not span the membrane but is suggested to form a horseshoe-like structure, with both N- and C-termini facing the cytosol (see review), while prohibitins possess transmembrane helices that, in mitochondria, protrude from the inner mitochondrial membrane into the intermembrane space (see figure 1-2) . In the bacterial HflK/C subfamily, the SPFH domain resides on the periplasmic side of the plasma membrane .

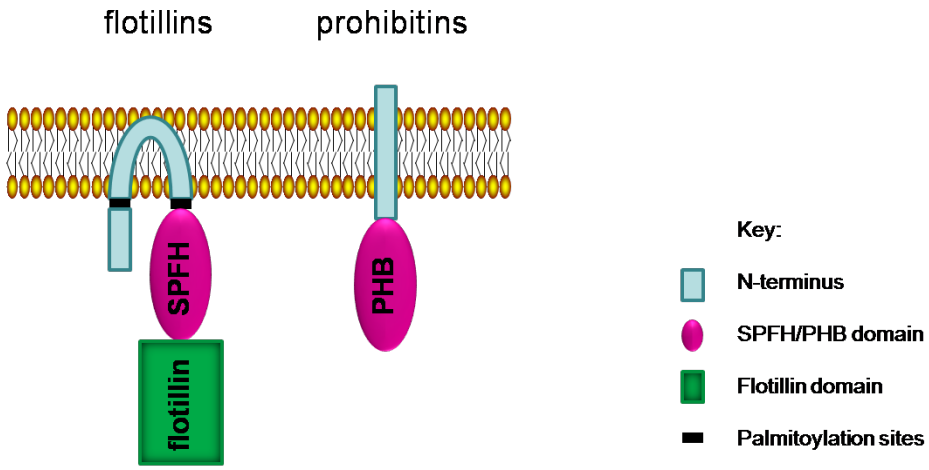

Figure -2: Membrane association found with flotillins and prohibitins. The N-terminus of flotillin integrates into the membrane in a horseshoe-like fashion whereas prohibitins have an N-terminal membrane helix. Palmitoylation sites as found in flotillins might aid membrane localisation.

Additionally, SPFH domain proteins tend to form oligomers mediated through their C-terminal domains, as shown for stomatin , podocin , prohibitin and flotillins . Similar structural features among this super-family suggest related functions for all SPFH proteins.

First structural data on SPFH proteins were obtained from an NMR structure of mouse flotillin-2 (PDB accession no. **1WIN**). As member of the SPFH protein family, flotillin-1 and its homologue flotilltin-2 are thought to bind to membranes and have thus been associated with lipid-rafts . Palmitoylation sites close to the N-terminus have been identified in flotillin-1 which would enhance membrane binding of the protein . Recent studies suggested a similar topology for flotillin-2, which is both palmitoylated and myristoylated close to the N-terminus . As observed in other SPFH family members, the C-terminal region contains a coiled coil domain which is thought to be

involved in homo-oligomerisation and commonly referred to as flotillin-domain in those proteins. The SPFH domain spans the first 250 amino acid residues of flotillin-2 as described in different prediction tools . Residues 1 to 123 of this region were synthesised and subjected to NMR analysis by Miyamoto and colleagues in 2004 (PDB accession no. **1WIN**, see figure 1-3).

Flotillin-2(1-123) presents itself as a compact, ellipsoid structure containing five α-helices and six β-strands. Two anti-parallel α-helices are packed against a strand of anti-parallel β-sheets; and the N-terminal and C-terminal sides of this structure are "sealed" by short α-helices. The flotillin domain starts at the C-terminus by a short α-helix. This NMR structure represents the only available experimental information on PHB proteins and might give first clues as to how the PHB domain in prohibitin 1 and 2 might look like.

Figure -3: NMR-structure of mouse flotillin-2 PHB domain (PDB accession no. **1WIN**).

1.2 Structural features of prohibitin proteins

1.2.1 Homology of prohibitin proteins

Prohibitins, the archetypal SPFH domain-containing proteins, are ubiquitously conserved in eukaryotes , and their SFPH domain is commonly referred to as PHB domain. PHB1 is the yeast orthologue of mammalian prohibitin 1 (BAP32), and its paralogue, prohibitin 2 (BAP37), is called PHB2 in yeast, respectively . Multiple sequence alignments of prohibitin proteins from different species show that both proteins are well conserved throughout the eukaryotic animal and plant kingdoms (see tables 1-1 and 1-2). While human and mouse prohibitin have identical BAP32 primary structures, identity of human prohibitin 1 to orthologues from yeast and plants decrease to around 50%. A much higher degree of identity can be found between prohibitin 1 from multicellular animal organisms such as *Caenorhabditis elegans* (65%) and *Xenopus tropicalis* (91%). On the other hand, both plant proteins from *Nicotiana benthamiana* and Petunia x hybrid show a high sequence identity of 96% amongst each other.

Table -1: Sequence identity of prohibitin 1 proteins in different species in percent [%].

	Mouse	**Human**	**Xenopus**	**Caenorhab-ditis**	**Nicotiana**	**Petunia**	**Yeast**
Mouse	100	—	—	—	—	—	—
Human	100	100	—	—	—	—	—
Xenopus	91	91	100	—	—	—	—
Caenorhabditis	65	65	66	100	—	—	—
Nicotiana	52	52	52	53	100	—	—
Petunia	53	54	53	53	96	100	—
Yeast	52	52	52	52	53	53	100

Table -2: Sequence identity of prohibitin 2 proteins in different species in percent [%].

	Mouse	**Human**	**Xenopus**	**Caenorhab-ditis**	**Nicotiana**	**Petunia**	**Yeast**
Mouse	100	—	—	—	—	—	—
Human	99	100	—	—	—	—	—
Xenopus	88	89	100	—	—	—	—
Caenorhabditis	62	63	61	100	—	—	—
Nicotiana	51	52	52	53	100	—	—
Petunia	60	60	62	62	96	100	—
Yeast	48	49	51	49	50	67	100

Human and mouse prohibitin 2 are different from each other in only two amino acids resulting in a sequence identity of 99% (see table 1-2). The next highest identity to human prohibitin 2 is observed with proteins from *X. tropicalis* (89%), followed by *C. elegans* (63%), Petunia x hybrid (60%), *N. benthamiana* (52%) and yeast (49%).
The generally high degree of conservation between prohibitins from unicellular organisms such as yeast, and multicellular organisms such as plants and humans emphasises their involvement in important cellular functions. On the other hand, prohibitins show a high degree of identity within mammalians or plants reflecting the evolutionary relatedness between different species and changes in the proteins during evolution.

1.2.2 Topology of prohibitins

In 1991, Nuell and co-workers predicted a 12 amino acid long hydrophobic N-terminal tail for yeast PHB1 from its primary structure , later specified as transmembrane domain encompassing residues 10 – 30 . A transmembrane domain for PHB2 was allocated to amino acids 36-54 . Sub-mitochondrial fractionation using yeast cells identified PHB1 and PHB2 as integral components of the mitochondrial inner membrane indicating that the N-terminal region is the membrane anchor, while the C-terminal region of each protein protrudes into the inter-membrane space.
Combining previous findings by other groups and secondary structure predictions using PSIPRED , extends of the three-divided topology of mammalian prohibitins 1 and 2 were suggested as seen figure 1-4.

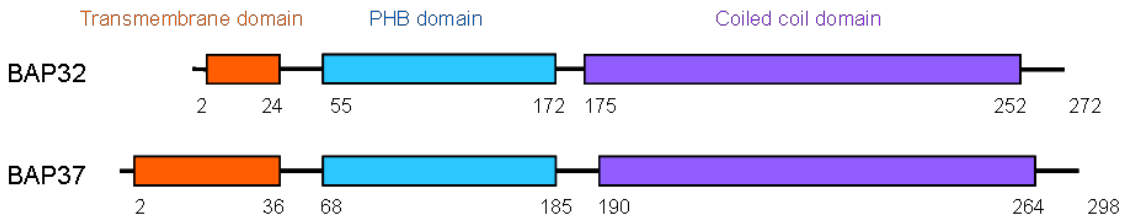

Figure -4: Domain topology of mammalian BAP32 and BAP37. Extends of transmembrane (orange), PHB domain (blue) and coiled-coil domain (purple) are indicated as residue numbers.

The N-terminal transmembrane domain (orange) of BAP32 spans residues 2-24, followed by the predicted PHB domain (blue, residues 55-172) and the C-terminal coiled-coil domain (purple, residues 175-252). BAP37 is divided into its N-terminal region (residues 2-36), the PHB domain (residues 68-185), and the coiled-coil domain from residue 190 to 264.

1.2.3 Complex formation between prohibitin 1 and prohibitin 2

In previous years, several observations have been made which led to a potential model where prohibitin 1 and prohibitin 2 interact strongly with each other, are interdependent in their stability , are co-localized in the cell and also co-precipitate. Observations suggested a physical, as well as a functional, interaction, which influences the function of mitochondria and thus the life span of the cell . The amount of both proteins produced in the cell was found to be equal despite different levels in different tissues, and prohibitin 1 is unable to functionally replace prohibitin 2 despite their highly similar sequences . In 1998, Berger and Yaffe suggested a complex formation of both proteins in the mitochondrial inner membrane which was supported by findings by Nijtmans and co-workers . They also suggested a barrel-like structure as seen in chaperones and proposed a similar function for prohibitins as a chaperon-like holdases . Evidence for such a complex in yeast was later provided by electron microscopy, and the complex formation could be assigned to the conserved C-terminal coiled-coil regions in both proteins . Electron microscope studies revealed an elliptical ring-like (32%) or more rectangular structure (68%) of the yeast prohibitin complex comprising 16 to 20 individual protein molecules (see figure 1-5) . The function of this large prohibitin complex in mitochondria is still unclear. In a recent study, a stretch of EA repeats at the start of the C-terminal domain was proven to be essential for oligomerisation of the protein .

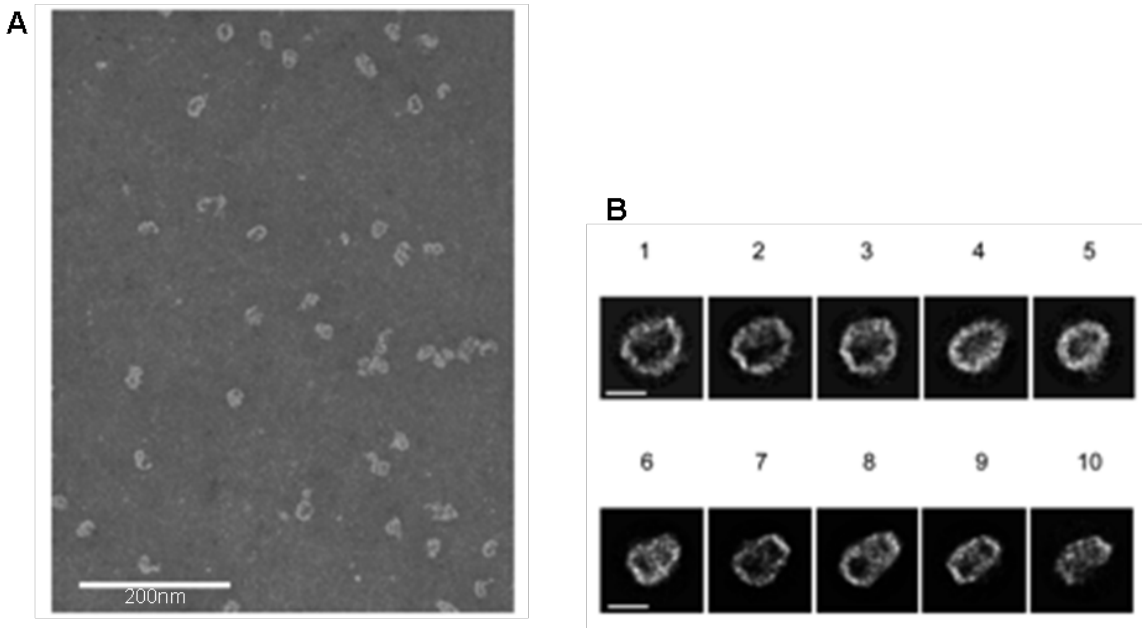

Figure -5: Micrograph showing prohibitin rings as observed in electron microscopy. Figure taken from . A - Representative section of an electron microscope micrograph, the bar is 200 nm. B - Class averages of typical end-on or side-on projection views, bar is 200 Å.

1.2.4 Complex formation with *m*-AAA-proteases

Membranes of mitochondria, chloroplasts and bacteria contain membrane embedded ATP-dependent proteases, termed AAA proteases (ATPases Associated with a variety of cellular Activities), to perform essential roles in cellular regulation and homeostasis . They degrade misfolded polypeptides , and are involved in maturation of target proteins such as the respiratory complex . AAA-proteases are well conserved throughout the animal and plant kingdom being divided in several sub-families with even greater conservation . AAA-proteases assemble to large complexes in the membrane, and are composed of up to 3 closely related subunits with molecular masses of 70–80 kDa . Human AAA-proteases contain 2 subunits, paraplegin and AFG3L2, whereas mouse expresses 3 different subunits, paraplegin, AFG3L1 and AFG3L2 . Most bacteria contain only one AAA protease subunit, such as FtsH from *Escherichia coli* which is thought to form a homo-oligomeric complex in the plasma membrane . FtsH-like proteases have also been found in plants . In yeast, two AAA-proteases are present within the inner membrane of mitochondria exposing their

catalytic sites either to the matrix (*m*-AAA protease) or the intermembrane space (*i*-AAA protease) . A direct interplay between *m*-AAA und *i*-AAA protease was found important for effective substrate recognition and proteolysis .

Prohibitins and *m*-AAA proteases have been found in a large superstructure within the inner mitochondrial membrane of yeast cells and were shown to interact physically in gel filtration experiments . These protein complexes with a diameter of 20–25 nm are thought to provide a scaffold within the membrane . Deletion of either *PHB1* or *PHB2* in yeast results in an accelerated degradation of non-assembled membrane proteins by the *m*-AAA protease , and a regulatory role for prohibitins was suggested where they would either interact directly with protease substrate proteins or modulate the enzymatic activity of the *m*-AAA protease. A genetic interaction with prohibitins has also been described for *YTA10* and *YTA12*, coding for subunits of the *m*-AAA protease in yeast that suggests additional functions of prohibitins which are not exerted via their physical interaction with the *m*-AAA protease. Additionally, a complex of two homologous prohibitin related proteins in *E. coli*,, HflK and HflC, has been found to reside on the periplasmic side of the plasma membrane and was found to assemble with FtsH , the bacterial *m*-AAA protease. Furthermore, HflK and HflC were found to interact directly with substrate polypeptides of FtsH.
The functional relationships of AAA proteases and prohibitins in the mitochondrion are schematised in figure 1-6. *i*-AAA protease and *m*-AAA protease are anchored to the inner mitochondrial membrane via N-terminal regions of their subunits, while the conserved C-terminal ATPase and metallopeptidase domains protrude into either the intermembrane space or the mitochondrial matrix . The inhibitory effect of prohibitins on the *m*-AAA protease is thought to be executed on the protein level , and is indicated by a grey arrow. ATP hydrolysis and protease function of the *m*-AAA protease are also indicated by grey arrows.

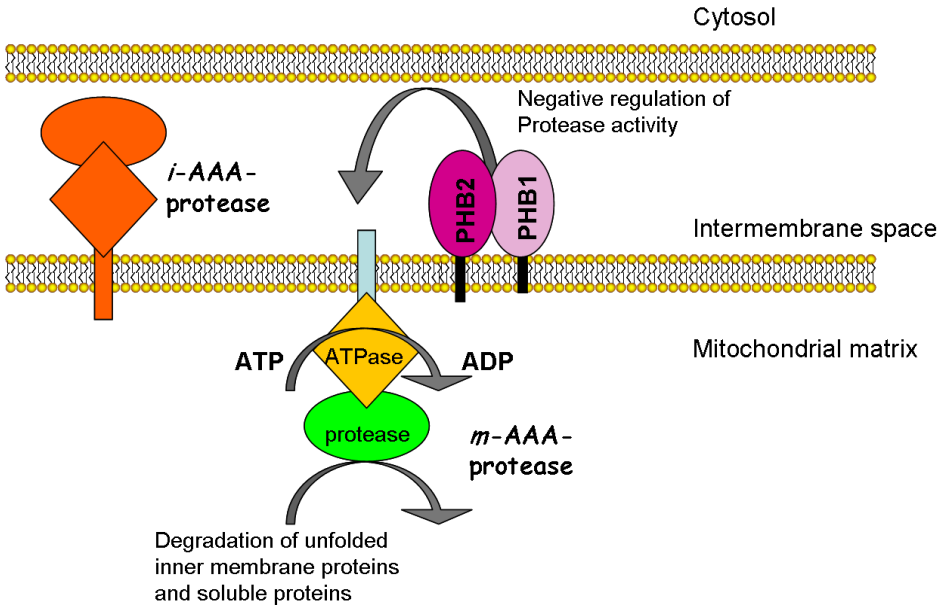

Figure -6: Schematic interpretation of the proposed interaction between prohibitins and AAA-proteases as they reside in the inner mitochondrial membrane.

ATPase and protease domains of the AAA protease FtsH have been crystallised in nucleotide-bound and apo state (PDB entries **1LV7**, **2DHR**, **1IXZ**, **1IY2** and). However, little structural information is available about the N-terminal region that anchors the protein to the membrane.

1.3 Functions of prohibitins in the cell

Prohibitins were first identified as negative regulators of cell division in cultured animal cells and human tumour cells . They were also thought to be involved in cancer development as a significant percentage of patients with sporadic breast cancer had mutations in the human prohibitin gene whereas studies of prohibitin homologues in yeast suggested that these proteins may be involved in cellular senescence . However, more recent studies showed that the cell-cycle arresting property of prohibitin is restricted only to certain cell types, and supposedly carried out by its 3'-untranslated region (3'-UTR) acting as a riboregulator .

A great variety of interaction partners for the prohibitin protein has been discovered in almost all cellular locations: mitochondria , nucleus , cytosol , plasma membrane and

endoplasmatic reticulum . A hypothesis has been put forward where the N-terminal sequences of PHB-domain containing proteins are responsible for the subcellular targeting of these proteins . BAP32 and BAP37 have also been shown to translocate to different cell compartments in the presence of extracellular and intracellular stimuli . The diversity of cellular locations and interaction partners reflects the wide range of important cellular functions assigned to these proteins such as protein turnover in mitochondria, regulation of gene expression, involvement in apoptosis and oxidative stress release.

Prohibitins interact with their target proteins mostly through their PHB domain and their C-terminal coiled-coil domain , but for most interactions it is not clear whether it is formed by the intact prohibitin complex or either monomer. Different groups report interaction of proteins with prohibitin monomers or dimers in different cell compartments such as the mitochondrial membrane , the nucleus and the cytosol . These controversial findings could be explained by the formation of a prohibitin dimer upon binding to membranes.

However, prohibitins seem to be able to interact with several target proteins simultaneously with moderate *in vitro* binding affinities . An overview of interaction partners of the BAP32:BAP37 complex in different cell compartments is given in figure 1-7. Depicted are extracellular ligands for a membrane bound complex, cytosolic proteins, cell cycle proteins and nuclear receptors and the *m*-AAA protease in mitochondria.

In recent years, prohibitin research has been focussing on prohibitin-ligand interactions, including protein-protein interactions, and interactions with peptides , sugars and other organic molecules .

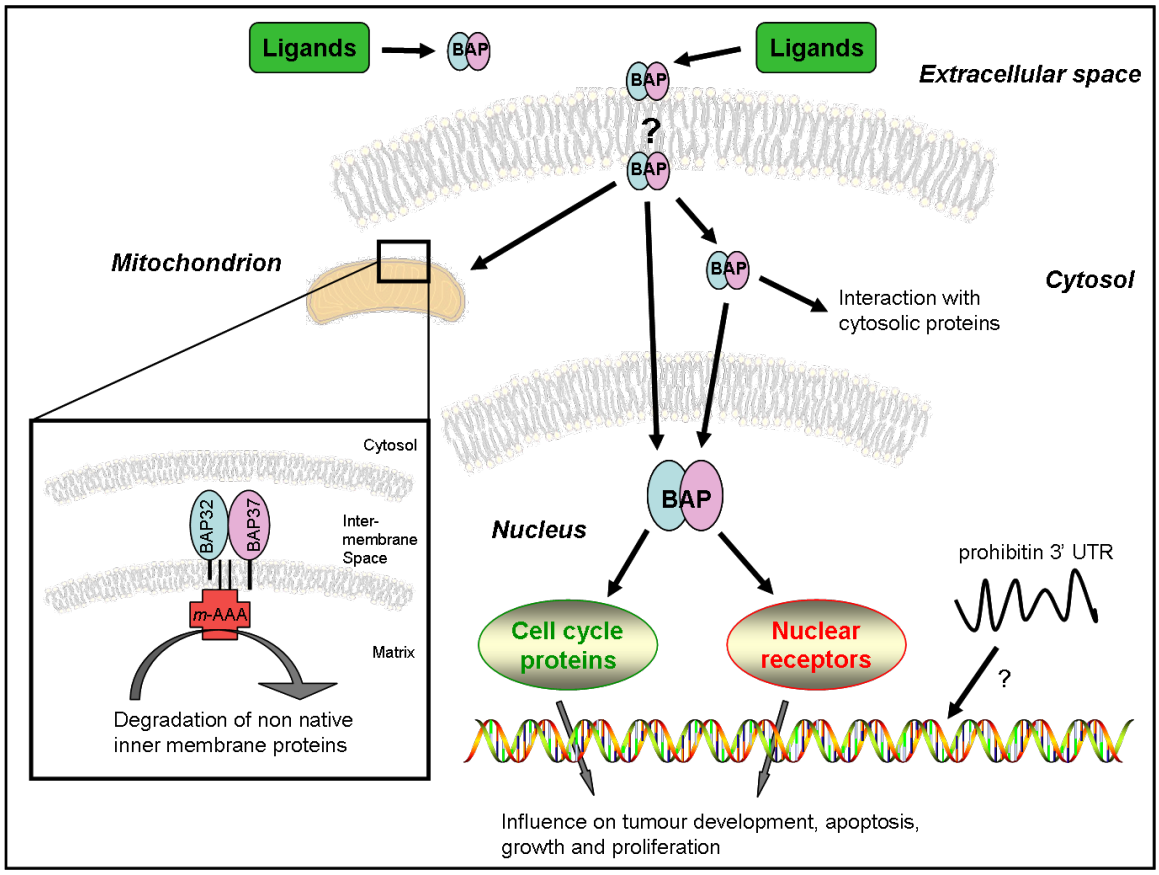

Figure -7: Interaction partners of prohibitin in different cell compartments. BAP32 (prohibitin 1) is shown as blue oval, and BAP37 (prohibitin 2) as purple oval.

1.3.1 Functions in cell cycle regulation

Prohibitin mRNA and its protein product are present in cells of all tissues in varying levels where they seem to have a natural function in the regulation of cell proliferation. Prohibitin mRNA levels were found to fluctuate throughout the cell cycle three- to four-fold and inhibit initiation of DNA synthesis with the largest inhibitory effect when the cells are entering G1 phase (and see figure 1-8).

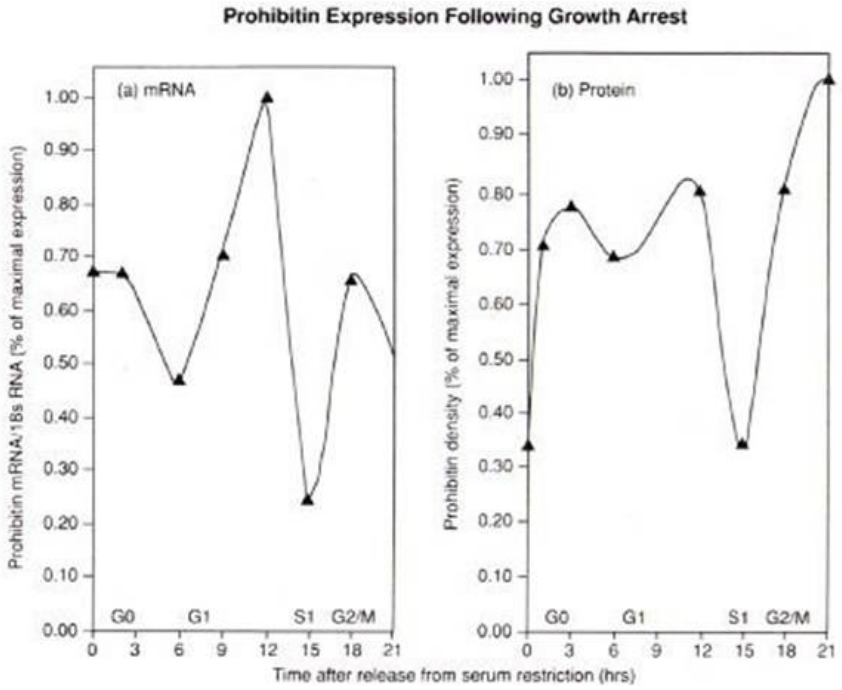

Figure -8: Progression of prohibitin 1 mRNA (a) and protein levels (b) in Rat1 cells through their cell cycle. Figure taken from .

Observations in higher species showed a correlation between the expression of PHB genes and ageing , and the life span of yeast cells increased upon the knock out of the prohibitin complex but the mechanisms by which expression of the *PHB* genes influences ageing are not yet fully understood. Interestingly, all immortal cell lines of the complementation group B were found to possess base changes in the prohibitin 3'UTR; resulting in loss of antiproliferative activity . Jupe and colleagues also found that all tumour cell lines express high levels of the PHB proteins, probably in an effort to produce more transcript that would increase anti-proliferative action.

In early studies, a shortened replicative life span was observed in yeast with disrupted prohibitin genes . While disruption of prohibitin genes in *Saccharomyces cerevisiae* does not result in a lethal phenotype , the deletion of a prohibitin homologue in *Drosophila melanogaster* and *Caenorhabditis elegans* is lethal during larval development. These findings were supported by results from recent studies, where severe growth inhibition and apoptosis upon knock-out or silencing of the prohibitin gene were observed in granulosa cells and with plant prohibitins . Furthermore, the transcription of multiple genes has been found to be modulated by increased cellular levels of prohibitin in transfection experiments involving prohibitin in cell cycle

regulation . These findings substantiate a proposed role for prohibitins in cell cycle regulation.

1.3.2 Extracellular prohibitin

Despite contrary statements about prohibitin 1 and 2 localizing to the plasma membrane and acting as a receptor for extracellular ligands, an immunohistochemical study revealed that prohibitin 1 is present in the vasculature of mouse and human white adipose tissue . A pro-apoptotic peptide was conjugated to a CKGGRAKDC motif which interacted with prohibitin 1 at the protein level possibly as part of a higher order complex. The peptide was also successful in reversing obesity in the mouse model . These findings deserve further attention, since the addition of prohibitin 1 to cultured adipocytes has been reported to result in inhibition of mitochondrial pyruvate carboxylase and subsequent suppression of glucose and fatty acid oxidation . The importance of these findings is evident when the use as a target for apoptosis inducing drugs to fight obesity is imagined.

Cell surface-associated prohibitins 1 and 2 have also been shown to interact with Vi capsular polysaccharide of *Salmonella typhi* in a human model intestinal epithelium cell line. *S. typhi* is a pathogen that enters the human body by intake of contaminated food or water causing typhoid fever and leading to considerable morbidity and mortality in third world countries . To date, the host-pathogen interactions of *Salmonella* remain incompletely characterised, and the virulence factor Vi capsular polysaccharide is currently one of the most efficient available vaccines for use in humans . Investigations on the interaction between prohibitins and the Vi capsular polysaccharide may provide leads for development of new drugs against *S. typhi* infection.

Table -3: Extracellular ligands targeting the prohibitin complex and involvement in cellular functions.

Extracellular binding partner	tissue	Prohibitin complex involved in

CKGGRAKDC	Adipose tissue	Extracellular recognition
Vi capsular polysaccharide	intestinal epithelial cells	Extracellular recognition, possibly inflammatory response
C3	Blood serum	Non-specific immune response

In 2007, Mishra and colleagues reported that prohibitin 1 binds to and activates C3, a component of the complement system involved in non-specific immune response to pathogens in the blood . Prohibitin 1 could be cross-linked to the human serum proteins C3a and C3b, descendents of C3, assigning a potential role for prohibitin in innate immunity and inflammation. This is in agreement with findings that prohibitins localise to the plasma membrane of human intestinal epithelial cells and lymphocytes . Intriguingly, during infection with *S. typhi*, serum complement activation is inhibited, if the strains carry the Vi antigen .

Recently, prohibitin 1 and prohibitin 2 were identified as antigens released from colorectal tumours *in vivo* . The source of circulating prohibitin is unclear but it may be shed from the plasma membrane or released from adipocytes and possibly other cells in lipid droplets . Translocation via lipid droplets might be one possible mechanism by which prohibitin could be transported to the endothelium, a mechanism that has been reported for lipoprotein lipase .

1.3.3 Interactions with cytoskeletal proteins

Employing an yeast two-hybrid screen, annexin A2 and α-actinin have been identified as binding partners for BAP32 and BAP37 . Similar to annexin A2 , α-actinin was found to interact with target proteins in a calcium-dependent fashion and to associate calcium-independently with membrane-bound proteins and adhesion proteins. Similarly, annexin A2 is a calcium-dependent actin binding protein , and mainly exists as a heterotetramer with S100A10 in the cell cytosol but can also bind to acidic phospholipid membranes in a calcium-dependent fashion . Using yeast two-hybrid screens, Bacher and colleagues found that each prohibitin was able to bind to each target protein, but stronger affinities were observed between BAP32 and annexin A2, and BAP37 and α-actinin, respectively . The association with annexin A2 links

prohibitins to lipid rafts, a notion that is further supported by the discovery of the PHB-domain containing proteins erlin-1 and erlin-2 in lipid rafts of the endoplasmic reticulum , and the association of lipid rafts with prohibitin 1 and prohibitin 2 on the cell surface . Notably, palmitoylated PHB domains of the prohibitin-related proteins podocin and mec-2 have been proven to be essential for the ability to bind cholesterol and thus locate the proteins to the cell membrane.

1.3.4 Nuclear prohibitin and regulation of gene expression

In recent studies, prohibitins were found to act as transcription regulators via an interaction with cell cycle regulators, transcription factors and nuclear receptors but detailed mechanisms remain to be elucidated . Interactions of both prohibitins with nuclear proteins are summarised in figure 1-9.

In 1999, Wang and colleagues found that prohibitin 1 could effectively interact with the cell cycle proteins Rb, p107 and p130 . Prohibitin 1 is also capable of physically interacting with p53 *in vivo* and *in vitro*, and was found to enhance p53-mediated transcriptional activity . Moreover, it was found to repress the activity of all five translation factors E2F1 to 5 supposedly by utilising the MAPK pathway , and thus inhibiting cell proliferation . Repression of E2F-mediated transcriptional activity requires the co-repressors HP1γ and Brg1/Brm , and is enhanced in response to estrogen antagonist treatment of breast cancer cells involving the estrogen receptor . Depletion of prohibitin, on the other hand, diminishes the growth-inhibitory effects of anti-estrogens. The regions on prohibitin 1 required for repression of E2F activity are the Rb-binding domain and an additional region mapped to the C-terminal part of the PHB domain (residues 185 to 214) . The Rb binding region on BAP32 spans residues 74-116, where three of four point mutations of prohibitin are found in sporadic breast cancer cells .

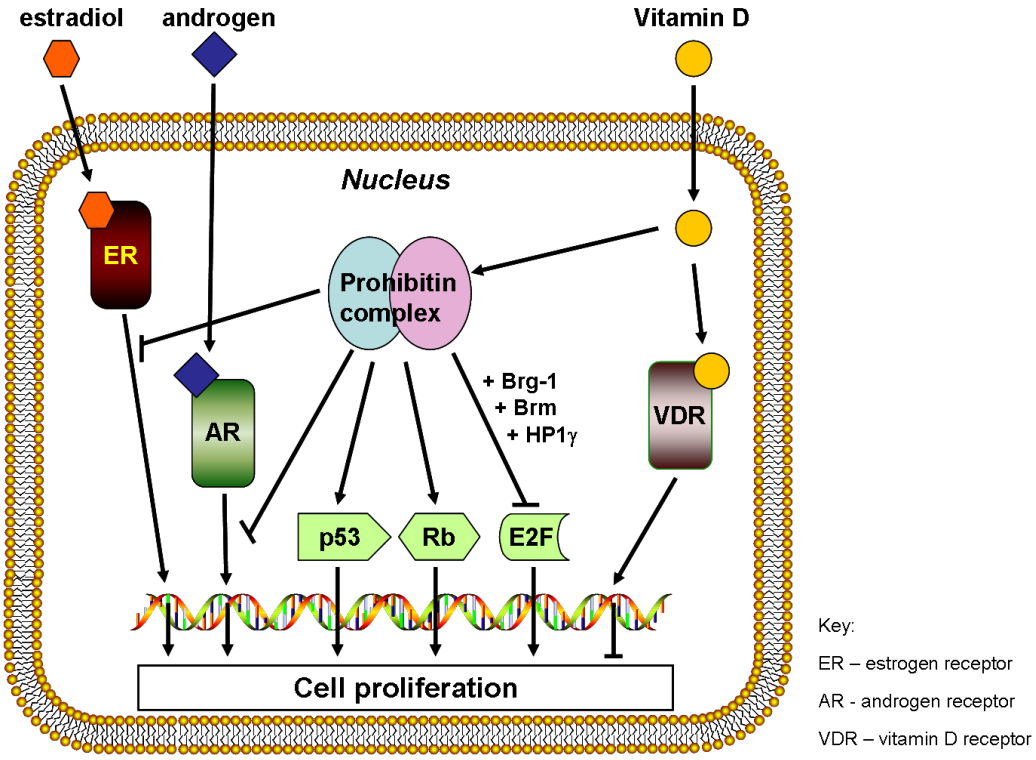

Figure -9: Role of the prohibitin complex in the nucleus. Prohibitin 1 and 2 were found to interact with nuclear receptors, DNA binding proteins and transcription factors.

Recently, prohibitin 2 was found to interact with the transcription factor families of MyoD and myocyte enhancer factor-2 (MEF2) possibly with the help of co-activators such as histone deacetylases . Amino acids 120-232 of prohibitin 2 were identified as the interaction interface with Akt, an indirect activator of the transcription factor families of MyoD and MEF2. Prohibitin 2 might thus act as a miogenic repressor by competing with Akt to prevent its interaction with MyoD and MEF2 .

In the nucleus, prohibitins were also found to interact directly with the steroid receptors estrogen receptor and androgen receptor . BAP37, originally known as repressor of estradiol activity (REA), binds directly to the estrogen receptor (ER) in the presence of its ligand estradiol repressing its transcriptional activity . While BAP37 possesses the common ER-binding motif L-X-X-L-L N-terminal of its PHB domain, residues 175-198 are also required for binding to ER . On the other hand, BAP32 was shown to repress androgen receptor (AR)–mediated transcription and androgen-dependent cell growth without an apparent direct interaction with AR . A binding site

for the vitamin D receptor has been identified in the promoter region of prohibitin 1, and cellular levels of the protein were increased after treatment with vitamin D .

The great variety of important nuclear binding partners shows the versatility of prohibitin action and highlights their involvement in important cellular functions. The prohibitin complex is mostly involved in regulating the activity of proteins which are responsible for regulating cell proliferation and cell growth rather than directly binding to specific sited on the DNA.

1.3.5 Implications for mitochondrial functions

Prohibitins were first located to the inner mitochondrial membrane , and have been implicated in various mitochondrial functions such as a chaperone, in scaffolding, programmed cell death and regulation of *m*-AAA-protease activity.
A recent study by Coates and colleagues reported that prohibitin 1 and prohibitin 2 were induced by metabolic stress caused by imbalances of mitochondrial and nuclear encoded proteins . An increase in improperly processed respiratory enzyme complexes would lead to oxidative stress due to leakage of electrons leading to the hypothesis of a chaperone function for prohibitins to stabilize mitochondrial proteins such as cytochrome C oxidase . This hypothesis was supported by findings showing that *in vitro* ageing is associated with increased oxidative stress in higher species .

Prohibitin 1 and 2 were found to assemble to hetero-oligomers in the inner mitochondrial membrane yielding high molecular weight complexes of about 1.2 MDa as shown for yeast , mammals and *C. elegans* . These high molecular weight prohibitin complexes are thought to play an important role in maintaining the integrity of mitochondrial membranes as prohibitin mutations in yeast are lethal when combined with disruption of the phosphatidylethanolamine (PE) biosynthetic pathway . A functional PE biosynthetic pathway is important as PE and phosphatidylcholine are the two major lipid constituents in mitochondrial membranes . Electron micrographs showing the high molecular weight complexes support the idea of a scaffolding function of prohibitin 1 and prohibitin 2 in mitochondria since the ring-like structures have a similar diameter to cristae junctions and pose a direct effect on the ultra-structure of the inner mitochondrial membrane . In tobacco, prohibitin depletion causes

abnormal mitochondria that lack inner cristae and contain fibre-like structures probably representing disintegrated inner mitochondrial membranes . The disrupted mitochondrial biogenesis or stimulated mitochondrial degeneration is accompanied by a reduced number and mass of mitochondria and excessive production of reactive oxygen species . Accumulation of aberrant mitochondria and defect in mitochondrial segregation from the mother to the daughter cell are frequent in cells possessing mutations in the prohibitin genes . A defect of the mitochondrial membrane potential and disruption of mitochondrial biogenesis have been found in *C. elegans* deletion mutants . RNA*i*-mediated elimination of prohibitin 2 was found to lead to mitochondrial fragmentation in HeLa cells .

Table -4: Proposed functions for prohibitins in the mitochondrion.

Implemented function as/in	Interaction partner	Reference
Chaperone	COX, respiratory chain proteins	
Maintenance of mitochondrial integrity	Prohibitin hetero-dimer complexes	
Programmed cell death	Prohibitin interacting proteins	
Regulation of *m*-AAA-protease activity	*m*-AAA-proteases	

Prohibitin's crucial role in mitochondrial integrity might entail their importance in programmed cell death, as suggested by recent studies in plants . Since prohibitins seem to maintain inner membrane proteins, modifications such as phosphorylation might change their functional properties or interactions with other proteins and finally lead to cell death. In this context, the high-molecular weight complexes of prohibitins formed with *m*-AAA protease is of particular interest. Recently, the PHB domain-containing protein QmcA was identified in *E. coli* as a factor involved in membrane protein quality control . As concluded from pulldown assays, QmcA interacts with FtsH to form oligomers just as prohibitin and *m*-AAA protease do.

1.4 Prohibitins in disease

1.4.1 Prohibitins in cancer

A potential role in tumour suppression for prohibitins was proposed when a growth arrest was found to occur in HeLa cells after microinjection of prohibitin transcripts . Later studies found that the ability to inhibit cell cycle activity is restricted to certain cell strains , and authenticated to the 3'-UTR of prohibitin mRNA where a polymorphism had been identified as a risk modifier in breast cancer in the presence of BRCA1 mutations .

Intriguingly, Sato and colleagues found that the prohibitin gene located on human chromosome 17q21 has mutations in exon 4 in four out of 23 sporadic human breast cancers . The four mutations are amino acid changes at positions 88 (Val to Ala) and 105 (Arg to His), as well as a frame shift leading to a truncation at position 53 . It was also suggested that a cell's sensitivity to the inhibition of cell cycle traverse is related to its prohibitin genotype and that the prohibitin protein expressed in immortalised populations is altered . Furthermore, a C to T change was observed in an intron which may interfere in the splicing process. Interestingly, almost all mutations reported in sporadic breast cancer lie within the Rb binding domain of prohibitin . Figure 1-10 shows the topology of the *PHB1* gene indicating the position of the 3'UTR and locations of mutations found within the gene.

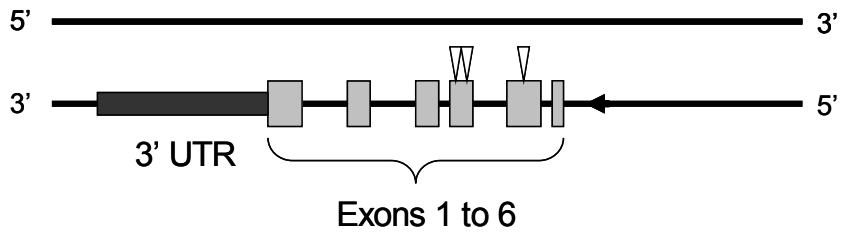

Figure -10: Topology of prohibitin 1 gene. *PHB1* is located on the minus strand of the DNA double helix (black lines). The gene's exons 1 to 6 are coloured in light grey, the 3'UTR is in dark grey. Light grey arrows indicate locations of mutations that have been identified in exons of the *PHB1* gene.

BAP32 has also been localised to the nuclei of breast cancer cells , and the cellular expression of the non-mutated protein is generally up-regulated in tumour cells as compared to normal cells . Notably, BAP32:BAP37 was observed to be secreted from

cultured colorectal tumour cells. While some cell surface localisation was observed, significant levels of both proteins were found in the blood serum . It is not entirely clear whether BAP32 and BAP37 are intentionally released into the blood or whether this is a direct consequence of the necrosis of tumour cells. In any case, these observations support a potential usability of prohibitins as tumour markers (see also).

The involvement of BAP32 in repression of estrogen-dependent transcription has brought the prohibitin proteins back into focus as potential targets for breast cancer therapy . Estrogen antagonists are the commonly used endocrine therapy in breast cancer, but are limited due to development of cellular resistance . The re-gained attention as potential cancer targets is also deserved by the finding that BAP32 is a novel target gene of vitamin D which stimulates down-regulation of proliferation through activation of its receptor. The growth-inhibitory effects of vitamin D in breast cancer cell lines were increased by over-expression of BAP32, and a vitamin D receptor binding site had been predicted in the promoter region of BAP32, but direct interactions on protein level remain to be clarified .
These findings encourage further investigations in this field, and might lead to the discovery of new anti-cancer drugs or therapies. A recent study elucidated the mechanisms of a synthetic drug that interferes with microtubule dynamics and thus exerts antimitotic actions . In this study, an E130K mutation in prohibitin 2 was identified to be responsible for occurrence of multidrug resistance in a *C. elegans* model which might also be responsible for resistance to other drugs binding to tubulin and camptothecin. In a quest for drug-regulated genes in osteosarcoma cells, the cytotoxic chemicals cis-platin, methotrexate and doxorubicin were found to significantly decrease the expression of prohibitin leading to apoptsis . The role of prohibitin in modulation of drug-induced apoptosis was further confirmed by the finding that its overexpression reduced chemosensitivity of the cells by about 50%.

Cancer cells are known to have increased reliance on anaerobic glycolysis compared with normal non-transformed cells due to their increased proliferation rate. An increased expression of prohibitin 1 may be part of a co-ordinated response in rapidly proliferating cells to allow for reduced oxidative stress in the presence of enhanced

anaerobic glycolysis. Vessal and colleagues found that prohibitin 1 inhibits pyrovate carboxylase in adipocytes and shifts their metabolism away from oxidative phosphorylation towards anaerobic glycolysis for faster ATP production. This might be the mechanism that links prohibitin expression levels and localisation to a high proliferation rate, and thus tumour development.

1.4.2 Mitochondrial disorders and apoptosis

Apoptosis is an important and controlled process to protect the organism from malfunctioning cells caused by different stimuli such as UV irradiation, reactive oxygen species, hormones and growth factors . Mitochondria play an important role in the signal transduction of apoptosis, since they release cytochrome C which triggers activation of caspases, apoptosis-inducing factor and Smac/Diablo in a process called mitochondrial permeability transition .

Very recently, BAP37 has been reported to interact with the anti-apoptotic protein Hax-1 , an integral membrane protein of the outer mitochondrial membrane that is exposed to the intermembrane space. Notably, the authors indicate that the interaction of BAP37 with Hax-1 is stonger than the BAP32-BAP37 interaction . The transforming growth factor-β (TGF-β) acts as a tumour suppressor via induction of apoptosis and inhibition of cell proliferation. Upon treatment with TGF-β, prohibitin translocates from the nucleus to the cell cytosol where it is strongly associated with the mitochondrial apoptosis-suppressor bcl-2 in human prostate cancer cells , and possibly repressing its activity. Table 1-5 summarises apoptotic processes where prohibitins were found to function as a regulator.

Table -5: Implementation for prohibitins in apoptosis.

apoptosis	inducer	regulation	References
drug-induced	cis-platin, methotrexate and doxorubicin	down-regulation of prohibitin expression	
stress-induced	calyculin A petunia-virus	hyper-phosphorylation of prohibitin 1 down-regulation of prohibitin 1	
hormon-induced	TGF-β	translocation of prohibitin from nucleus to cytosol	

Mitochondrial disorders can give rise to a broad spectrum of diseases such as myopathies, loss of hearing, optic neuropathy and the inflammatory disease ulcerative colitis . Disturbances in mitochondrial function might be common in aged population and probably contribute to age-related diseases, such as Type 2 Diabetes and Parkinson's disease .

Insulin resistance plays an important role in the pathogenesis of Type 2 Diabetes, and oxidative stress in ageing mitochondria leads to accumulation of superoxide. Superoxide then activates uncoupling protein 2 (UCP2) , an integral membrane protein that leaks protons across the inner membrane when activated. One might speculate that prohibitins could play a role in this process, especially when considering that prohibitin depletion leads to an excessive production of reactive oxygen species in plants . Prohibitin might act as a cellular defence against oxidant injury and thus be an interesting target for tissue injury and inflammatory diseases such as bowel and Crohn's disease . Several mitochondrial proteins have been found to be down-regulated in colon mucosa from patients with ulcerative colitis accompanied by pathological alterations of the mitochondrial ultra-structure . In a recent study, a significant reduction in prohibitin levels was found in the substantia nigra of patients with Parkinson's disease and related to deficiencies in complex I subunits of the respiratory chain .

1.4.3 Prohibitins and melanogenesis

Agents that promote pigmentation hold the potential to reduce UV-induced skin damage, carcinogenesis, and might also be the key in the treatment of hypopigmentation disorders such as certain forms of albinism. With a chemical genetics approach searching for pigment-enhancing chemicals, melanogenin has been found to enhance melanin production in melanocytes and to bind specifically to prohibitin . Melanogenin induced a dose-dependent up-regulation in both level and activity of tyrosinase, the rate-limiting enzyme in melanogenesis . Li and colleagues proposed a mechanism by which binding of melanogenin to prohibitin disrupts interactions between prohibitin and one or more transcriptional factors . The released transcription factors would be able to traffic to the nucleus, thus altering the level of tyrosinase gene transcription. Using RNA interference experiments, these authors also

observed an impaired melanin induction by melanogenin upon silencing of prohibitin expression .

1.4.4 Prohibitins as drug targets

Prohibitins have been found in the mitochondrion, the cytosol, the nucleus and extracellular where they interact with different targets such as nuclear receptors, cellular and mitochondrial proteins or organic molecules. If these interactions are impaired, serious diseases are introduced such as cancer, diabetes and intestinal inflammation. It is not surprising that prohibitins have been identified as drug target for many of those diseases . As prohibitins are implicated in basic functions of the cell, structural and functional information about these proteins is vital for understanding and curing prohibitin-related diseases. Table 1-6 summarises the different areas of disease in which prohibitins are thought to be involved.

Table -6: Potential mechanisms to target multiple prohibitin functions in various diseases.

	Potential mechanisms	Disease states
Mitochondrial prohibitin	Induction of apoptosis, stabilisation of mitochondrial function	Diabetes, obesity, metabolic syndrome, cancer, anti-ageing
Nuclear prohibitin	Disruption of interactions with Brg/Brm, E2F, Rb, p53, ER, AR	Breast and other cancers
Cell-surface prohibitin	Inhibition of inflammatory responses in the gut, vascular remodelling in adipose tissue, anti-angiogenesis	Intestinal infections, inflammatory bowel disease, obesity, diabetes, metabolic syndrome, cancer
Prohibitins 3'UTR	Inhibition of translation and RNA degradation	Breast and other cancers

This work aims at providing first insights into the atomic and molecular structure of prohibitins and characteristics of their possible interaction interfaces with target molecules. Understanding the mechanisms by which prohibitins are involved in gene regulation, mitochondrial biogenesis and tumour suppression is crucial in finding new ways in fighting common diseases such as cancer, adiposity or diabetes.

2 Results and Discussion

Prohibitin 1 and prohibitin 2 were overexpressed in *E. coli*, purified as inclusion bodies and refolded. The identity of the full-length protein's was verified by Edman degradation. Truncation mutants of both proteins were designed, overexpressed and refolded to improve solubility and stability of the protein complex. The N-terminally truncated prohibitin complex was analysed for its fold and stability using CD spectroscopy, and was subjected to gel filtration to investigate its oligomeric state. Homology models of the PHB domains of both proteins were generated and a hetero-dimer proposed. Additionally, possible interaction sites with melanogenin and other proteins were elucidated. Furthermore, the interaction between prohibitins and *m*-AAA-protease was investigated.

2.1 Production of recombinant full-length protein

Previously, prohibitin complexes were purified from yeast mitochondria with yields of around 1mg from a 20litre yeast culture . As over-expression of the protein complex leads to decreased cell growth, increasing the yield of protein product is rather difficult (T. Tatsuta, personal communication). To overcome this problem, the proteins were over-expressed in bacterial cells which resulted in production of inclusion bodies. In order to obtain properly folded native complex, protocols to purify and refold the proteins from inclusion bodies were established. Refolding of an isolated prohibitin protein was not successful in previous trials (A. Hofmann, personal communication). In order to improve solubility of the proteins, truncation mutants were generated lacking the predicted N-terminal hydrophobic tail and/or the predicted coil-coiled domain.

2.1.1 Expression and purification of protein from inclusion bodies

The construct His_6-BAP32:BAP37_pETDuet (kind gift from T. Tatsuta) was used for co-expressing His-tagged BAP32 and untagged BAP37 from mouse. BAP32 (276 amino acids, GeneID: 18673) has a molecular weight of 30kDa and a calculated pI of

5.22. BAP37 (GeneID: 12034) consists of 298 residues resulting in a molecular weight of 33kDa with a calculated pI of 10.22.

The complex was over-expressed in BL21(DE3) cells as stated in Materials and Methods, section 5.3.2. Processing 500ml of bacterial solution yielded up to 40mg of protein in inclusion bodies which could be purified to high purity. During this purification procedure both over-expressed proteins were enriched and separated from bacterial proteins (see figure 2-1).

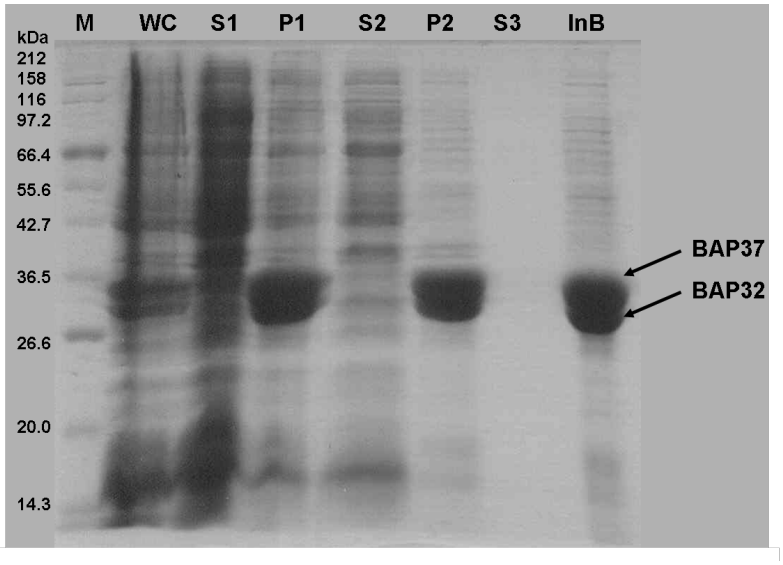

Figure -11: Protein expression in inclusion bodies. 10µl of supernatant fractions (S1, S2, S3), 5µl of pellet fractions (P1, P2) and 1µl of the inclusion body suspension (InB) were run on the gel for comparison.

Bacterial cells of *E.coli* strain BL21(DE3) were induced for only 2 hours with IPTG (final concentration 0.5µM) before harvesting. Cell pellets containing inclusion bodies were light brown in colour. Inclusion bodies were purified as stgated in section 5.3.4 and appeared as white solid particles. The proteins were unfolded and extracted from the inclusion bodies using urea buffer (8M urea, 50mM NaCl, 20mM Tris, pH 8.0).

Progress in protein purification was monitored by running samples of each purification step on a 12% SDS-PAGE (figure 2-1). Over-expressed His_6-BAP32 and BAP37 are clearly visible in the whole cell extract (WC) as distinct bands at 30kDa (BAP32) and 33kDa (BAP37). After cell lysis and high speed centrifugation (see section 5.3.3), His_6-BAP32 and BAP37 were exclusively found in the pellet fraction (P1). No protein was found in the soluble fraction (S1) or in the supernatants of further washing steps

(S2, S3, see section 5.3.3). Comparing pellet fractions P1, P2 and InB, an increase in purity caused by repeated washing and centrifugation steps can be clearly seen. The inclusion bodies (InB) were free from most contaminating proteins. Over-expressed His_6-BAP32 and BAP37 are the major proteins in the cell after induction indicating a very good level of over-expression of the target proteins.

2.1.2 Co-refolding of full-length BAP32 and BAP37

Pioneers in the prohibitin field such as Nijtmans, Coates and Berger found that both proteins co-localise in the cell, and are most stable in a complex with each other interacting via their natural interface. Therefore, refolding both proteins in the presence of each other was thought to lead to immediate complex formation which would aid the refolding process and help stabilize the proteins. Therefore, a simultaneous expression of both proteins followed by a co-refolding procedure was the approach chosen to produce the refolded proteins into a stable complex.

In general, refolding is a difficult, time-consuming and unpredictable procedure. Nevertheless, there are several suggested procedures, buffer compositions and additives that might lead to successful refolding . Refolding of solubilised inclusion body proteins is usually performed by rapid dilution or dialysis. Precipitation could result from rapid refolding under conditions that are very similar to the native solvent. In this case, gradual removal of the denaturant by dialysis or a stepwise dilution of the protein may lead to successful refolding. When removing the denaturant by dialysis, the protein is exposed to intermediate denaturant concentrations for a period of time. This could be beneficial for correct folding, as the protein can enter an intermediate folded state which might be important for finding the correct folding pathway. On the other hand, proteins in an intermediate folding state can also be prone to aggregation. Thus, the optimum procedure has to be determined on a case-by-case basis, because the preference for either refolding strategy cannot be predicted from the molecular properties of the protein.

In *in vitro* folding, misfolding, as well as aggregation, competes with the correct folding pathway . Aggregation may originate both from non-specific (hydrophobic) interactions of predominantly unfolded polypeptide chains, as well as from incorrect interactions of partially structured folding intermediates. When increasing the concentration of unfolded polypeptide chains, an increase in the rate of aggregated

protein is observed. Thus, aggregation predominates in renaturation experiments when a threshold concentration of denatured protein is exceeded . Therefore, renaturation must often be performed at an extremely high dilution .

Disulfide bond formation is always critical during refolding as the number of possible disulfide combinations increases dramatically with the number of cysteine residues present in the polypeptide chain. Therefore, substances functioning as "oxido-shuffling" reagents should be included in the refolding buffer if there are cysteine residues present in the protein to be folded. Reduced and oxidized glutathione (GSH, GSSG) are commonly used in this context, but other low molecular weight thiols such as cysteine/ cystine, cysteamine/ cystamine, or di-hydroxyethyl disulfide/ β-mercaptoethanol can be used as well, and may be superior for disulfide bond formation depending on the respective insoluble protein .

Considering literature about protein refolding, physical parameters such as pH, ionic strength, or temperature seem to have a tremendous effect on the efficiency of *in vitro* folding processes. Furthermore, buffer components or prosthetic groups may be essential for correct *in vitro* folding. For instance, addition of Tris buffer at a concentration of at least 0.4 M improved the refolding efficiency of various test proteins from *E. coli* inclusion bodies . L-Arginine functions as a very efficient low molecular weight "folding enhancer", and is known to have a positive effect on protein stability. Other additives like guanidine chloride, lauryl-maltoside, Chaps, mixed micelles consisting of Triton X-100 and phospholipids, glycerol, metal ions, and ligands can also enhance the refolding process . Nonionic, as well as ionic and zwitterionic detergents, have been found to have a favourable effect on renaturation, as very efficient protein folding at relatively high concentrations has been achieved using mixtures composed of detergents (e.g., Triton X-100 or lauryl-maltoside) and phospholipids . These mixed micelles contain both polar and nonpolar moieties that can interact with various sites of folding intermediates, thereby preventing misfolding or aggregation.

The following considerations for refolding the proteins were taken into account when designing a refolding procedure: 1) Both proteins possess a predicted membrane anchor, the presence of glycerol and detergent in the refolding buffer might be important to shield and stabilise the hydrophobic region. 2) There is only one cysteine

present in BAP32, addition of an "oxido-shuffling" reagent would not be necessary for correct refolding. Nevertheless, adding a reducing reagent might still be useful to prevent aggregation via formation of disulfide bonds between BAP32 monomers. 3) The prospective refolding buffer will need a suitable buffering agent at a relatively high concentration, and a neutral pH is recommended. 4) To enhance the refolding process, a certain amount of L-arginine (or other amino acid) should be included in the refolding buffer. 5) It is not known whether the prohibitin complex needs a ligand to help maintain its stability.

A "stepwise refolding" approach was preferred over the "fast dilution method" in order to keep the sample volume small. Furthermore, the proteins were purified after refolding by immobilised nickel affinity chromatography which would also indicate successful refolding. One of the proteins (BAP32) was constructed with an N-terminal His_6-tag, and can be purified by nickel affinity chromatography. If His_6-tagged BAP32 and the untagged BAP37 are successfully refolded in a complex, BAP37 will bind to BAP32 via its natural interface. The complex should bind to the nickel resin via His_6-tagged BAP32, and both proteins could be eluted from the column as a complex. The procedure is indicated in figure 2-2. First, the proteins are co-expressed in *E.coli* cells. After extracting the proteins from inclusion bodies using urea (A), both proteins are in their unfolded state. They undergo a refolding procedure (B), and are applied to a nickel affinity column for purification and to determine successful refolding (C).

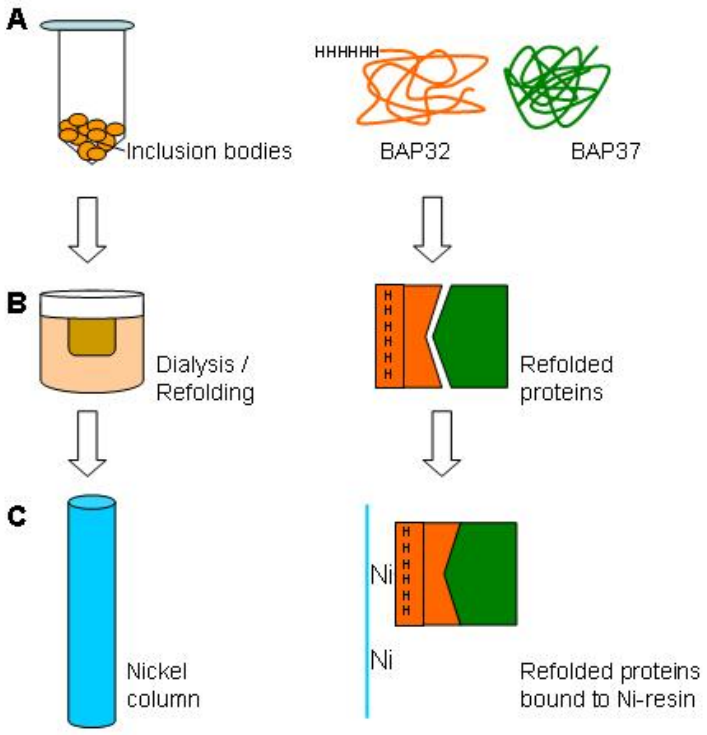

Figure -12: Strategy to refold the His_6-BAP32:BAP37 complex from inclusion bodies. After production in inclusion bodies (A), the unfolded proteins are subjected to refolding by dialysis (B) and purified using nickel affinity chromatography (C).

The unfolded proteins were subjected to several refolding trials using various refolding buffer compositions, including 1mM DTT, 1% Triton X-100 and 25mM dodecyl maltoside. The most successful refolding procedure was performed using a buffer that contained 0.5M Tris, 20% glycerol, 1% Nonidet-P40, 150mM KCl, 1mM DTT, 0.113M L-arginine, 0.275M L-serine, 11.86mM L-histidine at pH 8.0 (see section 5.3.4). Refolding was carried out twice by 1:10 dialysis of the unfolded proteins against the refolding buffer at 4ºC for at least 8 hours per step. The sample was then dialysed against a buffer containing only 150mM KCl, 100mM Tris, 10% glycerol, 1% Nonidet-P40 at pH 8.0 to reduce the amount of glycerol, DTT and amino acids in the protein solution. After the last refolding step, the protein was further purified using nickel affinity chromatography, where the protein complex could be eluted with 500mM imidazole (see figure 2-3).

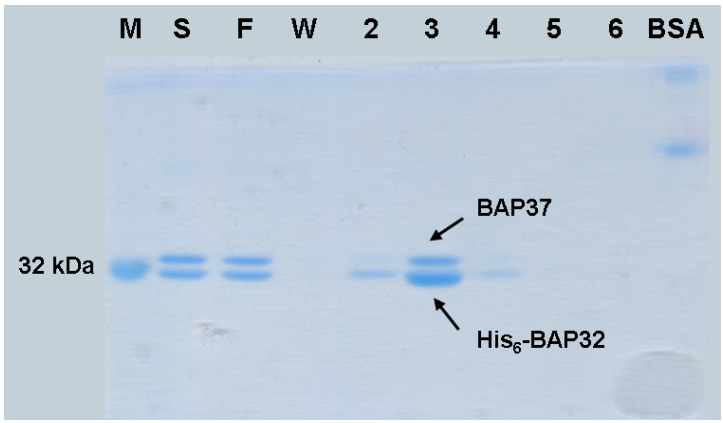

Figure -13: SDS-PAGE of nickel affinity chromatography of refolded His_6-BAP32:BAP37. The gel shows the marker (M) I lane 1, the refolding mixture (S) in lane 2, flow through (F) and wash (W) in lanes 3 and 4, and elution fractions 2 to 6 in lanes 5–9. BSA, applied in lane 10, was used as a calibrator to determinate the amounts of protein in the respective fractions.

Figure 2-3 shows all fractions of the purification step. The second lane (S) represents the refolded protein mixture that has been loaded onto the column. It contains both proteins in equal amounts as both proteins have been overexpressed with the same ratio. A significant amount of protein, but not all, can be found in the flow through (F), but nearly none in the washing step (W), which indicates binding to the column. The presence of some protein in the flow through is most likely due to improperly folded protein in the case of BAP37 and inaccessible His_6-tag in the case of BAP32. Inaccessibility of the His_6-tag might be caused by improper refolding. The bound proteins eluted with 0.5M imidazole in fractions 2-4 (lanes 5-7). Notably, the protein band representing BAP32 is stronger than the band representing BAP37 indicating an excess of BAP32 in the elution fractions. BAP32 possesses a His_6-tag, and is therefore able to bind to the nickel column both in its refolded as well as unfolded state. Not all of BAP32 would be refolded correctly, and not every molecule was able to form a complex with BAP37. One can expect a mixture of monomers (His_6-BAP32), probably unfolded, and refolded dimers (His_6-BAP32:BAP37) in the elution fractions. A BSA standard of known concentration (0.075mg/ml) was utilized to determine the concentration of total protein in each fraction as well as the amounts of each protein by densitometrical analysis using the software ImageJ . Using the respective volumes, the amount of protein present in each fraction could be determined (see table 2-1).

Table -7: Densitometric analysis of refolding yield of full-length His_6-BAP32:BAP37.

	Intensity of band		Protein concentration [mg/ml]			Distribution [%]		Protein yield [mg]
	His_6-BAP32	BAP37	His_6-BAP32	BAP37	complex	BAP37	His_6-BAP32	
S	3933	3872	0.092	0.090	0.182	49.61	50.39	29.06
F	3966	3460	0.092	0.081	0.173	46.59	53.41	25.92
W	211	151	0.005	0.004	0.008	41.71	58.29	0.84
fr. 2	2114	690	0.049	0.016	0.065	24.61	75.39	0.44
fr. 3	7787	4155	0.181	0.097	0.278	34.79	65.21	1.86
fr. 4	1479	603	0.034	0.014	0.048	28.96	71.04	0.33
								2.63 ≈ 9%
BSA	3223		0.075mg/ml					

The amounts of His_6-tagged BAP32 and untagged BAP37 are comparable at the beginning of the refolding experiment (see fraction S). A large amount of protein, both His_6-BAP32 and BAP37, did not bind to the column and was found in the flow through (F). In all elution fractions (fractions 2 to 4), His_6-BAP32 represents 65-75% of the total protein confirming observations made from the gel. 2.63mg protein could be eluted from the nickel column in this experiment which would give an approximate yield of refolding of 9% if all protein was refolded in a complex.

The sample still contains glycerol, a disadvantage when trying to concentrate the protein complex. Different methods were tried to concentrate the proteins, including Vivaspin concentration devices (VivaScience), Centricon concentration devices (Millipore) and removal of water using a dialysis bag placed in PEG, molecular weight 20000Da. Neither method led to high protein concentrations that could be used in crystallization trials. Moreover, glycerol and detergents also interfered with data aquisition from spectroscopic methods such as UV-spectroscopy and CD which makes any further analysis of the samples more difficult. The detergents Triton X-100, dodecyl maltoside and Nonidet-P40 were tested in order to improve the refolding yield and allow the solution to be more suitable for concentrating. However, no considerable difference in refolding yield or solubility could be observed with the different detergents. Furthermore, the usage of any detergent such as β-octyl glycoside in a refolding set up is very expensive and did not justify the minor improvement in refolding yield or solubility seen. Instead, truncation of the N-termini of both proteins has a better chance in increasing the refolding yield and solubility.

2.1.3 Identification of the full-length proteins by Edman degradation

To identify the proteins seen on the SDS-PAGE (see figure 2-3), Edman degradation was performed by the Mass Spectrometry facility using protein samples blotted on PVDF membrane by Western blotting. After a brief staining with Coomassie, each protein bands were cut out and used for Edman sequencing. The degradation experiment confirmed the identity of both proteins as His_6-BAP32 and BAP37. The first 17 amino acids of BAP32 and the first 10 residues of BAP37 could be clearly identified. In both cases, the starting methionine was processed.

Table -8: Results from Edman degradation of His_6-BAP32 and BAP37. Shown are the first 20 residues for each protein, and residues identified by Edman degradation are in bold.

Sequence BAP32	M **G S S H H H H H H S Q D P A A A** K V F
Sequence BAP37	M **A D L A A Q N** L K **D** L A G R L P A G P

2.1.4 Conclusions: Protein expression and characterisation

Full-length His_6-tagged BAP32 and BAP37 were over-expressed in BL21(DE3) cells resulting in inclusion bodies with a protein amount of up to 80mg per litre of bacterial culture. Inclusion bodies were purified to high purity using a protocol developed by C. Rückert (Institut für Immungenetik, Universitätsklinikum Charité, Humboldt-Universität zu Berlin, Germany). A novel approach was taken to refold BAP32 and BAP37 from inclusion bodies where the proteins were jointly subjected to the refolding procedure. As a result, the proteins could be eluted from a nickel column indicating a refolding of both proteins and subsequent complex formation. The proteins could be refolded with a refolding yield of up to 9%.

Both proteins, His_6-BAP32 and BAP37, were identified by Edman degradation using the respective bands from an SDS-PAGE which was first blotted onto a PVDF membrane.

Despite success in producing and refolding the proteins, difficulties were experienced in concentrating the sample due to the considerable amount of glycerol in the protein solution. Residual amounts of detergent hampered further analysis of the protein complex by spectroscopic methods such as UV and CD. In order to improve the

solubility of both proteins in aqueous solution, truncation mutants were generated lacking the hydrophobic N-terminal helix.

2.2 Generation and production of prohibitin truncation mutants

2.2.1 Secondary structure predictions

Secondary structure predictions of BAP32 and BAP37 were done using the PSIPRED server and revealed an overall similar secondary structure reflecting their high sequence similarity (see figure 2-4).

BAP32 showed an N-terminal helix encompassing the first 24 amino acids which was in good agreement with findings by other groups . This domain of BAP32 was previously predicted using the GCG software , and encompassed the first 20 amino acids. In both predictions, the next few amino acids downstream of the protein chain would form a β-sheet consisting of mostly hydrophobic amino acids. BAP37 showed a 40 amino acid spanning hydrophobic helix at its N-terminus thus allowing the protein to span a membrane.

Secondary structure predictions of both proteins revealed a PHB domain consisting of 6 β-sheets followed by 3 α-helices and one β-sheet. Extends of the secondary structure elements coincide nicely between both proteins (see figure 2-4).

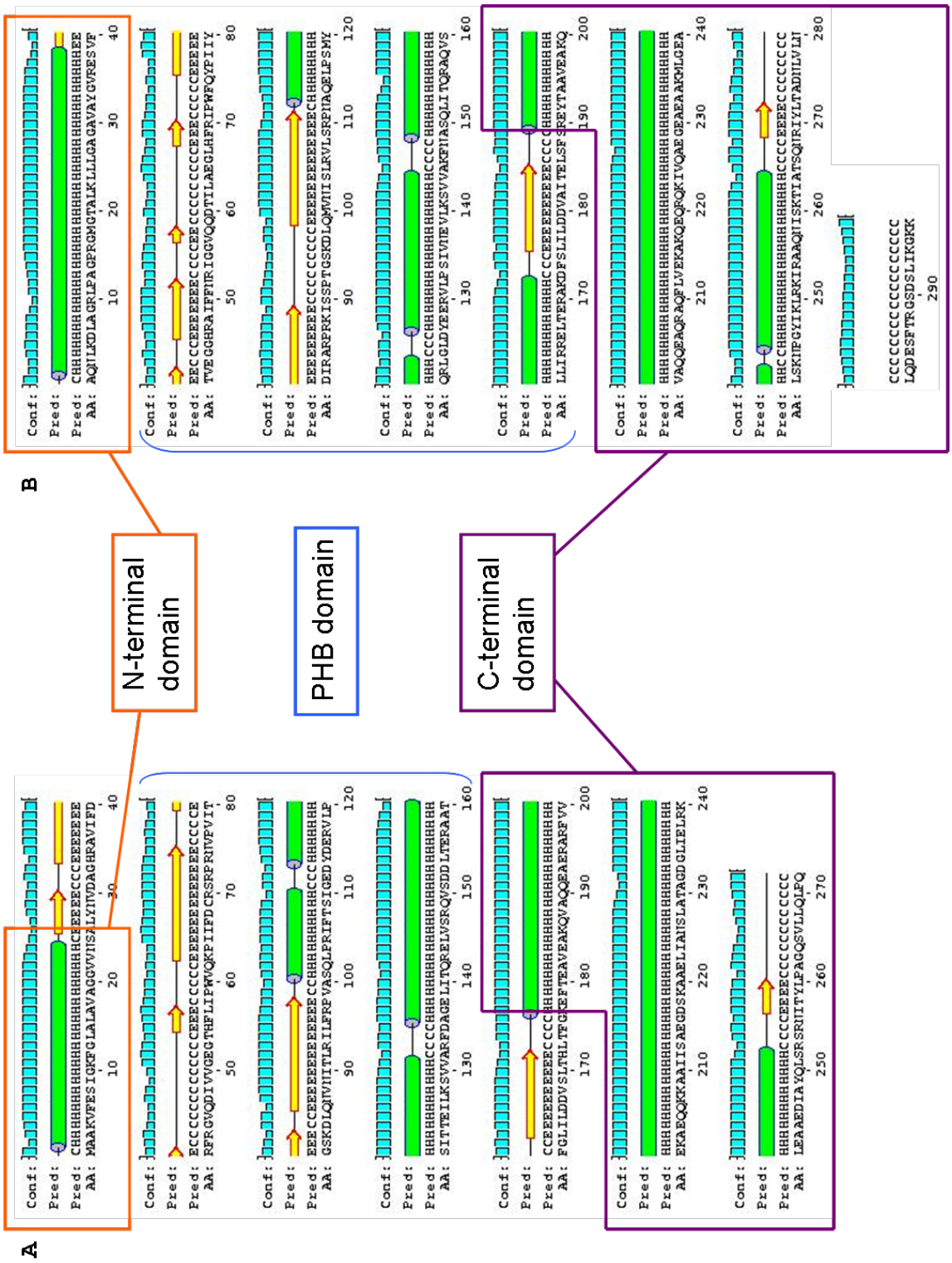
B
A
N-terminal domain
PHB domain
C-terminal domain

Previous page - Figure -14: Secondary structure prediction of BAP32 and BAP37. The N-terminal domain (orange), the PHB domain (blue) and the C-terminal domain (purple) are indicated. The predicted secondary structure (Pred) of the target amino acid sequence (AA) is displayed both as a letter code and in symbols. “H” or tubes indicate a helix, arrows or “E” symbolise strands, and coiled structures are indicated as black lines or “C”. The confidence of prediction for each amino acid is displayed as blue bars at the top.

The C-terminal domains of both proteins are large helices thought to be coiled-coil regions. In BAP37, this region spans residues 175 to 252 and is followed by a predicted β-sheet. The C-terminal region of BAP37 encompasses residues 190 to 264 and is also followed by a β-sheet. In contrast to BAP32, the C-terminal coiled-coil helix in BAP37 is predicted to be separated into two fragments around residues 243/244. As the predictions for those residues were made with low confidence, the helix might instead proceed in those two residues. On the other hand, there is a prediction, although with low confidence, for an α-helix around residue 231 of BAP 32. In this region, the predicted helix might also be separated into two fragments, similar to BAP37. This controversy might be solved by analysing structural data of this region.

In order to increase the solubility of each protein, the first 30 N-terminal amino acids of BAP32 and the first 40 amino acids of BAP37 were truncated. The predicted C-terminal coiled coil regions of both proteins are thought to allow the proteins to stick to artificial membranes e.g. in concentration devices. Therefore, constructs were generated that lack the C-terminal coiled-coil domain as well. In BAP32, the C-terminus was truncated at residue 178 whereas the C-terminus of BAP37 was truncated at residue 192.

2.2.2 Cloning of prohibitin truncation mutants

Two truncation variants were designed for each BAP32 and BAP37, one lacking the hydrophobic N-terminus, the other lacking both the hydrophobic N-terminus and the coiled-coil region at the C-terminus. Although constructs were generated in accordance with findings from secondary structure predictions, a few residues were included on either side of the respective domains to ensure proper formation of secondary structure elements. In figure 2-5, the constructs that have been produced are listed on the left side; the dimensions of the truncation mutants generated are shown as pictograms on the right.

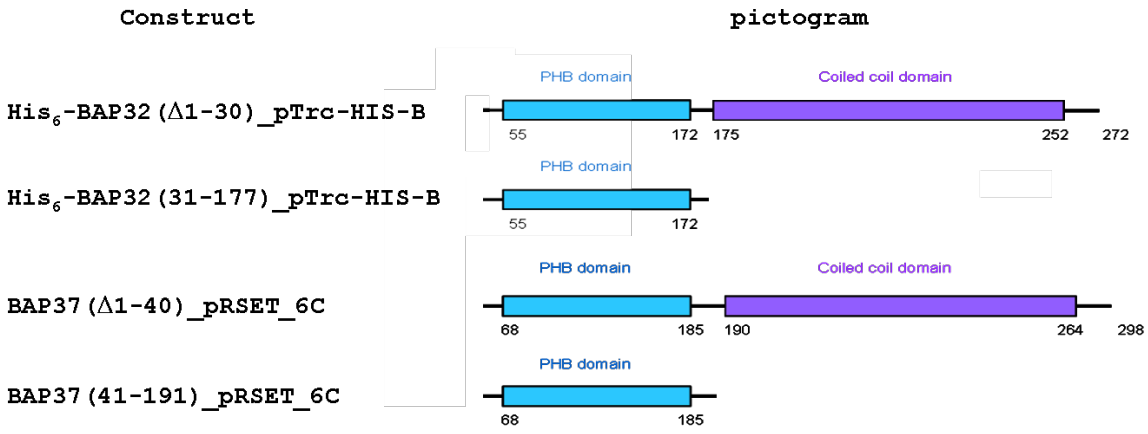

Figure -15: Truncation mutants created for BAP32 and BAP37, one lacking the N-terminus; the other lacking both the N- and C-terminus. PHB domains are shown in blue, coiled coil regions are in purple. Numbers indicate amino acid residues representing the edges of the domains.

All BAP32 constructs contain an N-terminal His_6-tag which is necessary for the refolding and purification procedure developed for the full-length protein complex (see section 5.3.4). Truncation mutants were generated using the construct received from T. Tatsuta (His_6-BAP32:BAP37_pETDuet) and according to procedures described in section 5.2.2. Each construct was verified by DNA sequencing.

2.2.3 Expression of truncation mutants

An expression trial with 250ml bacterial culture was performed inducing the expression plasmid His_6-BAP32(Δ1-30)_pTrcHis_B for 2.5 hours, 6 hours and overnight (see section 5.3.5). After harvest and cell lysis, a centrifugation step was introduced to separate the supernatant with soluble proteins from the cell pellet. Pellets from 2.5 hours and over-night induction were then treated with 8M urea to extract insoluble proteins. The extracts were analysed on SDS-PAGE where the truncated His_6-BAP32 (27kDa) could be found in the pellet of the lysed cells (see figure 2-6, lanes 2 and 3). This indicates protein expression is in inclusion bodies.

In order to confirm the presence and identity of the protein as His_6-BAP32(Δ1-30), an immobilised nickel affinity chromatography (IMAC) batch experiment (see section 5.4.4.)

was performed using the remaining urea-extract of the cell pellet from 6 hour induction (P_6). The strong band visible near the 26.5kDa marker band in the pellets $P_{2.5}$ and $P_{o/n}$, lanes 2 and 3, respectively, is also present in the first supernatant (F) and third supernatant (E) of the IMAC batch experiment carried out using pellet P_6. No protein was found in the second supernatant (W), lane 5.

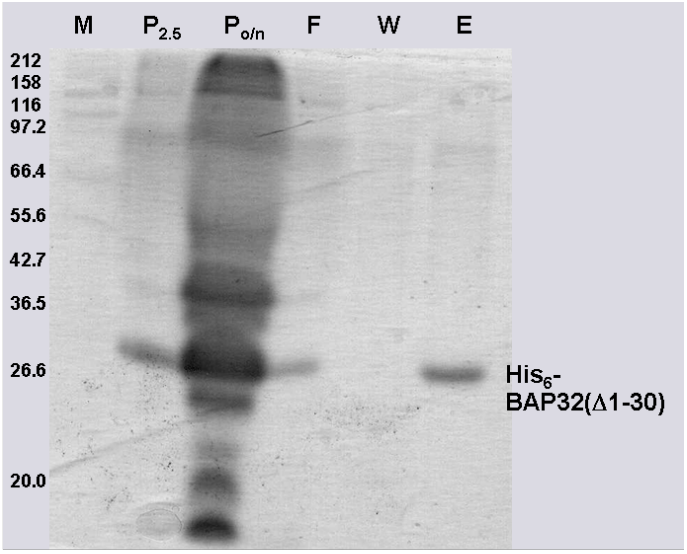

Figure -16: Expression and batch purification of His_6-BAP32(Δ1-30). The protein is visible as a thick band near the 26.5kDa marker in the pellet after 2.5 hours induction ($P_{2.5}$) and over-night ($P_{o/n}$) inductions. Fractions from IMAC batch experiment (first supernatant (F), second supernatant (W) and third supernatant (E)) are shown in lanes 4-6.

Furthermore, specific binding of this protein to the nickel resin indicates the presence of a His_6-tag, therefore confirming that the expressed protein was His_6-BAP32(Δ1-30). This result indicates that the N-terminally truncated BAP32 is produced as an insoluble protein, probably present in inclusion bodies. Truncation of the hydrophobic N-terminus did not result in a folded, soluble protein. In subsequent expression experiments carried out as stated in section 5.3.2., the other truncation mutants were also found to be expressed in inclusion bodies. The inclusion bodies were purified using the protocol stated in section 5.3.3. Although the amount of protein gained from one expression experiment varied with

the construct that was expressed, all purifications show an increase of purity and protein amount in the inclusion body fractions (see figure 2-7).

None of the truncation mutants were produced as soluble protein despite altering the expression conditions (IPTG concentration and induction temperature). Therefore, truncating the N-termini did not result in soluble protein which would be found in the cell cytosol.

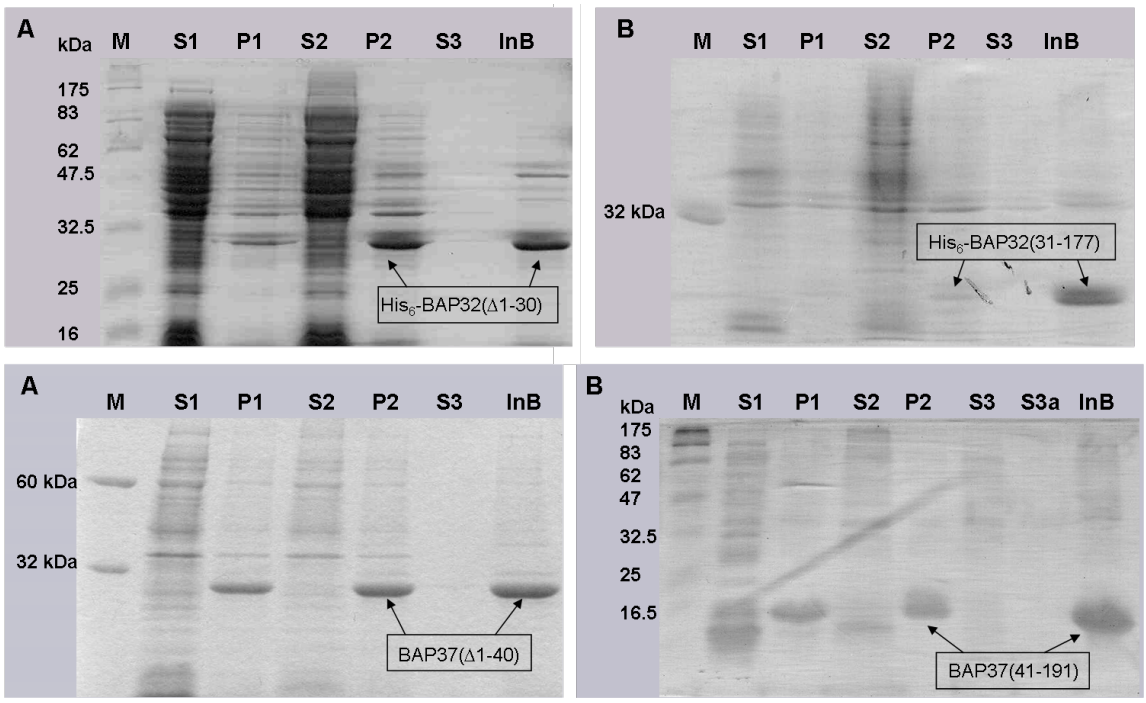

Figure -17: Expression of prohibitin truncation mutants. Increase of the purity of inclusion bodies of BAP32 truncation mutants (top panel) and BAP37 truncation mutants (bottom panel) can be seen on SDS-PAGE. For comparison, 10µl of all supernatants (S1, S2, S3), 5µl of pellet fractions (P1, P2) and 1µl of inclusion bodies (InB) were loaded on the gel.

There are various possible reasons why the proteins are still not produced as soluble proteins: a) all truncation mutants were produced separately, thus, no complex formation and subsequent stabilization of the proteins was possible during expression. b) The bacterial cell might not be able to properly fold these mammalian proteins due to lack of chaperones or other helper proteins. Therefore, the proteins still need to be refolded in a co-refolding approach similar to the procedure used for the full-length proteins.

Furthermore, all truncation mutants were subjected to refolding trials combining a BAP32-truncation mutant with different BAP37-truncation mutants in order to find a combination of truncation mutants that leads to a high refolding yield.

2.2.4 Co-refolding of truncation mutants with glycerol and detergent

As truncating the N-termini did not result in soluble proteins, a co-refolding approach similar to that used for the full-length proteins was the next step. BAP32 and BAP37 truncation mutants were co-refolded in different combinations (see table 2-3), trying to find a combination of two truncation mutants that produced water-soluble and stable prohibitin complex. Truncation mutants were refolded using the protocol developed for full-length His_6-BAP32:BAP37 (see section 5.3.4), and success of co-refolding was determined by nickel IMAC (see section 5.4.1.). The refolding yield was analysed densitometrically using the programme ImageJ .

Co-refolding of His_6-BAP32(Δ1-30) (27kDa) and BAP37(41-191) (16kDa) led to a decrease in sample volume in the dialysis bag to about 60% and heavy precipitation in the third dialysis step. The precipitation was centrifuged at 20000rpm in the Beckman centrifuge J2-21 for 30 minutes at 4ºC, and the remaining supernatant was applied to a nickel column. The SDS-PAGE showed only one band in the elution fractions and in accordance with a marker, this band could easily be assigned to His_6-BAP32(Δ1-30). The initial refolding mixture contained both proteins, but since His_6-BAP32(Δ1-30) could be eluted from the column this indicates that it was truncated BAP37 that had precipitated. Subsequent dialysis of the pooled elution fractions using a buffer containing 20mM tris, pH 7.5 and 100mM KCl led to precipitation of His_6-BAP32(Δ1-30) suggesting that the protein was kept in solution by the high amount of imidazole used for elution, and that the protein might not have refolded in the first place. Co-refolding of His_6-BAP32(Δ1-30) and BAP37(41-191) was not successful in producing soluble prohibitin complex.

After the third dialysis step in co-refolding His_6-BAP32(Δ1-177) with BAP37(Δ1-40), the sample volume decreased by about 30% and heavy precipitation was visible. The sample was centrifuged at 20000rpm in the Beckman centrifuge J2-21 for 30 minutes at 4ºC. The

remaining supernatant was applied to a nickel column, and the fractions from the nickel column and the precipitation were analysed on SDS-PAGE. Both proteins were found in the precipitate indicating an unsuccessful refolding procedure.

Only very little precipitation was observed during the refolding of His_6-BAP32(Δ1-30) and BAP37(Δ1-40), and the volume of the protein sample in the dialysis bag decreased slightly. Analysis of the fractions from nickel IMAC on SDS-PAGE revealed a double band in the elution fractions representing His_6-BAP32(Δ1-30) with 27kDa and BAP37(Δ1-40) with 29kDa. Some protein was found in the flow through, but none was found in the wash. Densitometric analysis using the BSA standard that was run with the samples estimates the protein found in the elution fractions to 54% of the initial protein amount. Elution fractions were pooled and subjected to a 1:20 buffer dialysis step twice with 20mM tris, pH 7.5 and 100mM KCl order to remove glycerol and Nonidet P-40. The pooled fractions did not precipitate during dialysis and could be concentrated using Vivaspin concentration devices (Vivascience) where a large amount precipitated. UV-spectrum and fluorescence spectrum taken from the sample were not interpretable. The sample was thus not used for further analysis, as traces of Nonidet P-40 and glycerol seem to affect any spectroscopic method. Refolding without using either glycerol or Nonidet P-40 might result in a complex suitable for spectroscopic analysis.

Results from all co-refolding trials carried out with full-length BAP32 and BAP37 and their truncation mutants are summarised in table 2-3. The pictograms show the topology of the proteins subjected to co-refolding trials including the N-terminal hydrophobic helix (orange), the PHB domain (blue) and the C-terminal coiled-coil region (purple). Furthermore, the refolding yield and maximum concentration of the purified complex are stated.

Table -9: Summary of results from co-refolding trials carried out with full-length His_6-BAP32 and BAP37 and their truncation mutants.

BAP37 \ BAP32	Δ N-terminus 	PHB domain 	Full length 
Δ N-terminus 	up to 54% refolded 0.1mg/ml	Both proteins precipitated	
PHB domain 	BAP37(41-191) precipitated completely, small fraction of His_6-Δ BAP32 could be eluted from column		
Full length 			2-9% refolding 0.71mg/ml 0.12mg/ml

From table 2-3, one combination was not tried: PHB domains only of both BAP32 and BAP37. This is because whenever a truncation mutant consisting of the PHB domain only was subjected to the refolding trial, the experiment resulted in precipitation of the protein with only the PHB domain, at the very least. Therefore, co-refolding of BAP32 and BAP37 PHB domain-truncation mutants would inevitably lead to precipitation of both components. Furthermore, co-refolding of His_6-BAP32(Δ1-30) and BAP37(Δ1-40) has already led to a successful refolding of both proteins.

2.2.5 Co-refolding of His_6-BAP32(Δ1-30) and BAP37(Δ1-40) without glycerol and detergents

All refolding trials with truncation mutants so far were carried out in the presence of glycerol and Nonidet P-40 which interferes with sample concentration and analysis by spectroscopic methods. His_6-BAP32(Δ1-30) and BAP37(Δ1-40) were therefore subjected

to a refolding trial lacking glycerol and detergents in refolding buffers. During refolding, slight precipitation was visible and was separated by centrifugation. The remaining supernatant was applied to the nickel column, and the protein eluted as a double band near the 32kDa marker representing both His_6-BAP32(Δ1-30) and BAP37(Δ1-40) (see figure 2-8).

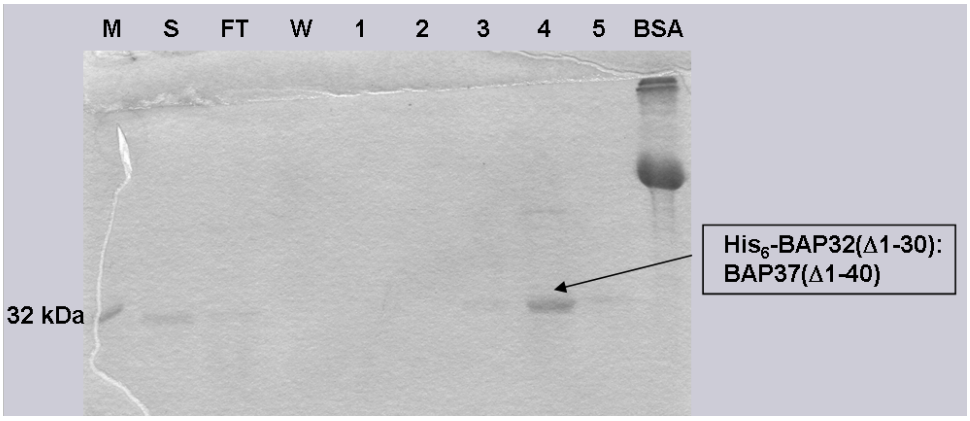

Figure -18: Co-refolding of His_6-BAP32(Δ1-30) and BAP37(Δ1-40) without glycerol or Nonidet in the refolding buffers. On this SDS-PAGE, protein bands can be seen in lanes for the loaded sample (S), flow through (F) and elution fractions 1 to 5. No protein band is present in the wash (W). 50μg BSA was run in lane 10 as a mass calibration standard for densitometric analysis.

Protein found in the flow through (F) indicates impaired binding of His_6-BAP32(Δ1-30) to the resin, possibly caused by misfolding or aggregation where the His_6-tagged N-terminus is not accessible. Densitometric analysis of the protein bands using the protein standard that was run with the samples revealed that 33% of the protein could be recovered from the column. The elution fractions 3 to 6 were pooled and concentrated by centrifugation at 4ºC and 4000g using Centricon devices with a molecular weight cut off of 10kDa (Millipore). The final concentration was determined via UV-spectroscopy to be 0.54mg/ml.

2.2.6 Protein engineering

The aim of this protein engineering approach was to replace the hydrophobic N-terminus of BAP32 with a self-folding water soluble helix instead of introducing a truncation. It is

still not known how secondary structures form, what triggers them to start at a certain amino acid residue or at which residue it is likely that a secondary structure element progresses. Truncation of the N-terminus of a protein might cause problems in folding the C-terminal protein since a crucial structural element will be missing.

In 1987, Shoemaker and colleagues investigated the secondary structure of the C-peptide helix of RNase A . This peptide, residues 3-13 in RNase A, is helical and only a few of its residues are in contact with the rest of the protein. The unusually stable C-peptide helix of RNase A was proposed to be an autonomous folding unit and would be stabilised by specific intra-helical side-chain interactions which may also provide start and stop signals for localising the helix . Marqusee and Baldwin investigated helix formation on artificial peptides of 17 amino acids in length, and found that certain criteria favour stability of a helix such as a (*i*+4)-spacing between charged groups within the helix rather than a (*i*+3)-spacing. Moreover, these artificial helices showed a helix content of up to 80% in 0.01M NaCl and at 1ºC which was temperature- and pH-dependent . Replacing the hydrophobic N-terminal helix by a soluble helix could increase the solubility and stability of the N-terminally truncated prohibitin complex to a great extent. As this N-terminal artificial helix would also self-induce its helix formation, secondary structure formation in the C-terminal protein sequence might be enhanced resulting in an increase of refolding yield.

2.2.6.1 Cloning and expression of His_6-helix-BAP32(Δ1-24)

The 16 amino acid long artificial helix AKAAAAKAAAAKAAAA was introduced at the N-terminus of His_6-BAP32(Δ1-24) as described in section 5.2.3.

Expression trials were undertaken to find optimal expression conditions for His_6-helix-BAP32(Δ1-24) in BL21(DE3) (see section 5.3.5.). All protein was found in the insoluble fraction. The best expression yield was obtained from induction at 37ºC, and there was little effect when the IPTG concentration was varied.

His_6-helix-BAP32(Δ1-24) was expressed (see section 5.3.2), the inclusion bodies purified (see section 5.3.3), and the purification process traced on SDS-PAGE (see figure 2-9). His_6-helix-BAP32(Δ1-24) has a molecular weight of 30kDa, and is detectable in the pellet

fractions P1 and P2 and in the inclusion body fraction InB. In the InB fraction, the protein appears as a strong band just below the 32.5kDa-marker.

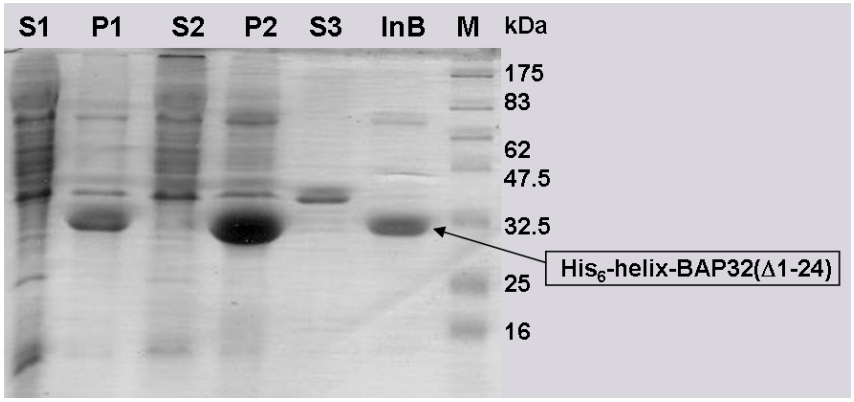

Figure -19: Protein production of His_6-helix-BAP32(Δ1-24) in inclusion bodies. The protein was purified in inclusion bodies from pellet fractions (P) of the washing steps, and appeared as a strong band near the 32.5kDa marker. No protein was found in the supernatants (S). For comparison, 10μl of the supernatant fractions, 5μl of pellets and 1μl of inclusion bodies were loaded onto the gel.

The protein could be purified to a high degree as there are only a few weak bands of contaminating proteins visible.

The artificial helix did not improve the solubility of BAP32 but this might also be due to the absence of its homologue BAP37 which is known to stabilize the protein. A co-refolding of His_6-helix-BAP32(Δ1-24) and BAP37(Δ1-40) using the protocol established for His_6-BAP32(Δ1-30):BAP37(Δ1-40) might produce a greater yield of refolded protein due to an increased solubility of the BAP32 truncation mutant.

2.2.6.2 Co-refolding of His_6-helix-BAP32(Δ1-24) and BAP37(Δ1-40)

During refolding of His_6-helix-BAP32(Δ1-24) and BAP37(Δ1-40), the sample volume decreased and precipitation was visible which was cenrifuged for 30 minutes and 4000rpm at 4ºC. Nickel affinity chromatography was applied as described in section 5.4.1., and an SDS-PAGE was run to determine successful refolding (see figure 2-10).

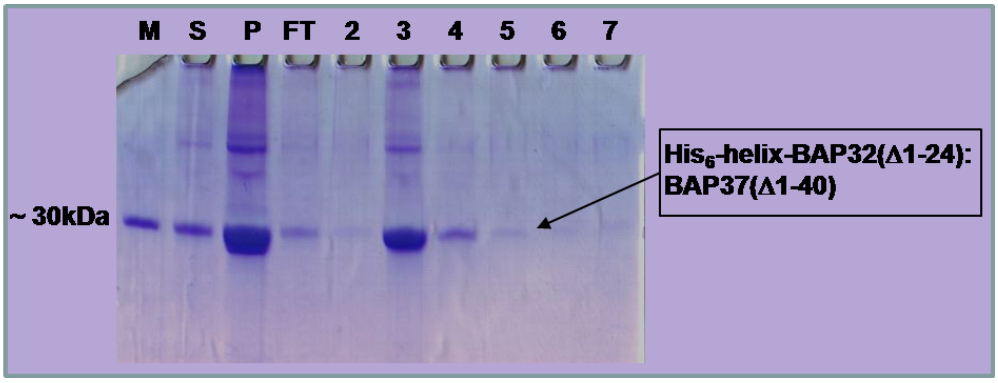

Figure -20: Co-refolding of His_6-helix-BAP32(Δ1-24) and BAP37(Δ1-40). Both proteins were found in the precipitate (P) after refolding, only His_6-helix-BAP32(Δ1-24) was present in the supernatant (S) after centrifugation of the refolding mix. His_6-helix-BAP32(Δ1-24) could be eluted form the column in fractions 2 to 5 (lanes 5-8).

The supernatant after centrifugation (lane 2, S) shows only one protein, and when compared to the third lane (precipitate, P) where both proteins are visible as a double band, the protein in the supernatant is thought to be His_6-helix-BAP32(Δ1-24). During refolding, a majority of both proteins were precipitated but since His_6-helix-BAP32(Δ1-24) was able to bind to the nickel column, it could be eluted from the column in fractions 2 to 7 (lanes 5-10). To determine the possible refolding of His_6-helix-BAP32(Δ1-24), elution fraction 3 (lane 6) was subjected to further dialysis in 20mM tris, pH 7.5 and 100mM NaCl in order to decrease the concentration of imidazole in the protein solution. Shortly after placing the dialysis bag in the new buffer, the protein precipitated which indicates that the protein was stabilised by high amounts of imidazole in the elution buffer, thus masking its insolubility.

2.2.7 Conclusions: Generation and production of truncation mutants

The prohibitin complex consisting of full-length BAP32 and BAP37 is not water-soluble due to hydrophobic membrane-anchoring helices at the N-termini of both proteins. N-terminal truncation mutants of both proteins were generated to overcome this problem. However, truncating the N-termini did not result in stable, water soluble BAP32 or BAP37. Co-refolding trials with different combinations of truncation mutants of both proteins led to the production of a stable complex using His_6-BAP32(Δ1-30) and BAP37(

Δ1-40). The refolding yield was 54% which decreased to 33% in the absence of glycerol and Nonidet-P40. The N-terminally truncated complex could be concentrated up to a concentration of 0.5mg/ml. Nevertheless, the main goal of production of a truncated prohibitin complex suitable for concentrating and application in further experiments was achieved. In subsequent experiments, the complex will be examined to further determine its state of folding and thermal stability using CD spectroscopy, and its size distribution using gel filtration analysis.

In 2005, Langhorst and colleagues found that truncation of the first EA repeat in the C-terminal helix lead to loss of oligomerisation function in stomatin and supposedly other SPFH family members . In BAP32 and BAP37, these EA-repeats are located at position 181/182 (BAP32) and at position 198/199 (BAP37) C-terminal to the PHB domain. The N-terminal and C-terminal truncation mutants of BAP32 and BAP37 were designed on the basis of secondary structure predictions, and the constructs were generated before this information was known. Assessing the truncation mutants generated in this work, the first EA-repeats both in BAP32 and in BAP37 were truncated in constructs lacking the C-terminal domains. That might be the reason why truncated proteins expressed from those constructs did not refold but rather precipitated. Their dimerisation potential might have been destroyed by truncating the protein before the first EA-repeat. This first EA-repeat is obviously present in the N-terminal truncation mutants that still contain the whole C-terminal region leading to refolding. On the other hand, coiled-coil regions are prone to aggregation and attachment to membranes, for example in centrifugation devices which might be the cause of protein loss in the concentration process. Design of truncation mutants lacking the N-terminal hydrophobic helix and the C-terminal coiled-coil domain but including the first EA-repeat C-terminal of the PHB domain might be the next step in improving refolding yield of those proteins and, equally, obtaining a high protein concentration suitable for crystallography.
Replacement of the hydrophobic N-terminal helix with an artificial soluble helix in BAP32 did not lead to refolding into a prohibitin complex. Here, the artificial helix did not

fold and the overall folding process of the protein might have been disturbed. Re-design of the construct will be necessary to achieve folding of the protein.

2.3 Biophysical experiments on prohibitin truncation mutants

Biophysical methods such as CD spectroscopy or gel filtration are used to analyse a protein solution with respect to its protein folding and oligomerisation state. The complex His_6-BAP32(Δ1-30):BAP37(Δ1-40) was successfully refolded without either glycerol or detergents which leaves the protein in a buffer suitable for spectroscopic analysis.

2.3.1 Gel filtration analysis of refolded His_6-BAP32(Δ1-30):BAP37(Δ1-40)

Gel filtration analysis is used to investigate the oligomerisation state of a protein and to determine the size of the different species. The gel filtration runs were carried out as stated in section 5.7.4.

Figure 2-11 shows a gel filtration run of N-terminally truncated prohibitin complex (thick line) overlaid by the calibration runs (thin line) which consists of Dextran Blue (2MDa), albumin (67kDa) and chymotrypsin (25kDa).

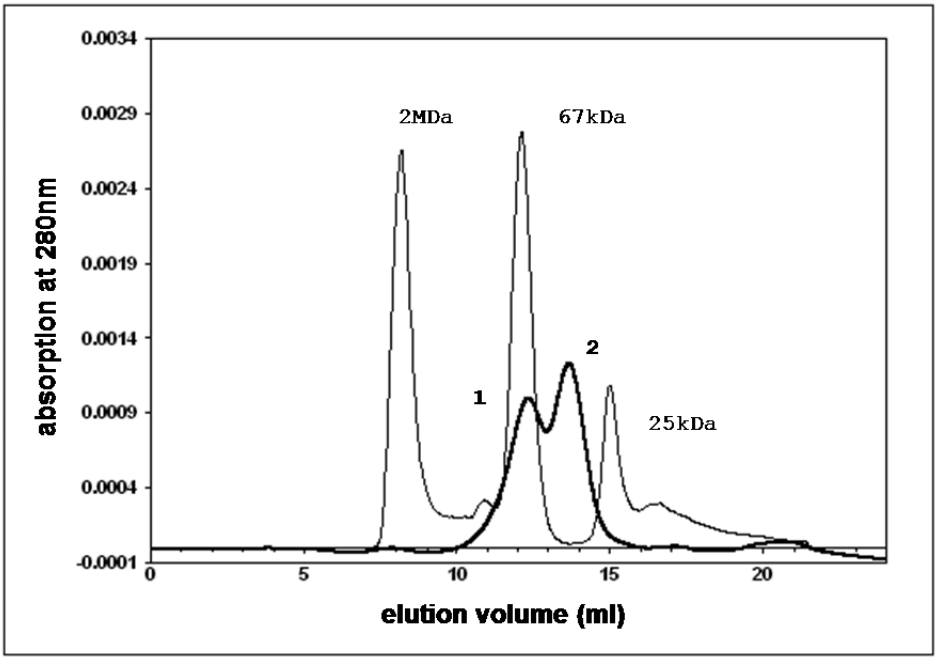

Figure -21: Gel filtration analysis of refolded His_6-BAP32(Δ1-30):BAP37(Δ1-40) complex shows two peaks at apparent molecular masses of 63kDa and 40kDa.

The trace of the prohibitin complex shows two peaks at 12.29ml and 13.65ml elution volume. K_{av} values were calculated for both peaks, which were converted into molecular weights using the equation generated from the calibration curve. His_6-BAP32(Δ1-30) has a predicted molecular mass of 27kDa and BAP37(Δ1-40) has a mass of 29kDa. The complex has a theoretical molecular mass of 56kDa. As His_6-BAP32(Δ1-30) and BAP37(Δ1-40) are the only components in the protein sample, the peak at the higher elution volumes could represent a monomer and the other a dimer. The theoretical molecular masses for either monomer (27kDa or 29kDa) or the dimer (56kDa) are lower than the respective molecular masses determined by gel filtration, 40kDa and 63kDa, respectively. The results are summarised in table 2-4.

Table -10: Analysis of the gel filtration experiment with His_6-BAP32(Δ1-30):BAP37(Δ1-40)

peak	elution volume [ml]	apparent molecular mass [kDa]	theoretical molecular mass [kDa]	Apparent species

1	12.29	63.2	56	dimer
2	13.65	40.0	27 and 29	monomer

Recent reports in the literature suggest that the presence of a His_6-tag can promote dimerisation of recombinant proteins . Attempts to verify the identity of the proteins represented by the peaks using SDS-PAGE analysis were not successful due to the low protein concentration in the elution fractions.

As the above calculations are only valid for globular proteins, prohibitin monomer and truncated prohibitin complex probably display an elongated shape which affects its hydrodynamic flow during gel filtration analysis. Determination of their Stokes' radii, R_s, could give clues about the dimensions of the protein species. Theoretical K_{av} values for His_6-BAP32(Δ1-30) and the truncated prohibitin complex were determined from their molecular masses using the formula obtained from the calibration runs (see section 5.7.4). Using the theoretical K_{av} values, their theoretical Stokes' radii could be calculated. Results reveal that the observed K_{av} values and Stokes' radii are greater than the theoretical values based on the molecular weight of each molecule (see table 2-5).

A greater difference in both K_{av} value and Stokes' radius were found for His_6-BAP32(Δ1-30) than for the prohibitin complex. The observed Stokes' radius of His_6-BAP32(Δ1-30) is 5.4Å bigger than the theoretical value which indicates an elongated shape of the particle. In contrast, the theoretical and the observed values for the Stokes' radius for the truncated prohibitin complex differ only by 2Å. The data suggest that the protein complex might still display a slightly elongated shape.

Table -11: Results for theoretical and observed K_{av} values and Stokes' radii R_s.

	observed K_{av}	theoretical K_{av}	observed R_s [Å]	theoretical R_s [Å]
His_6-BAP32(Δ1-30):BAP37(Δ1-40)	0.2617	0.2844	34.50	32.48
His_6-BAP32(Δ1-30)	0.3471	0.4207	27.32	21.91

2.3.2 CD spectroscopy of refolded His_6-BAP32(Δ1-30):BAP37(Δ1-40)

Circular dichroism was used to analyse the complex with respect to its secondary structure content and its fold stability. Presence of secondary structure elements in the protein complex was investigated by recording a wavelength spectrum and analysing it using implementations of two algorithms, the K2D neural network and a linear combination of Fasman spectra, within the programme ACDP which gave estimates for secondary structure element contents. Furthermore, CD spectroscopy was also used to determine the thermal stability of the protein complex by recording changes in the CD signal at a specific wavelength during heating of the sample.

2.3.2.1 CD wavelength spectrum and secondary structure prediction

The experimental spectrum in figure 2-12 (A) shows two minima at around 222nm and 208nm indicating the existence of α-helices. Furthermore, the spectrum displays a change of sign from 200nm towards lower wavelengths indicating a true fold of the protein (see figure 2-12, B).

The secondary structure was predicted using two algorithms, K2D and linear combination of Fasman spectra. The K2D algorithm predicts an α-helix content of 26%, a β-sheet content of 16%, and 57.7% as unordered. Using the linear combination of Fasman spectra, no α-helix content but 62% β-sheet were predicted. The least squares error was smaller for the fit using the K2D algorithm than for the fit using the linear combination of Fasman spectra.

A

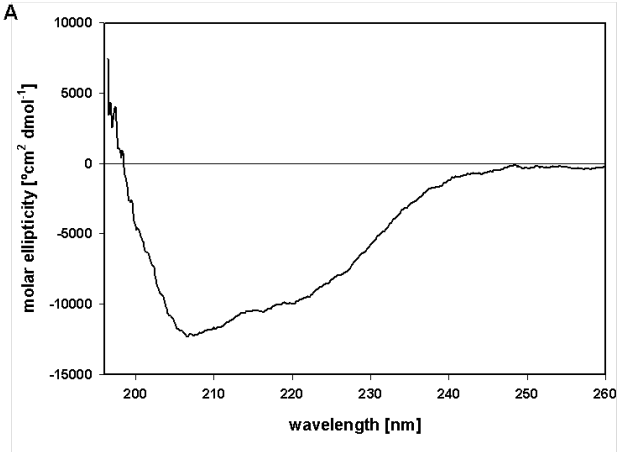

B

	K2D Neural Network	Linear combination of Fasman spectra
α-helix	0.26	0
β-sheet	0.16	0.62
unordered	0.577	0.37

Figure -22: CD spectrum of His_6-BAP32(Δ1-30):BAP37(Δ1-40) (A) and secondary structure prediction (B) using the programme ACDP .

Theoretical values for the proportion of residues in the respective structural element from the total number of residues were calculated from PSIPRED predictions and summarised in table 2-6. The N-terminal α-helices were excluded from the calculations as they are truncated in the protein sample.

Table -12: Theoretical distribution of residues in secondary structure elements

	Proportion of structured residues		
	BAP32(Δ1-30)	BAP37(Δ1-40)	complex
α-helix	0.58	0.50	0.53
β-sheet	0.21	0.20	0.21
unordered	0.21	0.30	0.26

With PSIPRED , a higher α-helical content was predicted for both proteins, a tendency that was also found using the K2D algorithm. Linear combination of Fasman spectra is not in agreement with secondary structure prediction, as no α-helical content was predicted. The K2D algorithm fits the experimental spectrum better in this case.

2.3.2.2 Thermal Denaturation

To determine the wavelength at which the complex His_6-BAP32(Δ1-30):BAP37(Δ1-40) experiences greatest change in its CD signal, corresponding to an unfolding, two wavelength spectra were recorded at two different temperatures, 15ºC and 90ºC (see figure 2-13 A). The spectrum recorded at 90ºC (dashed line) shows a flattening in the region from 235nm to 200nm as compared to the spectrum recorded at 15ºC (solid line) which indicates a loss of secondary structure caused by unfolding of the protein.

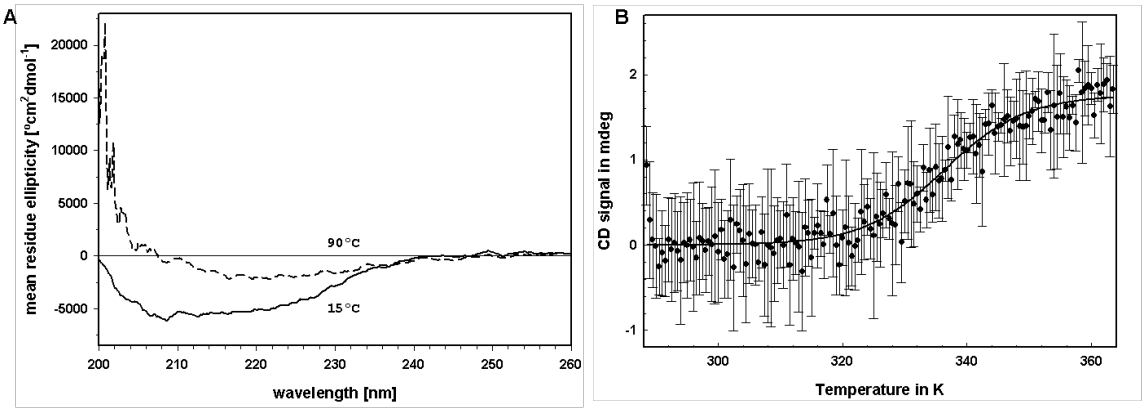

Figure -23: Thermal denaturation of His_6-BAP32(Δ1-30):BAP37(Δ1-40). A – The CD spectrum recorded at 90 ºC indicates less secondary structure of the protein as compared to the spectrum recorded at 15 ºC. B –Denaturation was monitored at 216nm and revealed a two-state transition process with a melting temperature T_m of 62ºC. Denaturation curve shows average of three independent experiments and respective error bars.

The greatest change in the CD signal during denaturation was observed at 216nm. Heat-induced unfolding was monitored 216nm in three independent experiments. The thermal denaturation curve displays a one-step transition process (figure 2-13 B) from native to unfolded protein. The data were fitted using a sigmoidal equation in the programme Sigma Plot giving a melting temperature, T_m, of 62ºC.

2.3.3 Conclusions: Biophysical experiments

Refolded N-terminally truncated BAP32/BAP37 complex was subjected to spectroscopic methods such as CD and gel filtration. In gel filtration, two peaks were visible at apparent masses of 63kDa and 40kDa which might represent the His_6-BAP32(Δ1-30):BAP37(Δ1-40) dimer and a BAP32(Δ1-30) or BAP37(Δ1-40) monomer, respectively.

The secondary structure of the complex was analysed using CD, and the spectrum shows a clear indication of the presence of secondary structure proving a folded state of a BAP-protein dimer without N-termini. The best prediction of secondary structure element contents was made using the K2D algorithm predicting both an α-helical and a β-sheet content. To assess its stability, the protein complex was unfolded by applying heat at a

defined rate. CD signal was measured at 216nm, the spectrum's minimum for β-sheets, resulting in a two-state unfolding curve with a melting temperature of 62ºC. The BAP complex consists of two molecules bound to each other via their natural interaction interface. In the thermal unfolding experiment, one might have expected an unfolding curve showing at least two transitions, one for dissociation of the dimer at lower temperatures and one at higher temperatures that represents unfolding of the monomers. There is no clear indication of a higher order unfolding process from the data obtained. Other methods such as fluorescence spectroscopy might give results that reflect both dissociation of the dimer and unfolding of the monomer.

This is the first time that a folded prohibitin complex was produced by recombinant expression and subjected to experiments assessing its biophysical properties. Using the given refolding protocol, it would be possible to produce His_6-BAP32(Δ1-30):BAP37(Δ1-40) in significant amounts and utilise it in crystallisation trials and binding studies with other proteins.

2.4 Computational experiments

In the absence of atomic details of prohibitin structures, and considering the difficulties faced with producing large amounts of soluble protein, a molecular modelling approach was undertaken in order to gain insights into the molecular structure of prohibitins. The structures of the PHB domains of BAP32 and BAP37 were modelled using the NMR structure of the band 7 (PHB) domain of the related mouse flotillin-2 as template (PDB accession number **1WIN**). Both models were used to create a hetero-dimer employing two different approaches.

In recent years, prohibitin research was focused on finding intracellular and extracellular binding partners. In this respect, possible interactions between BAP32 and melanogenin, a melanin production enhancer in the skin, were elucidated. Furthermore, possible interaction sites with other proteins were mapped onto the PHB domain models of BAP32 and BAP37 giving deeper insight into intracellular functions of prohibitins.

All modelling was done with the help of A. Hofmann, and work on melanogenin-binding to the PHB domain of BAP32 was done with the help of O. Kämäräinen.

Results from these studies were published in *Proteins* .

2.4.1 Molecular modelling

2.4.1.1 Alignment

In a first step to predict the three dimensional structure of prohibitin, a fold prediction model of prohibitin 1 was generated by Khurshid and co-workers (PDB accession no. **1LU7**). The only experimentally generated structure is an NMR structure of the band 7 (PHB) domain of mouse flotillin-2 (PDB accession no. **1WIN**), a distantly related protein within the SPFH super family. The theoretical model of the PHB domain of prohibitin 1 shares a similar shape with the experimentally determined flotillin-2 structure but the fold differs in the position and orientation of secondary structure elements (see also).

A sequence alignment of BAP32, BAP37 and flotillin-2 using Muscle , was slightly modified to satisfy conservations in the PHB domain region (boxed), and was combined with the secondary structure predictions for both prohibitins and the secondary structure elements found in the flotillin-2 NMR structure (see figure 2-14).

When comparing locations of secondary structure elements of BAP32 as seen in the fold prediction model generated by Kurshid and co-workers to predictions made by PSIPRED , one can identify some differences. In both predictions, the secondary structure elements encompass slightly different residues. β-sheets 2 and 4 are predicted to be shorter in the Kurshid model (full light grey arrows) but are roughly in the same region as predicted by PSIPRED (full middle grey arrows). Helices α1, α2and α3 are represented as two helices in the Kurshid model, and β5 was not predicted.

Following page: Figure -24: Sequence alignment for flotillin-2, BAP32 and BAP37 showing also their secondary structure elements. α-helices are displayed as cylinders, and β-strands are shown as arrows. Secondary structure predictions are indicated as full cylinders and arrows; experimental secondary structure of flotillin-2 (PDB accession no. **1WIN**) is represented by striped arrows/cylinders. The secondary structure obtained from the prohibitin fold prediction model (PDB accession no. **1LU7**) is shown in light grey.

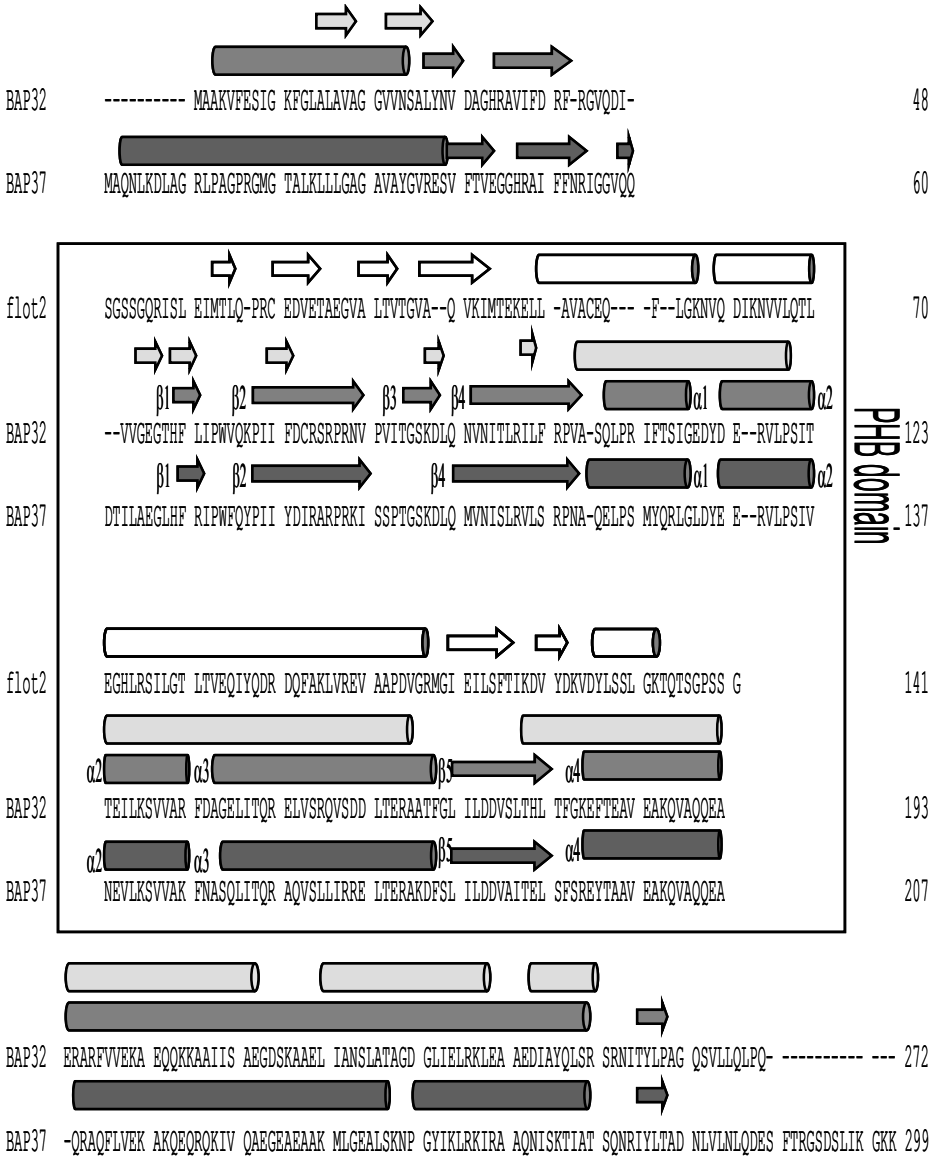

Legend

- Mouse Flotillin-2 NMR structure
- 1lu7 prediction of BAP32
- Prediction of BAP32 using PSIPRED
- Prediction of BAP37 using PSIPRED

Shortcomings in matching the two secondary structure predictions are mostly due to a poor prediction with confidences less than 0.5. For instance, the probability for helical geometry of helix α4 around residues 228/229 (BAP32) is less than 0.5 and thus it is quite likely, that α4 might also be divided into two segments as it is was predicted for BAP37.

2.4.1.2 Homology modelling of PHB domains of BAP32 and BAP37

Based on the agreement between the predicted secondary structures of BAP32 and BAP37 and on the experimentally determined structure of mouse flotillin-2, homology models for the PHB domains of both prohibitins were generated. The NMR structure of flotillin-2 (PDB accession no. **1WIN**) was used as a template for homology modelling with the programme Modeller 4 , see also section 5.9.2. Ramachandran plots were generated using PROCHECK to assess tensions in the proteins main chain angles (see Appendix). 87% of amino acids for the PHB domain of BAP32 were in most favoured regions and 11% in additionally allowed regions. No residues were found in disallowed regions indicating a good model for the protein. As for BAP37, 88% of amino acids were in most favoured regions. 10% of all residues were in additionally allowed regions. One residue, Leu99 was found in disallowed regions. Nonetheless, the model of BAP37 has almost all residues in most favoured regions and additionally allowed regions indicating a good model for the protein. However, prohibitins and flotillin-2 are distantly related proteins within the SPFH super family which might lead to slight differences in the fold of certain areas. Therefore, the calculated models have to be interpreted with caution and cannot substitute for experimental structures.

Homology models of BAP32 and BAP37 are shown in figure 2-15 in red and blue, respectively, and the predicted prohibitin fold by Khurshid and coworkers (PDB accession no. **1LU7**) is shown in green for comparison. The modelled PHB domains of both BAP32 and BAP37 adopt slightly elongated globular shapes where the two anti-parallel helices α 2 and α3 pack against the three-stranded anti-parallel β-sheet formed by β1/β2, β3/β4 and β5 (see figure 2-15).

Figure -25: Three-dimensional homology models of BAP32 (red) and BAP37 (blue) PHB domains in comparison with prohibitin fold prediction (green, PDB accession number **1LU7**). Figure prepared with BOBSCRIPT and rendered with PovRay .

The predicted helical segment α1 at the "bottom" (N-terminal) side of the protein appears like an extended loop and is probably an area of the model where the structure can be predicted with less confidence. The generated homology models have positional rms distances to the experimental flotillin-2 structure of 10.5 Å (BAP32) and 10.0 Å (BAP37). Models of the PHB domains of BAP32 and BAP37 differ by an rms distance of 3.1 Å.

While there are some similarities between the homology model presented in this work and the predicted BAP32 model by Khurshid and colleagues (PDB accession no. **1LU7**), the latter shows a much less globular fold. A β-sheet feature is present in the predicted model, but it is exclusively built by the N-terminal β-strands and there are no packing interactions to the two anti-parallel helices. Unfortunately, no further information about the fold

prediction model generated by Khurshid and colleagues is available limiting the space for interpretation.

In order to investigate the distribution of the electrostatic potential on the surface of the proteins, surface representations of the prohbitin models and flotillin-2 were prepared using PyMOL , and coloured according to their electrostatic potential with blue indicating positive and red indicating negative charge. The four structures within one panel show successive 90° rotations around the vertical axis (see figure 2-16).

A comparison of the surface properties of the proteins reveals interesting differences. The PHB domain of flotillin-2 is predominantly negatively charged with only a few isolated positive areas. In prohibitins, the surface appears to gradually have a more electropositive character. The surface of the PHB domain of BAP32 presents an electropositive patch at the C-terminal side (“top”) which is extended to the “bottom” side (membrane-proximal) in BAP37.

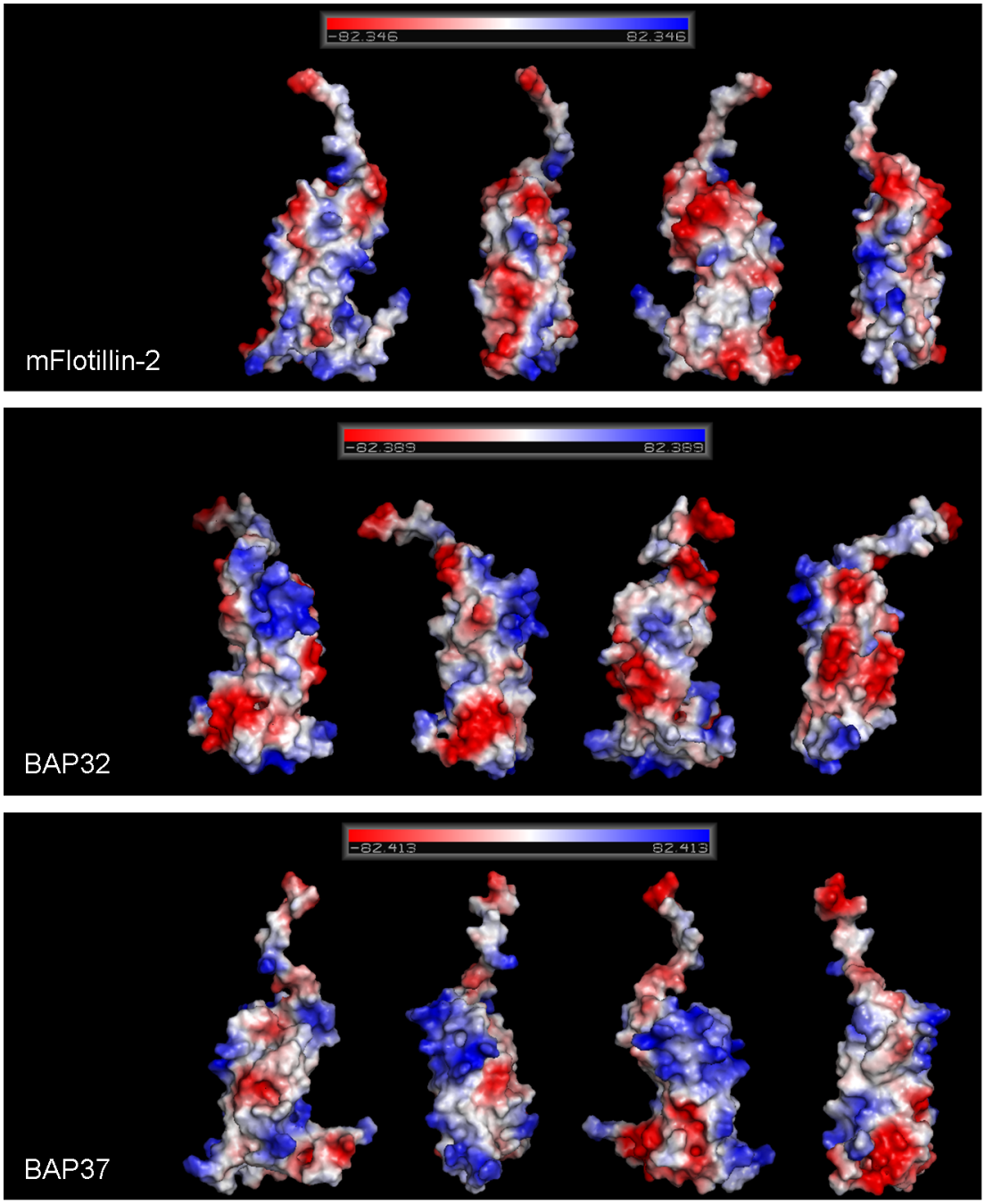

Figure -26: Surface representations of mouse flotillin-2 (top panel) and of modelled PHB domains of BAP32 (middle panel) and BAP37 (bottom panel). Each panel shows successive 90º rotations of the proteins around the vertical axis. Figure prepared with PyMOL .

2.4.1.3 Modelling of the N-terminal regions of BAP32 and BAP37

Results from the secondary structure predictions are well in agreement with the current state of knowledge where the N-terminal domains of prohibitins either form a membrane-anchoring α-helix (BAP32) or a transmembrane α-helix (BAP37). With a predicted length of 36 Å, the N-terminal α-helix in BAP32 would just be able to span the lipid bilayer whereas the N-terminal helical segment in BAP37 has an expected length of 56 Å and is thus long enough to reach well into the mitochondrial matrix.

In order to predict the nature of the anchor domain, models of the first 29 amino acids of BAP32 and the first 39 amino acids of BAP37 were generated using Garlic . Helical wheels were created from the same programme showing hydrophilic residues in blue, hydrophobic residues in red (see figure 2-17). The intensity of the colour describes the degree of hydrophilicity or hydrophobicity, respectively, with dark blue being very hydrophilic and dark red being very hydrophobic.

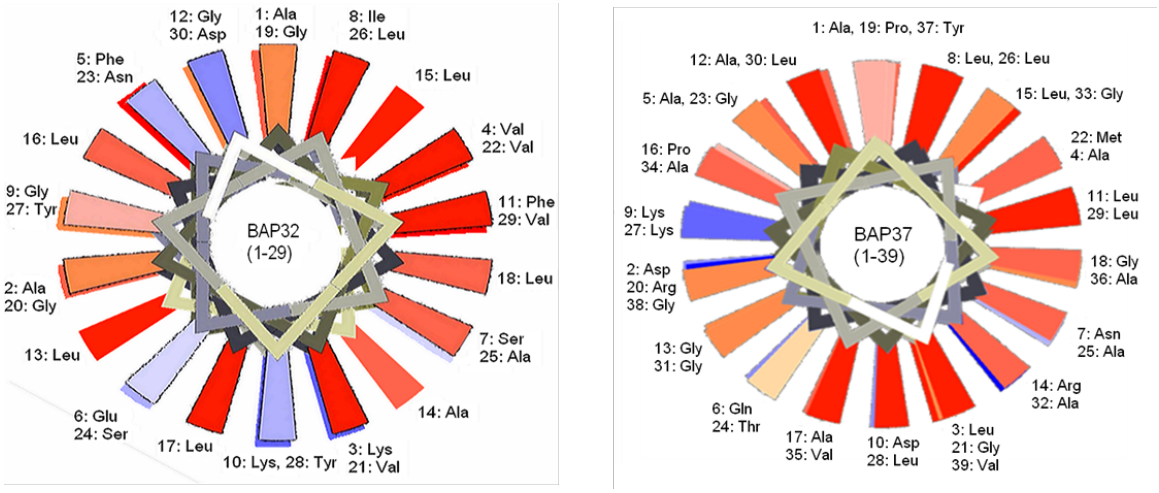

Figure -27: Helical wheels of amino acids 1 to 29 of BAP32 (left) and amino acids 1 to 39 of BAP37 (right). Hydrophobicity of residues is indicated by scales of red, and hydrophilic character is indicated in degrees of blue. Figure prepared using Garlic .

Both helices of the predicted membrane regions showed no true ampiphilic nature or a hydrophilic region, and is not as hydrophobic as expected for a membrane inserting segment. Surprisingly, about 20% of the residues present in the proposed membrane

regions are hydrophilic such as lysines and aspartates. BAP32 possesses lysines at positions 3 and 10, and an aspartate in position 30. Two lysines can be found in the N-terminal region of BAP37 at positions 9 and 27. Furthermore, the protein also possesses an arginine at position 14 and an aspartate at position 2.

Intriguingly, the few polar and charged residues are all positioned on one side of the helix but their exposure would be energetically unfavourable in a lipid bilayer. However, an exposure of those polar/charged residues to hydrophobic environment might be avoided by masking of the polar patches within a BAP32:BAP37 dimer. Homo-dimerisation was not considered as there is no experimental evidence for homo-oligomers . Helical models of BAP32(1-24) and BAP37(1-39) were dimerised using rigid body methods with the programme O where oppositely charged residues were brought in close contact to enable formation of hydrogen bonds, thus stabilising the dimer (see figure 2-18, A). Isoforms of side chains were also considered in this approach. The model of the helix dimer was further tested and its conformation improved by subjecting it to molecular dynamics simulations with GROMACS (done by A. Hofmann). Throughout the simulated time of 500 ps, the two helices stayed in contact with each other, and the simulated complex equilibrated as judged by analysis of rms distances and potential energies. However, several polar/charged residues remained on the outside surface of the helix dimer: Lys4 and Glu7 from BAP32 and Asp3, Gln7, Lys10, Arg15 and Arg21 from BAP37, and would still be in contact with the hydrophobic interior of the mitochondrial inner membrane. This result is best shown by calculating the electrostatic potential of the dimer surface with blue indicating positive and red indicating negative charge. Surface representations in 90º rotations around a vertical axis were generated using PyMOL (see figure 2-18, B).

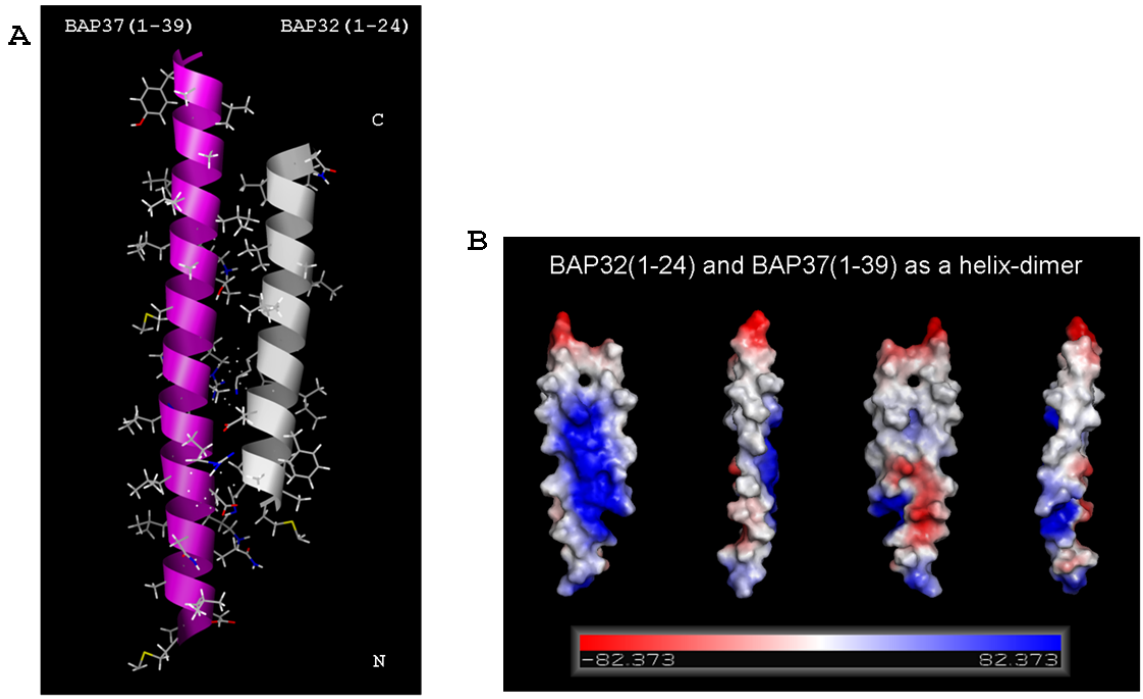

Figure -28: A – Models of the N-terminal helices BAP37(1-39) and BAP32(1-24) positioned in a helix dimer, B – Surface representations of the helix-dimer with electrostatic potential. Figure prepared with PyMOL .

One could speculate that these non-masked residues engage in interactions with transmembrane segments of *m*-AAA protease subunits in the mitochondrion, and thus be shielded from the hydrophobic environment.

Comparing the membrane helices of BAP32 and BAP37 with the N-terminal helices of their yeast homologues, one finds some interesting differences. Phb2, the yeast homologue of BAP37, possesses a N-terminal region that consists of a positively charged leader sequence and a hydrophobic α-helix, and was shown to be responsible for mitochondrial targeting of Phb2 . Furthermore, the N-terminal segment shows a much higher enrichment of basic residues giving rise to a truly amphipathic α-helix which is characteristic for mitochondrial sorting sequences. These authors have also been able to show that the presence of the N-terminal domain of Phb1, the yeast homologue of BAP32, is required for mitochondrial targeting. While the topology of residues on the helical wheel is very

similar for Phb1 and BAP32, the characteristic bipartite feature of Phb2 is not present in BAP37. These results suggest that mitochondrial targeting of BAP32 and BAP37 might be different from their homologues in yeast.

2.4.1.4 Analysis of the C-terminal coiled coil domain of BAP32 and BAP37

The C-terminal domain of both prohibitins presumably adopts a coiled coil structure , and further analysis using MultiCoil reveals that BAP32 shows a 30% probability to form a two-stranded coiled coil. BAP37, in contrast, is predicted to form a three-stranded coiled coil with a probability of almost 60%.

Generally, it is possible that the different strands of a multi-stranded coiled coil are provided by either the same molecule or a neighbouring molecule. Especially, if the coiled coil region is divided into two segments like in BAP37, it is quite possible that the second segment adopts an antiparallel orientation with respect to the first one and thus forms the second strand of a two-stranded coiled coil. As there is no structural information available, further predictions remain pure speculation.

2.4.1.5 The BAP32:BAP37 oligomer

A recent cross-linking study on isolated prohibitin complexes from yeast found that inter-molecular cross-linking occurred mainly between two PHB domains or two coiled-coil regions . Intra-molecular cross-linking between residues in close distance was also reported. Based on the finding that prohibitins exist as high molecular weight oligomers , a ring-like assembly of alternating prohibitin homologues has been proposed consisting of hetero-dimeric building blocks. This model is supported by recent electron micrographs of purified yeast prohibitin complexes revealing large ring-shaped structures whose formation could be abolished by truncating the C-terminal coiled-coil regions. So far, no experimental evidence has been obtained that would suggest formation of homo-oligomers . Two methods were employed to generate prohibitin hetero-dimers using the homology models of the PHB domains of BAP32 and BAP37: an automated modelling approach using the programme Hex and manual dimer generation with rigid body movement in the programme O .

Protein docking calculations using the programme Hex resulted in a model where α2 and α3 from BAP37 pack against β1 and α2 of BAP32 (see figure 2-19).

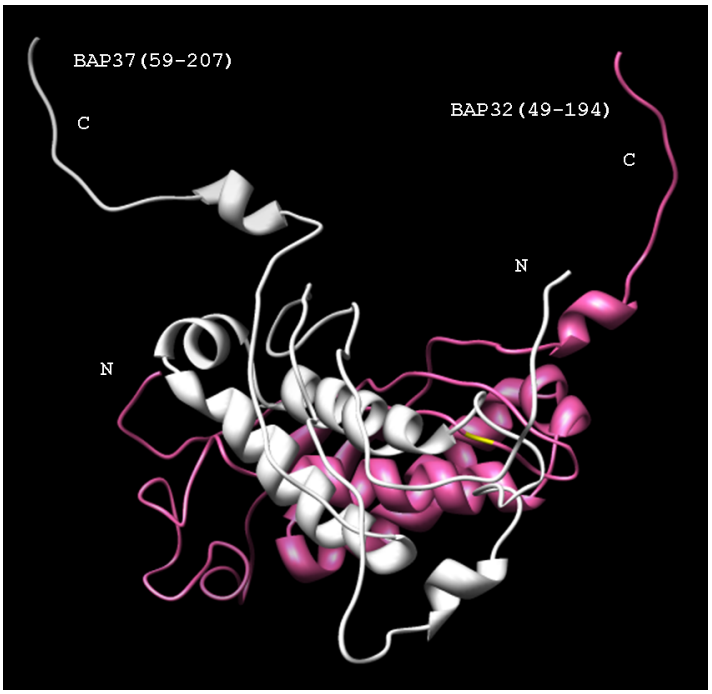

Figure -29: Docking of modelled PHB domains of BAP32 and BAP37 using the programme Hex . Cys69 of BAP32 is indicated in yellow. Figure prepared with PyMOL .

Overall, this leads to an orientation where both molecules are positioned next to each other with a tilt angle of about 120° between their long axes. Thus, they are aligned in an almost anti-parallel fashion. The dimer is held together mainly by van-der-Waals interactions, and only one hydrogen bond between Thr124 (BAP32) and Glu139 (BAP37) can be identified. The buried surface area is about 2700 $Å^2$ corresponding to 13% of the surface of each monomer. However, the Hex-derived model does not agree with results from the earlier cross-linking study with yeast prohibitin which showed that residues 74 and 154 in PHB1 were found to be cross-linked with residue 103 in PHB2 and residue 151 (PHB1) with 176 (PHB2). The respective residues in BAP32 and BAP37 identified by multiple sequence alignment are: 72 and 152 (BAP32) cross-linked to residue 86 (BAP37), and residue 149

(BAP32) linked to residue 159 (BAP37). Those residues are not in close proximity in the Hex-generated dimer.

In a second approach, the possibility of manually creating a model of a BAP32:BAP37 dimer using the programme O was attempted. Dimer formation was based on two criteria: the anticipated parallel orientation of the two protein molecules, as well as the spatial closeness of certain residues identified from cross-linking of prohibitin from yeast . Inevitably, this leads to a model where helices α2 and α3 from both molecules form a four-helix bundle (figure 2-20). In this model, both proteins align parallel with both N-termini pointing in the same direction satisfying requirements of their function as membrane anchors. The residues found to be cross-linked in both proteins are close to each other (14Å to 18Å) as shown in the inset.

The starting model was subjected to a molecular dynamics simulation in order to test the stability of the complex and to improve conformations which would maximise the interactions between both monomers (done by A. Hofmann). Within the timeframe of the simulation of 500ps, the potential energy decreased to a minimum, and the rms distance and the centre of gravity distance reached equilibrium. Depiction of the centre of gravity distance over time showed that, after initially drifting apart, both molecules anneal again resulting in a final distance of just over 25Å between their centres of gravity. The interaction interface covers about 1150Å^2 (6% of the total surface area of each individual protein molecule) which is a smaller area than was generated by the automated docking. Two hydrogen bonds can be identified, one between Glu90 (BAP32) and Arg174 (BAP37) and another between Asp104 (BAP32) and Ser231 (BAP37).

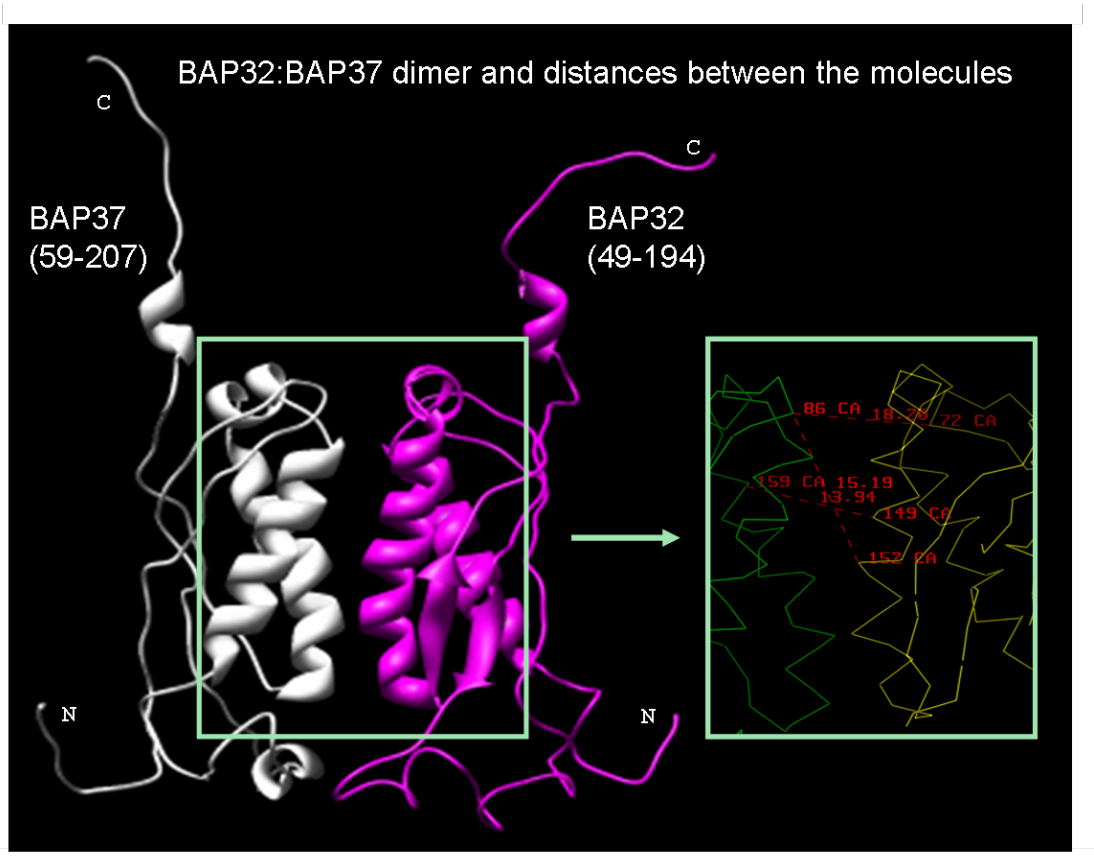

Figure -30: Manual modelling approach of PHB domains of BAP32 and BAP37 using O . Inset shows residues identified in cross-linking experiments in yeast prohibitin and their distances in the modelled dimer. Figure prepared with PyMOL .

The complex possesses pseudo-2-fold symmetry which establishes a prohibitin dimer as a building block for the ring-shaped high molecular weight complex and requires a different type of protein-protein interaction with the neighbouring prohibitin molecules in the ring. It is tempting to speculate that these interactions are provided by coiled-coil interactions between neighbouring BAP32 and BAP37 molecules. This speculation is in agreement with a report by Tatsuta and colleagues showing that C-terminally truncated yeast Phb1 is unable to form large assemblies . Furthermore, a number of residues in the coiled-coil region were found to be cross-linked in the study by Back and co-workers . One might therefore speculate that a cooperative effect based on coiled-coil strand exchange and four-helix-bundle formation enables the BAP32-BAP37 interaction which ultimately

results in formation of the large ring-shaped complexes. The fact that both proteins are membrane-bound through their N-terminal helices will most likely lower the activation energy for these interactions.

Intriguingly, all previous studies in this context agree that there is no prohibitin dimer detected in any aqueous environment such as the nucleus. It remains to be clarified whether the single proteins are stabilised by other binding partners instead. This would be necessary in order to mask the hydrophobic patches present in the N-terminal region and improve protein stability.

2.4.2 Modelling of melanogenin binding to BAP32

Melanogenin has been found to enhance melanin production in melanocytes and to bind specifically to prohibitin , proposing a functional role for prohibitin in melanin induction. Snyder and coworkers identified prohibitin 1 as a specific target for melanogenin by affinity chromatography with immobilised ligand and subsequent identification using mass spectrometry . It was further assumed that binding of the ligand would occur at a globular domain, i.e. the PHB domain of the protein. In order to investigate the interaction between melanogenin and BAP32, a docking study was carried out using the programme FlexX . The docking studies of melanogenin to the modelled PHB domain of BAP32 were carried out with the help of Outi Kämäräinen.

Melanogenin possesses three substituents at a central triazine ring: a polyether/amine chain, a mono-fluoro-benzyl group, and an ether-bonded penta-fluoro-hydroxy-benzol. By visual inspection and surface analysis of the BAP32 homology model, two potential binding pockets were identified within the PHB domain. The first pocket (pocket 1; see figure 2-21, A) is located at the membrane-proximal side of BAP32 and constituted by helix α1 at the bottom, strands β5 and β4 at the side and the linker region between the N-terminal membrane helix and the PHB domain at the back. A slightly smaller pocket (pocket 2; see figure 2-21, B) is located in a groove between helices α2 and α3 in between residues Thr124 and Phe134. Both pockets are lined with hydrophobic residues in the cavities and polar/charged residues at the protein surface.

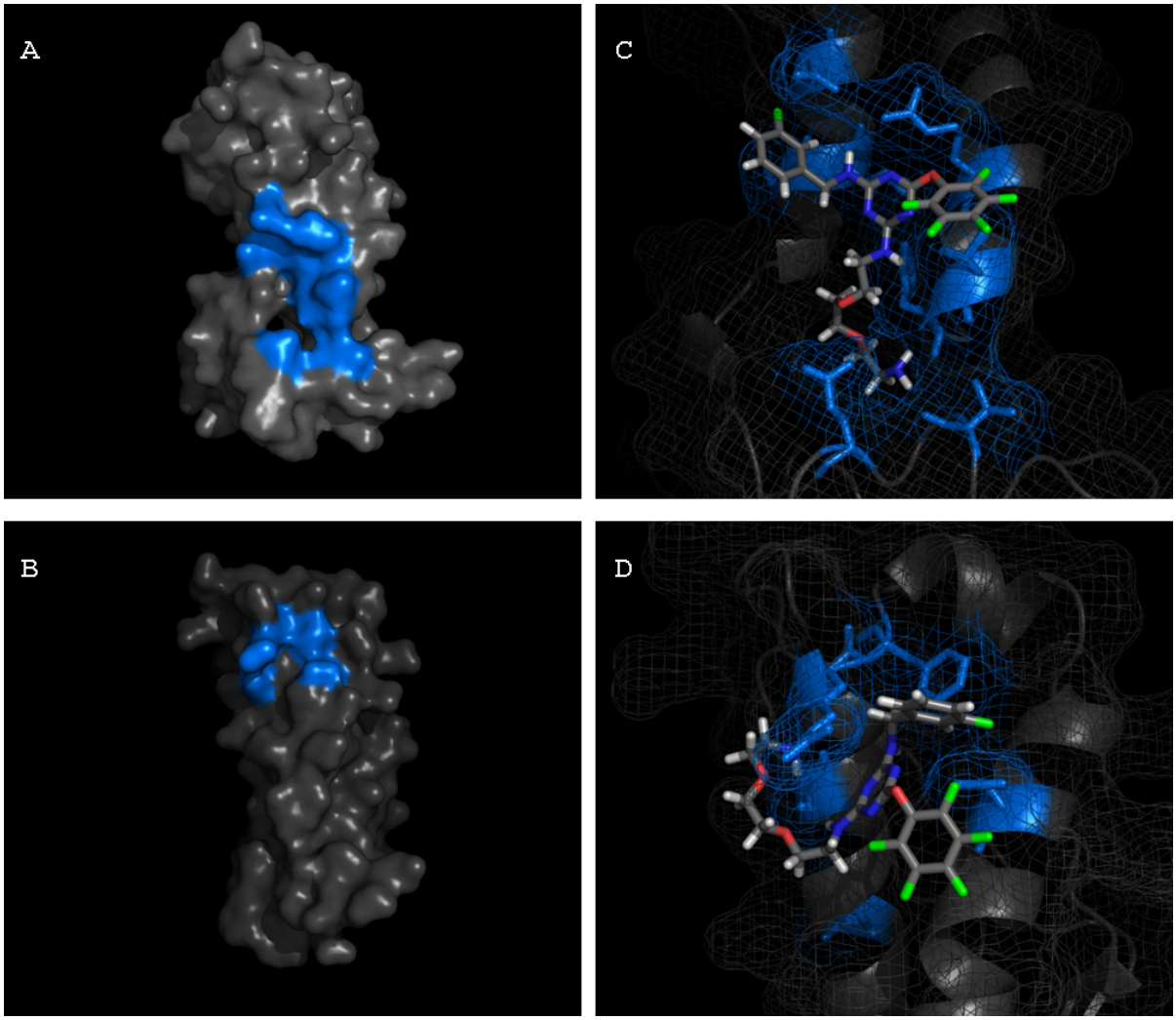

Figure -31: Docking of melanogenin to two predicted binding pockets on BAP32. Pockets are shown as blue areas (A and B), the position and conformation of melanogenin in pocket 1 (A) is shown in C, and melanogenin in pocket 2 is shown in D. Interacting side chains of the protein are coloured in blue, the melanogenin molecule is coloured by its elements. Figure prepared by N.-J. Hu with PyMOL .

Attempts to fit the ligand into pocket 2 yielded a conformation where the triazine ring, as well as the polyether/amine chain are neatly accommodated in a groove, and two aromatic rings of the organic molecule are sticking out from the protein surface. This binding mode with a buried surface of 737 Å^2 is stabilised by hydrogen bonds provided by Ser129, Arg133, Gln149 and Asp153.

Docking of melanogenin into pocket 1 yields conformations with much larger buried surface areas (839 Å^2) as compared to pocket 2. Here, the polyether/amine branch of the ligand protrudes into the cavity at the membrane-proximal side of the protein. The side chain amine group of Gln102 provides hydrogen bonds to interact with the two ether groups and the most extreme amine group of the ligand is held in position by hydrogen bonds with the backbone carbonyl groups of Phe161, Gln102, and Val99. At the protein surface, Thr160 and Arg157 provide hydrogen bonds to two nitrogen atoms of the triazine ring system which is further held in place by van-der-Waals interactions with Ile122. The fluorine of the mono-fluoro-phenyl group is hydrogen-bonded by the side chains of Ser121 and Glu125, and the penta-fluoro-substituted ring system is only loosely held in place by van-der-Waals interactions with Thr160. An alternative binding mode where the two aromatic ring systems have switched places has also been obtained with slightly less scoring values. It thus remains unclear which binding mode might be preferred.
A common observation for both pockets is that the penta-fluoro-substituted ring system is not fully coordinated by protein residues, sticking out of the protein surface and available for external interactions. This is somewhat surprising, since Snyder and coworkers found a melanogenin derivative with a 2,3,6-tri-fluoro-hydroxybenzol group to bind less well to prohibitin .

2.4.3 Binding of the prohibitin complex to other proteins

In various studies, BAP32 and BAP37 have been found to interact with other proteins in the cell cytosol and the nucleus that are involved in gene expression. However, only prohibitin monomers were shown to be involved in those interactions and not the BAP32:BAP37 complex. In all studies, the interaction sites were found to be localized mainly on the PHB domains of the respective prohibitin which appears to be the functional part of the proteins. Figure 2-22 visualises the interaction sites between prohibitins and Rb, E2F, estrogen receptor (ER) and Akt mapped onto the prohibitin homology models. Results from these studies were published as a review in *CCB*.

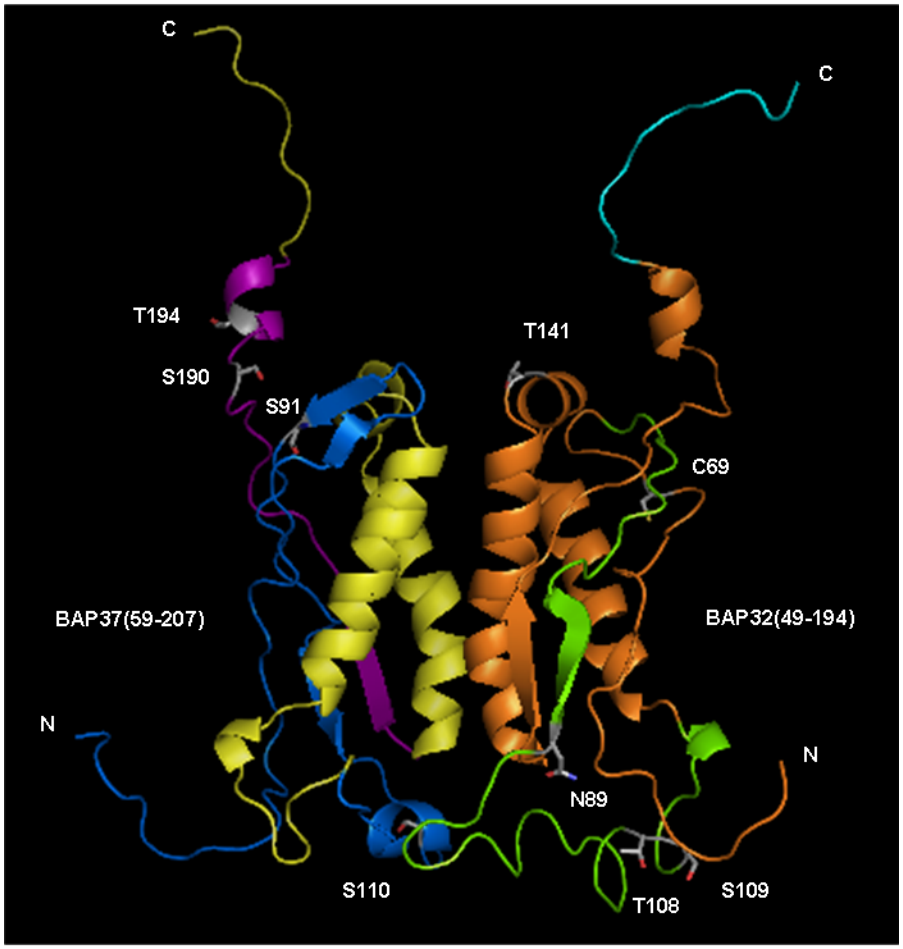

Figure -32: Interactions of PHB domains of BAP37 (blue) and BAP32 (orange) with target proteins identified by other groups in interaction assays. Figure prepared with PyMOL .

BAP32 interacts with Rb protein and the transcription factor E2F indicating a role in gene expression control. The Rb binding region on BAP32 (shown in green) spans residues 74-116, where three of four point mutations of prohibitin are found in sporadic breast cancer cells . Interestingly, those residues span the anti-parallel beta-sheet of BAP32, which is proposed not to interact with its homologue, BAP37, and would thus be potentially available for interactions with other target proteins. BAP32 also binds to the transcription factor E2F (shown in cyan) , and appears to act as a repressor in E2F-mediated transcription. Additional to the region at the C-terminal end of the PHB domain, this interaction also seems to require the RB-binding domain. Further research in this area

might give clues to the nature of this interaction and thus provide insights in the mechanism responsible for E2F repression.

Although there is a consensus Akt phosphorylation site present in prohibitin 2 (86-RPRKIS-91), phosphorylation of yeast prohibitin 2 could not be confirmed *in vitro* or *in vivo* . Prohibitin 2 might thus belong to the third class of Akt-interacting proteins where Akt functions by competitive binding to prevent its interacting proteins from binding other proteins. The proposed interaction site with Akt is coloured in yellow , which also includes the binding site for estrogen receptor (ER, purple) . BAP37 was found to bind directly to ER in the presence of its ligand estradiol. The Akt binding site on BAP37 attracts attention because it is located at the BAP32 interface. One might therefore speculate that BAP37 would only be able to bind to either protein. On the other hand, BAP32 and Akt might share similar structural features to be able to bind to the same interface on BAP37. This finding strengthens results from other studies where prohibitins were found to bind to proteins in their monomeric state.

Furthermore, putative phosphorylation sites are indicated by explicitly drawn residues. These modification sites were predicted using Expasy tools (www.expasy.org) and are analysed in detail in the following section. Additionally a putative palmitoylation site in BAP32 at Cys69 is indicated explicitly.

2.4.4 Prediction for posttranslational modifications

Posttranslational modifications were predicted for both proteins in order to evaluate possible conformational changes that could influence the function of prohibitins in the cell. Table 2-7 summarises the results from predictions that were run using Expasy tools (www.expasy.org) indicating also whether the predicted modification sites would be accessible in the model.

Table -13: Prediction for posttranslational modifications

Modification	Predicted in BAP32	Accessible in our model?	Predicted in BAP37	Assessed in our model?

Acetylation	No	n/a	No	n/a
Cellular localization	unknown	n/a	Unknown	n/a
Mito import sequence	32.5% yes	n/a	21.8% yes	n/a
N-glycosylation	N 89	Yes	N 103 N 259	No signal peptide
O-glycosylation	no	n/a	No	n/a
O-β-GlcNAc sites	S 147 (61%)	No	S 91 (46%) T 263 (58%)	Yes n/a
Phophorylation	S 109 (74.4%) S 151 (97.6%) T 108 (86.8%) T 141 (89.4%) T 155 (78.0%)	Yes No Yes Yes No	S 91 (90.3) S 92 (98.7) S 110 (86.9) S 176 (77.3%) S 190 (99.1%) S 267 (80.1%) S 291 (83.3%) S 293 (98.5%) T 170 (99.2%) T 194 (73.9%) Y 248 (94.4%)	No No yes No Yes n/a n/a n/a No Yes n/a
Kinase involved in phosphorylation (>70%)	T 155 (PKC) S 8 (PKC)	No n/a	S 91 (PKA) S 39 (PKA) S 110 (PKA) S 143 (PKC) T 155 (PKC) S 291 (PKA)	No No Yes No No n/a
Sulfation in Y	Y 155 (52%)		none	n/a

Predictions for post-translational modifications indicate that both proteins would not be acetylated by N-acetyltransferase A nor possess O-glycosylation sites.

Their cellular localization was predicted unknown due to the absence of an N-terminal pre-sequence, and the possibility of a mitochondrial import sequence was predicted with only 32.5% for BAP32 and 21.8% for BAP37. This might reflect a ubiquitous distribution of both proteins in the cell exerting functions in different cell compartments. An interaction with a target protein or a post-translational modification of the proteins might specify their cellular localisation.

Although BAP37 possesses two N-glycolysation recognition sequences (Asn-Xaa-Ser/Thr), glycolysation is unlikely because it does not possess a signal peptide that would expose the protein to the N-glycosylation machinery, and thus may not be glycosylated *in vivo* even though it contains potential motifs. On the other hand, BAP32 does possess a signal peptide, and an N-glycolysation site has been predicted for asparagine 89 which is located at the membrane proximal side (see figure 2-22). This residue lies within the suggested Rb interaction site with BAP32, and might therefore only be used when this interaction is not intended or BAP32 does not reside in the cytosol. Predictions for O-ß-N-acetylglucosamine (O-ß-GlcNAc) attachment sites in eukaryotic protein sequences revealed that BAP32 possesses one site at residue S147 which is not accessible according to our model. Two O-ß-GlcNAc sites were detected in BAP37, S95 and T267, where the latter lies in the C-terminal coiled-coil region and cannot be assessed by our model. Residue S95 was predicted with 46% confidence level and resides in the membrane-distal part of the protein.

Proteins can be phosphorylated at serine, threonine and tyrosine residues which plays an important part in modifying their functions. In 2D-gel electrophoresis, several prohibitin species were found which indicated that the proteins are phosphorylated . In context with investigations on E2F interaction sites on BAP32, Wang and colleagues proposed a possible involvement of JNK1 in phosphorylating the prohibitin .

Possible phosphorylation sites were predicted for both prohibitins and evaluated on whether they were used *in vivo*. Phosphorylation sites on membrane-proximal side are unlikely to be used when the prohibitins are in the membrane bound complex because they are not accessible. Some proposed phosphorylation sites lie within the protein interface in the BAP dimer and are unlikely to be used in the dimerised state. Looking at a membrane-bound BAP dimer, only three phosphorylation sites are likely for each BAP protein, T108, S109, T141 in BAP32 and T194, S190, S110 in BAP37. As visualised in figure 2-22, some of those residues lie within the interaction interfaces with other proteins. In BAP32, T108 and S109 lie within the Rb binding site, in BAP37, T194 and S190 are part of the interaction interface with Akt and estrogen receptor. It is therefore tempting to speculate

that phosphorylation is used in prohibitins to modify the interaction interfaces with other proteins, allowing or disallowing an interaction.

Lipo-conjugation of the PHB domain as observed with podocin and mec-2 that are two PHB domain containing proteins , and might be another possible posttranslational modification. As palmitoylation occurs at accessible cysteine residues, but only BAP32 (one cysteine at position 69; see figure 2-22), and not BAP37 (no cysteine) is anticipated to possess this feature. Based on a preliminary secondary structure alignment of BAP32 with podocin and mec-2, Cys69 seems to be located in a similar position to the conjugated cysteines in podocin and mec-2 .

2.4.5 Conclusions: Computational experiments

In the absence of experimentally determined three-dimensional structures of both prohibitins, homology models provide valuable insight into the structural features of prohibitins, their interactions in the dimer and with other proteins. Dissecting the proteins into the three domains, the N-terminal hydrophobic helix, the PHB domain and the distal C-terminal coiled-coil region, allows some structural predictions.

Based on helical wheel interpretations and models of the N-terminal α-helices, an unusually high content of charged and polar amino acid was discovered within the mainly hydrophobic membrane-inserting helices. Partial masking of those residues could be achieved by dimer formation of the N-terminal transmembrane helices of both BAP32 and BAP37. Homology models of the PHB domains of BAP32 and BAP37 were generated using an NMR structure of the related mouse flotillin-2 as a template (PDB accession number **1WIN**). The domain adopts a slightly elongated globular shape where the two anti-parallel α-helices pack against a three-stranded anti-parallel β-sheet. In a cross-linking study , two groups of prohibitin 1-prohibitin 2 interactions had been found: between the respective PHB domains and between coiled-coil domains. It seems likely that the main interactions between the globular PHB domains of BAP32 and BAP37 occur only on one side engaging in formation of the dimeric building block for high molecular weight assemblies observed in electron micrographs . One can imagine a prohibitin dimer

residing in the inner mitochondrial membrane where both the PHB domains and N-terminal α-helices of BAP37 and BAP32 engage in protein-protein interactions.
The C-terminal coiled coil domains will most likely be involved in inter-molecular interactions as well, although it is not clear at this point, whether these interactions occur within the dimeric building block or between two of these building blocks. Formation of ring-like assemblies would require interactions between the dimeric building blocks that could be provided by interactions between either the N-terminal helices (within the membrane) or the C-terminal coiled coil domains. Alternatively, the ring-like assembly could also be promoted by an external factor such as the *m*-AAA protease.

Measurement of extends of the generated model reveals a width of 37Å, 16Å in the y-direction, and 42Å (BAP32) or 45Å (BAP37) in the z-axis. Tatsuta and colleagues found ellipsoid ring-like assemblies of yeast prohibitin subunits with an outer diameter of 270Å x 200Å and an inner diameter of 160Å to 90Å . One can calculate the average ring thickness to be 55Å which coincides nicely with the z-dimension of the prohibitin complex. The combination of results from this study with findings from electron micrographs lead to the conclusion that the prohibitin complex is likely to lie flat on the membrane inserting its N-termini into the membrane. A spatial closeness between the PHB domain and the membrane would be a preferred scenario for a possible palmitoylation of cysteine 69 in BAP32. Palmitoylation of the cysteine would create a second membrane anchor within BAP32 that could promote membrane binding of the complex thus decreasing the activation energy necessary for this process. An elliptical prohibitin ring with an inner diameter of 160Å x 90Å would lead to a perimeter of approximately 816Å. 22 modelled prohibitin dimers would fit into the ring which is in agreement with Tatsuta and colleagues who proposed the presence of 16 to 20 molecules of both yeast prohibitin 1 and prohibitin 2 .

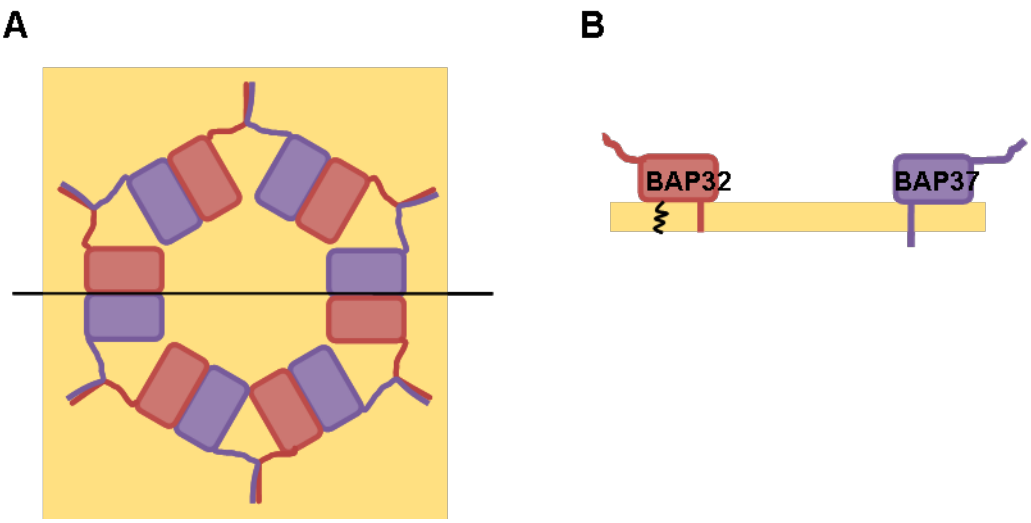

Figure -33: Suggested model of prohibitin dimer residing in the inner mitochondrial membrane. A – *Top view*: Ring-like assemblies are formed by hetero-dimeric building blocks consisting of BAP32 (red) and BAP37 (purple). B – *Side view*: Both proteins are anchored to the membrane via their N-terminal hydrophobic helices whereas the C-terminal helices are engaged in formation of inter-molecular coiled-coil structures. BAP32 potentially possesses a second membrane anchor, palmytoylated Cys69 (black wave).

The homology models generated in this work were used to depict the interaction of prohibitin 1 with melanogenin, to map interaction sites of target proteins on both prohibitins and to investigate possible posttranslational modifications.

Results from the docking studies of modelled PHB domain of BAP32 with melanogenin suggest that the larger pocket in BAP32 constituted by helix α1, and strands β5 and β4 is a likely binding pocket for melanogenin although the model does not explain the apparent discriminating effect of the fluoro-substituents in position 4 and 5 of the penta-fluoro-hydroxy-benzol group of melanogenin, but this might well be due to shortcomings of the homology model of the BAP32 PHB domain. A different conformation of amino acid residues in the area of the binding pocket might easily lead to a different conformation of the bound ligand, for example, a change of positions between the penta- and mono-fluoro-substituted ring systems.

Both prohibitin 1 and prohibitin 2 have been found to interact with a variety of proteins . In these studies, the respective interactions were described for only one of the prohibitin homologues. The interaction sites lie mostly within the PHB domain of the proteins and could be mapped onto the homology models. One could therefore speculate that a complex consisting of both prohibitins acts as a mediator between several proteins, such as Rb and E2F (interacting with BAP32) on the one hand, and ER receptor (interacting with BAP37) on the other. Furthermore, these functions might be activated by phosphorylation since some phosphorylation sites are situated in the proposed binding sites of Rb/E2F (see figure 2-22).

Interestingly, a recent study elucidating the mechanisms of a synthetic hemiasterlin variant identified the E130K mutation in prohibitin 2, located in the proposed Akt/ER binding site, to be responsible for the occurrence of multidrug resistance in a *Caenorhabditis elegans* model . Hemiasterlin is a naturally occurring peptidic toxin that interferes with microtubule dynamics and thus exerts antimitotic actions. A hemiasterlin analogue is currently being evaluated in clinical trials for cancer chemotherapy. The prohibitin 2 missense mutation confers drug resistance not only in the case of hemiasterlin, but also for other drugs binding to tubulin and camptothecin. While direct binding of hemiasterlin to prohibitin 2 is reported to be unlikely, the location of Glu-130 in the region of prohibitin 2 binding to Akt, MyoD and α-actinin might indicate the direction of further studies to elucidate the molecular mechanism.

The interactions of prohibitins with different proteins might be modulated by post-translational modifications within the PHB domain enabling a wide range of cellular functions. Phosphorylated species of prohibitins were found in 2D-gel electrophoresis experiments in plants , and it was also shown that purified JNK1 successfully phosphorylates prohibitin *in vitro* . Examination of the proposed PHB domain dimer model of BAP32 and BAP37 returns three possible phosphorylation sites in each BAP32 (T108, S109, T141) and BAP37 (T194, S190, S110), all being located within protein-protein interaction sites.

Bacher and coworkers reported that both isolated prohibitins, BAP32 and BAP37, preferably form homotetramers as well as calcium-independent heteromeric complexes.

Affinities for homo- and heteromers were reported in the order of 10^{-7} M . Potentially, BAP32 could form dimers via its cysteine residue in position 69 and is a substrate of a disulphide isomerise . Since BAP37 does not have any cysteine residues, the BAP32:BAP37 interactions cannot involve disulfide bonds. These findings remain to be elucidated further as homomers have not been reported in other contexts.

Structural information about the prohibitin complex at atomic detail will undoubtedly be useful in understanding the molecular mechanisms of protein turnover in mitochondria, as well as in structure-based lead compound discovery for novel drugs in a variety of diseases. It would also help to understand protein-protein interactions as seen in the nucleus, where the prohibitins seem to act as monomeric binding partners being engaged in gene regulation processes with respect to proliferation control.

Initial crystallisation trials did not result in the formation of crystalline material, most likely because the protein solution is not homogenous (presence of monomers and dimers), and the concentration is low. Improvement of protein production and purification protocols might result in higher refolding yield where isolation of the dimer would be feasible.

2.5 Interaction of prohibitins with *m*-AAA-proteases

It is known from previous studies that *m*-AAA-proteases interact with prohibitins but little is known about how this interaction is established . The highly conserved proteins are an interesting target in prohibitin research as they are thought to interact physically with the prohibitin complex. *m*-AAA-proteases display a three-divided topology: an N-terminus with two transmembrane segments, APTase domain and protease domain . In mitochondria, the poorly investigated N-terminus is thought to anchor the *m*-AAA-protease in the inner mitochondrial membrane possibly forming a loop in the intermembrane space. An interaction between the prohibitin complex and the *m*-AAA-protease could possibly be established either in the inner mitochondrial membrane via their respective N-termini or in the intermembrane space via the N-terminal loop of the *m*-

AAA-protease and the prohibitin PHB domain. Since no structural information is available about the intermembrane space (IMS) region of *m*-AAA-protease, thus, further investigation was focussed on this domain.

2.5.1 Multiple sequence alignment and secondary structure prediction

Sequences from *m*-AAA-protease subunits of FtsH (*E.coli*), Yta10 and Yta12 (yeast), AFL3G2 and paraplegin both from mouse and human were aligned using the programme ClustalW . Information about their secondary structure was gained either from crystal structures (FtsH ATPase domain, PDB accession number **1LV7**, and peptidase domain, PDB accession number **2DI4**) and/or PSIPRED secondary structure predictions. The multiple sequence alignment was adjusted to preserve structural features and conserved residues in the ATPase domain and protease domain. The remaining N-terminal sequences were analysed and compared both in their amino acid sequences and their predicted secondary structures. Interestingly, the N-termini of the aligned sequences showed high similarity in their secondary structure elements, and were therefore combined to a conserved secondary structure named intermembrane space (IMS) region. The IMS region consists of a hydrophobic α-helix (residues 3 to 21), a region of relatively hydrophilic residues structured in α-helices and β-sheets followed by another hydrophobic α-helix (residues 97 to 121). The first and last helices of the N-terminus are long enough to span a membrane and therefore are most likely transmembrane helices. In order to strengthen this hypothesis, the topology of FtsH as an integral membrane protein was predicted using MEMSAT . It revealed two possible transmembrane helices, one from amino acids 2 to 20 (in→out), the other spanning amino acids 97 to 124 (out→in). Therefore, both helices were annotated TM1 and TM2, respectively.

Figure 2-24 presents an overview of the topology of *m*-AAA-protease subunits summarising the new features that have been found in this study. The N-terminal IMS region is shown in cyan including the sequence alignment of different *m*-AAA protease subunits. The ATPase domain is depicted as a yellow diamond and the protease domain is shown as a green ellipsoid. The conserved secondary structure features of the IMS region are shown in the bottom line, α-helices (α) and β-sheets (β) are shown as red tubes or

green arrows, respectively, and are numbered accordingly. The sequence alignment included in figure 2-24 shows hydrophobicity of amino acid residues as varying degree from strongly hydrophobic (coloured in red) to strongly hydrophilic (in blue). The sequence alignment also shows that certain amino acid residues are either conserved or semi-conserved in nearly all aligned sequences revealing a consistent pattern in the properties of α-helices and β-sheets.

.

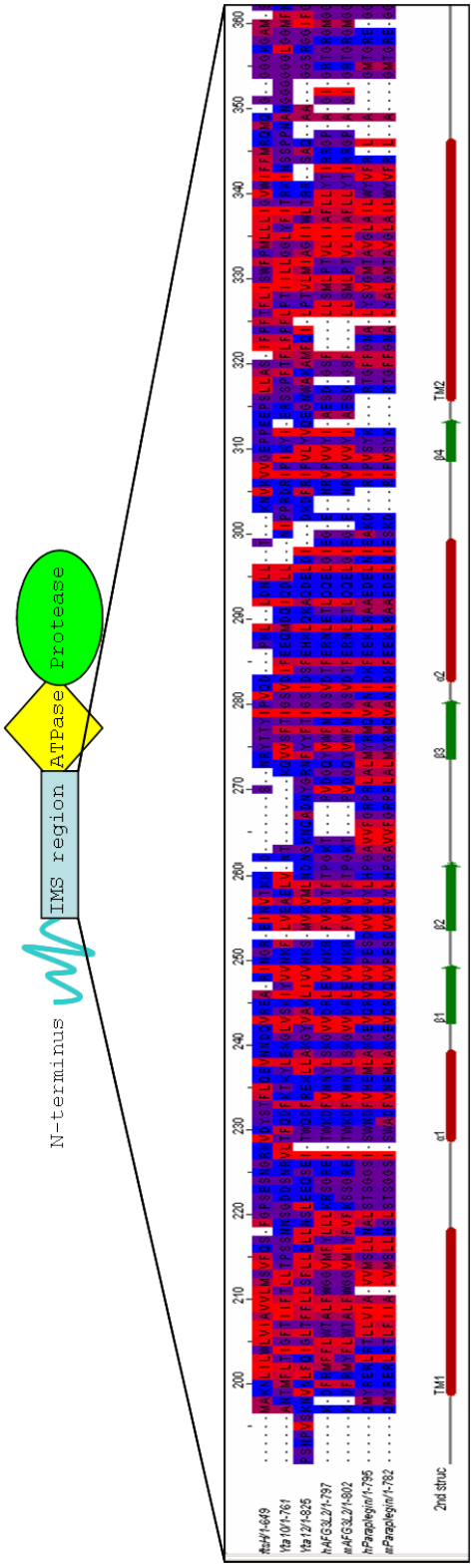

Figure 2-24: Identification of IMS region in m-AAA-proteases from different species. In the sequence alignment, hydrophobic residues are coloured in red and hydrophilic residues in blue. Secondary structure elements are depicted as green arrows (β-sheets) and red tubes (α-helices). Figure prepared with Jalview [1].

These findings led to the conclusion that the N-terminal regions of *m*-AAA-proteases might have a conserved fold that could provide a possible interaction interface for interaction with other proteins, and could therefore be important in exerting cellular functions. It is known that *m*-AAA-proteases interact with prohibitins in the inner mitochondrial membrane forming a large multimeric complex . A structurally defined N-terminal region of the *m*-AAA-proteases might be the key to answering the question of how this interaction might be established.

In the PDB, this domain is referred to as FtsH_ext for bacterial *m*-AAA-proteases (*E. coli* and *T. thermophilus*) but no structural information is available. In order to extend this term to include *m*-AAA-proteases from other species, this region will be called inter-membrane-space (IMS) region for the continuation of this work.

2.5.2 Cloning of FtsH-IMS region from E.coli genomic DNA

Genomic DNA from *E.coli* strain BL21(DE3) was isolated as stated in section 5.2.6., and used as template in a PCR reaction to gain the construct His_6-FtsH(20-97)_pRSET_C (see section 5.2.2.). The resulting protein has a molecular weight of 13488 g/mol including the hexa-His-tag and linker sequence.

2.5.3 Expression and purification of FtsH-IMS region

The IMS region of FtsH was expressed in BL21(DE3) cells (see section 5.3.1) and purified using immobilised metal chromatography and anion exchange chromatography (see sections 5.4.1. and 5.4.2.).

Figure 2-25, A, shows the result of the first purification step, immobilised metal chromatography, on an SDS-PAGE where the protein appears as a strong band near the lysozyme single marker band (14kDa) which has a similar molecular weight to the FtsH-IMS region. No protein was found in the flow through (FT). The protein was eluted from the column in fractions 10 to 17 which corresponds to imidazole concentrations of 0.12M to 0.18M. Fractions containing the protein showed other bacterial proteins at higher molecular weight which were separated in the next purification step, anion exchange chromatography.

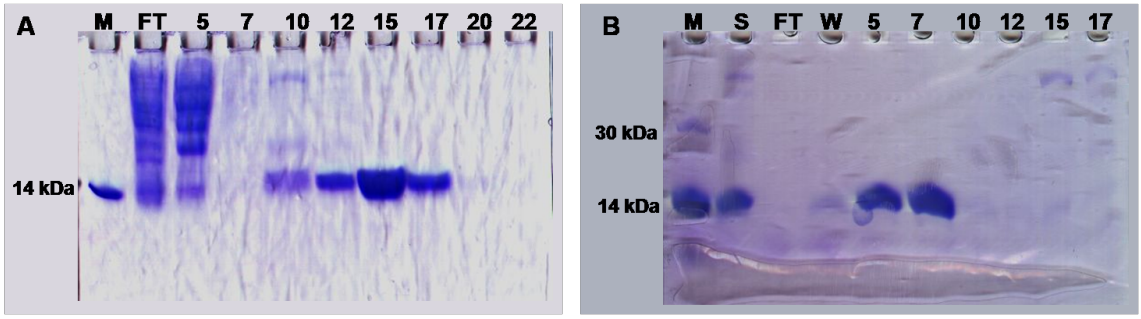

Figure -34: Purification of His_6-FtsH(20-97) using nickel affinity (A) and anion exchange chromatography (B). Gels show the marker (M) in lane 1, sample (S), flow through (FT) and wash (W) in following lanes. Elution fractions are labelled by their fraction numbers.

Results from anion exchange chromatography are shown in figure 2-25, B, where the protein appears as a strong band near the lysozyme marker. The sample (S) applied to the anion exchange column is shown in lane 2. No protein was found in the flow through of the column (lane 3, FT). After extensive washing of the column (lane 4, W), the eluted protein could be found in all fractions up to fraction 7 (lanes 5 and 6) corresponding to a NaCl concentration of up to 150mM. The other proteins eluted at a higher NaCl concentration and could thus be separated from the FtsH-IMS region. After pooling the fractions containing the protein, FtsH-IMS region could be concentrated up to 160mg/ml using Amicon Ultra concentration devices with 5kDa molecular weight cut off. The purity was determined to be greater than 95% as judged by SDS-PAGE.

2.5.4 Biophysical characterization

2.5.4.1 Mass spectrometry

The molecular mass of the purified protein was determined using mass spectrometry (MALDI-MS). Sample preparation and layout of the experiment were as described in section 5.7.1. The mass spectrum in figure 2-26 shows a single dominant peak at 13471g/mol which is in the range of the expected 13488g/mol. The protein could be identified as His_6-FtsH(20-97).

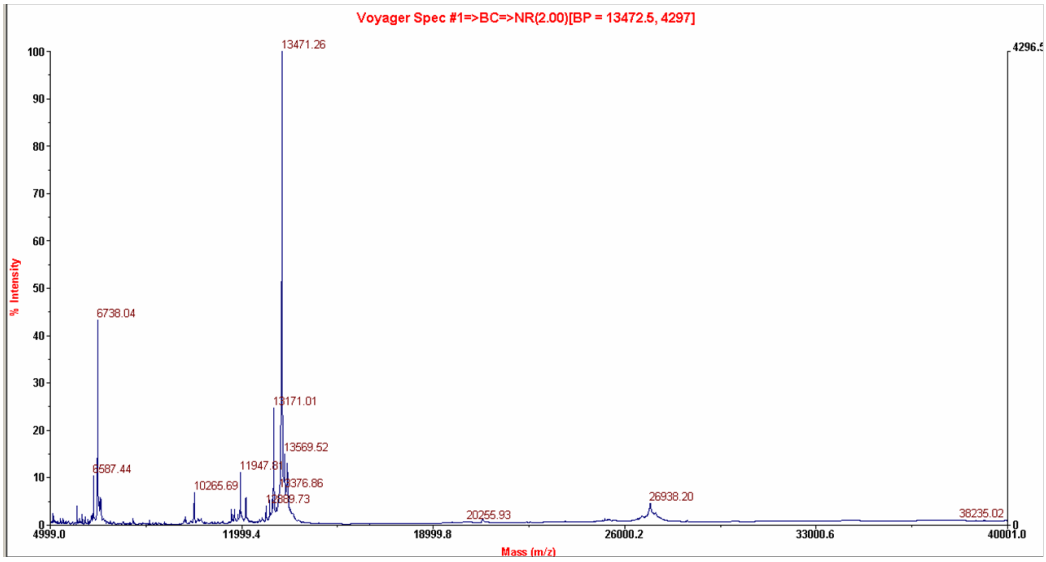

Figure -35: Mass spectrum of FtsH-IMS region. The single peak at 13471g/mol corresponds well with the expected molecular mass of 13488g/mol.

The identity of the protein fragment was verified by trypsin digest and subsequent analysis by mass spectrometry (see figure 2-27).

1	11	21	31	41	51
MRGSHHHHHH	GMASMTGGQQ	MGRDLYDDDD	KDRWIRPRDQ	SFGPSESNGR	KVDYSTFLQE
61	71	81	91	101	111
VNNDQVREAR	INGREINVTK	KDSNRYTTYI	PVQDPKLLDN	LLTKNVKVVG	EPPEEPS

Figure -36: Results from mass spectrometry of the trypsin-digested FtsH-IMS region. Protein residues in red were identified by mass spectrometry. Underlined residues indicate possible protease cleavage sites after basic residues according to trypsin specifity.

A custom search database had to be set up, because the FtsH-IMS region is a very small part of the full-length protein FtsH, and scores from the default set up were not sufficient to verify the identity of the FtsH-IMS region. The custom search database found that 64% (76 of 117 amino acids) of the peptides matched that of the protein (see figure 2-27).

2.5.4.2 Circular dichroism (CD)

CD spectroscopy was utilised to analyse the fold of the protein and its thermal stability. The fold of the protein was investigated by recording a CD spectrum and analysing it using the programme ACDP with implementations of two algorithms, K2D Neuronal Network and Linear Combination of Fasman Spectra, to predict secondary structure contents. Thermal stability of the protein was investigated by recording the change in the CD signal at a specific wavelength during heating of the sample.

2.5.4.2.1 Wavelength spectrum

The smoothed experimental spectrum from 260nm to 190nm in figure 2-28 (A) shows two minima at around 208nm and 222nm indicating the presence of α-helices. Furthermore, the spectrum reaches the positive at 196nm indicating a true fold of the protein.

A

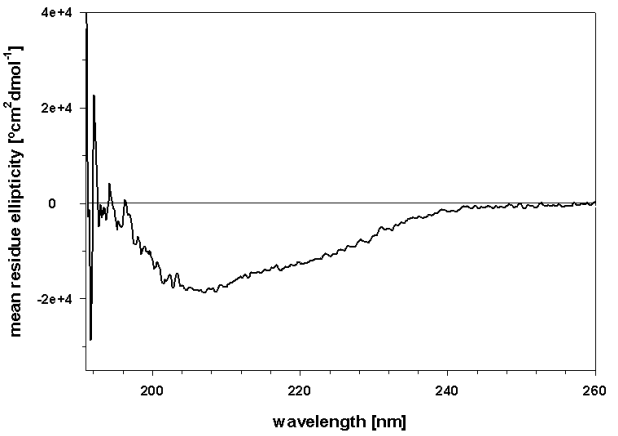

B

	K2D Neural Network	Linear combination of Fasman spectra
α-helix	0.287	0.07
β-sheet	0.272	0.38
unordered	0.439	0.55

Figure -37: CD wavelength spectrum (A) and secondary structure prediction (B) of FtsH-IMS region using the programme ACDP .

The spectrum was best described with a Fasman Fit giving a lower least squares error than the K2D Neural Network. The Fasman algorithm predicted 7% of the residues to be organised in an α-helix, 38% in a β-sheet and 55% to be unordered (see figure 2-28, B). Using the K2D neural network algorithm, an α-helix content of 28.7% and β-sheet content of 27.2% were predicted, 43.9% of the residues were predicted as unordered. Theoretical values for the ratio of residues in the respective structural element from the total number

of residues were calculated from PSIPRED secondary structure predictions. Here, 25.3% of the residues were predicted to be structured in α-helices, 37.3% in β-sheets and 37.3% as unordered. The α-helical content seems to be underrepresented in the Fasman calculation whereas the K2D fit is in better agreement with the PSIPRED secondary structure prediction despite a higher error.

2.5.4.2.2 Thermal denaturation

FtsH-IMS region was subjected to thermal denaturation from 20ºC to 90ºC as described in section 5.7.2. Unfolding experiments were monitored at 222nm which provided the greatest change in the CD signal during the denaturation process (see figure 2-29).
Three independent experiments were carried out, the data averaged and fitted using a sigmoidal equation in the programme Sigma Plot . The denaturation curve shows a two-state transition curve with a melting temperature, T_m, of 49ºC.

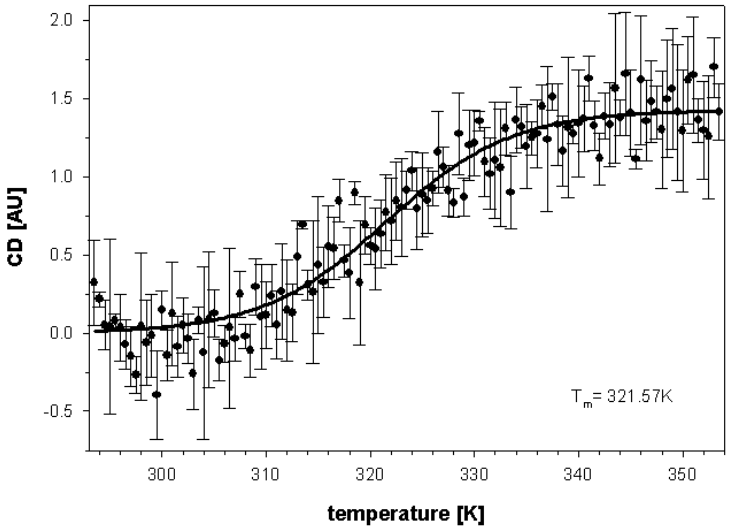

Figure -38: Thermal denaturation of FtsH-IMS region displays a two-state transition curve with a melting temperature T_m of 49ºC. Shown is the average of three independent experiments and their standard deviation.

2.5.4.3 Gel filtration analysis

The oligomerisation state of FtsH-IMS region was investigated using gel filtration analysis as stated in section 5.7.4. The absorption peaks were fitted using the programme PeakFit , and the positions of the peak maxima were determined.

Figure 2-30 shows a gel filtration run of FtsH-IMS region overlaid with a calibration run with Dextran Blue (2MDa), BSA (68kDa) and cytochrome C (12.4kDa). It reveals one peak which a shoulder which was fitted as two peaks with apparent molecular masses of 29kDa (peak 1) and 15kDa (peak 2) (see table 2-8).

Results suggest that the FtsH-IMS region eluted as a mixture of dimers and monomers with dimers as the predominant species (see table 2-8). As the protein was purified to 99% as judged by SDS-PAGE analysis, both peaks are resumed to represent oligomeric species of FtsH-IMS region. The oligomerisation state of the protein and its possible shape will be investigated in further experiments such as SAXS.

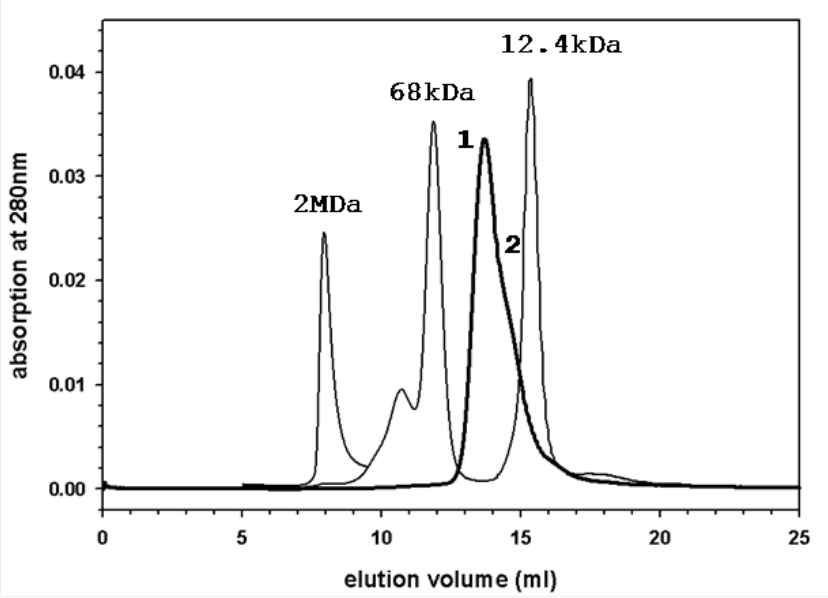

Figure -39: Gel filtration analysis of FtsH-IMS region. The major fraction of the protein eluted as peak 1 at an apparent molecular mass of 29kDa possibly representing a dimer. A second peak (peak 2) that is seen as a shoulder of the first peak eluted at 15kDa.

Table -14: Analysis of gel filtration experiment with FtsH-IMS region.

peak	elution volume	Apparent molecular	Apparent species

	[ml]	weight [kDa]	
1	13.7	29.3	dimer
2	14.7	15.2	monomer

2.5.4.4 Small angle X-ray scattering (SAXS)

SAXS analysis was used to gain information about the shape of the protein and to confirm the proposed dimer formation of the FtsH-IMS region. The experiment was carried out in the laboratory of our collaborator, Jan Pedersen (University of Aarhus, Denmark).

The sample showed aggregates which made analysis of the scattering curves difficult. The best set of data could be recorded using 5mg/ml of protein. After processing the data, they could be fitted with the programme GNOM which determined the molecular mass to be between 30.0kDa to 37.4kDa. Results indicate a protein dimer which is consistent with the gel filtration analysis.

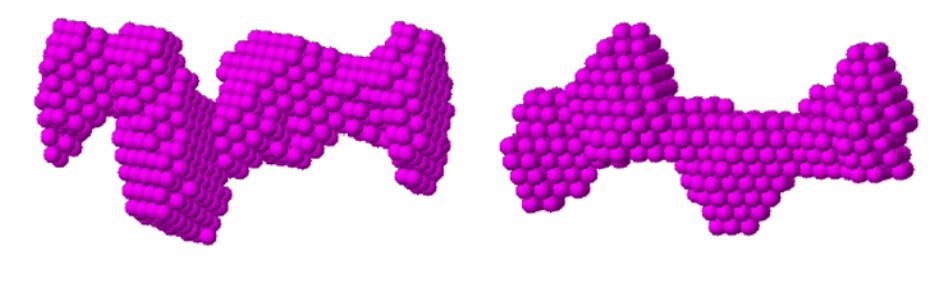

Figure -40: Shape restoration of FtsH-IMS region dimer using the programme Dammin .

Shape restoration from SAXS data was carried out using the dummy bead modelling program Dammin . The particle looks very much like a dimer and displays an elongated shape with a maximum radius, R_{max}, of 95Å. Figure 2-31 shows the reference model for 10 Dammin models found using data recorded with 5mg/ml protein.

2.5.5 Crystallization of FtsH-IMS region

The purified FtsH-IMS region was subjected to crystallisation trials but no crystals have been obtained so far.

2.5.6 Conclusions: FtsH-IMS region

In mitochondria, prohibitins have been found to physically interact with *m*-AAA-proteases forming a high molecular weight complex . The *m*-AAA-protease is anchored to the inner mitochondrial membrane by the N-terminal domain of its subunits, while the well conserved C-terminal ATPase and metallopeptidase domains protrude into the mitochondrial matrix . Although the X-ray structures for both the ATPase domain and protease domain have been solved , only little structural information is available on the N-teminal domain. In yeast, it is thought that both *m*-AAA-protease subunits, Yta10 and Yta12, anchor the protease to the inner mitochondrial membrane via two tramsmembrane helices . Interactions between the dimeric building blocks of BAP32:BAP37 and the *m*-AAA-protease could be established in either the membrane or the intermembrane space.

Comparing a multiple sequence alignment of different *m*-AAA-protease subunits with secondary structure predictions and available crystal structures revealed a high conservation of the ATPase and protease domains. Furthermore, another structurally conserved region was discovered: the N-terminal intermembrane space region referred to as FtsH-IMS region in this work. In order to investigate the structure of this region, the N-terminal region of FtsH (residues 20 to 97) was cloned, expressed and purified using immobilised nickel affinity and anion exchange chromatography. The identity of the protein was confirmed by mass spectrometry. The folding state of the protein was investigated by CD spectroscopy revealing α-helix and β-sheet contributions to the secondary structure indicating a folded state. Monitoring differences in the CD signal at 222nm, a two-state transition curve upon heat induced denaturation could be recorded suggesting one folding unit for the protein. The melting point of the protein was determined to be 322K (49ºC).

Gel filtration analysis revealed a major peak at an apparent mass of 29kDa, suggesting a FtsH-IMS region dimer as the predominant species in solution. As the theoretical molecular mass of a dimer is smaller than the value determined with gel filtration (27kDa), the dimer is likely to possess an elongated shape. To obtain information about its molecular shape, the protein was subjected to SAXS analysis. Fitting the SAXS data using

the programme GNOM and analysis by the programme Dammin confirmed a possible dimer formation. Here, the average molecular weight of the particles could be determined to be between 30 to 37.4kDa, which is in good agreement with findings in the gel filtration analysis. Using the SAXS data, a dimer was modelled with an elongated shape, and an R_{max} of 95Å was estimated but this is value is likely to be biased towards higher numbers due to the presence of aggregates in the solution.

Dimer formation of the IMS-region might give clues as to how the *m*-AAA protease is assembled in the inner mitochondrial membrane. Previous findings suggest that the protein is present as hexamers in the membrane which is thought to be important for its function . Furthermore, a varying composition of *m*-AAA-protease subunits within one hexamer was observed which, in combination with a proposed IMS-region dimer, leads to a model where the *m*-AAA protease might consist of three, possibly different, dimers of *m*-AAA-subunits.

Including findings from the present work in the existing knowledge of oligomer formation in the inner mitochondrial membrane, one could imagine a module that consists of a building block of BAP32:BAP37 and an *m*-AAA-protease subunit.

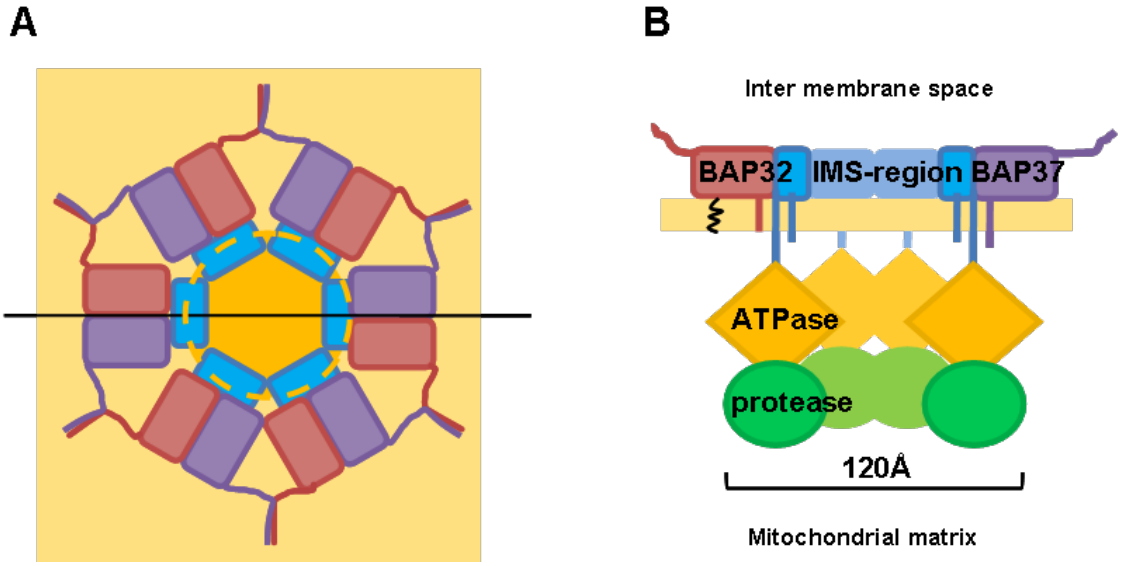

Figure -41: Suggested model of membrane-bound prohibitin and their interaction with *m*-AAA-protease subunits. A – *Top view:* The prohibitin hetero-dimer (red and purple) interacts with the IMS-region (cyan) of *m*-AAA protease (yellow) forming modules to build large assemblies in the membrane. B – *Side view*: The ring formed by BAP32, BAP37 and the IMS-region is anchored to the membrane via N-terminal hydrophobic helices of the three proteins and a possible additional anchor formed by the palmitoylated Cys69 of BAP32. The *m*-AAA-protease resides on the matrix-side of the membrane and is shown with its ATPase (yellow) and protease domain (green).

In this module, the inter-membrane-space regions of the *m*-AAA-subunits would interact with either BAP32 or BAP37 or both proteins and with themselves as indicated in figure 2-32. BAP32 (red) and BAP37 (purple) interact to form a dimeric building block. The N-terminal transmembrane helices of BAP32 (red) and BAP37 (purple) and of the *m*-AAA-protease (cyan) could interact with each other in the membrane, which would satisfy the need to mask the remaining exposed polar residues of the two prohibitin membrane helices. Additionally, the N-terminal IMS region of *m*-AAA-protease (cyan) which is exposed to the inter-membrane space might interact with the PHB domains of the BAP32:BAP37 building blocks. These proteins assemble to ring-like structures in the membrane which have an average inner diameter of 125Å . This value coincides nicely with the value for the diameter of the cytosolic region of the FtsH hexamer as had been found in the crystal structure, 120Å . Therefore, a model is proposed where the *m*-AAA-protease is located in the middle of the ring exposing the well conserved ATPase domain (yellow) and protease domain (green) to the other side of the inner mitochondrial membrane, to the mitochondrial matrix. It follows that the N-termini of BAP32 and BAP37 would point to the inside of the ring whereas the C-terminal coiled-coil regions would point away from the ring.

2.6 Concluding remarks on prohibitins and outlook

The main goal of this work was to gain insights in the molecular structure of prohibitins and their complex formation. Both proteins were produced as recombinant proteins in *E. coli*, refolded into the stable complex and their biophysical properties analysed. Refolding of N-terminal truncation mutants gave a refolding yield of 33%, and provided protein suitable for analysis employing spectroscopical methods such as CD. Replacement of the hydrophobic N-terminal helix with an artificial self-folding soluble helix did not lead to

successful refolding of the complex possibly due to misfolding of the artificial helix or interference with the folding process of the protein.
In a recent study, EA repeats located C-terminal of the PHB domain were found to be important for oligomerisation . BAP32 possesses four EA-repeats in the C-terminal coiled-coil region, the first being located at position 181/182. The first of five EA-repeats of BAP37 is located at position 198/199. In the present work, C-terminal truncation mutants of BAP32 and BAP37 were generated excluding the EA-repeats which might have caused those proteins to fail to refold. Truncation of the C-terminal region is desirable as coiled-coil regions tend to stick to artificial membranes, e.g. in concentration devices. Therefore, constructs of BAP32 and BAP37 including residues 181/182 (BAP32) and residues 198/199 (BAP37) might lead to refolding of proteins with improved suitability for concentrating.
Furthermore, the refolding protocol could be optimised in the future also including binding partners that have been identified in functional studies such as the pro-apoptotic peptide or the *Salmonella* polysaccharide . Although the main aim, crystallising the protein complex, was not achieved, valuable information could be obtained from biophysical studies. In future studies, the refolded full-length prohibitin complex could be analysed as to its ability to bind to lipid layers using a Langmuir surface film balance. The proposed dimer formation of the N-terminal helices of both prohibitins in the inner mitochondrial membrane could also be assessed by experiments using a Langmuir balance. In this context, the proposed oligomer formation with transmembrane helices from *m*-AAA-proteases could also be investigated. Modelling of *m*-AAA-transmembrane regions and elucidation of a possible interaction interface with the prohibitin transmembrane dimer that was already modelled might give first insights as to whether an interaction is likely.

PHB domains of BAP32 and BAP37 were subjected to molecular modelling using the NMR structure of mouse flotillin-2 (PDB accession number **1WIN**) as template. Manual dimerisation of the modelled PHB domains according to findings from cross-linking experiments gave first insights in how a prohibitin dimer might look like. This prohibitin

dimer would be the building block that can assemble large prohibitin oligomers. The interaction with *m*-AAA-proteases in the inner mitochondrial membrane could either be mediated via their N-terminal membrane helices or via a newly found structural feature within *m*-AAA-proteases, the IMS region. This region is predicted to possess a distinct fold conserved in many *m*-AAA-proteases, and was investigated further.
FtsH-IMS region could be purified to over 95% purity, and was subjected to CD spectroscopy, gel filtration and SAXS experiments. In CD experiments, FtsH-IMS region appears as a single folding unit although formation of dimers in solution was proven by gel filtration and SAXS. In future studies, gel filtration experiments under different buffer conditions could be carried out to gain information about the nature of the dimer interaction interface. Gel filtration under high salt conditions such as 1M NaCl would disrupt interactions via salt bridges whereas SDS would disrupt hydrophobic interactions. Furthermore, the interaction interface of the FtsH-IMS region monomers could be mapped by subjecting the purified dimer to cross-linking experiments, subsequent trypsin digest and mass spectrometry. Crystallisation trials were set up but did not lead to crystal formation. Another method to gain information about the three-dimensional structure of FtsH-IMS region would be to perform NMR experiments. Once an experimental three-dimensional structure could be obtained, intermembrane regions of other *m*-AAA-proteases such as paraplegin, AFG3L1 and AFG3L2 could be modelled using the experimental three-dimensional structure of FtsH-IMS region as template. Subsequent docking studies could then be used to investigate a possible interaction between prohibitin PHB domains and *m*-AAA-protease IMS regions.

Proposed functions for the prohibitin complex include regulation of *m*-AAA-proteases in the inner mitochondrial membrane, scaffolding functions in the mitochondrion, gene regulation in the nucleus and exposure as an extracellular receptor. Investigations into the structure and biophysical properties of the prohibitin complex might give important clues to their true function in the cell and their mechanism of interaction with other proteins, sugars and small molecules. The modelled prohibitin dimer generated from the modelled PHB domains was used to elucidate possible interaction interfaces with their proposed

interaction partners. Results showed that the dimer could interact with different nuclear target proteins at the same time, and could thus serve as a mediator for gene expression in the cell.

Prohibitins exert basic functions in the cell, and are therefore considered as potential drug targets in various diseases such as adiposity, diabetes and cancer, especially sporadic breast cancer. While the prohibitin proteins are involved in cell cycle regulation, senescence and morphological change of mitochondria under oxidative stress, the 3'UTR of its mRNA is thought to be responsible for its function as tumour suppressors. It is not clear whether the prohibitin mRNA interacts directly on the DNA causing silencing of genes needed for progression into the S-phase or via formation of an RNA-protein complex. In this context, the term riboregulator was introduced to describe cellular effects caused by prohibitin mRNA . Experimentally, a pull-down assay could be performed where the 3'UTR of the mRNA is covalently bound to a matrix and the binding proteins are extracted from cytosolic or nuclear fractions. Proteins identified by this method would be good targets for developing anti-cancer drugs besides providing insights into cancer development.

2.7 References

PART B

Biochemical and structural characterisation of Annexin B1

Table of contents

PART B: Biochemical and structural characterisation of Annexin B1

3 Introduction to Annexin B1

3.1 Annexins in plant and animal kingdom

Annexins are water-soluble, calcium-dependent phospholipid binding proteins. Members of the annexin family are ubiquitously distributed in different tissues and cell types of higher and lower eukaryotes. To date, more than 160 unique annexin proteins have been found in more than 65 different species ranging from fungi and plants to non-vertebrates and higher vertebrates . More than one thousand proteins of the annexin superfamily have been identified in major eukaryotic phyla, but annexins are absent from yeasts and prokaryotes. A recent review by Moss and Morgan classes annexins in five subfamilies A to E . Annexins common to vertebrates were summarised in the annexin subfamily A; other annexins have been assigned to subfamilies B (invertebrates), C (fungi and some groups of unicellular eukaryotes), D (plants), and E (protists). At least 40 additional subfamilies await formal classification into these families. Most eukaryotic species have one to twenty annexin (*ANX*) genes; even the primitive unicellular protist *Giardia* has at least seven . The 12 human annexin genes range in size from 15kb (*ANX*A9) to 96kb (*ANX*A10) and are dispersed throughout the genome on chromosomes 1, 2, 4, 5, 8, 9, 10 and 15 . Annexins display a high level of conservation throughout their amino acid sequences. The overall three-dimensional structure is divided into a C-terminal core domain and the N-terminal domain. The N-terminal domains of annexins are highly variable and confer specific properties to each particular protein.

Implications of annexin proteins for health and disease are increasingly being appreciated, and the term ‘annexinopathies’ has been put forward for annexin-related diseases . The importance of annexins A1 for inflammation and annexin A2 for plasminogen-dependent fibrinolysis has long been acknowledged, and in recent years, the role of membrane-bound annexin A5 as a protective shield has clarified the molecular mechanisms of its

anticoagulant properties . Altered gene regulation and/or distribution of annexins have been observed for a variety of conditions.

Annexins were also found in parasitic organisms where they might be located extracellularly and thus could be involved in host attachment and invasion. Annexin B1 had recently been identified in the larval stage of the porcine tapeworm *Taenia solium* . First applications were focussed on the ability of annexin B1 to displace phospholipid-dependent coagulation factors and to prolong clotting times of human serum emphasising its potential for antithrombotic treatments. The combination of thrombus-targeting and thrombolytic properties has also been suggested for the protein . Possessing anticoagulant activity, this protein carries a significant therapeutic potential due to its thrombus-targeting and thrombolytic properties.

3.2 Structural features

3.2.1 Four-helix-bundle repeat and calcium binding sites

In 2001, Pidcock and Moore conducted a study investigating metal binding sites in proteins as observed in different crystal structures . Interrogation of files deposited in the protein data base (PDB) in the years between 1994 and 1999 revealed 515 crystal structures of calcium-containing proteins. Forty of the final 44 data sets with a resolution better than 2.3Å were selected for further analysis, and three general types of calcium binding sites in proteins were identified. Type I calcium binding sites bind calcium ions with a continuous short sequence of amino acids similar to those seen in lectins, human α-lactalbumin and flavodoxin. The type II binding site in contains a main binding sequence and an additional amino acid far removed from the main binding sequence. This type of motif can be found in annexins, amylase and collagenase. In the third category, type III calcium binding sites, the residues involved in calcium binding are remote from one another in the sequence, as exemplified by adamalysin. Calcium binding sites are generally located at the protein surface and in regions of loops or turns.

All annexins share a C-terminal core region in the shape of a slightly curved disc made up of four similar domains. Each domain is approximately 70 amino acids long and generated by five α-helices, termed A to E. Figure 3-1 shows the ribbon diagram of full-length annexin A5 and the calcium-binding sites on the convex side of the protein (PDB accession number 1AVR).

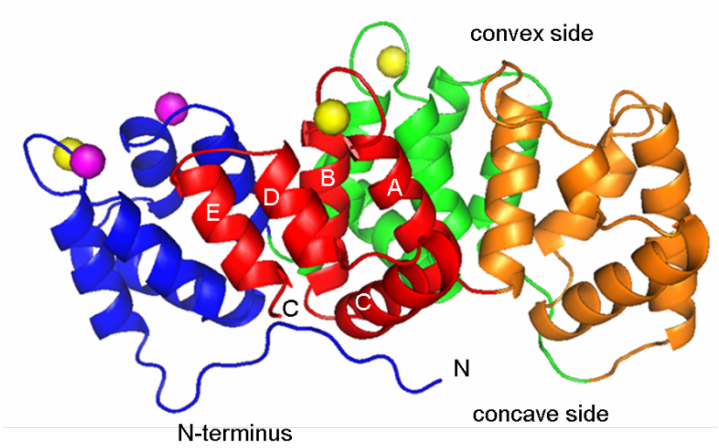

Figure -1: Ribbon diagram of human annexin A5 (PDB accession number **1AVR**). Calcium ions in type II calcium binding sites are represented by yellow spheres, Calcium ions in type III calcium binding sites are represented by magenta spheres. Domains I to IV are coloured in blue, green, orange and red, respectively. Numbering of helices A to E is shown exemplarily on domain IV.

Annexins possess both type II and type III calcium binding sites but the type II sites remain the main structural feature. Its binding motif is formed by residues from loops between helices A/B and D/E. Type II calcium binding sites can be found in each of the four domains, and are characterised by the endonexin sequence K-G-X-G-T residing in the loop between helices A and B. Additionally, an amino acid residue possessing bidentate properties, such as aspartic acid (D) or glutamic acid (E), and sitting 38 residues along the protein backbone is necessary to complete the endonexin sequence (see figure 3-2). In the type II calcium binding site the calcium ion is coordinated by main chain oxygens from residues in the endonexin sequence, two water molecules and the two oxygens from the acidic residue.

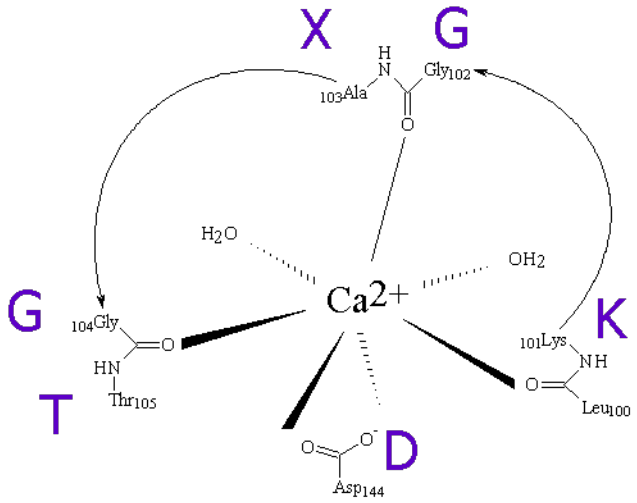

Type II calcium binding site:
Endonexin sequence
K-G-X-G-T-{38}-D/E

Figure -2: Type II calcium binding site formed by the endonexin sequence in annexins. The calcium ion is coordinated by main chain oxygens, two water molecules and an amino acid with bidentate features.

The type III calcium binding site is mainly found in the loop between helices D and E of each annexin domain. Calcium ions in the traditional type III calcium binding site are coordinated by two backbone carbonyl oxygen atoms, one acidic residue located approximately eight residues downstream in sequence and one to three water molecules.

The ubiquity and versatility of annexins suggest some fundamental role for the unique C-terminal core domain in cellular physiology, possibly involving adhesion mechanics, membrane traffic, signal transduction and/or developmental processes. The core domains of most vertebrate annexins have been analyzed by X-ray crystallography, revealing a great conservation of their secondary and tertiary structures despite only 45-55% amino-acid identity among individual members. Annexin B1 shares 35% amino acid identity with hydra annexin B12 and human annexin A5, and molecular modelling suggests a similar three-dimensional structure as observed with other annexins .

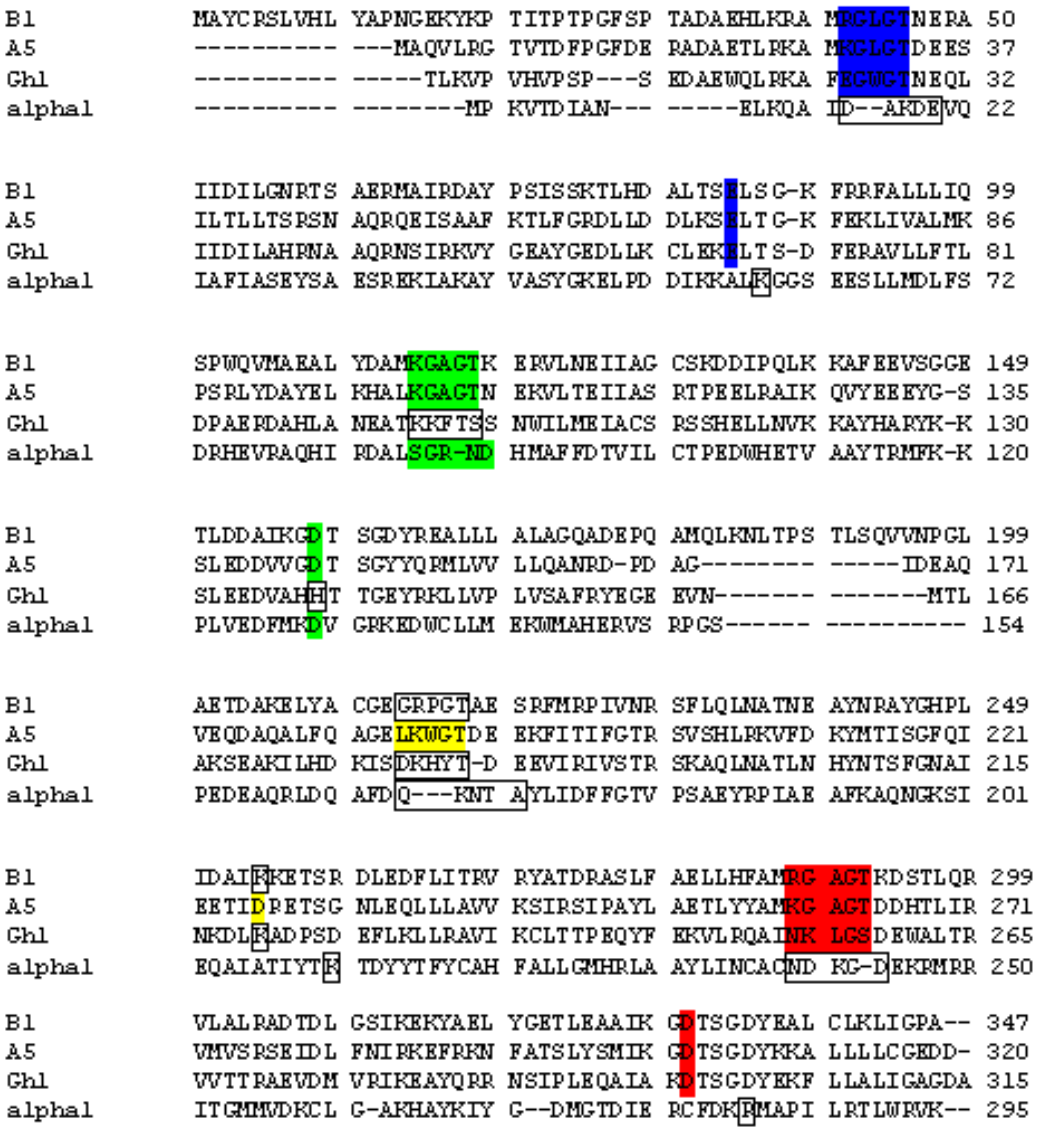

Figure -3: Alignment of annexins from different species and indication of their type II calcium binding sites. Type II calcium binding sites of annexins B1, A5, Gh1 and α-1 giardin are highlighted in blue, green, yellow and red, respectively. Dysfunctional calcium binding sites are shown as boxed residues.

Figure 3-3 shows a sequence alignment of annexin B1, mammalian annexin A5, plant annexin Gh1 and α-1 giardin from the protozoan *Giardia lamblia*. These annexins are members of annexin subfamilies B, A, D and E. Their functional type II calcium binding sites are highlighted by colouring the respective residues whereas non-functional binding

sites are indicated by boxed residues. Distinct features of annexin B1 include the slightly longer N-terminal domain (about 30 amino acids as compared to α−1 giardin), as well as an extended connector region between repeats II and III. The connector region of this protein comprises 30 amino acids compared to annexin A5 which has a connector of 14 residues.

3.2.2 Conservation of type II calcium binding sites in annexins

Mutations of the acidic residue disrupts the type II calcium binding sites in some annexins which, as a consequence, show altered calcium binding behaviour with great consequences for their cellular functions.

Mammalian annexin A5 is the only annexin shown in the multiple sequence alignment (figure 3-3) that possesses four intact type II calcium binding sites. In annexin B1, the calcium binding site in domain III is disrupted due to a lysine instead of an acidic residue in position 254 preventing a calcium coordination by the endonexin sequence . The plant annexin Gh1 from cotton possesses only 2 intact binding sites in domains I and IV, and α-1 giardin has only one in domain II. Strikingly, the type II calcium binding sites seem to be conserved to varying degree in different subfamilies. Mammalian annexins generally possess four intact calcium binding sites, whereas annexins from subfamily B possesses only three. Plant annexins of subfamily D have two functional calcium binding sites and annexins E only one or none (see figure 3-4).

		Domains				
		I	II	III	IV	
ANXA1 – A11, ANXA13	**A5**	+	+	+	+	mammals
ANXB1 – B21	**B1**	+	+	-	+	invertebrates
ANXC1 – C6						fungi
ANXD1 – D16	**Gh1**	+	-	-	+	plants
ANXE1 – E5	**α1-giardin**	-	+	-	-	protist

Figure -4: Functionality of type II calcium binding sites in different annexin subfamilies. Annexins from different sub-families A to E and one representative member are shown in blue (mammals), brown (invertebrates), black (fungi), green (plants) and yellow (protists). The predicted presence of type II calcium binding sites in each domain is indicated by "+".

This is of course a generalisation observed in a large number of members of the respective subfamilies and should therefore be treated with caution. Despite exceptions that can be found in each subfamily, a general tendency remains striking and may be worth further investigation with respect to evolution of calcium binding mechanisms in annexins.

3.2.3 Oligomer formation in annexins

Annexins are preferably monomeric cytosolic proteins, although higher oligomers have also been found. In 2002, Hofmann and colleagues investigated oligomer formation in plant annexins and observed a trimer formation of up to 80% in solution with annexins 23(Ca38), 24(Ca32), and Anx(Gh1) in gel filtration experiments. For Anx(Gh2), analytical gel filtration indicated the presence of a dimeric species in solution. The presence of calcium quantitatively suppressed oligomerisation and yielded almost pure monomer. In sedimentation equilibrium experiments, monomer–trimer equilibriums were found where the trimer constitutes 55% to 65% of the total protein content in standard

buffer conditions. Association constants range from 0.9×10^{-10} M^2 to 1.7×10^{-11} M^2 at protein concentrations of about 1mg/ml. Both ultracentrifugation and gel filtration results suggest that plant annexins investigated in that study exhibit calcium-independent self-association.

This behaviour certainly distinguishes the plant members of the annexin family from their mammalian counterparts. The oligomerisation states of mammalian annexins A1, A4, A5, A6, the heterotetramer [AnxA2 p11]2 , and annexin A7 have been investigated in solution using ultracentrifugation techniques. For all of these proteins, formation of a calcium-dependent monomer–dimer equilibrium has been observed with weak association constants in the range of 10^{-3} M. These studies were carried out using sedimentation equilibrium experiments in the presence of 10mM $CaCl_2$. Annexin A1 was found in preparations from human placenta where the dimer is particularly abundant accounting for approximately 20% of the protein. Here, the dimer consists of two covalently linked monomers probably generated by a transglutaminase. Annexin B12 undergoes a transition from soluble monomer to membrane surface trimer upon addition of calcium at neutral pH. Although annexins are generally water-soluble cytosolic proteins, AnxB12 was found to be membrane-inserted at pH 4.5 and present as a monomer in its transbilayer form . Anx A4 and Anx A5 have also been found to show trimerisation upon calcium-dependent binding to membranes.

3.3 Role and functions in the cell

Annexins are generally cytosolic proteins, although some, such as annexins A11 and A2, have been found in the nucleus under particular circumstances . The expression level and tissue distribution of annexins span a broad range, from abundant and ubiquitous (annexins A1, A2, A4, A5, A6, A7, A11) to selective or restrictive such as annexin A3 in neutrophils, annexin A8 in the placenta and skin, annexin A9 in the tongue, annexin A10 in the stomach and annexin A13 in the small intestine .

Members of this family are versatile adapter and regulator proteins in membrane-associated processes. Accordingly, a role in endo- and exocytosis has been assigned for

many annexin proteins such as annexins A1 to A4 and A13 . Despite being intra-cellular proteins, extra-cellular functions have also been described for several annexins. While annexin A2 is known to act as a co-receptor for plasminogen and tissue plasminogen activator on the surface of endothelial cells , annexin A1 has been observed to bind to an extra-cellular domain of β2 integrin . Annexin A5 was found to bind to the intra-cellular part of the β5 integrin receptor subunit . Annexins A2 and A5 have repeatedly been reported to act as cellular receptors for cytomegalovirus and hepatitis B virus , although this is still a matter of discussion within the community. Frequently, annexins are found to interact with cytoskeletal proteins. Annexins A1 , A2 , as well as the plant annexins p34 and p35 from tomato , exhibit binding to F-actin, while others, for example plant annexins from corn , bell pepper and cotton , tested negative in this context. Interactions between annexin A1 and profilin have also been demonstrated .

Interactions are either mediated through their C-terminal core domain or their N-terminus. The C-terminal core domain with its four repeats of five α-helices is conserved in all annexins exerting similar functions such as calcium- and phospholipid-binding. In contrast, the N-terminus is unique to each protein and thought to be responsible for the wide range of functions observed with annexins. In vertebrate annexins, its size varies from 11 to 19 residues (annexins A3 to A6, A10, A12, A13), 33 and 42 residues (annexins A2 and A1) to more than 100 residues in annexins A8 and A11. The N-terminal domain harbours binding sites for other proteins (annexins A1, A2, A11) and phosphorylation sites (annexins A1 and A2). As well as using their N-terminal domains, annexins also employ posttranslational modifications to specify their interactions such as phosphorylation, myristoylation and surface remodelling.

3.3.1 Calcium dependent membrane binding

It is known that annexins bind to liposomes in the presence of calcium (reviewed in). This feature implicates annexins in platelet activation and coagulation as well as membrane association. Cryoelectron and atomic force microscopy of annexins bound to model membranes have provided compelling images of the proteins forming two-dimensional lattices of membrane domains organizing the interface between the cytoplasm (or

cytoskeleton) and the cytoplasmic face of cellular membranes (reviewed in). Thus, a potential role in membrane scaffolding has been proposed.

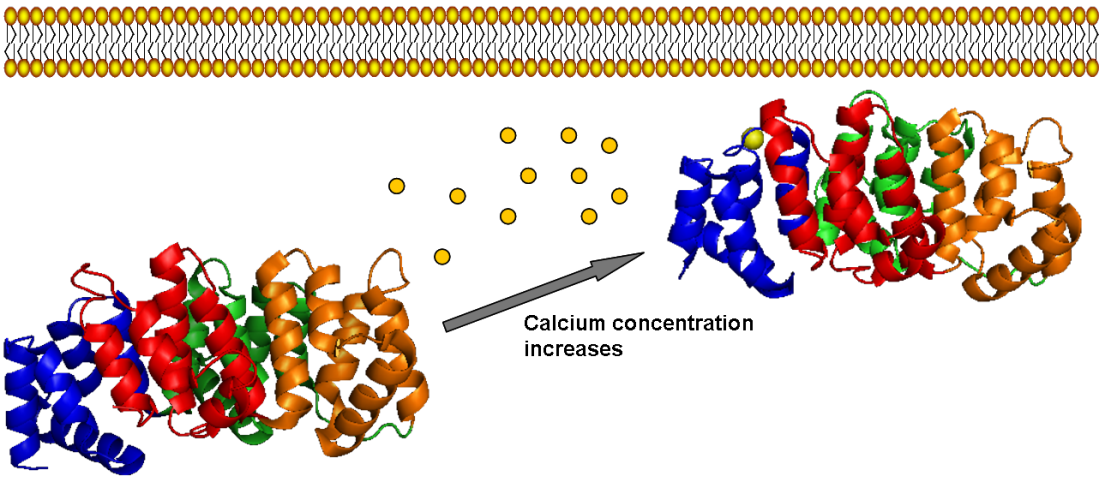

Figure -5: Calcium-dependent membrane binding of annexins. Annexins bind to phospholipid membranes upon an increase in the calcium concentration in the cell. Shown is annexin α-11 giardin from G*iardia lamblia* in its apo form (PDB accession number **2II2**) and its calcium-bound state (PDB accession number **2IIC**). Domains I to IV are highlighted in blue, green, orange and red, respectively, and calcium ions are shown in yellow.

As most annexins reside in the cellular cytosol, their membrane binding and membrane-domain organizing function must be activated. Intracellular calcium mobilization induced by various stimuli triggers recruitment of annexins to membranes in several cell models (see figure 3-5). The free Ca^{2+} concentration required for membrane translocation differs between different annexins (see). These findings connect calcium-induced membrane binding of annexins to calcium signalling in the cell. However, although Ca^{2+}-dependent phospholipid binding is shared by all annexins, individual members differ significantly in their Ca^{2+} sensitivity and phospholipid headgroup specificity.

Calcium-dependent membrane binding is mediated through calcium ions that are coordinated in type II or type III calcium binding sites. Mammalian annexins seem to rely almost entirely on a calcium-mediated binding mode regardless of the vesicle composition . The protozoan annexin α-11 giardin does not posses any proposed type II calcium binding sites, and was recently crystallized with one calcium ion coordinated in a type III

calcium binding site (PDB accession number 2IIC) . Emphasis on the importance of this structural feature with respect to its functional aspects was taken when this protein was found to be unable to bind to phosphatidyl-serine (PS)/phosphatidylcholine (PC) (1:5) vesicles *in vitro* . However, recent findings suggest that some plant annexins employ a second, calcium-independent mechanism that may utilise conserved exposed surface residues . A large number of reports analyzing Ca^{2+}-regulated phospholipid binding of annexins *in vitro* have been published underlining diverse functions in structural organization of the cell, intracellular signaling by enzyme modulation and ion fluxes, growth control, and action as atypical calcium channels .

Recent studies revealed a participation of the N-terminal domain in membrane binding which was influenced by the presence of calcium ions. In annexin A3, the local mobility of Trp5 of the N-terminus is increased by calcium binding whereas interaction of the protein with membranes reduces the Trp5 mobility back to its level in the absence of Ca^{2+} . Annexin A1 undergoes a conformational change upon Ca^{2+}-dependent binding to lipid bilayers exposing a secondary, less headgroup-specific binding site . When great differences were observed in X-ray structures of annexin A1 including (PDB accession number 1HM6) or lacking (PDB accession number 1AIN) its N-terminal region, an involvement of the N-terminal domain in this new lipid binding mechanism was evident. In the absence of calcium, the amphipathic α-helix of N-terminal domain is buried in the core domain causing a large conformational change and disabling the type II calcium binding site. Upon calcium and membrane binding, the N-terminal domain becomes solvent exposed and engages in membrane aggregation whereas the type II calcium binding site of repeat III regains its original conformation .
These findings indicate a conformational change of the protein both upon calcium binding and membrane binding.

3.3.2 Calcium dependent heparin binding

The glycosaminoglycan heparan sulphate is ubiquitously distributed on the surface of cells and acts as a regulator of ligand-receptor encounters , promotes protein assembly and thus

coordinates a variety of cellular functions. Heparan sulphate has a variable heparin-like structure but more N-acetylated and less N- or O-sulphonated groups than heparin. Heparin itself is a highly potent anticoagulant due to its ability to activate serine protease inhibitors such as antithrombin .

Several annexins, including annexins A1 , A2 , A4 , A5 , A6 and Nex-1 , are known to possess glycosaminoglycan-binding properties. In 2003, Weiland and colleagues found that α-1 giardin, an annexin from the parasite *Giardia lamblia*, displayed Ca^{2+}-dependent binding to glycosaminoglycans (GAGs), in particular heparan sulphate, a common GAG in the intestinal tract . In immuno-EM experiments and immunofluorescence studies, this immunodominant GAG-binding protein localised to the plasma membrane with some protein on the extracellular side during the early stages of the parasite infection implicating involvement in parasite-host attachment.

Crystal structures in complex with heparin-derived tetrasaccharides (HTS) have been published for annexins A2 (PDB accession numbers 2HYU, 2HYV and) and A5 (PDB accession number 1G5N and). The crystal structure of complexed annexin A5 revealed two binding sites, a calcium-mediated binding site residing on the convex side (HTS-1) and a calcium-independent site on the concave side (HTS-2) of the protein (see figure 3-6). Apart from involving calcium ions in HTS binding, the HTS-1 site has another important determinant: a basic cluster residing near the calcium binding loops IAB and IDE of domain I including the residues Arg25, Lys29, Arg63 and Arg151. This site is mainly involved in binding heparin once the initial recognition and binding of heparin has occurred via the HTS-2 binding site at residues Arg207 and Arg208. A proposed third heparin binding motif that was not complexed with HTS in the annexin V crystal structure lies on the concave surface and includes Arg-285, Lys-286, Arg-289 and Lys-290.

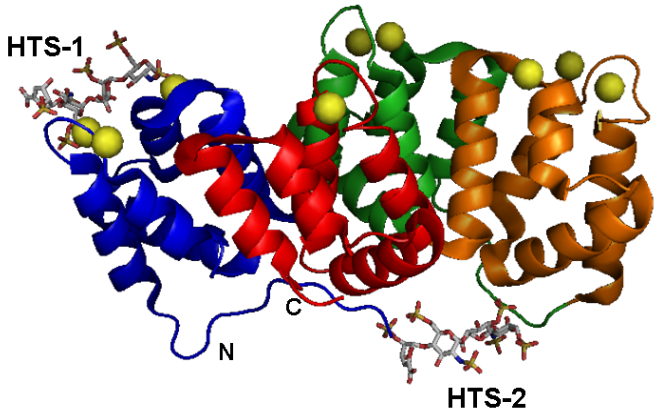

Figure -6: Crystal structure of annexin A5 in complex with two heparin tetrasaccharides (PDB accession number **1G5N**). Annexin domains are coloured in blue, green, orange and red, calcium ions are shown as yellow spheres. The heparin tetrasaccharides are bound on opposite sides of the protein (HTS-1 and HTS-2).

Subsequent binding of annexin A5 to the membrane surface would release the glycosaminoglycan from the HTS-1 site since its affinity for the phospholipid membrane is considerably higher . In this latter state, the protein is attached to the membrane surface via its convex site and the heparin is bound with the binding sites only on the concave side.

In that study, Capila and coworkers also presented a model where the heparin chain is wrapped around the annexin molecule occupying both binding sites. While binding of the carbohydrate to the site on the concave surface of the protein most likely does not interfere with the essential annexin-membrane association, the site on the convex surface would be affected by membrane binding.

However, *in vitro* studies showed that heparin binding cannot compete effectively with phospholipid membrane binding to annexin A5 . Therefore, heparin might be displaced from the binding site on the convex surface of annexin A5 by phospholipid molecules, e.g. when membrane binding occurs. In the soluble state, calcium binding contributes to the overall affinity of the annexin A5-heparin interaction. Thus, the annexin A5 -heparin interaction is calcium-dependent *in vitro*, but is thought to carry less significance *in vivo* .

In contrast, heparin binding to annexin A2 occurs only on one binding site on the convex side of domain IV . In this study, three heparin oligosaccharides (tetramer, hexamer, octamer) were co-crystallised with annexin A2. All oligosaccharides were bound near the IV-AB and IV-DE loops mainly involving the first four to five non-reduced heparin residues. Residues six to eight were not observed in the crystal structures indicating that only the first four residues from the non-reducing end are critical for heparin recognition and binding. Comparing their findings with results from the previously published study by Capila and coworkers , Shao and colleagues concluded that calcium-dependent heparin binding can arise from two mechanisms: calcium-dependent conformational changes in the protein that produce a favourable heparin-binding site (indirect mechanism), and/or a protein-calcium-heparin ternary complex formation (direct mechanism). Both mechanisms are evident in the annexin A2-heparin oligosaccharide complexes involving different calcium ions on the protein surface . The crystal structure of annexin A5 in complex with Ca^{2+} and heparin tetrasaccharide shows a calcium-dependent mode of oligosaccharide binding that is very similar to the indirect mechanism observed in annexin A2. In the annexin A5-heparin-tetrasaccharide complex, the oligosaccharide does not coordinate the protein-bound calcium ion but instead binds solely to protein atoms residing in a conformationally sensitive I-AB Ca^{2+}-binding loop. The Ca^{2+}-independent annexin A5-oligosaccharide binary complex occurring on the concave surface of that protein is not observed in the annexin A2 crystal structures. Heparin-binding sites at this location may be precluded in annexin A2 as a consequence of A2t heterotetramer formation, which involves the concave side of the protein surface .

3.4 Parasite annexin B1 and its medicinal potential as a drug target

In an attempt to find novel antigens for vaccine development against cysticercosis, annexin B1 from *Cysticercus cellulosae* had originally been identified by immunological screening of a *C. cellulosae* expression library . In this study, *Cysticercus*-infected serum

from both pigs and humans recognized annexin B1 indicating an extracellular location of this protein.

Cysticercosis, the common parasitic infection induced by a larval stage of *Taenia solium*, seriously affects human health manifesting itself mostly in causing inflammatory reactions in the central nervous system, muscles, subcutaneous tissue and the globe of the eye . Mature tapeworms harm their human hosts by stealing vital nutrients causing severe malnutrition, greater intestinal disturbance, pain, and inflammatory response but symptoms are still generally mild and the pathology minor. Of great clinical importance is the larval infection of humans with *T. solium,* cysticercosis. Tapeworm eggs that are ingested from human faeces develop into larvae that infest specific sites in the central nervous system. Here, they can induce epilepsy, mental disturbances, meningeal syndrome, and can even cause death. Dead or dying parasites provoke an inflammatory response and seizures which lead to swelling of the respective areas. Human cysticercosis is a serious and widespread disease, being especially common in Latin America, Asia, Africa, the Phillipines and parts of Southern Europe . The disease is frequently found among Mexican agricultural workers in California and other Western states. Cysticercosis can be treated requiring chemotherapy followed by surgery for ophthalmic or brain involvement whereas tissue infection can be treated with anti-inflammatory drugs. Side effects of the drugs such as dizziness, vomiting and temporary hair loss are common. New therapies could help to lower infection rates and side effects in humans and to reduce great economic losses in live stocks in developing countries.

Annexin B1 cDNA encodes a 347 amino acid long protein (GenBank accession no. AF147955) with a molecular mass of 38kDa and a predicted pI of 5.6. Yan and colleagues also found that annexin B1 shows high affinity to thrombocytes and anticoagulant activity *in vivo*. Large amounts of non-fusion, full-length protein was previously produced in *Escherichia coli* in a soluble form and purified by employing either ion-exchange chromatography or a procedure on the basis of its PS-binding affinity . Application as a novel imaging agent , anticoagulant and thrombolytic agent have been suggested, and PS-binding properties of annexin B1 lead to the development of a radiopharmaceutical for

apoptosis imaging *in vivo* . Western blot analysis revealed that annexin B1 existed in the cystic fluid of *T. solium* cysticerci and sera of pigs infected with cysticercosis. Using monoclonal antibodies, annexin B1 was also detected in the surrounding host-derived layer with granulomatous infiltration, the distribution of annexin B1 being in accordance with the degree of inflammation. Those results imply that annexin B1 may be secreted at the host-parasite interface .

Investigating specific features of annexin B1 such as membrane- and heparin-binding properties could lead to development of new therapies against infestation with the parasite tapeworm *T. solium*. Therefore, membrane- and heparin binding behaviour of annexin B1 will be investigated in this work. Furthermore, its oligomerisation behaviour and molecular three-dimensional structure will be researched.

4 Results and Discussion of Annexin B1

In this work, annexin B1 was overexpressed and purified using ion exchange and heparin affinity chromatography. The protein's identity was verified by protein mass spectrometry finger printing, and its fold and stability were determined using CD spectroscopy. Annexin B1 was investigated for its liposome- and heparin-binding properties employing biochemical assays. The oligomerisation state was examined by gel filtration analysis, fluorescence spectroscopy and mass spectrometry. Annexin B1 was also subjected to crystallization trials.

4.1 Protein expression and purification

The construct annexin B1(P346H)_pRSET_6c was transformed into competent bacterial cells of the strain BL21(DE3) and overexpressed as described in section 5.3.1. The purification of annexin B1 was carried out in two steps; anion exchange chromatography followed by heparin affinity chromatography as a further purification step (see sections 5.4.2 and 5.4.3).

Fractions from each purification step were analysed on SDS-PAGE. Figure 4-1 A shows fractions resulting from anion exchange chromatography. The protein is already visible as a band near the 36.5kDa marker in the sample lane (S) that was loaded onto the column. After loading, some annexin B1 was washed off the column (W), probably because the capacity of the column was exceeded. Annexin B1 was eluted from the anion exchange column in elution fractions corresponding to 120-300mM NaCl (lanes 6-10) where it is visible as a band near the 36.5kDa marker (lane 1).

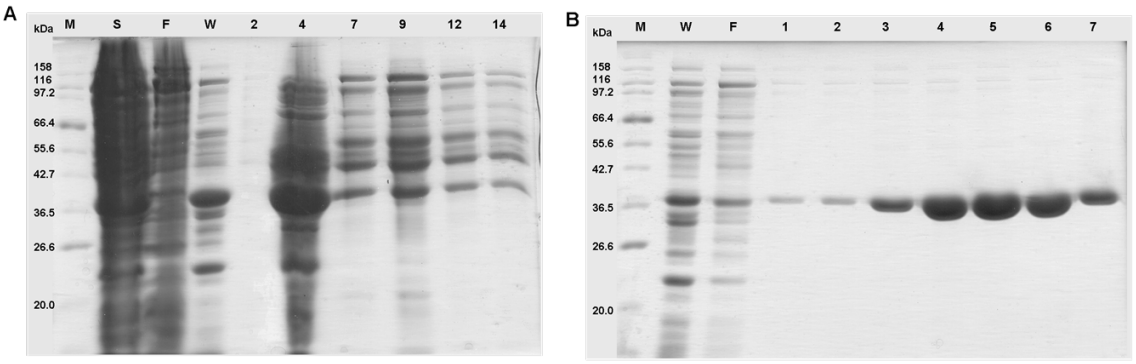

Figure -7: Purification of Annexin B1 using anion exchange chromatography (A) and heparin affinity chromatography (B). The protein appears near the 36.5kDa single maker (M). Lanes are labelled protein sample (S), flow through (FT) and wash (W). Numbered lanes represent elution fraction colleted from the respective column.

The fractions containing annexin B1 from the anion exchange purification were pooled, dialysed against a buffer containing 20mM Tris, pH 9.0, 250mM NaCl and 5mM $CaCl_2$, and subsequently applied to a heparin column. During heparin affinity purification, some protein was found in the flow through (F) and wash (W) fractions. Annexin B1 was eluted from the heparin column using a buffer containing 20mM Tris, pH 9.0, 250mM NaCl and 10mM EDTA, and appeared as a single band around 36.5kDa (see figure 4-1 B, lanes 4 - 10).

Annexin B1 was successfully purified as an untagged protein employing the two-step-purification procedure. This protocol yielded up to 10mg of protein per 1 litre bacterial culture with a purity greater than 95%. Identity and purity of the protein were verified by mass spectrometry.

4.2 Biophysical experiments

4.2.1 Mass spectrometry

The mass of the purified protein was determined using ESI-mass spectrometry. Sample preparation and experimentation were done by the COIL facility (University of Edinburgh) and as described in section 5.7.1.1. The mass spectrum showed a dominant single peak at 38241Da which was higher than the expected average molecular mass of

37998Da which may result from matrix adducts or salt present in the sample. An experimental mass 243Da higher than the theoretical value lies within an acceptable range. The protein was also subjected to trypsin digest and subsequent analysis using a MALDI-TOF mass spectrometer (see section 5.7.1.2.). The identity of full-length annexin B1 from *T. solium* was verified by mass spectrometry using the Mascot database (see figure 4-2).

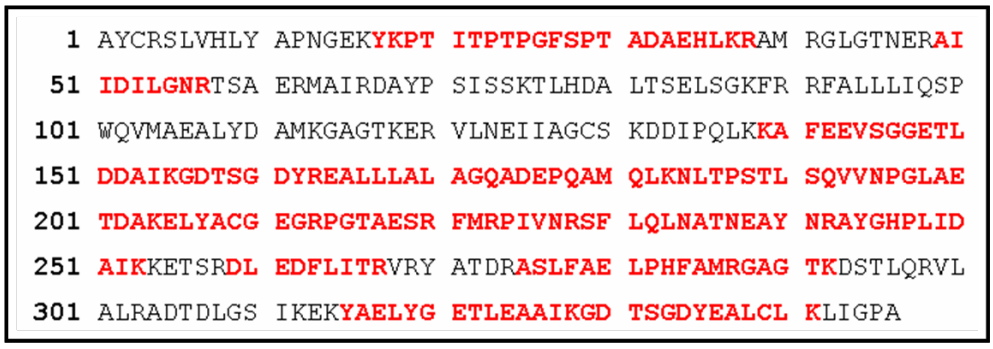

Figure -8: Mass spectroscopy analysis of trypsin digested annexin B1 proved identity of the protein. Residues in bold red represent peptides found within the database analysis.

4.2.2 Circular dichroism

4.2.2.1 Fold determination

Protein fold and stability were analysed using CD spectroscopy as described in section 5.7.2.1. Spectra were recorded in the presence (solid line) and absence (dashed line) of 5mM calcium showing similar progressions for both. CD spectra showed highly negative values from 240nm to 200nm with a change in sign from 200nm to 190nm (see figure 4-3) indicating a folded protein. Furthermore, the spectrum in figure 4-3 A, shows two minima at around 222nm and 208nm characteristic for the presence of α-helices.

A

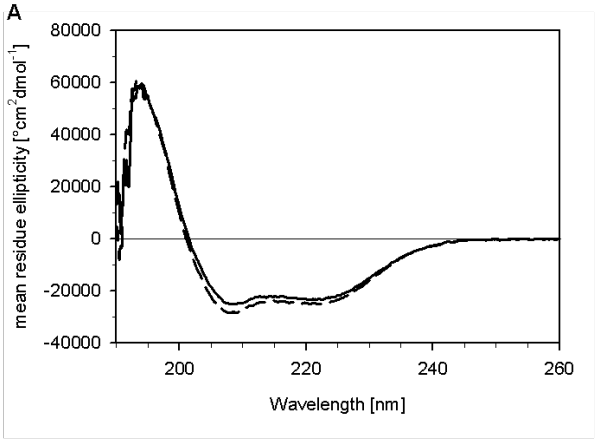

B

	K2D Neural Network	Linear combination of Fasman spectra
α-helix	0.825	0.60
β-sheet	0.0	0.16
unordered	0.163	0.24

Figure -9: Results from CD wavelength scans. A - CD spectra of AnxB1 in the absence (dashed line) and presence of 5mM calcium (solid line). B - Secondary structure prediction of the spectrum without calcium using implementations of the K2D neural network and a linear combination of Fasman spectra within the programme ACDP .

CD spectra recorded in the presence and absence of 5mM calcium both show similar progression. Secondary structure prediction using the tools in the programme ACDP revealed α-helices to be the dominant species with a ratio of 82.5% as determined using the K2D algorithm or 60% as determined using a linear combination of Fasman spectra (see figure 4-3 B). Both methods calculated a low amount of unordered structure, 16.3% with the K2D algorithm and 24% with the linear combination of Fasman spectra application. Furthermore, 16% β-sheet was predicted using the latter algorithm. However, it is known that all annexins investigated so far, possess a tight fold of exclusively α-helices. It is therefore unlikely to find β-sheets as a secondary structure element in annexin B1. Additionally, the K2D algorithm also presents the lower least squares error with 2.01 x 10^8 compared to 5.68 x 10^8 for the linear combination of Fasman spectra. The K2D algorithm fits the experimental CD spectrum of annexin B1 better than the linear combination of Fasman spectra.

4.2.2.2 Thermal stability

Thermal unfolding of annexin B1 was carried out by applying heat at a constant heating rate monitored by CD spectroscopy. The CD wavelength spectrum shows two minima at

208nm and 222nm which indicate the existence of α-helices. Denaturation experiments were monitored at 222nm providing the greatest change in the CD signal during the denaturation (see section 5.7.2.2.). Denaturation experiments were also carried out in the presence of 1mM DTT and 5mM $CaCl_2$. Endogenous levels of calcium are considered to be negligible as the last purification step involves usage of 10mM EDTA which would sufficiently remove all calcium. Three independent datasets were recorded for each experiment and fitted using a sigmoidal equation in the programme Sigma Plot (see figure 4-4 A).

A

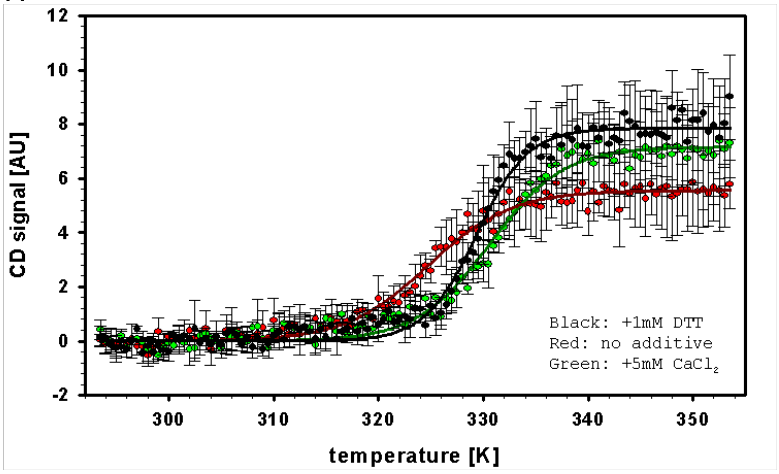

B

	T_m [K]
no agent	324.8
1mM DTT	329.4
5mM $CaCl_2$	330.6

Figure -10: Determining thermal stability of annexin B1 in presence of calcium or DTT. The protein unfolds in a two-state process (A) with a melting temperature depending on the added compound (B).

Denaturation studies indicate a heat-induced single transition unfolding process depending on the added compounds, DTT or $CaCl_2$ (see figure 4-4 A). The DTT curve (black) as well as the $CaCl_2$ curve (green) displays a steeper progression and a shift of the transition point towards higher temperatures as compared to that of the untreated sample (red). The corresponding melting temperatures T_m were therefore different for each set of experiments (see figure 4-4 B). Without adding any compound, the melting temperature was determined to be 52ºC; adding DTT or $CaCl_2$ resulted in melting temperatures of 56ºC and 58ºC, respectively.

The results indicate that both DTT and $CaCl_2$ have a stabilising effect on annexin B1 which is indicated by a shift of the melting temperature towards higher values as compared to untreated sample.

4.2.3 Gel filtration analysis

The oligomerisation state of annexin B1 was investigated using gel filtration analysis. Calibration utilising globular proteins of known size was used to determine the size of the different species. Gel filtration runs were carried out as stated in section 5.7.4. Figure 4-5 shows a gel filtration run of annexin B1 (solid line) overlaid with the calibration runs (dashed line). The absorption peaks of the annexin B1 run were fitted using the programme PeakFit to determine the positions of the peak maxima.

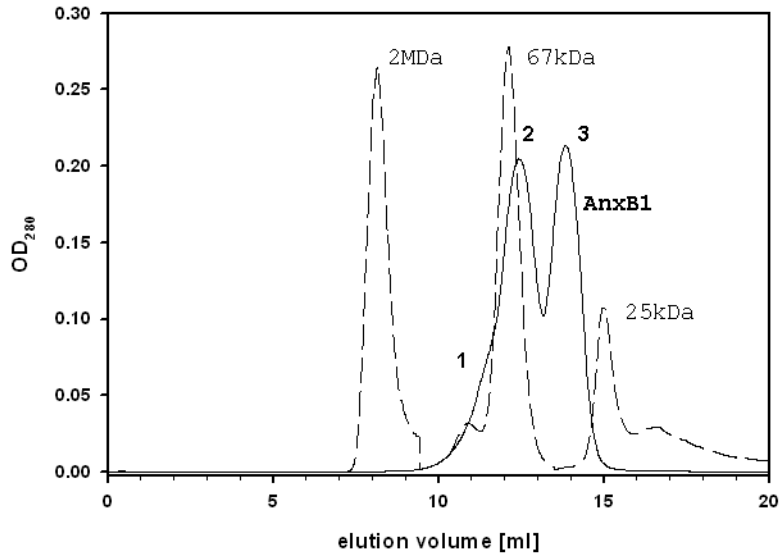

Figure -11: Gel filtration analysis of AnxB1 at a concentration of 5mg/ml. Representative gel filtration run of annexin B1 (solid line) overlaid by calibration runs. The molecular masses of the calibrators are indicated accordingly.

The gel filtration run of annexin B1 in figure 4-5 was fitted with three peaks with maxima at 11.18ml (peak 1), 12.44ml (peak 2) and 13.88ml (peak 3), respectively. Peaks 2 and 3 are clearly visible in the trace whereas the first peak is only visible as a preceding shoulder

of the second peak. As the protein was purified to a purity greater than 95%, proteins represented by the peaks are presumed to be oligomeric species of annexin B1. K_{av} values were calculated for all peaks (see table 4-1), which were converted into molecular masses using the equation generated from the calibration curve (see section 5.7.4.1.). Furthermore, a proposed oligomer species was assigned to each peak. The calculated molecular weight of peak 3 (37kDa) is in good agreement with the expected molecular weight of an annexin B1 monomer of 38kDa. Peak 2 could represent an annexin B1 dimer, and peak 1 a trimer.

Table -1: Results of the gel filtration analysis of annexin B1.

peak	elution volume [ml]	K_{av}	molecular mass [kDa]	species
1	11.18	0.192	92.0	Trimer
2	12.44	0.271	60.1	Dimer
3	13.88	0.362	37.0	Monomer

The highly pure annexin B1 sample is not homogeneous and contains monomers, dimers and trimers according to gel filtration analysis. Investigations on conditions for oligomer formation and the interacting residues were undertaken in further experiments which are described in section 4.3.

4.2.4 Conclusions: Biophysical experiments

The identity of annexin B1 was verified by full-length mass spectrometry and peptide mass finger printing. The purified protein was subjected to CD experiments where its secondary structure and fold stability was investigated. The spectra show that annexin B1 is folded and has a high α-helical content. Thermal denaturation experiments revealed a one-step unfolding transition with a transition temperature, T_m, of 52ºC. In additional denaturation experiments adding 1mM DTT or of 5mM $CaCl_2$ to the protein sample, a shift in T_m towards higher temperatures was observed indicating a stabilising effect on the

protein. Using gel filtration, the oligomerisation state of annexin B1 was investigated where it was determined to be a mixture of monomers, dimers and trimers in solution. In order to learn more about the oligomerisation behaviour of annexin B1, more gel filtration runs under different buffer conditions, fluorescence experiments and mass spectrometry analysis were carried out (see following section).

4.3 Investigation on dimer formation

4.3.1 Gel filtration analysis

Gel filtration runs of annexin B1 were carried out to analyse dimer formation under different conditions: 5mM and 15mM $CaCl_2$, 20mM EDTA, 10mM DTT, 1mM DTT or 0.8mM H_2O_2. The protein concentration in all gel filtration runs was kept at 1mg/ml. 5mM calcium and 20mM EDTA represent concentrations of the compounds used for purifying the protein. Gel filtration runs in the presence of 15mM calcium were carried out to investigate calcium-dependent oligomerisation of the protein as was previously observed with annexins 23(Ca38), 24(Ca32), Gh1 and Gh2 . 1m DTT and 0.8mM H_2O_2 represent 40 times molar excess of compound over protein.

Elution of the protein was monitored at 280nm measuring the absorption of the protein. Traces showed appearance of up to four peaks representing different oligomeric states of annexin B1. Assignment of peaks to monomers, dimers or trimers of annexin B1 was done by determining their apparent molecular masses using the molecular mass calibrators (see section 5.7.4). In all runs, the peaks representing the individual oligomeric state of the protein appeared at around the same elution volume. These experiments have been repeated with samples from different protein batches to account for any artefact resulting from contamination or specificities within the batch. In order to assess how much of the protein was present in an oligomeric state, the areas under the peaks were determined using the programme PeakFit . The area under a peak is dependent on the concentration or amount of the protein eluting in this fraction, and the sum of all areas represents 100% of the protein subjected to the gel filtration experiment. Each area under a peak was then

calculated as share of the sum of all areas. Shares of monomer (black), dimer (middle grey), trimer (dark grey) and aggregates (light grey) on the total amount of protein are depicted in figure 4-6.

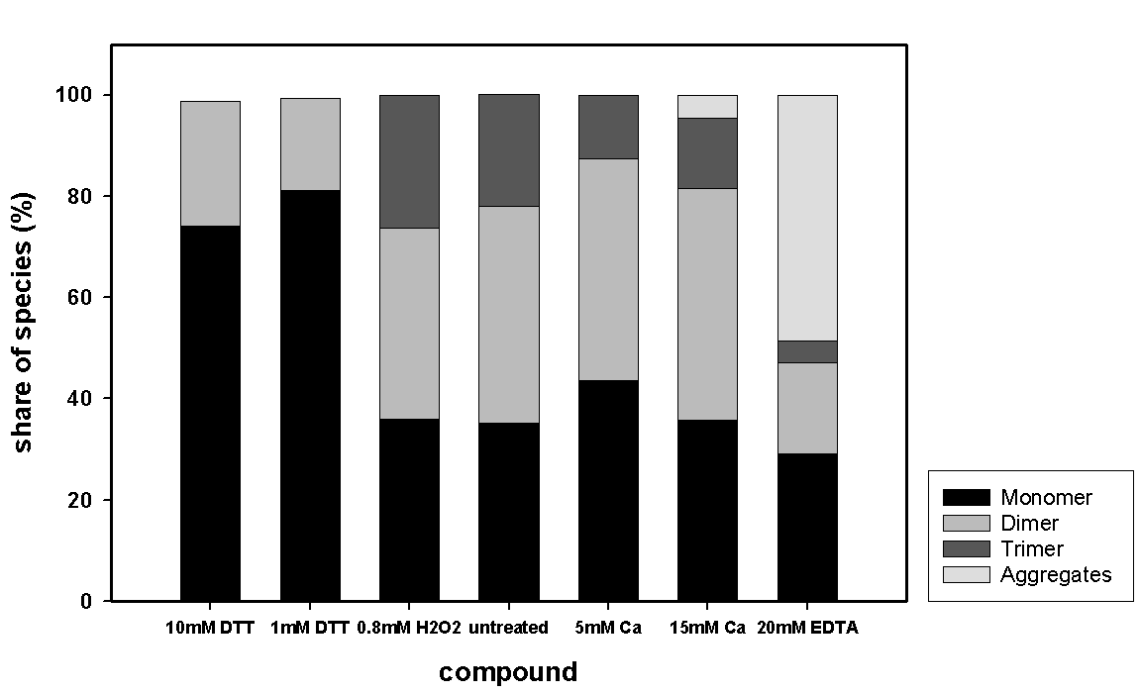

Figure -12: Oligomer formation of AnxB1 in presence of different compounds analysed by gel filtration. Shown are the species observed under different conditions: monomers (black), dimers (middle grey) and trimers (dark grey) as share of total protein amount in the sample. The protein was treated with 10mM DTT, 1mM DTT, 0.8mM H_2O_2, 5mM $CaCl_2$, 15mM $CaCl_2$ or 20mM EDTA prior to the experiment. In all experiments, peak centre and area under the peak differed by less than 1% for each species.

In two samples, 15mM $CaCl_2$ and 20mM EDTA, a proportion of the protein eluted at molecular masses greater than 600kDa or in the void volume of the column and was therefore considered to be aggregated protein and excluded from further analysis.

Results from gel filtration experiments show that the formation of monomers, dimers and trimers can be influenced by treating the protein with different agents. In the untreated sample and samples treated with 10mMDTT, 1mM DTT, 0.8mMH_2O_2 and 5mM $CaCl_2$, the protein was present as monomers, dimers and trimers. Interestingly, addition of 1mM DTT mainly promoted formation of monomers, and only 20% of dimers were observed in this sample. Treatment of annexin B1 with 0.8mM H_2O_2 caused a slight increase in trimer

content although all three species could be observed. This suggests that, in comparison with the untreated sample, the oxygen in the air is sufficient to oxidise the protein.
In the presence of 5mM $CaCl_2$, the monomer content was slightly higher than in the untreated sample. Contrary to findings from plant annexins , annexin B1 did not show a suppressed oligomerisation but rather aggregation as seen in samples treated with 15mM $CaCl_2$. On the other hand, deprivation of calcium ions by treatment of the protein with 20mM EDTA also led to aggregation (see figure 4-6).
The results from gel filtration runs suggest that dimer formation is partly dependent on the presence of calcium ions, although depletion of those ions leads to aggregation of the protein. The biggest shift in the monomer/dimer equilibrium could be observed by adding 1mM DTT. Monomer formation was increased by incubating the protein with 1mM DTT which suggests a Redox dependency and the involvement of disulfide bonds in dimer formation. This hypothesis was further investigated by native gel analysis, fluorescence spectroscopy and mass spectroscopy in the following sections.

4.3.2 Native gel

A native gel was run as stated in section 5.5.4 to determine particle sizes present in the protein sample. Bands on the gel were analysed by determining their R_f value and assigning molecular masses using the molecular mass marker as reference. The gel shows multiple bands from different species (figure 4-7) and /or different charged states of the protein species. A comparison of an untreated sample (sample 2, lane 3) with those treated with different compounds, showed the appearance or disappearance of some bands.

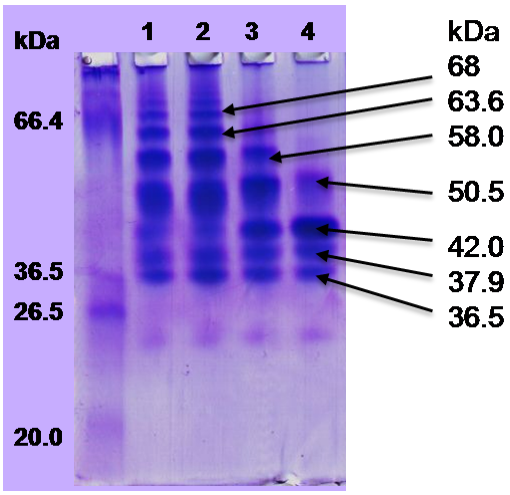

Figure -13: Native gel of annexin B1 under different conditions: 50 times molar excess of H_2O_2 (sample 1), untreated sample (sample 2), 5 times molar excess of DTT (sample 3), 50 times molar excess of DTT (sample 4). Lane 1 shows the molecular weight marker.

This experiment was repeated several times with different protein batches due to low resolution of the bands or the quality of the gel. Figure 4-7 is a representative native gel of annexin B1. The sample with 50 times molecular excess of DTT (sample 4) shows only 4 bands, among them a very strong band at 42.0kDa, presumably the annexin B1 monomer. In comparison to the untreated sample (sample 2), bands at higher molecular mass have disappeared in the DTT treated sample. This effect was less pronounced in the sample with only 5 times molecular excess of DTT (sample 3). Here, a strong band at 42kDa is visible suggesting a mainly monomeric protein. Treating the protein with 50 times molecular excess of H_2O_2 seems to preserve species distribution as compared with the untreated sample (sample 1). These findings are consistent with our previous results from gel filtration experiments (section 4.3.1).

Results from gel filtration and native gel suggest that oligomer formation of annexin B1 is Redox dependent. Although treatment with H_2O_2 does not significantly change the oligomeric state of annexin B1, DTT treated protein shows a higher proportion of monomeric species. It is likely that the oxygen present in the air is sufficient to fully oxidize the protein. To gain further insight into the oligomer formation of annexin B1,

experiments employing fluorescence spectroscopy and mass spectrometry were performed (see following sections).

4.3.3 Molecular modelling of Annexin B1

The crystal structure of annexin A8 (PDB accession number **1W3W**) was chosen as a template for homology modelling of annexin B1 based on the highest amino acid sequence identity to annexin B1 (39.7%). Modelling was carried out as stated in section 5.9.2., and Ramachandran plots were generated to assess tensions in the protein main chain angles (see Appendix). 95.1% of amino acids were in most favoured regions and 3.9% were in additionally allowed regions indicating a good model of annexin B1.

The C-terminal core domain of annexin B1 is completely modelled whereas the first 23 N-terminal amino acids are not present due to the lack of an N-terminal domain in the template used (see figure 4-8).

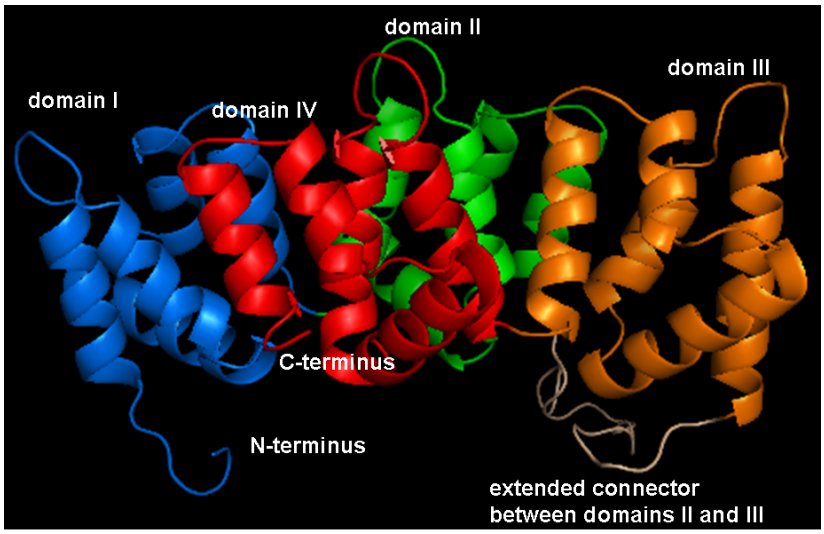

Figure -14: Homology model of annexin B1 based on the crystal structure of annexin A8. Domains I to IV are indicated in blue, green, orange and red, respectively. The extended connector between domains II and III is coloured in wheat. The N-terminal region is not present in the model due to shortcomings in the template. Figure prepared with PyMOL .

This homology model of annexin B1 will be used to analyse and visualize results from fluorescence spectroscopy and mass spectrometry.

4.3.4 Fluorescence spectroscopy

Annexin B1 possesses 9 phenylalanines, 13 tyrosines and one tryptophan which can be used for intrinsic fluorescence spectroscopy. Using the intrinsic fluorescence of proteins one can obtain information about the folded state of the protein and its change during unfolding. Fluorescence, especially of tryptophans and tyrosines, depends significantly on their environment, e.g. solvent, pH, and presence of a quencher, or a neighbouring group in the protein. Unfolding of a protein domain is thought to take place in one step whereas unfolding of a second domain in the protein or dissociation of a dimer might occur in two steps. Annexin B1 was subjected to fluorescence-monitored unfolding experiments with urea under different conditions in order to assess oligomer formation. In the presence of a dimer, two transition processes might be observed when unfolding the protein.

4.3.4.1 Spectra of folded and unfolded protein

Two excitation wavelengths were used to monitor fluorescence: 280nm (experimental setup A, excitation of mainly tyrosines) and 295nm (experimental setup B, excitation of tryptophans only). Emission spectra were recorded from 300nm to 400nm (experimental setup A) and 310nm to 400nm (experimental setup B), respectively. Examples of the fluorescence emission spectra of annexin B1 for the native (solid line) and denatured states (dashed line) in the presence of 1mM DTT are shown in figure 4-9. Here, the native protein has a greater intrinsic fluorescence than the denatured protein. After excitation at 280nm, the emission maximum of the native state of mostly monomeric annexin B1 is 343nm compared to 359nm for the unfolded state, indicating a wavelength shift of 16nm to higher wavelengths during unfolding. This behaviour could be observed in all experiments regardless of the compound used or the excitation wavelength applied. A red shift in the emission wavelength with maximum fluorescence intensity, λ_{MAX}(emission), represents a characteristic feature of fluorescent amino acid residues being exposed to aqueous (polar) environment suggesting progressive unfolding of the annexin with increasing concentration of denaturant .

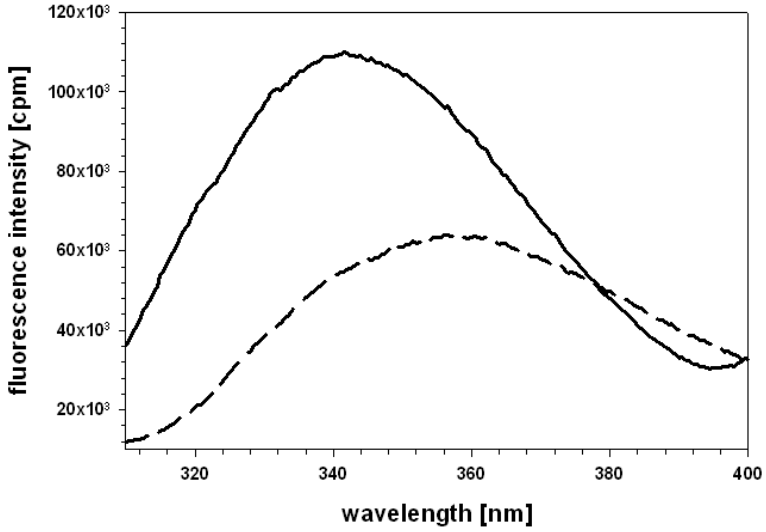

Figure -15: Fluorescence emission spectra for native (solid line) and denatured (dashed line) states of annexin B1 at 23°C, excitation at 280nm. Samples were treated with 1mM DTT to promote formation of monomers as seen in gel filtration experiments.

Different phenomena such as shift of λ_{MAX}(emission) or change of fluorescence intensity dependent on the added compounds could be observed in the fluorescence experiments.

The λ_{MAX}(emission) of the untreated sample is significantly higher compared to samples treated with DTT or $CaCl_2$ regardless of the excitation wavelength (see table table 4-2). The averaged emission maximum for the untreated sample is 355nm and decreased to 342nm in the presence of $CaCl_2$. In contrast, all unfolded protein samples showed their emission maximum at either 359nm or 360nm (excitation of mainly tyrosines) and 355nm (excitation of mainly tryptophans). Thus, the difference in fluorescence intensity between the folded and unfolded state is greater in DTT- or calcium-treated samples. This also indicates that the fluorescence-emitting residues present in the protein experience a greater change in their environment when treated with DTT or $CaCl_2$ than in the untreated sample. Treatment of the protein with DTT or $CaCl_2$ might have led to conformational changes which caused a burial of the fluorophores in an apolar environment, e.g. within the protein or between two protein molecules. Fluorophores in an apolar environment show fluorescence at lower wavelengths.

Table -2: Fluorescence emission maxima obtained in experimental setups A and B.

	Untreated		1mM DTT		5mM $CaCl_2$	
Excitation at	280nm	295nm	280nm	295nm	280nm	295nm
λ_{MAX}(Folded) [nm]	355	350	343	346	342	347
λ_{MAX}(Unfolded) [nm]	360	355	359	355	359	355

Interestingly, the fluorescence intensity at λ_{MAX}(emission) decreased or increased upon unfolding of the protein sample in different fluorescence experiments (see table 4-3). Compared to untreated annexin B1 and treatment with 5mM $CaCl_2$, fluorescence intensity decreased upon treatment with DTT both when excitation occurred at 280nm and 295nm.

Table -3: Fluorescence intensity at emission maxima in experimental setups A and B.

	Untreated		1mM DTT		5mM $CaCl_2$	
Excitation at	280nm	295nm	280nm	295nm	280nm	295nm
I_{MAX}(Folded) [cpm]	86066	44385	174835	89251	107421	49882
I_{MAX}(Unfolded) [cpm]	120939	62552	126473	61740	114335	59515

A decrease in fluorescence intensity can be explained by the fluorophors becoming fully exposed to the solvent. Here, the contact of fluorophores with polar solvent molecules causes a decrease in the energy of the excited fluorophor, and the emission intensity decreases. An increase in fluorescence intensity at λ_{MAX} upon unfolding, as observed with the untreated sample and the sample treated with 5mM $CaCl_2$, might be caused by neutralisation of quenching effects upon unfolding of the protein. The quencher has to be near the fluorophor and could either come from residues within the protein or from another protein molecule in close proximity (ie. oligomerisation). Notably, fluorescence intensities of DTT-treated samples were higher than those of untreated or calcium-treated sample.

4.3.4.2 Denaturation curves

Denaturation curves were generated by monitoring the change of fluorescence intensity, I, at two wave lengths, $\lambda_{MAX}$of the folded protein (I_{folded}) and of the protein in the unfolded

state ($I_{unfolded}$). In order to increase the signal-to-noise ratio and to account for wavelength shifts of the wavelength maxima, denaturation curves were plotted as $I_{folded}/I_{unfolded}$ (see figure 4-10). Data for experimental setups A and B were analysed separately, and fitted in the programme SigmaPlot using a sigmoidal curve determining the half maximal denaturant concentration, $c_{1/2}$(urea), for each sample. Results show that the denaturation of annexin B1 is different for samples treatment with 1mM DTT or 5mM $CaCl_2$ as compared to the untreated sample in both experimental set ups.

In the experimental setup A (excitation of mainly tyrosines), denaturation curves of protein samples treated with 1mM DTT or 5mM $CaCl_2$ show a sigmoidal progression with a large change in $I_{folded}/I_{unfolded}$ (see figure 4-10 A). The sigmoidal shape is much less pronounced in the untreated sample where data show a nearly linear progression with negligible change in value between 0M urea and 8M urea. Interestingly, in 8M urea, $I_{folded}/I_{unfolded}$ is nearly equal for all samples. $c_{1/2}$(urea) decreased from 4.2M to 3.4M upon treatment of the protein with 1mM DTT, and to 3.7M under 5mM $CaCl_2$ (see figure 4-10 B).

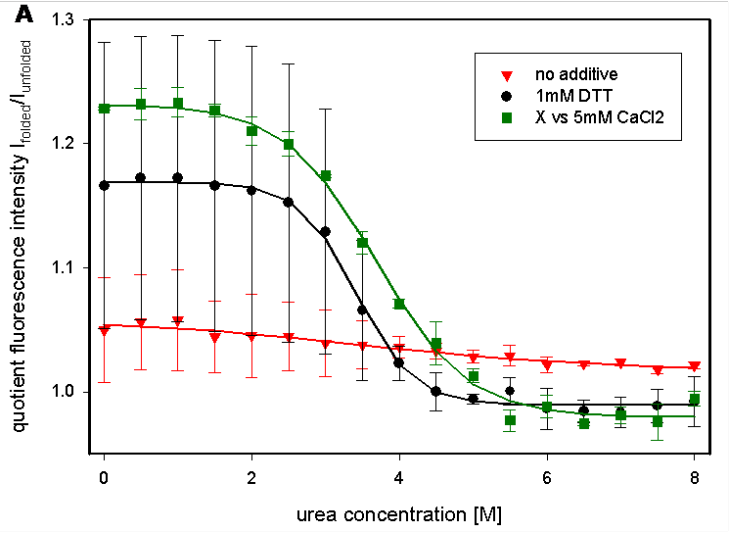

B

Agent	$c_{1/2}$ (urea) [M]
No agent	4.2
1mM DTT	3.4
5mM $CaCl_2$	3.7

Figure -16: Experiment A: Chemical denaturation of annexin B1 using urea monitored by fluorescence, excitation at 280nm. A – Denaturation curves of untreated protein (red) and samples

treated with 1mM DTT (black) or 5mM $CaCl_2$ (green). B – Table showing the half maximal denaturant concentrations $c_{1/2}$(urea) for each compound.

Denaturation curves recorded with an excitation wavelength of 295nm (experimental setup B) are shown in figure 4-11 A. All curves were fitted with a sigmoidal function. The change of I_{folded}/ $I_{unfolded}$ in this set of experiments is not as pronounced as in the previous data sets. Fluorescence intensities measured with excitation at 295nm were generally lower than those recorded with excitation at 280nm which might be due to the fact that only one fluorophor was excited. In samples treated with 1mM DTT or 5mM $CaCl_2$, the half maximal denaturant concentrations were determined to be 3.3M and 3.7M, respectively (see figure 4-11 B). In contrast, $D_{1/2}$ for untreated annexin B1 was determined to be 2.8M.

A

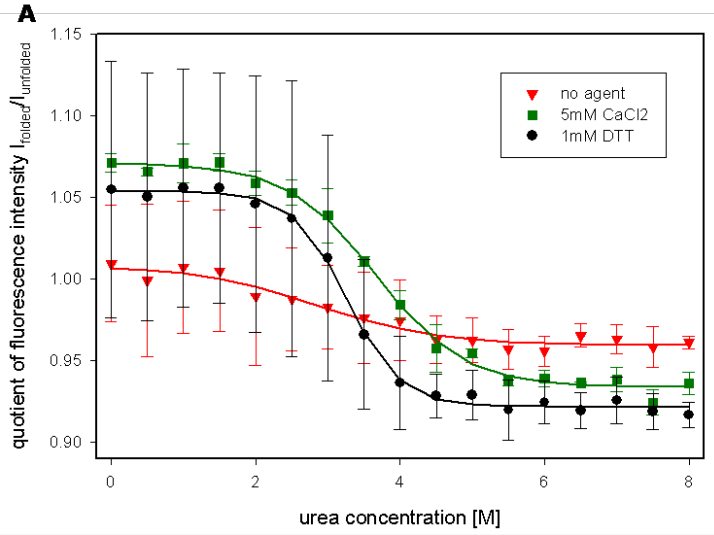

B

Agent	$c_{1/2}$ (urea) [M]
No agent	2.8
1mM DTT	3.3
5mM $CaCl_2$	3.7

Figure -17: Experiment B: Chemical denaturation of annexin B1 using urea monitored by fluorescence, excitation wavelength 295nm. A – Denaturation curves of untreated protein (red) and samples treated with 1mM DTT (black) or 5mM $CaCl_2$ (green). B – Table showing the half maximal denaturant concentrations $c_{1/2}$(urea) for each reagent.

Comparison of $c_{1/2}$(urea) values determined in experimental setup A with values obtained in experimental setup B yields a great difference. $c_{1/2}$(urea) values for samples treated with 1mM DTT or 5mM $CaCl_2$ are within the same range in both experimental setups whereas $c_{1/2}$(urea) values for untreated sample are significantly different. In experimental setup A

(excitation at 280nm), $c_{1/2}$(urea) is 4.19M, and in experimental setup B (excitation at 295nm) $c_{1/2}$(urea) was determined with 2.84M.

Relating to gel filtration experiments previously performed, the untreated sample consists of 35% monomers, 43% dimers and 22% trimers as determined by gel filtration. In the untreated samples, the difference between $c_{1/2}$(urea) determined from experiment A and experiment B suggests that tyrosines and Trp102 experience the unfolding process differently. Trp102 reports its exposure to a polar environment at a lower urea concentration than tyrosines. In comparison, the sample treated with 1mM DTT consists of 80% monomers and 20% dimers. Therefore, changes in fluorescence upon unfolding observed in this sample can be related to an unfolding of an annexin B1 monomer. $c_{1/2}$(urea) values are similar in both experimental setups indicating an environmental change at the same urea concentration for both, tyrosines and Trp102. Here, Trp102 is as susceptive to changes in its environment as are the tyrosines present in the protein. Similar observations were made when the protein was treated with 5mM $CaCl_2$ indicating a similar exposure of Trp102 and tyrosines to the environment as compared to the DTT-treated sample. Interestingly, the oligomer distribution in the calcium-treated sample is comparable to that of the untreated sample.

4.3.4.3 Conclusions

Three main phenomena were observed upon chemical unfolding of annexin B1: (i) shift of emission maxima to higher wavelength when exciting the protein both at 280nm and 295nm, (ii) decrease of fluorescence intensity during unfolding for samples treated with 1mM DTT but increase of fluorescence intensity for untreated samples and samples treated with 5mM $CaCl_2$ in both experimental setups and (iii) similar $c_{1/2}$(urea) values for samples treated with 1mM DTT and 5mM $CaCl_2$ in both experimental setups but a lower $c_{1/2}$(urea) value in experiment B for the untreated sample.

A shift of emission maxima to higher wavelengths can be explained by a change from an apolar to a polar environment experienced by the fluorophors. Tyrosines as well as Trp102 experienced the same change in environment indicating unfolding of the protein upon

treatment with urea. While a decrease in fluorescence intensity upon unfolding is an indicator of unfolding, an increase in fluorescence intensity as seen for the untreated sample and sample treated with 5mM $CaCl_2$ indicates that the fluorophores are released from a quencher. The quencher could be a residue within the molecule or from a neighbouring molecule in the case of oligomer formation. However, both, the shift in wavelength and change in fluorescence intensity, suggest that annexin B1 was unfolded by subjecting the protein to increasing urea concentrations.

$c_{1/2}$(urea) value determined from denaturation curves for the untreated protein are lower when monitored by fluorescence emission of Trp102 than when monitored by fluorescence emission of mainly tyrosines. Inspecting the homology model of annexin B1, Trp102 can be found on the concave side of the protein but slightly inserted into the core domain. It is located between domains I/IV and II/III (see figure 4-12), which have previously been described as modules of an annexin monomer .

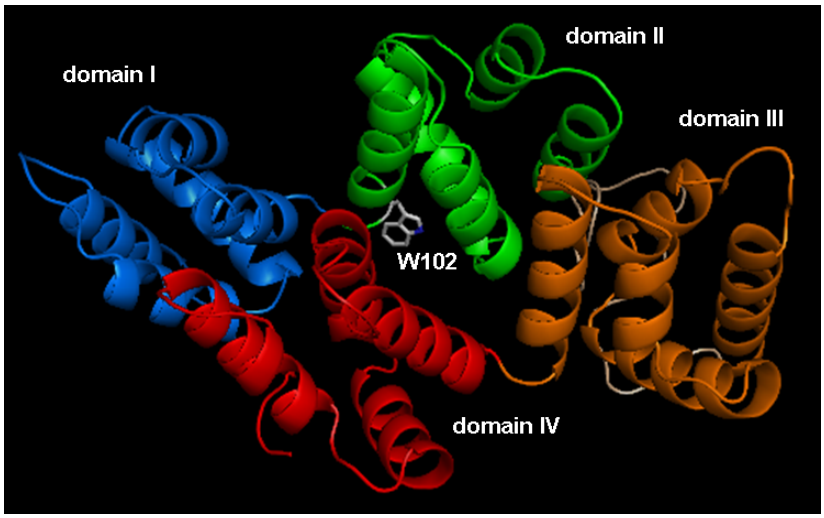

Figure -18: Top view of modelled annexin B1. Domains I to IV are indicated in blue, green, orange and red, respectively. Trp102 is drawn explicitly and coloured by its elements. Figure prepared with PyMOL .

Intra-modular contacts are tight and mediated by hydrophobic interactions whereas interactions between the two modules are less tight and mostly provided by polar charged residues therefore forming a unique channel across the protein. In a chemical unfolding

experiment, urea is thought to interact directly with the protein showing shorter residence times around nonpolar residues as compared to polar residues . Therefore, the less tight polar interactions between the two modules would disrupt at a lower urea concentration than the tighter hydrophobic interaction within the modules. As Trp102 is located between domains I/IV and II/III, it would report unfolding at lower urea concentrations than other residues elsewhere in the protein. Therefore, Trp102 is likely to monitor the disruption of salt bridges between domains I/IV and domains II/III at the first stages of unfolding.

Samples treated with 5mM $CaCl_2$ or 1mM DTT show a similar progression of their unfolding curves in both experiments, and $c_{1/2}$(urea) values were determined to be in the same range. This is in contrast to $c_{1/2}$(urea) values obtained for the untreated sample, and does not seem to be related to the oligomeric state of the protein. The untreated sample and the calcium-treated sample both show a similar distribution of oligomers whereas mostly monomers are found upon treatment with DTT. Comparing denaturation curves from DTT-treated samples and untreated samples, no additional transition stages could be observed in the untreated sample that would reflect the dissociation of a protein oligomer. It must therefore be concluded that either dissociation of an oligomeric species coincides with unfolding of the annexin B1 monomer or that fluorescence spectroscopy is not a suitable method for analysing oligomer formation of annexinB1.

A similar behaviour of DTT- and calcium-treated sample in fluorescence experiments could be due to a possible conformational change within the protein upon compound binding. It is known that annexins undergo conformational changes upon calcium binding that could affect the C-terminal or the N-terminal domain as seen with annexin A1 . A stabilisation of calcium-bound annexins against thermal denaturation had also been observed . Crystal structures of the apo- and calcium bound form of annexin B1 could shed light on a possible conformational change upon calcium binding, and deliver a possible explanation for the fluorescence data obtained with the calcium-treated sample.

4.3.5 Mass spectrometry

Gel filtration experiments strongly suggested that oligomer formation in annexin B1 is Redox dependent. SDS-PAGE analysis of elution fractions from gel filtration experiments

confirms annexin B1 as the only protein present (data not shown). In an attempt to map the interaction sites on the protein that are responsible for oligomer formation, annexin B1 was subjected to cross-linking experiments. Different cross-linkers were used to cross-link annexin B1 but no distinct bands were visible on SDS-PAGE that would have been suitable for trypsin digest and mass spectrometry. Therefore, the naturally occurring linkages of two annexin B1 molecules via disulfide bonds were used to investigate possible interaction sites involved in oligomer formation. Comparison of peptide mass fingerprinting results from different oligomeric species was used to identify cysteine residues involved in oligomer formation.

The different oligomer species were separated by denaturing but non-reducing gel electrophoresis, which denatured the protein sample and applied a negative charge but would preserve any possible disulfide bonds between annexin B1 monomers. The samples were mixed with loading dye lacking DTT but included SDS and heated to denature but not reduce the sample. Present disulfide bonds will still be intact, and their presence or absence can be traced back to treatment with different compounds. The resulting SDS-PAGE shows protein bands with varying intensity in each lane (see figure 4-13), where the migration of the respective species is now only dependent on size. Annexin B1 was treated with 20mM EDTA (sample 1), 15mM $CaCl_2$ (sample 2), 5mM $CaCl_2$ (sample 3) and 1mM DTT (sample 4) and subjected to electrophoresis (see section 5.5.3.). The molecular masses of the protein bands were estimated using their R_f values and marker proteins (lane 1).

The gel shows bands of similar molecular weight in each lane indicating monomeric (34.7kDa), dimeric (64.3kDa) and trimeric (88.5kDa) annexin B1. Formation of tetramers and higher species could be observed in some samples. Bands were cut out and labelled according to the number of the lane: 1 (20mM EDTA), 2 (15mM $CaCl_2$), 3 (5mM $CaCl_2$), 4 (1mM DTT), and 5 (untreated sample). For each lane, the band at the respective monomer size was labelled with “a”, the band supposedly representing dimer was designated “b”, trimers “c” and tetramers “d” (see figure 4-13).

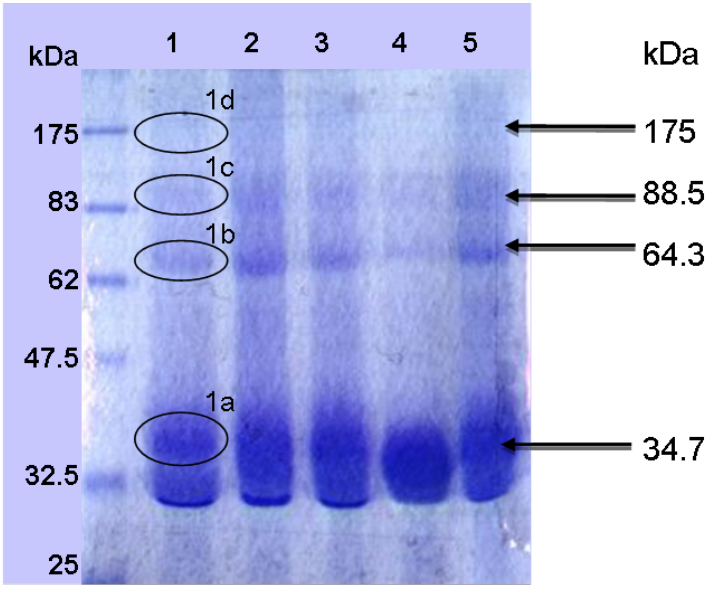

Figure -19: Annexin B1 run under different conditions on a denaturing, non-reducing SDS-PAGE. Lane 1 is broad range marker. Samples treated with 20mM EDTA (sample 1, lane 2), 15mM $CaCl_2$ (sample 2, lane 3), 5mM $CaCl_2$ (sample 3, lane 4) and 1mM DTT (sample 4, lane5) are run along with untreated sample (sample 5, lane 6). Examples for bands that were cut out are indicated on the gel.

In order to verify the identity of the proteins of each band, an in-gel trypsin digest was performed (see section 5.7.1.2) with samples incubated with 20mM EDTA and 15mM $CaCl_2$, and the resulting peptide mixtures were subjected to mass spectrometry (peptide mass fingerprinting). The results for each sample are summarised in table 4-4 stating the probability based Mowse score with which annexin B1 was identified including the sequence coverage. **T**he oligomeric species are also indicated, as well as the compounds with which the samples were treated.

Sequence coverages from all peptide mass fingerprint experiments were greater than 67% verifying annexin B1 from *Taenia solium* as the protein represented by the protein bands. As SDS-PAGEs and full-length mass spectrometry showed annexin B1 to be of high purity, it is concluded that the protein bands visible on the gel were due to homo-oligomerisation. This also supports the hypothesis of an oligomer formation through disulfide bonds.

Table -4: Mass spectrometry results from in-gel digest.

agent	sample	anxB1 score	Sequence coverage [%]	species
20mM EDTA	1d	236	67	Tetramer
	1c	238	71	Trimer
	1b	225	71	Dimer
15mM $CaCl_2$	2d	256	69	Tetramer
	2c	219	63	Trimer
	2b	256	72	Dimer
5mM $CaCl_2$	3d	119	57	Tetramer
	3c	85	40	Trimer
	3b	95	45	Dimer
1mM DTT	4a	102	54	Monomer

Annexin B1 possesses 4 cysteins in positions 4, 130, 210 and 340 which are indicated in figure 4-14. Cysteine-containing peptides that can theoretically be obtained from trypsin digest are underlined, and the respective cysteine is indicated in bold red.

```
        10         20         30         40         50         60
AYCRSLVHLY APNGEKYKPT ITPTPGFSPT ADAEHLKRAM RGLGTNERAI IDILGNRTSA
        70         80         90        100        110        120
ERMAIRDAYP SISSKTLHDA LTSELSGKFR RFALLLIQSP WQVMAEALYD AMKGAGTKER
       130        140        150        160        170        180
VLNEIIAGCS KDDIPQLKKA FEEVSGGETL DDAIKGDTSG DYREALLLAL AGQADEPQAM
       190        200        210        220        230        240
QLKNLTPSTL SQVVNPGLAE TDAKELYACG EGRPGTAESR FMRPIVNRSF LQLNATNEAY
       250        260        270        280        290        300
NRAYGHPLID AIKKETSRDL EDFLITRVRY ATDRASLFAE LPHFAMRGAG TKDSTLQRVL
       310        320        330        340
ALRADTDLGS IKEKYAELYG ETLEAAIKGD TSGDYEALCL KLIGPA
```

Figure -20: Trysin digest of annexin B1. Cysteine containing peptide fragments resulting from trypsin digest are underlined, and the respective cysteine is shown as bold red letter.

In order to preserve disulfide bonds for mapping of cysteins involved in oligomerisation, the protocol for peptide mass finger printing was altered slightly. The step involving IAA and DTT in the sample preparation was omitted which reduced the score in the finger printing slightly (see table 4-4). Annexin B1 treated with 5mM $CaCl_2$ (samples 3b, 3c, 3d) and 1mM DTT (sample 4a) were cut out from the gel. For analysis, peptide masses

identified by mass spectrometry of samples treated with 5mM $CaCl_2$ (comprising dimers, trimers and tetramers) were compared to peptide masses identified in the sample treated with 1mM DTT (mostly monomers).

After mass spectrometry, a peptide list containing all fragments present in the respective samples was obtained. If two cysteine-containing fragments are linked via a disulfide bond, their respective individual peptide masses should not be present in the peptide list but a number that is the sum of the two individual peptide masses (also subtracting masses for 2 protons). The molecular mass of each cysteine-containing peptide was combined with the molecular mass of another cysteine-containing peptide, and 10 possible peptide masses were determined. Each peptide list obtained from mass spectrometry of samples 3b (dimer), 3c (trimer), 3c (tetramer) and 4a (monomer) was analysed for presence of those peptides. Table 4-5 summarises results from mass spectrometry experiments stating the disulfide-bonded peptides (column 1) with their expected molecular masses (column 2). Their presence or absence in the mass spectrum of an annexin B1 sample is indicated by (+) or (-). A peptide fragment was considered as present when the peptide mass that was determined in the experiment was within 1 Dalton of the theoretical value (personal communication with A. Cronshaw).

Since annexin B1 possesses four cysteines, the possibility of intra-molecular disulfide formation cannot be out ruled when those residues are close in space to each other. Therefore, disulfide-bond containing peptide fragments that were identified in mass spectrometry could belong to either intra- or inter-molecular disulfide bonds. To address this problem, the previously generated molecular model of annexin B1 was used to visualise the positions of all cysteines in the protein.

Table -5: Disulfide-bonded peptides identified with mass spectrometry and their assignment to oligomer species.

C-C fragment	Expected MW	Sample 3d tetramer	Sample 3c trimer	Sample 3b dimer	Sample 4a monomer
AYCR + AYCR	1022.4	+	+	–	–
AYCR + VLNEIIAGCSK	1656.8	+	+	+	+

AYCR + GDTSGDYEALCLK	1881.8	+	+	+	+
AYCR + ELYACGEGRPGTAESR	2206	+	+	+	–
VLNEIIAGCSK + VLNEIIAGCSK	2291.2	–	–	–	–
VLNEIIAGCSK + GDTSGDYEALCLK	2516.2	+	+	+	+
VLNEIIAGCSK + ELYACGEGRPGTAESR	2840.4	+	+	–	+
GDTSGDYEALCLK + GDTSGDYEALCLK	2741.2	+	+	–	–
GDTSGDYEALCLK + ELYACGEGRPGTAESR	3065.4	+	+	+	+
ELYACGEGRPGTAESR + ELYACGEGRPGTAESR	3389.6	–	–	–	–

Figure 4-15 shows a cartoon of the annexin B1 model (green) with cysteine-containing fragments highlighted in light pink and cysteine residues drawn explicitly as red sticks. The 23 N-terminal amino acids including Cys4 are not present in the model due to an absence in the template but are indicated by a green dashed line. Cys 4 is indicated as a red dash to indicate its proposed position in the model. Cysteines in domains II, III and IV are all surface exposed, Cys130 points towards the concave side of the protein whereas Cys210 and Cys340 point towards the side.

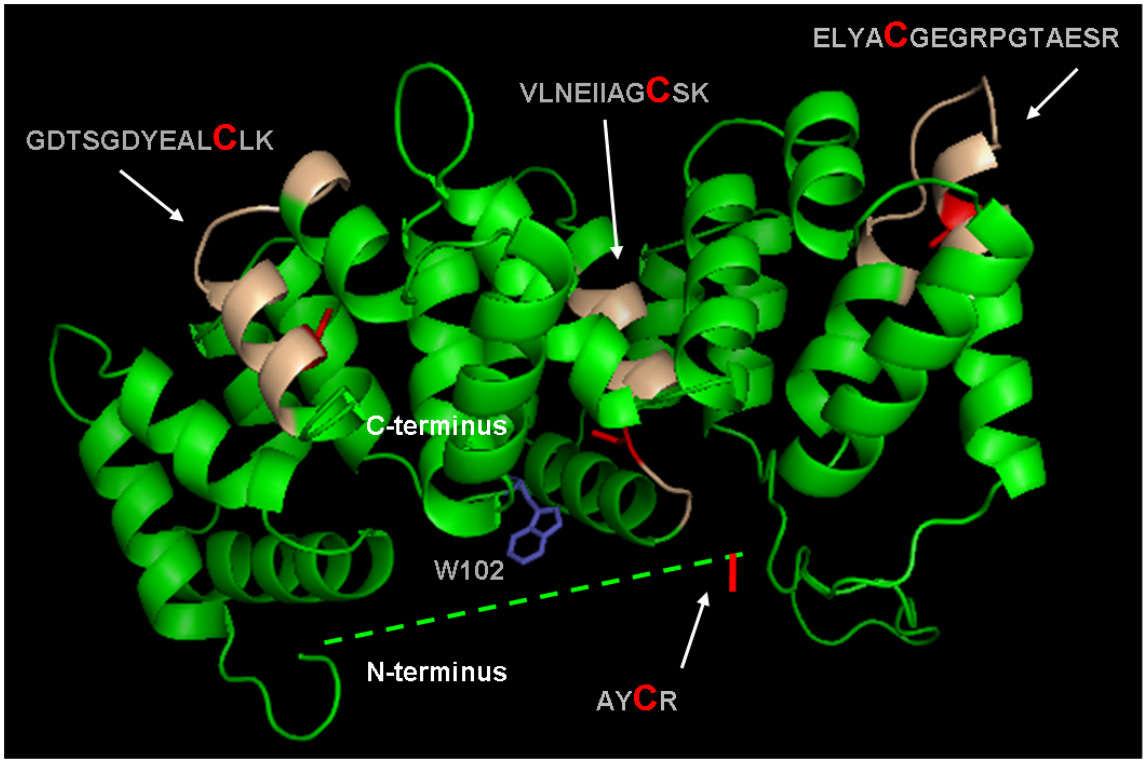

Figure -21: Annexin B1(24-347) modeled on annexin A8. Cysteines are shown as red sticks, and the corresponding peptides identified in mass spectrometry are highlighted in wheat and labelled accordingly. The N-terminus in this model is missing due to its absence in the template but is indicated as a dashed green line. Figure prepared with PyMOL

In the homology model, Cys130 (domain II) lies on the concave side of the protein. The N-terminus of the protein could align to the concave side of the protein and shield Cys130 form formation of inter-molecular disulfide bridges. Considering a very flexible 26 amino acid long N-terminus of annexin B1 and a relative closeness in space between cysteines 4 and 130, one could also speculate that both residues engage in an intra-molecular disulfide bridge. This hypothesis is supported by mass spectrometry data where the corresponding fragment, AYCR + VLNEIIAGCSK, was observed in sample 4a (monomer). In contrast, fragments AYCR + AYCR, AYCR + ELYACGEGRPGTAESR and GDTSGDYEALCLK + GDTSGDYEALCLK, involving Cys4, Cys210 and Cys340, are likely to result from inter-molecular disulfide bridges since peptide masses of those fragments were not identified in mass spectrometric analysis of sample 4a (monomer).

Summarising the results from mass spectrometry experiments and findings from the homology model, two main conclusions can be drawn: (i) Cys210 (domain III) and Cys340 (domain IV) are likely to be surface exposed and could take part in formation of Redox dependent oligomers. (ii) Cys4 or Cys130 are potentially involved in formation of intra- and inter-molecular disulfide bridges (see table 4-6).

Table -6: Involvement of cysteines in formation of intra- and inter-molecular disulfide bridges.

cysteine	domain	formation of disulfide bridge	
		intra-molecular	inter-molecular
Cys4	I	potentially with Cys130	potentially
Cys130	II	potentially with Cys4	not likely
Cys210	III	not likely	likely
Cys340	IV	not likely	likely

True involvement of these four cysteines in oligomer formation can only be assessed by mutational studies which will be considered for further work on that topic. The best candidates for those studies would be Cys210 and Cys340 of domains III and IV, respectively. Mutations of these residues to serines, for example, might impair oligomer formation.

4.3.6 Conclusions: Investigations on dimer formation

Gel filtration data and native gels showed that annexin B1 was present as a mixture of oligomers of different sizes in solution ranging from monomers to tetramers. Treating the protein with different compounds revealed that oligomer formation of annexin B1 is Redox-dependent. Using a non-reducing but denaturing SDS-PAGE and peptide mass fingerprinting, all species in a protein sample could be identified as annexin B1 indicating disulfide-dependent homo-oligomerisation. Although the presence of disulphide bonds in the in the protein in its intracellular form is highly unlikely, cell-surface exposed protein may form disulphide-dependent oligomers as part of its mechanism to interact with host cell surface molecules.

The protein possesses four cysteine residues that could be involved in oligomer formation, one in each domain. Comparison of peptide mass fingerprinting experiments in concert with findings from molecular modelling revealed Cys210 and Cys340 of domains III and IV likely to be involved in the formation of inter-molecular disulfide bonds suggesting a side-to-side oligomer of annexin B1. Cys130 lies on the concave side of the protein and is not likely to be involved in homo-oligomerisation but rather in the formation of an intra-molecular disulfide bond with the N-terminal Cys4. Disulfide bonding of the N-terminal Cys4 and Cys130 might have implications for the protein's function as the flexible N-terminus would be locked into the core domain.

Denaturation experiments were monitored by fluorescence and carried out with untreated sample and samples treated with 1mM DTT and 5mM $CaCl_2$. DTT was added to the sample to promote presence of monomers, whereas addition of 5mM $CaCl_2$ was used to study the influence of calcium on the stability of the protein and its unfolding process. All samples report unfolding in one step despite their presence in multiple oligomeric states. The mostly monomeric DTT-treated sample reports $c_{1/2}$(urea) values for excitation at 280nm excitation at 295nm (Trp102) to be in the same range. This is in contrast to findings with the untreated sample consisting of monomers, dimers and trimers where tyrosines report unfolding at a higher urea concentration than Trp102. Homology modelling shows that Trp102 resides in the cleft formed by domain I/IV and II/III. Upon treatment with low urea concentrations, weak polar interactions between the modules are distorted causing exposure of this residue to the environment. At higher urea concentrations, the mostly hydrophobic interactions within the modules are disrupted, and the protein unfolds which is reported by tyrosine residues. Results suggest that, upon unfolding, fluorescence spectroscopy is likely to monitor processes within the monomer rather than dissociation of protein oligomers.
The homology model also suggests that Trp102 is located towards the concave side of the protein (see figure 4-15), in close proximity to Cys130. In a scenario where the N-terminal domain nestles to the core domain and forms a disulfide bridge with Cys130, Trp102 might experience quenching by residues in close proximity such as Tyr3, Tyr 11 or Tyr18

of the N-terminal region. Upon treatment with urea, the N-terminal domain might loose its structure releasing Trp102. This change in environment might also contribute to results from fluorescence spectroscopy where fluorescence intensities of DTT-treated native protein were generally higher than those of the untreated or calcium-treated sample. Validation of a close proximity, and thus possible quenching, could be achieved when examining a crystal structure of the protein.

4.4 Biochemical characterization

4.4.1 Liposome binding behaviour

The calcium-dependent membrane binding of annexin B1 was investigated employing an assay developed by A. Hofmann and R. Huber . The experiments were carried out using large unilamellar vesicles (LUVs) with two different PS:PC ratios, 1:3 and 3:1. The amount of protein that had bound to the membrane in a calcium dependent manner was determined densitometrically and expressed as a degree of binding.

Annexin B1 displays calcium-dependent binding behaviour to PS/PC (1:3) vesicles to a moderate extent with a maximum binding of 30% in 10mM calcium (figure 4-17 A, closed circles). In contrast, the binding is more enhanced with more acidic PS/PC (3:1) vesicles where the maximum binding degree in 10mM calcium is 90% (figure 4-16 A, open circles). Here, binding of annexin B1 to PS/PC (3:1) vesicles reaches a maximum in 3mM $CaCl_2$. The half-maximum calcium concentration, $c_{1/2}$, of 0.1mM is at the lower end of the range observed with several plant annexins . The results are summarised in table format in figure 4-16 B stating $c_{1/2}$ and degree of binding in 0mM and 10mM calcium.

A

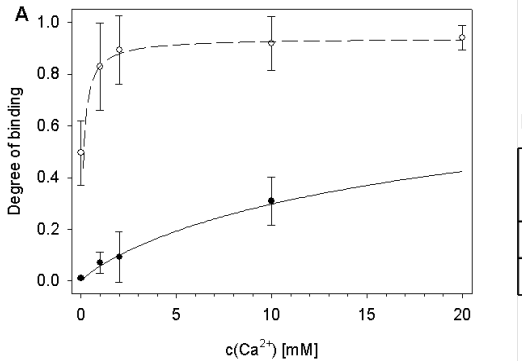

B

Liposome composition	$c_{1/2}(Ca^{2+})$ [mM]	Binding at $c(Ca^{2+})$ 0 mM [%]	Maximum binding at $c(Ca^{2+})$ 10 mM [%]
PS/PC (1:3)	-	0	30
PS/PC (3:1)	0.13	0.5	90

Figure -22: Results from annexin B1 liposome binding assays. A - Calcium-dependent binding of the protein to PS/PC vesicles of the molar ratios 1:3 (closed circles) and 3:1 (open circles) is shown as degree of binding. B – Table showing $c_{1/2}$ and degree of binding at a calcium concentration of 0mM and 10mM.

More interestingly, annexin B1 exhibits calcium-independent binding with a binding degree of about 50% for PS/PC (3:1) liposomes. This behaviour is akin to that seen with bell pepper and cotton annexins, although the latter proteins have a less stringent requirement for PS in this context . One can therefore speculate that annexin B1 employs a similar mechanism whereby exposed residues on the convex surface engage in direct interactions with the membrane .

4.4.2 Heparin binding behaviour

While experimenting with the purification procedure, annexin B1 was discovered to bind to heparin in the presence of calcium. In order to investigate the binding behaviour in more detail, a heparin binding assay was developed using heparin residues on a Heparin Sepharose resin (Amersham Biosciences). This assay is designed in the same way as the liposome binding assay used in section 4.3.2. Reversible heparin binding was assessed by first binding the protein to the resin, washing, and subsequent release of the protein by applying EDTA. The supernatant of the EDTA washes were run on an SDS-PAGE and the binding behaviour was evaluated using densitometric analysis. Calcium-dependent heparin binding was investigated with both annexin B1 (figure 4-17 A) and annexin A1 (figure 4-18 B). From previous studies it is known that annexin A1 binds to heparin in a calcium-

dependent manner , therefore it was used as a control in the assay. No protein was found to bind to the heparin resin in the absence of calcium implying a truly calcium-dependent process. Both proteins show reversible (closed circles or triangles) and irreversible binding (open circles or triangles) to heparin.

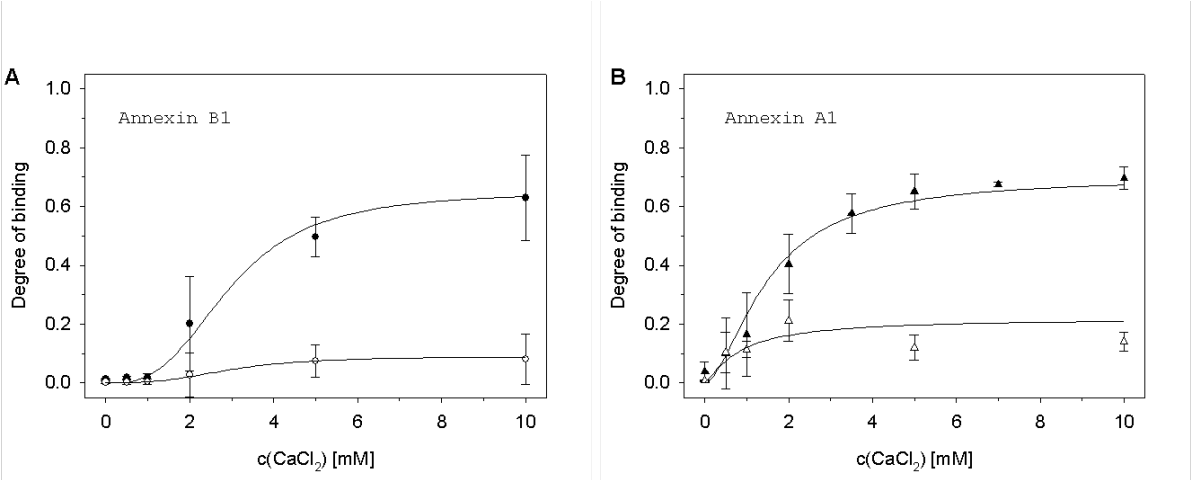

Figure -23: Reversible (closed signs) and irreversible (open signs) binding of annexins B1 and A1 to heparin.

For the reversible binding, annexin B1 data suggest a cooperative binding behaviour with respect to calcium concentration that can be fitted with a Hill equation using a Hill coefficient of n=3. For comparison, annexin A1 displays a binding behaviour with less cooperativity (n=1.7; figure 4-19 B). Comparing the binding curves of the two proteins, it can be ruled out that the lag phase observed with annexin B1 is due to an artefact within the assay.

Both annexin B1 and annexin A1 show calcium dependent binding to heparin with 70% maximum binding degree. The heparin sepharose resin pellet after the EDTA wash step was analysed and some protein could be detected. The amount of irreversibly bound protein increases with higher calcium concentrations and reaches between 10% and 20% in 10mM calcium for both annexins (see open circles and triangles in figures 4-17 A and B). Results from a precipitation assay show that only insignificant amounts of annexin B1 precipitate in the range between 0mM to 10mM calcium. A possible explanation for this calcium-independent heparin binding could be a mechanism where the protein is

dependent on calcium ions to form initial interactions with heparin. Once bound, a fraction of the protein might undergo a shift in the binding mode which "irreversibly" attaches it to the glycosaminoglycan.

4.4.3 Conclusions: Biochemical assays

Annexin B1 binds both to phospholipid vesicles and heparin in a calcium-dependent manner. Moderate binding of annexin B1 can be observed when binding to PS/PC vesicles in a molar ratio of 1:3, but the binding is enhanced with vesicles with a higher PS content. Interestingly, annexin B1 also displays calcium independent binding to the latter vesicles with a half-maximal calcium concentration of 0.1mM. Annexin B1 also binds to PS-rich vesicles in the absence of calcium, a behaviour that had previously been observed with several plant annexins . Here, basic residues on the protein surface such as Trp35, Trp107 and Lys190 (annexin 24(Ca32) numbering) are involved in binding acidic phosphatidyl-serine-rich phospholipid vesicles. This mechanism might also be responsible for calcium-independent membrane binding of annexin B1.

Results from heparin binding assays show that annexin B1 possesses lectin properties. The protein binds to glycosaminoglycan in a calcium-dependent manner and displays cooperativity with respect to calcium. This feature might be traced back to the number of functional calcium binding sites in the protein as fitting the binding curve with a Hill equation revealed a Hill coefficient of n=3.

For annexin A5, a model of heparin binding has been put forward where recognition and binding of heparin occurs via two binding sites (HTS). One could envision a similar mechanism with annexin B1, where the calcium-dependent binding step occurs through the calcium binding sites on the convex side. Assuming the presence of further heparin binding sites elsewhere on the protein surface, annexin B1 can remain bound to the glycosaminoglycan even in the absence of calcium ions. In this context, the amino acid sequence alignment of annexins A5 and B1 reveals that only the HTS-1 site of annexin A5 (Arg25, Lys29) is conserved in annexin B1 by Lys38, Arg42, which could mediate heparin binding via calcium ions. The binding sites on the concave surface (HTS-2) are

not observed with annexin B1, although a K-E-K motif is present instead of the R-K-X-X-R-K motif of HTS-3 (see table 4-7).

Table -7: Heparin binding sites observed in annexin A5 and predicted for annexin B1.

	AnxA5	AnxB1	prediction
HTS-1	basic cluster: Arg-25, Lys-29, Arg-63, (Arg-151)	Lys-38, Arg-42, Lys-76	functional
HTS-2	charged N-terminus and Arg-206, Lys-207	—	Not present
HTS-3	Arg-285, Lys-286, Arg-289, Lys-290	Lys313, Glu314, Lys315	predicted

However, two other sites in annexin B1 merit attention. The motifs Arg91-Arg92 and Lys139-Lys140 on the concave sides of domains I and II respectively could be potential calcium-independent heparin binding sites. A further possible motif, Lys254-Lys255 is found in the DE loop of domain III, which is located in the anticipated dysfunctional canonical calcium binding site. Nevertheless, occupation of this site by heparin would compete with binding to the membrane surface. Further studies would be necessary to test these hypotheses.

4.5 Crystallography

A crystal could be obtained from a factorial condition (0.1mM sodium acetate, pH 5.3, 2M sodium formate, see figure 4-19), and with a protein concentration of 10mg/ml in the drop.

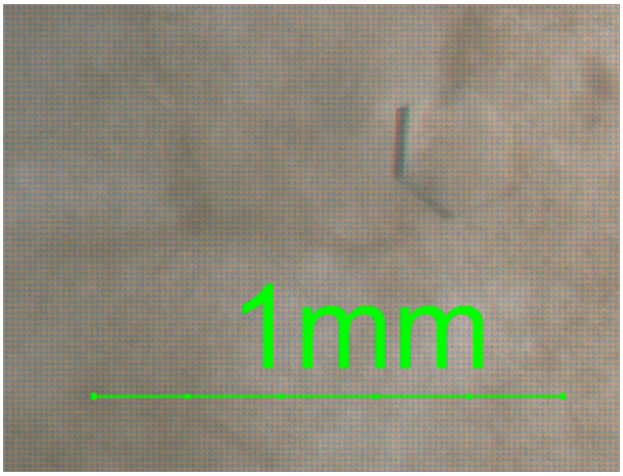

Figure -24: Annexin B1 crystal obtained from 0.1mM sodium acetate, pH 5.3, 2M sodium formate.

Crystallisation conditions were optimised to 0.1mM sodium acetate, pH 5.0, 1.45M sodium formate, and crystals grew to a size of 0.86mm x 0.11mm x 0.11mm. Resolution of the best data set recorded at the ESRF in Grenoble was 3.8Å (see figure 4-20), but it was not possible to index the data and determine the cell parameters with confidence.

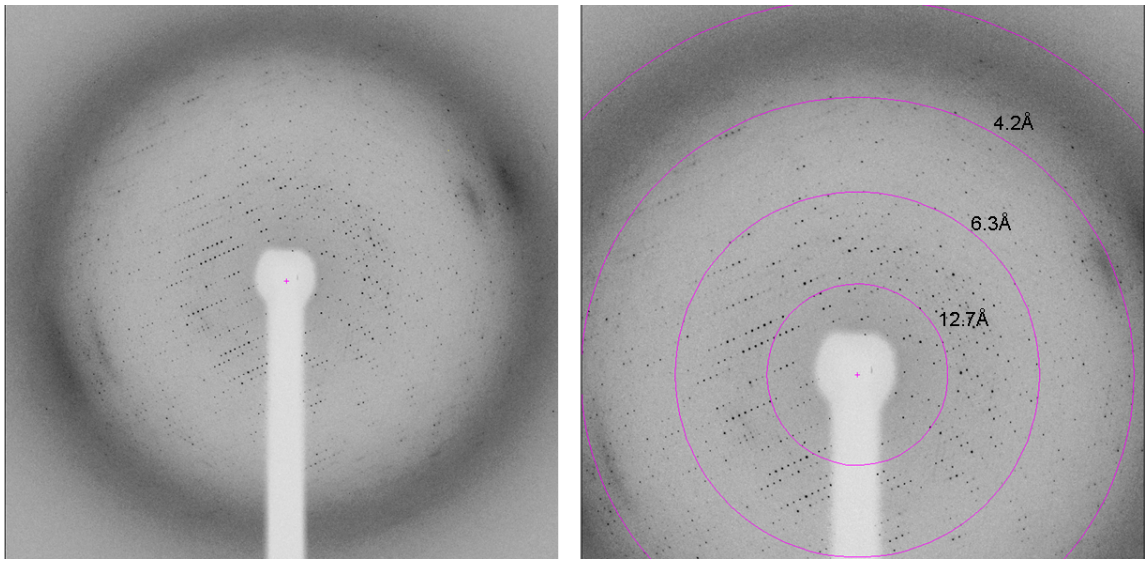

Figure -25: Diffraction pattern of annexin B1 crystal.

4.6 Concluding remarks on AnxB1 and future direction

The pig tapeworm *T. solium* is a parasite that infests the human gut leading to greater intestinal disturbance, pain, and inflammatory response. Humans who ingest *T. solium* eggs may develop the larval infection resulting in the serious disease cysticercosis which can induce epilepsy, mental disturbances, meningeal syndrome, and can even cause death. This parasite causes great economic loss in Latin America, Asia, Africa, the Phillipines and parts of Southern Europe where it also a threat to public health. Reasearch on annexin B1 was aimed to investigate biophysical and biochemical properties of the protein that could be exploited for finding new drug leads to fight infestation with the parasite tapeworm. In this study, membrane- and heparin-binding properties of annexin B1 have been investigated, and first insights into annexin B1 oligomer formation in solution have been gained. Crystallisation trials yielded first crystals that diffracted to 3.8Å but the three-dimensional structure could not be solved.

4.6.1 Membrane binding

Biochemical assays revealed that annexin B1 binds to phospholipids in a calcium-dependent manner supposedly via its type II calcium binding sites. A calcium dependent phospholipid binding mode is reminiscent of the binding behaviour of mammalian annexins which rely almost entirely on a calcium-mediated binding mode regardless of the vesicle composition . Results from this work show that annexin B1 binds more readily to vesicles containing a higher ratio of PS which is a natural component of the cell membrane. In the absence of stimulation, PS is almost exclusively located on the cytoplasmatic side of the cell membrane. By contrast, after stimulation by e.g. thrombin or collagen, PS becomes exposed to the outer side of the plasma membrane at a proportion depending on the nature of the stimulus . There is ample evidence that PS exposure is of crucial importance in cellular physiology being involved in the regulation of haemostatic mechanisms by providing a procoagulant surface on activated platelets, monocytes and endothelial cells . PS exposure is also required in the anticoagulant protein C pathway

leading to the inactivation of factors Va and VIIIa at the membrane interface. Other annexins such as the mammalian annexins A1 and A5 have been known to display anticoagulant activity, which had recently been shown for annexin B1 as well . Notably, the glycoprotein lacadherin is able to compete with factors V and VIII for membrane binding sites at acidic PS functioning as anticoagulant. One could imagine a similar mechanism for binding of annexin B1 to PS-membranes resulting in anticoagulant function.

Interestingly, calcium-independent membrane binding reminiscent of plant annexins was also observed whereby conserved surface exposed residues, including Trp35, Trp107 and Lys190 [annexin 24 (Ca32) numbering] might engage in direct interactions with the membrane . One can therefore speculate that annexin B1 might employ a similar mechanism. In annexin B1, only Lys190 is semi-conserved as Arg214 but it is possible to identify a number of exposed basic residues on the convex surface of the protein such as Arg191, Arg236, Arg265 and Lys232. The involvement of these basic residues would help to explain the observation that a high PS content in the membrane is required in order to bind annexin B1 in the absence of calcium . This property might be important when the protein is directed to bind to specific, PS-rich sites within the membrane. These specific membrane patches could reside in the tape worm itself or in the membrane of a host cell. Too little is known about the localisation of annexin B1 *in vivo* to draw any further conclusions regarding the utilisation of this property. An involvement of these basic residues in membrane binding could be verified by employing mutagenesis studies.

One could imagine that the calcium-independent membrane binding mechanism might assist the calcium-dependent mechanism in annexins where functional calcium binding sites are destroyed by mutation in the endonexin sequence. For instance, the protist-derived annexin α-1 giardin has only one proposed intact type II calcium binding site in domain II whereas helminth annexin B1 has three in domains I, II and IV (see figure 3-3). Plant annexins generally possess two type II calcium binding sites. In contrast, most mammalian annexins possess four intact type II calcium binding sites. The development of four canonical calcium binding sites in certain annexins (predominantly later in evolution) might have made the calcium-independent mechanisms obsolete. The observation of

calcium-independent membrane binding by annexin B1 fits well with this hypothesis, since one can anticipate a disrupted canonical calcium binding site in domain III of this protein. In future studies, membrane binding of α-1 giardin will be assessed where a more calcium-independent mechanism is hypothesized. Outcome of this study will help understand the evolution of calcium binding sites in annexins.

4.6.2 Lectin properties

Binding to carbohydrates of proteoglycans or glycosaminoglycans might be a crucial step in attachment, invasion and cytolysis of intestinal epithelium by parasites. As annexin B1 has been demonstrated to be highly immunogenic [31] and is potentially present on the surface of *C. cellulose*. Results from this work show that annexin B1 binds to heparin in a calcium-dependent and cooperative manner. The assumption of three calcium-dependent calcium binding sites in annexin B1 coincides with the fact that annexin B1 has three canonical type II calcium binding sites. It remains to be clarified whether all three binding sites engage in calcium-dependent glycosaminoglycan binding. A model for heparin binding had been proposed for annexin A5 , where two main heparin binding sites engage in recognition and/ or binding of heparin. Only one of the heparin binding sites is conserved in annexin B1 involving residues Lys38 and Arg39 but further basic surface-exposed residues could be identified on the surface of the protein which could be involved in heparin binding.

Interestingly, several viruses and parasites are thought to have infection strategies based on binding to glycosaminoglycans in the extra-cellular matrix. Prominent examples of proteins with lectin properties are microbial adhesions, including the influenza hemaglutinin, as well as the adhesins from *Shiga* toxin and *Entamoeba histolytica* . Heparan sulphate binding has been found with α-1 giardin, one annexin of the protozoan parasite *G. lamblia*. This protein has also been found to bind to epithelial cells of the small intestine, mast cells and connective tissue. Annexin B1 has been demonstrated to be highly immunogenic , and is potentially present on the surface of *C. cellulosae* . The binding of the protein to glycosaminoglycans such as heparin may therefore be a

mechanism used by *C. cellulosae* to attach to and invade host tissue. This finding opens possibilities for drug design at the heparin binding sites of the protein. Drugs designed to interfere with heparin binding are suitable as they might prevent parasite attachment and invasion of host tissue. Therefore, crystallisation of annexin B1 in complex with heparin tetrasaccharides is considered a goal for further studies in this area. Crystal structures of annexin B1 in complex with heparin tetrasaccharides could be used to investigate the heparin binding sites.

4.6.3 Redox-dependent oligomer formation

Biophysical studies revealed that annexin B1 is present as a mixture of different oligomers in solution, and that their formation is Redox-dependent. Two of the four cysteines present in the protein are likely to be involved in this process, Cys210 (domain III) and Cys340 (domain IV). This led to the hypothesis that side-to-side oligomers are formed which could, on a lipid layer, result in formation of rod-like structures such as the ones found with plant annexins . Coating of target membranes to establish and/or regulate lateral membrane domains is likely to be a key element of annexin function . Formation of 2D crystals of annexins on the surface of membranes was first observed in electron and atomic force microscopy experiments for some mammalian annexins, including AnxA5 and AnxA6 . In a later study, formation of elongated rods reminiscent of 2D crystals was also observed with plant annexins Anx24(Ca32) and Anx(Gh1) . These rods were presumably made up by annexin dimers implying protein-protein interactions as a very important factor for formation of those structures. In that study, a hypothesis had been put forward, where an extended annexin oligomer would be able to provide interaction sites for two membranes at both ends. Those “connecting” rod-like structures would be able to initiate and/or assist in membrane-fusion events in endo- and exocytosis. The same mechanism could also play a role in the cell’s attachment to other (extracellular) structures like infection of a host by a parasite. On the other hand, supra-molecular assembly of annexins on membrane surfaces might provide a platform for binding other proteins and thus carry out scaffolding functions for the cell.

Disulfide-dependent oligomer formation was shown to be responsible for activation and/or functionality of proteins from different organisms and cellular compartments such membrane-bound transcription factor ATF6 and prostanoid IP receptor . The serum protein Acrp30/adiponectin activates different signal transduction pathways in its trimeric and hexameric form , and the activity of the cytosolic thimet oligopeptidase is dependent on the location of dimer forming disulfide bonds, rather than their existence *per se* . Disulfide-dependent oligomer formation might have implications for the function of annexin B1 in a cellular context. Results from this work suggest the formation of an intra-molecular disulfide bridge between Cys130 and N-terminal Cys4 on the concave side of the protein. Reduction of the disulfide bridge would release the N-terminus to exert specific functions, e.g. in membrane binding, as has been found for annexins A3 and A1 . In the case of annexin A3, the local mobility of Trp5 is dependent on Ca^{2+} binding and membrane association of the protein. The N-terminal region of annexin A1 consists of an amphipathic α-helix which is buried into the core domain and becomes solvent exposed upon calcium and membrane binding. Additionally, the N-terminal domain of annexin B1 might also show secondary structure as had been found with annexin A1. The presence of a disulfide bond between Cys130 and Cys4 of annexin B1 needs to be validated in a crystal structure of the protein.

In future studies, the cysteine residues could be mutated to serine residues to study their effects on oligomer formation. Truncation of the N-terminal region might reveal insights into its function and might give clues to the protein's function in the cell. Binding studies on lipid monolayers using a Langmuir balance and electron microscopy **c**ould provide information about oligomer formation on membranes which might be different from findings in solution.

4.6.4 Crystallisation

In initial trials, annexin B1 could be crystallised and yielded a crystal that diffracted up to 3.8Å but the data set could not be indexed. There are several methods by which crystallisation of a protein could be improved to yield a crystal suitable for X-ray diffraction and structure determination. Those methods include modification of the protein

on the DNA level and on the protein level. Annexin B1 possesses a 13 amino acid longer N-terminus as compared to annexin A5 which might be very flexible and hinder a defined arrangement of protein molecules in the crystal. Truncation of the N-terminus at the DNA-level is currently underway, and the truncated protein will be subjected to crystallisation trials as soon as it is available. Other possible modifications of the protein include mutation of surface-exposed cysteine residues to alanines. In this work, cysteine residues have been shown to be involved in Redox-dependent oligomer formation, and their mutation might result in a protein that is mainly monomeric in solution. Modification of the protein, e.g. methylation of surface-exposed lysine residues, might improve the crystallisation properties. This protein engineering approach benefits from being conductible without the necessity to re-clone the DNA and therefore being less time-consuming. Annexin B1 possesses a total of 20 lysines which could potentially be methylated. Addition of cross-linkers or ligands (DTT, HTS, calcium) might also aid packing of the protein into a crystal that diffracts to higher resolution. Co-crystallisation of annexin B1 with HTS and calcium would provide valuable information about the architecture of the heparin binding site and suggest ways for interfering with the binding. A three-dimensional structure would be the first step in structure based drug design for this protein.

The most interesting finding in this present study was that annexin B1 possesses features from both mammalian and plant annexins. It binds to heparin in a calcium-dependent fashion which is reminiscent of mammalian annexins but binds to acidic phospholipids in a manner like plant annexins do. It is tempting to speculate that the ability to bind to heparin or to phospholipid membranes might have undergone a certain development in evolution which might have been intertwined with the development of calcium binding sites. In this scenario, the development of type II calcium binding sites, supposedly later in evolution, might have made a calcium-independent binding mode to phospholipids obsolete. Heparin binding is promoted by type II calcium binding sites and was, so far, only observed for mammalian annexins and annexin B1. As our results suggest cooperativity with respect to calcium, the number of type II calcium binding sites in the

protein might be important. Mammalian annexin A1 shows a stronger binding to heparin at lower calcium concentrations as compared to annexin B1, and it remains to be tested to which degree plant annexins and annexins from subfamily E would bind to heparin.

References

PART C

Materials and Methods

Table of Contents

5 Materials and Methods

5.1 General lab equipment, reagents and media

5.1.1 General lab equipment

Block heater QBT1, Grant Instruments, Cambridge, UK
MS1 Minishaker, IKA -Werke GmbH & CO. KG, Staufen, Germany
IKAMAG® Magnetic stirrer, IKA -Werke GmbH & CO. KG, Staufen, Germany
J2-21 centrifuge with rotor JA-20, Beckman Coulter Inc., High Wycombe, UK
J6-MC centrifuge with rotor TY.J5 4.2, Beckman Coulter Inc., High Wycombe, UK
Megafuge 1.0R with swing bucket rotor, Heraeus, Hanau, Germany
Biofuge fresco, Heraeus, Hanau, Germany
Biofuge pico, Heraeus, Hanau, Germany
Innova 4330 incubator, New Brunswick Scientific, Edison, USA
PE360 balance, Mettler-Toledo international inc., Columbus, USA
AB104 balance, Mettler-Toledo international inc., Columbus, USA
Microwave oven, Panasonic UK Ltd
PowerPac 300, Bio-Rad Laboratories, Inc, Hercules, California, USA
SDS-PAGE equipment: Hoefer Inc., 953 Indiana Street, San Francisco, California 94107
DNA-gel equipment: Orchard House, The Square, Hessle, East Riding of Yorkshire, HU13 0AE, UK
Stuart 3D rocking platform STR9, Barloworld Scientific, Stone, UK
U-100 UV/VIS Spectrophotometer, Hitachi High-Technologies Corp., Tokyo, Japan
Gel drying processor AE-3700, Atto, Tokyo, Japan
UV transluminator UVT-28M, Herolab GmbH Laborgeräte, Wiesloch, Germany
Gene flash, Syngene Bio imaging, Cambridge, UK
Soniprep 140, MSE (UK) Ltd., Lower Sydenham, London, UK
pH meter 140, Corning Inc., Corning, New York, USA

Scotsman ice machine, Scotsman Ice Systems, Vernon Hills, Illinois, USA
Puritec Select water purifier, Onedo Industrial Solutions, Vaucresson, France
Biocad® 700e Workstation (Applied Biosystems)

5.1.2 General Reagents

Purchased from Sigma-Aldrich Company Ltd, Gillingham, Dorset, UK:
Acetonitrile, NH_4HCO_3, APS, ampicillin, L-Arginine, benzamidinium chloride, bromphenolblue, $CaCl_2$, CHCA, Coomassie Brillant Blue R, deoxycholic acid, DTT, EDTA, $NiSO_4$, NonidetP40, sorbitol, galactose, glycine, L-Histidine, HEPES, IAA, IPTG, isopropanol, lactate, Lysing enzyme, lysozyme, $MnCl_2$, MOPS, PMSF, K_2HPO_4, KH_2PO_4, L-Serine, sinapinic acid, SDS, TEMED, TRIS, Triton X-100, xylene cyanol

Purchased from Fisher Scientific UK Ltd, Loughborough, Leicestershire, UK:
acetic acid (glacial), EtOH, glycerol, HCl, NaCl, NaOH, $MgCl_2$, KCl, sucrose, urea,

Purchased from Promega
trypsin

Purchased from Invitrogen Corporation, Paisley, UK:
Agarose

Purchased from VWR International Ltd, Ashbourne, Ireland:
imidazole

Purchased from Severn Biotech Limited Kidderminster, Worcestershire, UK:
Design a Gel Acrylamide Solution, 30% (w/v) acrylamide, acrylamide to bis-acrylamide ratio 37.5:1
Purchased from Pierce, Rockford, Illinois, USA:
Gelcode Blue Stain Reagent
Purchased from Oxoid Ltd., Basingstoke, Hampshire, UK:
tryptone, yeast extract

5.1.3 Media

5.1.3.1 LB medium

10g Tryptone (1%), 5g yeast extract (0.5%) and 5g NaCl were dissolved and made up to 1 litre with water. The medium was autoclaved.

5.1.4 Other materials

Vivaspin concentration devices, VivaScience, Unit 6, Stroud Business Centre, Oldends Lane Industrial Estate, Stonehouse, GL10 3RQ, Glouchestershire, UK
Centricon, Amicon Ultra, Millipore, 112 Talavera Road, North Ryde, NSW 2113, Australia
Dialysis bags, Spectrum Laboratories Inc, 18617 Broadwick street, Rancho Dominguez, CA 90220, USA

5.1.5 Crystallisation equipment

24-well plates, 22mm siliconized circular cover slides, high vacuum sealant and synthetic CryoLoops were purchased from Hampton Research, 34 journey, Aliso Viejo, CA 92656-3317, USA

5.2 Molecular biology

5.2.1 Plasmids

Plasmids are circular, double-stranded DNA (dsDNA) molecules that are separate from the cell's chromosomal DNA. Plasmid vectors contain essential nucleotide sequences required for their use in DNA cloning: a replication origin and a region in which exogenous DNA fragments can be inserted. The plasmid also harbours a selective gene,

the most commonly used being the ampicillin-resistance gene (*amp*^{r}), encoding β-lactamase, which inactivates the antibiotic ampicillin. During cell division, at least one copy of the plasmid DNA is segregated to each daughter cell, and any DNA sequence inserted into such a plasmid is replicated along with the rest of the plasmid DNA. Expression vectors can produce protein upon induction with IPTG (isopropyl-beta-D-thiogalactopyranoside).

List of plasmid vectors:

pETDuet-1	Novagen, EMD Biosciences, Inc, Darmstadt, Germany
pTrcHis_B	Invitrogen Corporation, Paisley, UK
pRSET_6c	Schoepfer, 1993
pRSET_C	Invitrogen Corporation, Paisley, UK

5.2.2 Molecular cloning

The essence of recombinant DNA technology is the preparation of large numbers of identical DNA molecules through linkage of a DNA fragment with a vector. This way, identical copies of a DNA fragment can be produced (cloning).
Rare specific DNA sequences can be directly amplified to large amounts through an alternative to cloning, called the polymerase chain reaction (PCR). In a PCR, two synthetic oligonucleotides (primers) complementary to the 3′ ends of the plus and minus strand of the target DNA segment are used as primers for DNA chain synthesis done by a temperature-resistant DNA polymerase for instance from *Thermus aquaticus* (*Taq* polymerase). Oligonucleotides, deoxynucleotides and DNA polymerase are mixed with the target DNA and subjected to repeated heating and cooling cycles.

Prohibitin truncation mutants were generated from the tandem vector His_6-BAP32:BAP37_pETDuet (a kind gift from T. Tatsuta) as template which was digested to gain the DNA for the respective proteins which would serve as templates for PCRs. BAP32 was originally cloned into the first multiple cloning site of pETDuet using the

restriction sites for *BamHI* and *EcoRI*, BAP37 was cloned into the second multiple cloning site via restriction sites for *NdeI* and *XhoI*. Using suitable primers in the PCRs, truncated versions of the proteins were produced. Each PCR was optimised in its annealing temperature to give maximum yield of product. The amplified product was subsequently ligated into expression vectors pTrc_His_B (BAP32) or pRSET_C (BAP37). The different truncation mutant constructs, their respective PCR primers and annealing temperatures are summarised in table 5-1.

Following page: Table -1: Used primers and annealing temperatures for cloning of prohibitin truncation mutants

Truncation of	restriction site coding primer/	restriction site non coding primer/	annealing temperature
N-terminus	BAP32_1F/ *Bam*HI	BAP32_1R/ *Eco*RI	42
N-terminus, C-terminus	BAP32_1F/ *Bam*HI	BAP32_2R/ *Eco*RI	46
N-terminus	BAP37_2F/ *Nde*I	BAP37_1R/ *Xho*I	48
N-terminus, C-terminus	BAP37_2F/ *Nde*I	BAP37_2R/ *Xho*I	46
N-terminus	BAP32_2F/ *Hind*III	BAP32_3R/ *Eco*RI	44

Construct name
HIS_6-BAP32(Δ1-30)_pTrcHisB
HIS_6-BAP32(31-177)_pTrcHisB
BAP37(Δ1-40)_pRSET6C
BAP37(41-191)_pRSET6C
HIS_6-BAP32(Δ1-24)_pTrcHis_B

List of primers

BAP32_1F coding, BAP32(Δ1-30), *Bam*HI
5'-C GCG GAT CCC GAT GCT GGA CAC AGA GCT GTC-3'

BAP32_1R non-coding, BAP32, *Eco*RI
5'-CCG GAA TTC TCA CTG GGG AAG CTG GAG AAG CAC GG-3'

BAP32_2R non-coding, BAP32(1-177), *Eco*RI
5'-CCG GAA TTC TCA CTT CCC GAA GGT CAG ATG TGT CAG-3'

BAP32_2F coding, BAP32(Δ1-24), *Eco*RI
5'-C CGG AAT TCT GCT TTG TAT AAT GTG GAT GC-3'

BAP32_3R non-coding, BAP32, *Hind*III
5'-CCC AAG CTT TCA CTG GGG AAG CTG GAG AAG CAC-3'

BAP37_1F coding, BAP37, *Nde*I
5'-GGG TTT CAT ATG GCA GAT CTC GCA GCC CAG AAC TTG-3'

BAP37_1R non-coding, BAP37, *Xho*I
5'-CCG CTC GAG GTC ATT TCT TAC CCT TAA TGA GGC TGT-3'

BAP37_2F coding, BAP37(Δ1-40), *Nde*I
5'-GGG TTT CAT ATG CGC GAA TCC GTG TTC ACC GTG GAA GGC GG-3'

BAP37_2R non-coding, BAP(1-191), *Xho*I
5'-CCG CTC GAG TCA TCG GCT GAA GCT CAG CTC TGT GAT-3'

HIS_6-FtsH-IMS region was generated from *E. coli* genomic DNA using suitable primers in a PCR reaction with an annealing temperature of 48ºC, followed by double digestion using *Eco*RI and *Xho*I and ligation into cut pRSET_C vector. The success of the ligation was analysed by analytical digestion of the ligated plasmid and sequencing.

List of primers

FtsH_1F N-terminal loop, extra-membrane domain, coding, *Xho*I
5'-CC GCT CGA GAT CAG AGC TTT GGG CCC AGC GAG-3'

FtsH_1R N-terminal loop, extra-membrane domain, non-coding, *Eco*RI
3'-GGC GGA CTT CTT GGT TCG ATC CTT AAG GCC-5'

All primers were purchased from MWG, Ebersberg, Germany. Identity of each construct was verified by DNA sequencing.

5.2.2.1 PCR

The PCR is mostly dependent on the annealing temperature of the primers, the magnesium concentration and the amplifying system. PCR conditions were optimized in annealing temperature whereas the magnesium concentration was kept constant for all PCRs at 4mM.

Amplifying system: *Taq* DNA polymerase, Promega UK Ltd., Southampton, UK
Taq DNA polymerase, Roche Diagnostics Ltd., Burgess Hill, UK
PCR machine: MJ research PTC-200, GMI Inc., Minnesota, USA

An example of the reaction mix and the used PCR protocol is stated below (see table 5-2). The reactions were analyzed on a 1% agarose gel stained with SYBR Safe™ DNA gel stain (Invitrogen Corporation, Paisley, UK). The appropriate DNA bands were cut out and gel extracted using the gel extraction kit from Qiagen following the manufacturer's protocol.

Table 5-2: Examples for a PCR mix and a PCR protocol

Mixture
32µl sterile water
4µl 10x Thermo Pol buffer
4µl or 6.5µl 25mM $MaCl_2$
1µl 100pmol Primer F
1µl 100pmol Primer R
0.4µl 3.2pmol dNTPs (25mM)
0.5µl template DNA
1µl Taq Polymerase

Protocol		
Denaturation	94ºC for 5:00	
Denaturation	94ºC for 1:30	╗
Annealing	42ºC for 1:30	╠ 30x
Elongation	72ºC for 2:30	╝
Elongation	72ºC for 10:00	

5.2.2.2 Restriction digest

To clone specific DNA fragments into a plasmid vector, the PCR products and an appropriate vector were digested using restriction enzymes. In this reaction, single-stranded regions ("sticky ends") of complementary sequences were created at the respective restriction-sites. Pairing of matching single-stranded regions from a DNA fragment with single-stranded regions from a cut vector in a ligation reaction leads to formation of a chimeric molecule, the new plasmid.

Digests of PCR products or vectors were carried out as subsequent single (one restriction enzyme) or one double digest (two restriction enzymes at a time) by incubation of the DNA with the appropriate restriction enzymes and buffers at 37ºC for 2 to 4 hours. During digestion of a vector, 1/10 volume of CIP was added for the last 30 minutes to remove phosphates at the restriction sites which reduces re-ligation of the vector in the subsequent ligation reaction. All digests were analysed on a 1% agarose gel stained with SYBR Safe™ DNA gel stain (Invitrogen Corporation, Paisley, UK). The DNA bands were cut out and extracted using the gel extraction kit from Qiagen and following the manufacturer's protocol.

List of enzymes:

restriction endonucleases: *Nde*I, *Eco*RI, *Hind*III, *Xho*I, *Bam*HI, all purchased from New England Biolabs, Ipswich, Massachusetts, USA

other enzymes: Calf Intestinal Alkaline Phosphatase (CIP) purchased from New England Biolabs, Ipswich, Massachusetts, USA

5.2.2.3 Ligation

In recombinant DNA technology, purified DNA ligase is used to covalently join the ends of restriction fragments in an ATP dependent chemical reaction.

The digested PCR products and vectors were evaporated at 50ºC in a heating block to increase their concentration. Ligation reactions were carried out in a total volume of 20µl at 16ºC at least overnight, and up to 4 days. The reaction set up included 4µl T4 ligase and

2µl 10x T4 DNA ligase buffer, PCR product and vector. Success of the ligation was determined by transforming the ligation reaction mix into XL1Blue cells and incubating the plate overnight at 37ºC. Resulting colonies were used to inoculate 8-10ml LB media with which a MINI prep (Qiagen) was carried out the following day using the manufacturer's protocol. Analytical digest and sequencing of the gained plasmid DNA confirmed the success of the ligation and the identity of the construct.

Enzme:T4 DNA Ligase, New England Biolabs, Ipswich, Massachusetts, USA
Cells: XL1Blue *E.coli*, Stratagene, La Jolla, California, USA

5.2.2.4 Sequencing

A PCR reaction was set up using the plasmid, T7 sequencing primer and Big Dye Term Mix, and following the protocol stated in table 5-3. The Big Dye Terminator Mix (Applied Biosystems, Foster City, California, USA) contains a polymerase, unlabelled and labelled nucleotides in buffer. Whenever a labelled nucleotide is used by the polymerase in the elongation process, the chain terminates. Statistically, all terminated chains have different lengths with one labelled nucleotide at the end. The mix is the run on a gel and analysed by a software that detects intensity and identity of the fluorescently labelled nucleotides at the ends of the DNA oligomers. Sequencing was done by the DNA sequencing facility at the School of Biology, The University of Edinburgh.

Table 5-3: PCR mixture and temperature protocol used for sequencing.

Mixture	**Protocol**	
4µl Big Dye Term Mix	Denaturation	96ºC for 0:20
1-5µl DNA template	Annealing	50ºC for 0:20
1µl T7 sequencing primer	Elongation	60ºC for 4:00
sterile water to 20µl	25 repeats	

T7 sequencing primer: 5'-TAA TAC GAC TCA CTA TAG GGA GA-3'

5.2.3 Generation of a BAP32 construct with an artificial N-terminal helix

The construct His-BAP32(Δ1-24)_pTrc_His_B was generated in two steps: first, BAP32(Δ1-24) was amplified in a PCR using the primers BAP32_2F and BAP32_3R creating restriction sites for *Eco*RI and *Hind*III. The PCR product was digested and cloned into pTrc_His_B to create the intermediate construct His_6-BAP32(Δ1-24)_pTrcHis_B. Afterwards, the intermediate construct was cut with *Bam*HI and *Eco*RI in two subsequent single digests to create sticky ends for ligation with the hybridized oligomers coding for the artificial helix. 1/10 volume CIP was added to the last 30 minutes of the second digest to remove phosphates at the restriction sites.

The artificial helix AKAAAAKAAAAKAAAA was translated into a DNA code and purchased from MWG (Ebersberg, Germany) as two oligomers of 54 nucleotides. For usage in the later ligation, the oligomers were designed with complementary sticky ends as theoretically gained from a *Bam*HI/ *Eco*RI restriction digest of the intermediate construct, and a phosphate at both 5' ends was introduced to enable ligation (see figure 5-1). The lyophilised oligomers were dissolved in STE buffer (10 mM Tris pH 8.0, 50 mM NaCl, 1 mM EDTA) at a concentration of 8 OD_{260} units/ 100µl. The two strands were mixed together in equal molar amounts (5µl + 5µl). After heating to 94°C in a heating block, the block was allowed to gradually cool down to room temperature enabling a slow annealing of both strands. The resulting product was a stable, double-stranded DNA that was used for ligation into the cut intermediate construct. The ligation and sequencing was carried out as stated above.

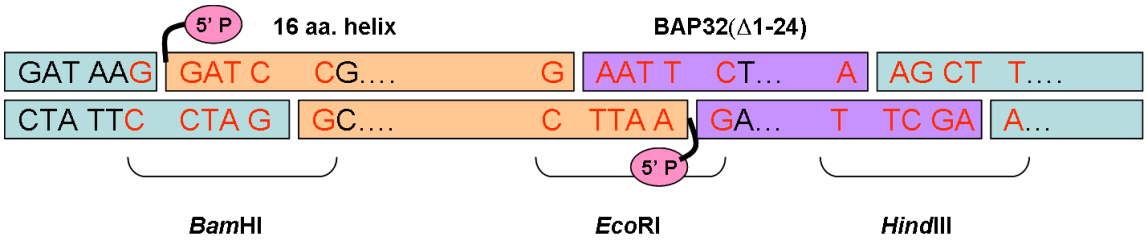

Figure -1: Cloning strategy for generating HIS_6-helix-BAP32(Δ1-24)_pTrcHIS_B. The oligomers for the 16 residues long artificial helix (pink) is cloned into the vector pTrc_His_B (blue) using a *Bam*HI restriction site. BAP32(Δ1-24) (purple) is inserted upstream of the helix via *Eco*RI and *Hind*III sites. Oligomers for the artificial helix were designed including a phosphate residue at the 5'end to enable ligation.

List of oligomers:

coding, synth. helix, *Bam*HI/*Eco*RI

5'-pGATCCGGCTAAGGCCGCGGCAGCTAAAGCCGCGGCAGCTAAGGCAGCTGCCGCG-3'

non-coding, synth. helix, *Eco*RI/*Bam*HI

5'-pAATTCGCGGCAGCTGCCTTAGCTGCCGCGGCTTTAGCTGCCGCGGCCTTAGCCG-3'

5.2.4 Transformation

Transformation describes a genetic alteration of a cell caused by the uptake and expression of foreign DNA regardless of the mechanism involved. The selective gene on the plasmid provides the transformed cell with a resistance against this antibiotic which is used to differentiate between successfully transformed and not transformed cells.

List of cell strains:

BL21(DE3) *E.coli*	Invitrogen Corporation, Paisley, UK
DH5α *E.coli*	Invitrogen Corporation, Paisley, UK
XL1Blue *E.coli*	Stratagene, La Jolla, California, USA
Rosetta 2(DE3) E.coli	Novagene, Merck Pty., Kilsyth, Victoria, Australia

All transformations involved in this work were done either by heat shock or electroporation. For transformation by heat shock, one aliquot of competent cells was thawed on ice and 1µl plasmid DNA was added. After incubation on ice for 10 minutes, the cells were placed in a heat block at 42ºC for 4 minutes (heat shock) to enable transformation. The cells were incubated on ice for further 10 minutes, afterwards mixed gently with 800µl LB media and incubated at 37ºC for 45 minutes. Cells were then

harvested by centrifugation at 3000 g for 5 minutes at room temperature in a Biofuge pico. Finally, the cell pellet was resuspended in a small volume of LB media and plated on an agar plate containing an antibiotic (e.g. ampicillin) as a selection tool. The plate was then incubated at 37ºC over night.

Competent cells used for transformation by electroporation were washed three times with 400µl glycerol in order to remove remaining salt surrounding the cells. After adding 1µl plasmid DNA, the cells were incubated on ice for 15 minutes. The cells were transferred to the precooled electroporation cuvette, and the cuvette was placed in the electroporator (*Gene Pulser* with *Pulse Controller* and *Capacitance Extender*, Bio-Rad Laboratories, Inc, Hercules, California, USA) and electroporated. If no sparks have appeared during pulsing the cells, the electroporation was considered successful. The cells were transferred into 800µl LB warm media immediately. After incubating the cells for ca. 45 minutes at 37ºC while shaking, the cells were centrifuged at 3000rpm for 7 minutes in a Biofuge pico at room temperature. The cells were plated on an agar plate and incubated over night at 37ºC.

5.2.5 Plasmid DNA preparation

Plasmid preparations were carried out using Qiagen MINI or MIDI plasmid kits (QIAGEN Ltd., Crawley, West Sussex, UK), and following the manufacturers protocols.

For preparation of plasmid DNA, a single colony of transformed DH5α or XL1Blue cells was picked from an agarose plate to inoculate 7ml (MINI) or 100 ml (MIDI) LB media containing 100µg/ml ampicillin. After incubation over night at 37ºC in an orbital shaker, the cells were spun down at 3000g, 4ºC for 15 minutes in a Megafuge 1.0R. Plasmid DNA was isolated from the cells following the instructions for the plasmid purification kit (MINI or MIDI) by Qiagen. For convenience, step 13 and 14 of the MIDI prep protocol were altered as follows: after elution of the plasmid DNA from the column with buffer QF and subsequent addition of 3.5ml isopropanol, the solution was aliquoted into 6 Eppendorf tubes and spun for 45 minutes at 13.000 rpm using a Biofuge fresco. The pellets were washed with 200µl 70% ethanol and pooled into one tube. This tube was spun again for 30 minutes at 13.000 rpm. The ethanol was removed, and the tube was left to dry over night

to remove residual ethanol. Finally, the DNA was resolved as recommended in the Qiagen protocol.

5.2.6 Isolation of genomic DNA

For cloning of FtsH-IMS region into pRSET_C, genomic *E.coli* DNA was isolated and used as a template in the PCR reaction. 20µl of untransformed DH5α cells were used to inoculate 20ml LB media without an antibiotic. Bacteria were pelleted by centrifugation at 3000g for 15 minutes in a Megafuge 1.0R, the supernatant was discarded and all liquid was completely removed. For purifying the genomic DNA, two QIAGEN protocols (for MIDI prep and for Isolation of genomic DNA) were combined as follows. The cell pellet was resuspended in 3.5 ml Buffer B1 with 10 µl RNase A solution (100 mg/ml) by vortexing. 100 µl lysozyme stock solution (100 mg/ml) was added, and the mix was incubated at 37°C for 30 minutes. After adding 1.2 ml of Buffer B2, the tube was mixed by inverting the tube several times and by vortexing for a few seconds. During the following incubation at 50°C for 30 minutes, the QIAGEN MIDI prep column was equilibrated with 10 ml of Buffer QBT. After the column was allowed to empty by gravity flow, the sample was vortexed for 10s at maximum speed and applied to the equilibrated column and allowed to enter the resin by gravity flow. The column was washed 2 times with 10 ml of Buffer QC, and the genomic DNA was eluted with 5 ml of Buffer QF. Afterwards, the DNA was precipitated by adding 3.5 ml (0.7 volumes) room-temperature isopropanol. The tube was inverted 10 to 20 times, and the DNA spooled using a curved glass rod. The end of the rod containing the DNA was immediately transferred into a microcentrifuge tube, and 300µl 10mM Tris-HCl, pH 8.5, was added. After dissolving the DNA overnight on a shaker at room temperature, the microcentrifuge tube was centrifuged at 13000rpm (Biofuge fresco) for 10 minutes at 4ºC. The dissolved DNA was transferred into a fresh microcentrifuge tube and stored at -20ºC.

Buffer compositions:

B1: 18.61g $Na_2EDTA{\cdot}2H_2O$ and 6.06g Tris base are dissolved in 800ml distilled water, and 50ml 10% Tween-20 solution and 50ml 10% Triton X-100 solution are added.

After the pH is adjusted to 8.0 with HCl, the volume is brought to 1L with distilled water.

B2: 286.59g guanidine HCl are dissolved in 700ml distilled water, and 200ml of 100% Tween-20 are added. The volume is adjusted to 1L with distilled water.

QBT: 43.83g NaCl and 10.46g MOPS (free acid) are dissolved in 800ml distilled water, and the pH is adjusted to 7.0 with NaOH. Afterwards, 150ml pure isopropanol and 15ml 10% Triton X-100 solution (v/v) are added. The volume is brought to 1L with distilled water.

QC: 58.44g NaCl and 10.46g MOPS (free acid) are dissolved in 800ml distilled water and the pH adjusted to 7.0 with NaOH. 150ml pure isopropanol are added and the volume is brought to 1L with distilled water.

QF: 93.5g NaCl and 6.06g Tris base are dissolved in 800ml distilled water, and the pH is adjusted to 8.5 with HCl. 150ml pure isopropanol are added and the volume is brought to 1L with distilled water.

5.3 Protein production

5.3.1 Protein expression for FtsH-IMS region and annexin B1

A single colony of transformed BL21(DE3) was picked from a plate to inoculate the preculture of 1L LB media containing 100µg/ml ampicillin. After incubation over night at 37ºC in an orbital shaker, the preculture was diluted into 7L fresh LB media (containing 100µg/ml ampicillin) and grown at 37ºC while shaking until the OD_{600} exceeds 1. The cells were induced with 0.5mM IPTG (final concentration) and incubated overnight at 37ºC in an orbital shaker incubator. After harvesting the cells at 3000g, 4ºC for 20 minutes (J6-MC centrifuge, Beckman), the cell pellet was resuspended in buffer D1 (100 mM NaCl, 1.5 mM EDTA, 5 mM benzamidinium chloride, 1 mM PMSF, 0.1% Triton X-100, 20 mM Tris, pH 8.0) and stored at -20ºC until further use.

5.3.2 Protein expression for prohibitins

A single colony of transformed BL21(DE3) was picked from a plate to inoculate the preculture of 0.5-1L LB media containing 100µg/ml ampicillin. After incubation over night at 37ºC in an orbital shaker, the preculture was diluted into 3L fresh LB media (containing 100µg/ml ampicillin) and grown at 37ºC until the OD600 exceeds 1. The cells were induced with 0.5mM IPTG (final concentration) and incubated for further 3 hours at 37ºC. The cells were harvested at 3000g, 4ºC for 20 minutes (J6-MC centrifuge, Beckman). The cell pellet was resuspended in 20ml lysis buffer (25% sucrose, 1mM EDTA, 50mM Tris/HCl, pH 8.0, 1mM PMSF in isopropanol) and stored at -20ºC until inclusion bodies were prepared.

5.3.3 Preparation of inclusion bodies

The isolation of the inclusion bodies was carried out in accordance to a protocol provided by C. Rückert (Institut für Immungenetik, Universitätsklinikum Charité, Humboldt-Universität zu Berlin, Germany) and as previously described in Garboczi *et al*., 1992 .
One litre frozen cell pellets were thawed, resuspended and 1ml lysozyme solution (10mg/ml lysozyme in lysis buffer) was added. After incubation on ice for 30 minutes, 200µl 1M $MgCl_2$ and 20µl 1M $MnCl_2$ were added. The cells were then sonicated 5 times for 5 seconds each time at 35% amplitude, with 10 seconds break between the pulses to enhance the lysis process. The lysate was centrifuged for 10 minutes at 4°C, 10000 x g in a Beckman centrifuge J2-21, to remove light cellular components and particles of the cytosole. The light brown pellet was then resuspended in 20 ml detergent buffer (200mM NaCl, 1% deoxycholic acid, 1% Nonidet-P40, 2mM EDTA, 20mM Tris, pH 8.0) with 40µl 1M DTT. After another sonication step and centrifugation, the pellet was washed in 20ml Triton buffer (100mM NaCl, 1mM EDTA, 0.5% TritonX-100, 50mM Tris, pH 7.5) with 40µl 1 M DTT and then sonicated again. Afterwards, the solution was incubated on ice for 10 minutes and centrifuged again. The washing step in Triton buffer followed by sonication and centrifugation was repeated two more times but without the incubation on ice. The last pellet (inclusion bodies) appeared to be white and was resuspended in 4ml inclusion bodies buffer (20mM Tris, 150mM NaCl, pH 7.5) with 40µl 1M DTT, aliquoted

to 1ml aliquots into microcentrifuge tubes and stored at -20°C. Stepwise purification of the inclusion bodies was traced on SDS PAGE.

5.3.4 Refolding

Microcentrifuge tubes containing inclusion bodies were thawed, and centrifuged for 10 minutes at 4°C, 10000 x g in a Biofuge fresco. The pellets were resuspended in 1ml urea buffer (8M urea, 50 mM NaCl, 20 mM Tris, pH 7.5) and incubated for 2 hours at room temperature while shaking. A centrifugation step in a Biofuge fresco for 20 minutes at 10000 x g, 4°C, separates the supernatant containing BAP32 and BAP37 or their truncated forms from the inclusion body membrane. A refolding protocol was established according to the suggestions made by . To avoid protein precipitation, the protein solution was diluted with urea buffer to a concentration of ~1mg/ml protein. The proteins are refolded by stepwise dialysis using 10 times the amount of refolding buffer compared to the dialysis sample. The protein solution is transferred into a dialysis tube (heated 100mM EDTA for 10 minutes prior to use, MWCO 6000 – 8000Da) and dialysed against refolding buffer A (0.5M Tris, 20% glycerol, 1% Nonidet-P40, 150mM KCl, 1mM DTT, 0.113M L-Arginine, 0.275M L-Serine, 11.86mM L-Histidine, pH is adjusted to 7.5) overnight at 4ºC. The next morning, the tube is transferred into fresh refolding buffer A and dialysis continues for at least another 8 hours at 4ºC. Finally, the dialysis tube is transferred into refolding buffer B (150mM KCl, 100mM Tris, 10% glycerol, 1% Nonidet-P40, pH adjusted to 8.0) and dialysed overnight at 4ºC. The content of the dialysis tube was applied to an equilibrated nickel column for protein purification (see section 5.4.1).

5.3.5 Protein expression in expression trials

A single colony of transformed BL21(DE3) was picked from a plate to inoculate the preculture of 20ml LB media containing 100µg/ml ampicillin. After incubation over night at 37ºC in an orbital shaker, 2ml of the preculture was diluted into 20ml fresh LB media (containing 100µg/ml ampicillin) and grown at 37ºC until the OD600 exceeds 1. A sample was taken (20µl) before the cells were induced. The cells were induced with varying final IPTG concentrations: 0.125mM, 0.25mM, 0.375mM and 0.5mM. All cultures were

incubated for further 7 hours at 37ºC or 30ºC, and another sample was taken. The samples representing uninduced and induced cells were run on SDS-PAGE. After incubation over night at 37ºC or 30ºC, respectively, the cells were harvested for 15 minutes at 3000 x g, 4ºC (J6-MC centrifuge, Beckman). The cell pellet was resuspended in 1ml lysis buffer (25% sucrose, 1mM EDTA, 50mM Tris/HCl, pH 8.0, 1mM PMSF in isopropanol) and subjected to three freeze-thaw cycles to lyse the cells. After centrifugation for 40 minutes at 13000rpm and 4ºC (Biofuge fresco), 20µl of supernatant and pellet were analysed on SDS-PAGE.

5.4 Protein purification and concentration

Annexin B1 and $HisS_6$-FtsH-IMS were expressed as soluble proteins in the cell cytosol. Cells from expression experiments of both proteins were harvested and frozen at -20ºC. For purification, frozen cell pellets were thawed and refrozen three times to lyse the cells. Afterwards, the resuspended cell pellets were sonicated three times for 15 seconds on/ 15 seconds off at 15 micron amplitude. High-speed centrifugation at 23000 rpm for 30 minutes at 4ºC (Beckman centrifuge J2-21) separated the cell cytosol (supernatant) from insoluble parts of the cell such as membranes and cell organelles. The supernatants containing the proteins were subjected to individual purification protocols. Purification of annexin B1 included anion exchange and heparin affinity chromatography; whereas His_6-FtsH-IMS was purified employing immobilised metal affinity chromatography (IMAC) and anion exchange chromatography as a polishing step.
Prohibitins were subjected to immobilised nickel affinity chromatography after refolding of the proteins.

5.4.1 Immobilised metal affinity chromatography (IMAC)

IMAC is useful for purifying histidine-tagged proteins, but generally applicable to most proteins with exposed histidine, cysteine, and tryptophan residues. The highly selective affinity depends upon the metal ion used such as Ni^{2+} and Co^{2+} which is bound to the chelating ligand nitrilotriacetic acid (NTA) on highly cross-linked agarose beads (Ni-NTA

Sepharose™ 6 Fast Flow, QIAGEN Ltd., Crawley, West Sussex, UK). Free coordination sites of the nickel ion interact with the imidazole rings of the histidine-tag thus binding the protein. Imidazole itself can also bind to the nickel ions, and can be used to elute the His_6-tagged protein. Other methods to elute the bound protein include reducing the pH to 4.5–5.3 which will protonate the histidine residues or using reagents such as EDTA or EGTA to chelate the nickel ions, and this way removing them from the NTA groups including the protein.

The Ni-NTA resin used for purifying the intermembrane space region of FtsH was equilibrated with 20mM Tris, pH 7.5, 100mM NaCl. The supernatant from the high-speed centrifugation step was diluted 1:3 with 20mM tris, pH 7.5, 100mM NaCl and applied to the equilibrated column. The Ni-NTA resin was eluted with a step gradient of 20, 50, 100, 150 and 250mM imidazole in 20mM Tris, pH 7.5, 100mM NaCl. 50ml imidazole solution was used for each step. Fractions were collected and proteins were detected using SDS-PAGE.

For purifying prohibitins, the Ni-NTA resin was equilibrated with refolding buffer B, and the contents of the dialysis bag after refolding was applied onto the column. After a washing step with buffer B, the protein complex was eluted from the column with 50ml 500mM imidazole in refolding buffer B.

5.4.2 Anion exchange chromatography

In anion exchange chromatography, positively charged exchange groups are linked to a sepharose resin (Q-Sepharose, Amersham Biosciences, GE Healthcare UK Ltd, Little Chalfont, Buckinghamshire, UK) giving the resin an overall positive charge. Negatively charged patches in proteins can bind to the resin and thus attach the protein to the resin. Proteins can then be eluted with high salt solution such as 1M NaCl or a change in pH.

Anion exchange chromatography was employed as a second purification step for His_6-FtsH-IMS. Pooled fractions from the nickel affinity step were dialysed 1:10 over night at 4ºC in 20mM tris, pH 9.0. After application onto the equilibrated column and washing, the protein was eluted using a linear gradient from 0M to 1M NaCl in 20mM Tris, pH 9.0 with a total volume of 400ml.

Supernatant containing annexin B1 was dialysed 1:10 in equilibration buffer (20 mM Tris, pH 9.0) over night at 4 ºC. After applying the supernatant to the equilibrated column, the column was washed extensively with equilibration buffer. To elute the protein, 500ml of a linear gradient from 20mM to 1M NaCl in equilibration buffer was applied, and the protein eluted from 150mM to 300mM NaCl. After detecting the proteins using SDS-PAGE, the protein containing fractions were pooled and dialysed against the equilibration buffer for heparin affinity chromatography as the next purification step.

5.4.3 Heparin affinity chromatography

Heparin Sepharose™ 6 Fast flow (Amersham Biosciences, GE Healthcare UK Ltd, Little Chalfont, Buckinghamshire, UK) allows separation of biomolecules with an affinity for heparin, a naturally occurring glycosaminoglycan with a molecular weight distribution from 5kDa to 30kDa.

Purification by heparin affinity chromatography was used as the second purification step in purifying wild type annexin B1. The pooled fractions obtained from the anion exchange step were dialysed over night against the equilibration buffer for heparin affinity chromatography (5mM $CaCl_2$, 250mM NaCl, 50mM Tris, pH 9.0) and loaded onto a heparin sepharose column. After extensive washing, the protein was eluted by applying buffer containing EDTA (10mM EDTA, 250mM NaCl, 50mM Tris, pH 9.0). Fractions were analysed on SDS-PAGE, and annexin B1 containing fractions were pooled and concentrated.

5.4.4 Nickel affinity chromatography batch experiment

Batch experiments were carried out to detect His_6-tagged prohibitin proteins in a protein mixture. 700µl of Ni-NTA resin (Amersham Biosciences) was transferred to a microcentrifuge tube and spun down for 3 minutes at 3000 x g, 4ºC in a Biofuge fresco. The supernatant was then removed, and the resin was washed 3 times with 500µl refolding buffer B. After the protein solution was applied onto the resin, the microcentrifuge tube was centrifuged for 3 minutes at 3000 x g, 4ºC, and the first supernatant was kept as fraction F. Afterwards, the resin was washed again with 500µl refolding buffer B.

Centrifuging the tube produced a second supernatant kept as fraction W. The proteins were eluted from the resin by adding 500µl of 500mM imidazole, and the third supernatant after centrifugation was kept as fraction E. All fractions were analysed using SDS-PAGE.

5.4.5 Concentrating protein

Different methods can be employed to concentrate a protein sample such as ultra filtration or dialysis. Ultra filtration using Vivaspin (Vivascience) or Centricon (Millipore) devices removes species smaller than the molecular weight cut off of the filtering device by centrifugal force. Concentration using a dialysis tube in a bed of PEG, MW 20000, or in a highly concentrated sucrose solution might be preferred when the protein sample tends to stick to the membranes of centrifugation devices. Here, molecules smaller than the molecular weight cut off of the dialysis membrane and water pass through the membrane driven by the force to generate a concentration equilibrium with the surrounding environment. On the other hand, small molecules present in PEG20K or sucrose molecules might pass through the dialysis bag in the other direction. In some cases, this might aid protein stability or solubility, but it is considered a contamination.

5.4.6 Determination of protein concentration

Concentrations of proteins were determined using UV spectroscopy and employing the Lambert-Beer-law. It describes the relationship between UV absorption of a sample with its concentration via the extinction coefficient:

$$A = \varepsilon \cdot c \cdot d \qquad [1]$$

The absorption, A, is the product of the extinction coefficient ε, the concentration c and the path length d.

A UV-spectrum of the protein was recorded from 500nm to 210nm. After baseline correction, the absorption value was used to calculate the protein concentration.

5.5 Gel electrophoresis

5.5.1 DNA gel electrophoresis

Mixtures of DNA fragments can be separated by agarose gel electrophoresis. When applying an electric field to a DNA mixture, the negatively charged DNA molecules will separate according to their size only because it is proportional to their charge. For 100ml of 1% agarose gel, 1g agarose was mixed with 100ml TAE buffer (40 mM Tris, 20 mM acetic acid (glacial), 1 mM EDTA, pH= 8.4) and heated in a microwave until it was dissolved. 8µl SYBR Safe™ DNA gel stain (Invitrogen Corporation, Paisley, UK) was added to the melted agarose in order to stain the DNA fragments for visualisation. The solution was poured into a horizontal gel chamber (SciePlas, Gentaur, Av. de l'Armèe 68, B-1040 Brussels, Belgium) and left to harden. After cooling, the comb is removed and the gel placed in the electrophoresis apparatus. Samples were mixed with 6 times DNA loading dye (30% (v/v) glycerol, 0.25% (w/v) bromphenolblue, 0.25% (w/v) 0.1 g xylene cyanol), loaded onto the gel and subjected to electrophoresis. The gel was run in TAE buffer at 140V for 20 to 30 minutes using a Bio-Rad PowerPac. DNA was visualized using a UV transluminator and could be photographed using the gene flash imager. DNA that was used for further experiments could be excised and extracted from the agarose gel using a Qiagen gel extraction kit and following the instructions as stated in the manufacturer's protocol.

5.5.2 Reducing SDS-Polyacrylamid gel electrophoresis (SDS-PAGE)

In SDS-PAGE, proteins are separated according to their molecular weights. The protein samples are mixed with loading dye (100mM Tris (pH= 6.8), 200mM DTT, 4% (w/v) SDS, 0.2% (w/v) bromphenolblue, 20% (w/v) glycerine ad 50ml H_2O) that contains SDS and DTT. The negatively charged anionic detergent SDS denatures secondary and non–disulfide–linked tertiary structures and thus applies a negative charge to each protein in proportion to its mass. This way, the distance of migration through the gel can be assumed to be directly related to the size of the protein. DTT reduces disulfide bonds, and heating of the samples for 5 minutes at 95ºC unfolds the proteins completely. Usage of a protein

size marker allows an estimation of the molecular weight of the proteins in question. 8 SDS-PA gels were prepared in a caster using the following recipe:

Table 5-4: Recipe for reducing and denaturing SDS-PAGE

	Separation gel			Stacking gel
Ingredient	16%	14%	12%	5%
H_2O	24ml	30ml	36ml	41.6
2M TRIS (pH 8.8)	17ml	17ml	17ml	-
1M TRIS (pH 6.8)	-	-	-	7.5 ml
SDS (10%)	0.9ml	0.9 ml	0.9 ml	0.6 ml
AA / Bis-AA	48 ml	42 ml	36 ml	10 ml
APS	200µl	200µl	200µl	200µl
TEMED	100µl	100µl	100µl	100µl

First, the separation gel was prepared. When polymerised, the stacking gel was poured on top of the separation gel, and the combs were placed. After the stacking gel was polymerised, the comb could be removed leaving wells for loading the samples. The gel is placed vertically in the electrophoresis apparatus, and both chambers are filled with running buffer (25mM Tris, 250mM glycine, 0.1% (w/v) SDS). An electric field of 140V was applied for 1 hour causing the negatively-charged proteins to migrate across the gel towards the anode. All gel equipment was from Hoefer Inc, 953 Indiana Street, San Francisco, CA 94107, USA. SDS-PAGEs were stained with Coomassie solution (2.5 g Coomassie Brilliant Blue R250, 100 ml HAc (glacial), 450 ml MeOH, 450 ml H_2O) for 20 minutes and destained with destaining solution (250ml methanol, 80ml acetic acid brought up to 1L with water) over night.

Prohibitins and annexin B1 were mostly run on a 12% or a 14% gel, whereas FtsH-IMS was run on 16% SDS PAGEs.

5.5.3 Non-reducing SDS-PAGE

Non-reducing SDS-PA gel was used to investigate DTT dependent oligomer formation of annexin B1. The gel was prepared like a reducing SDS-PA gel but no DTT was used in the protein loading dye. The samples were denatured using SDS in the gel and in the loading dye. Furthermore, the samples were also heated prior to use. The gels were run in running buffer (25mM Tris, 250mM glycine, 0.1% (w/v) SDS) at 140V for 1 hour and treated as stated above.

5.5.4 Native gel electrophoresis

In native gels, proteins separate according to their size, shape and natural charge. Native gals were prepared as stated for SDS-PAGEs (see section 5.5.2.) but SDS was replaced by the respective amount of water. Protein samples were mixed with native loading dye (100mM TRIS (pH= 6.8), 0.2% (w/v) bromphenolblue, 20% (w/v) glycerine ad 50ml H_2O), and the samples were not heated. After assembling the gel in the electrophoresis apparatus, the gel was run in native running buffer (25mM Tris, 250mM glycine) for up to 6 hours at 80V and room temperature. Gels were stained with Coomassie solution for 20 minutes and destained with destaining solution.

5.6 Biochemical assays

5.6.1 Western Blot

The SDS-PAGE was blotted onto a PVDF membrane using a current of 30mA for 60 minutes. The PVDF membrane was stained with Coomassie solution for a few seconds and destained extensively with destaining solution.

5.6.2 Co-pelleting assay

To assess the membrane binding behaviour of annexin B1, a co-pelleting assay was conducted in accordance to a protocol established by Hofmann & Huber in 2003. In this assay, the protein is co-pelleted with lipid vesicles by centrifugation at ultra-high speed, and the amount of protein copelleted with liposomes can be quantified directly using densitometric analysis of a SDS-PAGE. Phospholipid vesicles were prepared from 1,2-

dioleoyl-*sn*-glycero-3-phosphoserine (PS) and 1,2-dioleoyl-*sn*-glycero-3-phosphocholine (PC) (both from Avanti Polar Lipids Inc., Alabaster, Alabama, USA) according to the protocol by Reeves & Dowben . The vesicles were converted into large unilamellar vesicles (LUVs) by five freeze-thaw cycles and subsequent extrusion (11 times) through 0.1 µm filter membranes using an extruder (Avanti Polar Lipids Inc., Alabaster, Alabama, USA) at 37°C. A total of 0.2µmol phospholipids for each individual sample (500µl) was mixed with protein buffer with varying calcium concentrations (0, 1, 2, 10 and 20mM). Afterwards, 0.5nmol protein in liposome buffer is added to each sample. It binds to the liposomes according to the calcium concentration in the buffer. As a control, a sample of 0.1nmol protein in 100µl of 10% SDS was prepared at this stage (master sample). All samples were incubated for 10 minutes and centrifuged for 45min and 13000rpm at 4°C to remove unbound protein from the liposome suspension. The pellets were resuspended with 50µl of 10% SDS and subjected to SDS-PAGE to detect the remaining protein (see figure 5-2).

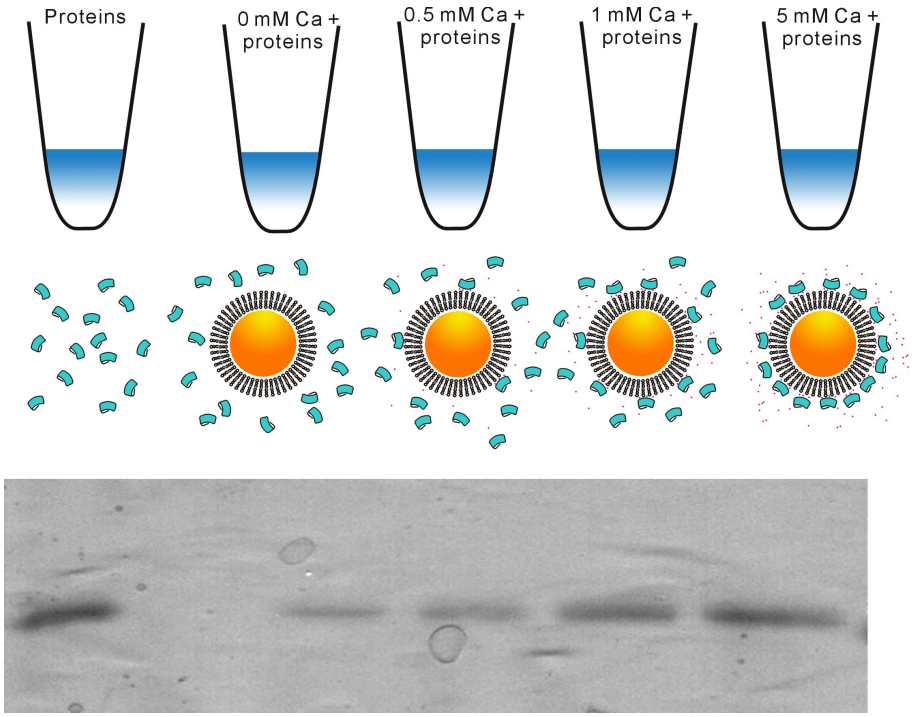

Figure -2: Co-pelleting assay. *Top panel*- Microtest tubes containing liposomes and protein at different calcium concentrations. *Middle panel* – Calcium-dependent binding to liposomes. *Bottom panel* – Detection of liposome-bound protein using SDS PAGE. Figure prepared by N.-J. Hu.

Gels were stained with Coomassie solution, destained with destain solution and analysed densitometrically using the programme ImageJ . Each calcium concentration was assessed three times independently. Curve fitting was performed with SigmaPlot .

5.6.3 Heparin binding assay

For assessing calcium-dependent binding of annexin B1 to heparin, a centrifugation assay using heparin sepharose was developed. 1 ml suspension of heparin Sepharose™ 6 Fast flow (Amersham Biosciences, GE Healthcare UK Ltd, Little Chalfont, Buckinghamshire, UK) was equilibrated by washing three times with 3.5 ml protein buffer (100mM NaCl, 20mM Tris, pH 8.0) and subsequent centrifugation at 3000rpm and 3min, at 4°C. The resin was resuspended in 4 ml protein buffer and distributed into six aliquots. After centrifugation, the supernatant was removed, and the resin was resuspended in 390µl protein buffer containing varying concentrations of calcium (0, 0.5, 1, 2, 5 and 10mM). Finally, 10µl of the protein (1mg/ml – 5mg/ml) was added to each aliquot. After 10 minutes incubation at room temperature, the samples were subjected to centrifugation and the supernatant removed. The pellets were then washed with 400µl protein buffer with the appropriate calcium concentration and the samples were centrifuged again. The protein was eluted from the resin with 400µl of protein buffer containing 30mM EDTA. The amount of reversibly bound annexin could be determined by running the supernatant from the EDTA elution on SDS-PAGE (see figure 5-3) and analysing the protein bands by densitometric analysis using the programme ImageJ . Each calcium concentration was assessed three times independently. Curve fitting was performed with SigmaPlot .

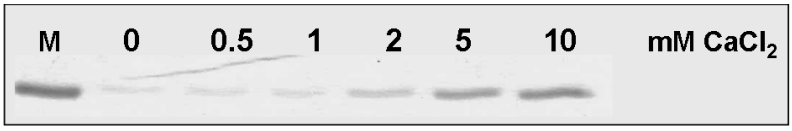

Figure -3: Example of an SDS PAGE for Heparin binding assay. Shown are supernatants from EDTA elutions.

5.6.4 Chemical cross linking

Cross-linking reagents contain reactive ends that are able to form a covalent bond to specific functional groups (primary amines, sulfhydryls, etc.) on proteins. Using analytical methods such as trypsin digest and mass spectrometry on the covalently linked protein molecules, protein interfaces can be determined. Annexin B1 was cross-linked using the reagents listed in table 5-5 also stating their specificity and reaction conditions.

Table 5-5: Cross-linking reagents, their specificity and experimental setup

Reagent	Specificity	Stock solution [mM]	Reaction buffer	Quenching with
Bissulfosuccinimidyl (BS^3)	lysine	8	PBS pH 8.0	1M TRIS pH 7.5
Dimethyl suberimidate (DMS)	Primary amines	35.7	PBS pH 8.0	1M TRIS pH 7.5
Dithiobis[succinimidylproprionate] (DSP)	Primary amines	10	PBS pH 8.0	1M TRIS pH 7.5
1-ethyl-3-[3-dimethylaminopropyl] carbodiimide hydrochloride (EDC)	Glutamic acid Aspartic acid	52.2	MES pH 6.0	10% β-Mercaptoethanol
4-(N-maleimidomethyl) cyclohexane-1-carboxylate, Sulfosuccinimidyl (Sulfo-SMCC)	Primary amines Sulfhydryl groups	10	PBS pH 8.0	1M TRIS pH 7.5
N-Cyclohexyl-*N'*-(2-morpholinoethyl)carbodiimide methyl-*p*-toluenesulfonate (CMC)	Glutamic acid Aspartic acid	10	MES pH 6.0	1M TRIS pH 7.5
Glutaraldehyde (GA)	Non specific	100%	PBS pH 8.0	1M TRIS pH 7.5

Reactions of all cross-linkers except glutaraldehyde were set up with 4mM cross-linker, 0.04mM protein and the appropriate amount of buffer giving a total volume of 20µl. The samples were incubated at room temperature or at 4ºC for varying amounts of time. Glutaraldehyde was used as 0.1% of the total reaction volume. Reactions were quenched with either 1µl of 1M TRIS pH 7.5 or 0.28µl of 10% β-mercaptoethanol. All samples were analysed on a denaturing SDS-PAGE under reducing conditions except samples cross-linked with DSP which would be cleaved by DTT.

5.7 Biophysical experiments

5.7.1 Mass spectrometry

Mass spectrometry is an analytical tool used for determining the molecular mass of peptides or proteins in a sample to a great accuracy. Mass spectrometers can be divided into three fundamental parts, namely the ionisation source, the analyser, and the detector. In electrospray ionisation mass spectrometry (ESI-MS), the liquid protein sample is ionised when it is forced through a small capillary and evaporates into a gas-filled chamber. When the protein exists as a lone ion, it moves to the analyser. This method is used to determine the full-length mass of the protein by obtaining mass spectra. In the case of peptide analysis by Matrix Assisted Laser Desorption Ionisation (MALDI), molecules in the sample are ionised due to bombardment with a pulsed nitrogen laser with a wavelength of 337nm producing mostly single protonated molecules. This method is mainly used to analyse proteins and peptide fragments. All mass spectrometry experiments were carried out at the COIL facility, University of Edinburgh where a time-of-flight analyser (TOF) measured the time it took for the peptide ions to travel through a field free region known as the flight, or drift, tube under high vacuum. Here, particles were separated according to their mass-to-charge (m/z) ratios. After inserting the plate in the mass spectrometer, the laser was fired, the energy arriving at the sample/matrix surface optimised, and data accumulated until an m/z spectrum of good intensity and signal-to-noise-ratio had been amassed as judged by eye. The m/z scale of the mass spectrometer was calibrated with either myoglobulin (full-length protein analysis) or trypsin digested trypsin (peptide analysis). Trypsin calibration was done either independently (external calibration) or pre-mixed with the sample (internal calibration). The spectra were analysed using the software Data explorer and compared to the peptide data base SwissProt (www.expasy.org).

5.7.1.1 ESI-MS

Full-length of annexin B1 was analysed by Sam Clokie in the COIL facility, University of Edinburgh, and the result was presented as a spectrogram including mass values for the respective peak.

5.7.1.2 MALDI-MS

Full-length protein analysis of HIS_6-FtsH-IMS was done using MALDI-MS. Different dilutions of sample were used in the experiment, the highest being 3µl of 10mg/ml protein mixed with 27µl of 50mM ammonium bicarbonate (ABC). After spotting 0.5µl of the protein sample onto the plate, it was covered with 0.5µl of sinapinic acid serving as a matrix. The sample was allowed to dry prior to insertion into the mass spectrometer.

For analysing peptides, the protein was digested with trypsin, a serine protease that specifically cleaves at the carboxylic side of lysine and arginine residues with stringent specificity. The peptides gained from in-solution or in-gel digestion are purified and concentrated, then analyzed by mass spectrometry to determine their molecular masses. The list of peptide masses obtained from the experiment was analysed using the programme Data Explorer , and peaks were compared to the Mascot database or the peptide data base SwissProt (www.expasy.org). Protein samples were digested using three different protocols depending on digestion in-solution or in-gel and the sample quality. After digestion over night, 0.5µl of the reaction mix and 0.5µl of α-cyano-4-hydroxycinnamic acid (CHCA) were spotted on a gold plate, left to dry and inserted into the mass spectrometer.

For basic in-solution digestion, 1µl porcine trypsin (Roche) was added to 3µl of 10mg/ml protein premixed with 27µl of 50mM ammonium bicarbonate and incubated over night at 32ºC. For better resolution in the mass spectrogram, beneficial in case of a low quality sample, 3µl of 10mg/ml protein was mixed with 27µl of 50mM ammonium bicarbonate. DTT was added to a final concentration of 5mM and the sample was heated to 60ºC for 30 minutes. After cooling down to room temperature, iodoacetamide was added to a final concentration of 15mM, and the sample was incubated for 30 minutes in the dark at room

temperature. Afterwards, 1µl trypsin was added and the sample was either incubated at 37ºC for 2 hours or at 32ºC overnight to gain the desired peptides.

For in-gel digestion, a SDS-PAGE was run, stained with GelCode Blue Stain Reagent and destained with water. The protein bands were cut out tight and placed in a microcentrifuge tube. 300µl buffer1 (200mM ammonium bicarbonate in 50% acetonitrile) were added to the samples and left to incubate at room temperature for 30 minutes. This was repeated twice to remove all SDS in the gel. The gel was incubated in 300µl buffer 2 (200mM DTT, 200mM ammonium bicarbonate, 50% acetonitrile) for one hour to reduce the protein. The gel was washed three times in 300µl buffer 1 before alkylating the cysteines in 100µl buffer 3 (50mM iodoacetamide, 200mM ammonium bicarbonate in 50% acetonitrile) at room temperature in the dark for 20 minutes. The gel pieces were washed three times with 500µl buffer 4 (20mM ammonium bicarbonate in 50% acetonitrile) before cut into 2mm x 1mm big pieces. After spinning down at 13000rpm and 4ºC using a bench top centrifuge, the supernatant was removed and the gel pieces covered with 100% acetonitrile. The gel pieces shrink and turn white from dehydration. The acetonitrile is then removed, and the gel pieces are allowed to dry. Gel pieces are swollen in trypsin solution (1µl trypsin stock solution and 29µl 50mM ammonium bicarbonate) at 4ºC. Finally, the samples are incubated at 32ºC for 22 hours. The next day, samples are sonicated shortly prior to spotting onto the plate.

Results were analysed using the probability based Mowse score, -10*log(P), where P is the probability that the observed match is a random event. Scores greater than 67 are considered significant ($p<0.05$) and indicate that the protein is the most probable identification.

5.7.2 Circular dichroism spectroscopy

Circular dichroism (CD) is a phenomenon resulting from the interaction of circular polarised light with chiral molecules such as amino acids. The amide groups of the peptide bonds are the actual chromophors in CD. The chiral centres of the protein molecules affect the velocity of the right- and left-handed component of the circular polarised light leading

to a difference in absorption of both components which is measured. The restricted arrangement of the amino acids/ peptide bonds in secondary structure elements in proteins is also an influential factor in CD causing coupling of absorption effects by the peptide bonds. Consequently, the shape of the resulting CD spectrum allows conclusions towards the presence of a secondary structure element such as α-helix and β-sheet. Proteins containing multiple secondary structure elements show a superposition of their respective spectra.

A CD cuvette with a light path of 1mm (Hellma GmbH & Co. KG, Müllheim, Baden, Germany) and a Jasco J-810 spectropolarimeter equipped with a Peltier element were used for all experiments. The data collected in CD experiments were deconvoluted using the programme ACDP to calculate mean residue ellipticity, Θ_{mean}, thus normalising the data against path length, protein concentration and extinction coefficient of the protein.

5.7.2.1 Wavelength scan

Wavelength scans were performed by measuring the CD signal in the wavelength range from 260nm to 190nm or 200nm at a set temperature, e.g. 20ºC. After transformation of the data into mean residue ellipticity using the programme ACDP , the secondary structure was predicted using implementations of the K2D algorithm and Fasman deconvolution in the programme.

CD wavelength spectra of annexin B1 (1.8 μM) were recorded either in buffer 1 (50 mM NaCl, 5 mM Tris, pH 8.0) or in buffer 2 (20mM NaCl, 5mM Hepes, pH 7.5). Experiments in the presence of calcium or DTT were carried out with the addition of 5mM $CaCl_2$ or 1mM DTT in the buffer, respectively.

Wavelength spectra of His_6-BAP32(Δ1-30):BAP37(Δ1-40) were recorded in 100mM Tris, pH 7.5, 100mM KCl at a protein concentration of 0.054mg/ml.

CD signals of His_6-FtsH-IMS region were monitored at a protein concentration of 0.04mg/ml in 5mM Hepes, pH 7.5, 20mM NaCl.

5.7.2.2 Temperature scan

Denaturation curves provide valuable information about the protein, its fold and conformational stability. They are very helpful in measuring differences in conformational stability between folded and unfolded protein and how modifications of the protein might influence both conformational states. Even though equilibrium measurements are made, conclusions about the mechanism of the folding of the protein can be drawn, e.g. how many separate folding units are present in the protein and how stable they are in relation to each other. And finally, unexpected results may provide valuable information about the protein such as a possible influence of disulphide bonds on the protein stability. In general, the greater the change in a physical property of a protein is when it unfolds, the more usable is the technique for following unfolding.

A folded protein can be unfolded either by heating (thermal unfolding) or by adding a denaturant such as urea (chemical unfolding). Secondary structure elements show spectra with specific minima, 208nm and 222nm for α-helices, and 216nm for β–sheets which can be used to monitor unfolding. The wavelength for recording the temperature scan was chosen by the criterion of a large difference between thre CD signal of the protein at low temperature (10ºC) compared to the CD signal at high temperature (90ºC). The temperature scan was performed by measuring the CD signal at that specific wavelength in the temperature range from 10ºC or 20ºC to 80ºC. Data were recorded using the following parameters: temperature slope 1K/minute or 20 K/hour and a data pitch of 0.5 or 0.2. For investigation of the thermal denaturation of FtsH-IMS region and annexin B1, the CD signal at 222nm was recorded whereas the unfolding behaviour of the BAP complex was monitored at 216nm. Unfolding experiments were performed three times independently. Changes in the CD signal were used to construct an unfolding curve which was fitted with SigmaPlot using a sigmoidal equation.

5.7.3 Fluorescence spectroscopy

Absorption of light with a wavelength in the range of ultra violet or visible light leads to excitation of electrons in a protein molecule. Fluorophores in a protein are tyrosine, phenylalanine and tryptophane side chains. When the molecule returns to its ground state,

fluorescence might occur. Fluorescence is characterised by a) an independence of emitted light with regards to the excitation wavelength, b) a shift towards higher wavelengths of the emitted spectrum as compared to the absorption spectrum and c) a mirrored progression of both spectra when because the excited state and the ground state show similar vibration structures.

Changes in the intrinsic protein fluorescence that occurred during chemical unfolding were monitored by fluorescence spectroscopy using urea as denaturant at various concentrations. 2µl of 1.3mg/ml annexin B1 were added to 298µl buffer containing urea at concentrations from 0 to 8M in 0.5M increments and incubated for 1.5 hours at room temperature to reach equilibrium. Samples were measured in a Fluoromax spectrometer by Jobin Yvon using a quartz cuvette (Starna). Unfolding experiments under 1mM DTT or 5mM $CaCl_2$ were carried out by adding 1µl 300mM DTT or 1.5µl 1M $CaCl_2$ to the sample tubes. Samples were incubated with the respective agent and urea 1.5 hours prior to measurement to reach equilibrium, and measured with two different excitation wavelengths, at 280nm and at 295nm. Emission was monitored from 300nm to 400nm for the excitation wavelength at 280nm (experimental setup A), and from 310nm to 400nm for excitation at 295nm (experimental setup B). Experiments were repeated three times independently. In order to determine changes in fluorescence intensity and the spectrum itself, the quotient of fluorescence intensities at the respective wavelength maxima of folded (0M urea) and unfolded (8M urea) protein was used. All curves were generated and fitted with SigmaPlot using a sigmoidal equation to determine $c_{1/2}$(urea), the urea concentration at which half of the protein is denatured.

5.7.4 Gel filtration analysis

A Superose® 12 HR 10/30 column (Amersham Biosciences, GE Healthcare UK Ltd, Little Chalfont, Buckinghamshire, UK) was run on a Biocad® 700e Workstation or a BioLogic® HPLC syatem (Biorad) allowing a separation in the range of 1kDa-3kDa. The cross-linked, agarose-based Superose resin consists of beads of a narrow particle-size distribution of 8-12µm in diameter. Separation is achieved by filtering the sample through a tightly packed network of beads, allowing large particles to leave the column quickly,

whereas small particles remain longer on the column, and thus are eluted with longer separation times.

Gel filtration experiments were carried out to investigate dimer formation of annexin B1 under different buffer conditions. Gel filtration buffers consisted of 20mM Hepes, pH 7.5 and 100mM NaCl completed with 1mM DTT, 5mM, 15mM calcium chloride, 20mM EDTA, or 0.8mM H_2O_2 depending on the experiment carried out. His_6-FtsH-IMS region was run in 20mM HEPES, pH 7.5 and 100mM NaCl. Preparative size exclusion chromatography was used to separate refolded His_6-BAP32(Δ1-30):BAP37(Δ1-40) complex from His_6-BAP32(Δ1-30) or BAP37(Δ1-40) monomers using their different size and shape. The running buffer consisted of 20mM TRIS, pH 7.5 and 100mM KCl. All buffers were filtered through a 0.22μm filter (Whatman) and degased before use.

Gel filtration experiments were performed at a flow rate of 0.5ml/min. After equilibrating the column with up to three column volumes of buffer (~ 75ml), 1ml of sample was loaded. Proteins were separated on the column for 2 column volumes, and their absorption was monitored at 280nm. All sample runs were analyzed using the programme PeakFit version 4.0 to determine the maximum of the elution peak.

5.7.4.1 Relating elution volumes to molecular weight values

In order to estimate the sizes of molecules eluted from the column, the column was calibrated with Dextran Blue (2MDa), albumin (62kDa) and chymotrypsinogen A (25kDa) or Dextran Blue (2MDa), aldolase (160kDa), BSA (68kDa), myoglobin (17kDa) and cytochrome C (12.4kDa) using the same general setups of the runs. In different calibration experiments, Dextran Blue eluted with 7.82 ml to 8.14ml in different calibration runs which represents the void volume of the column (1st peak, figure 5-4, A). All calibration proteins are of globular shape, and therefore the experimentally determined relationship between molecular weight of the protein and its retention time from the column is only valid for globular proteins.

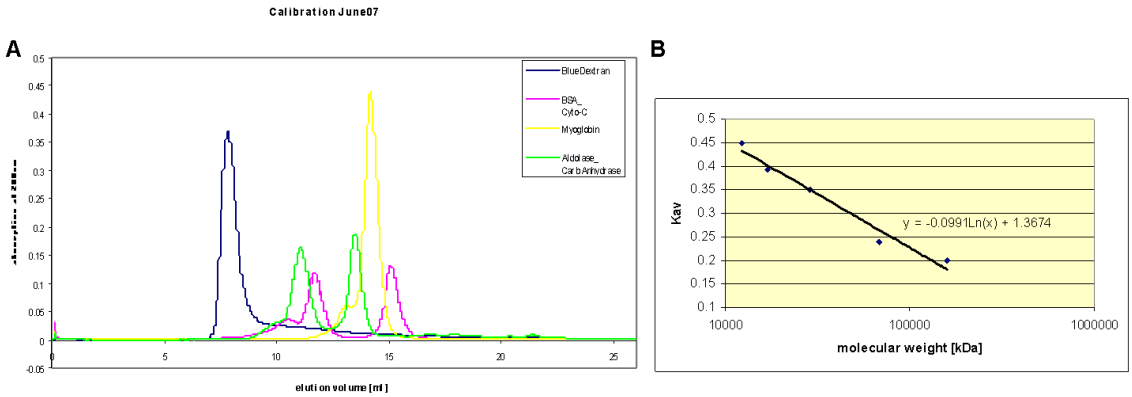

Figure -4: Calibration of Superose 12 HR 10/30 column using known protein standards.

The elution volumes of the proteins were used to calculate the gel phase distribution coefficient, K_{av}, values using the formula:

$$K_{av}=(V_e-V_o)/(V_t-V_o) \qquad [2]$$

where V_e is the volume at which the protein elutes, V_o is the void volume and V_t the total column volume (bed volume). K_{av} values were plotted against the respective molecular weights on a logarithmic scale. The data were fitted with Excel using a logarithmic regression (see figure 5-4, B). The equation of the trend line was subsequently used to determine the molecular weight of proteins in question.

5.7.4.2 Relating elution volume to Stokes' radius

In cases of elongated proteins or denatured proteins where calibration using globular shaped proteins fails, it can be useful to relate the elution volume to another molecular parameter, the Stokes' radius R_s. For elongated proteins, the Stokes' radius would be higher than the radius of a globular protein of the same molecular mass.

The Stokes' radius for albumin and chymotrypsinogen are known to be 35.5Å and 20.9Å, respectively, and can be used to create a plot of R_s vs. $(-\log(K_{av}))^{1/2}$ (Figure 5-5). The data

points were fitted in Excel using a linear regression. Stokes' radius of the protein in question can be calculated from the respective equation.

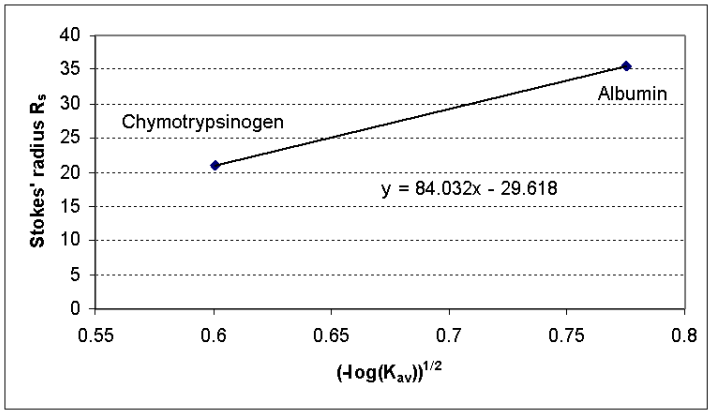

Figure -5: Plot for calculating Stokes' radii.

5.7.5 Small angle X-ray scattering (SAXS)

SAXS experiments were carried out by our collaborator, Jan Skov Pedersen at University of Aarhus in Denmark. It is a technique where X-rays (wavelength 0.1 to 0.2nm) experience elastic scattering by a non-crystalline sample that is recorded at very low angles (typically 0.1° - 10°). This way, structural information on the order of submicrometers (50Å to 250Å) can be obtained allowing conclusions about the shape and size of macromolecules such as proteins. His_6-FtsH-IMS region was subjected to SAXS at concentrations of 10mg/ml, 5mg/ml and 2.5mg/ml. Data showing least aggregation were obtained at 5mg/ml. They were improved by excluding some data points at the beginning of the scattering curve eliminating contributions from aggregates and higher oligomers, and were analysed by the collaborators using the programme Gnom . From the data, a reference model could be created employing the dummy bead programme Dammin . Using the information of the protein sequence, the dummy residue programe Gasbor was used to create the most probable model of an His_6-FtsH-IMS region dimer. The results

were presented by the collaborator as a report showing both the data curves and calculated models.

5.8 Crystallography

Crystallography is the experimental science of determining the arrangement of atoms in solids (crystals). In a protein crystal, X-rays are scattered by the electrons of all atoms leading to an overall scattering pattern as waves will add constructively or destructively to varying degrees. This diffraction of the unit cell is repeated on a lattice that determines the space group. The combination of the diffraction pattern resulting from the unit cell and the diffraction pattern resulting from the lattice gives the diffraction pattern of the complete crystal. The diffraction pattern of a crystal can be expressed mathematically, and an image of the crystal structure can be calculated. In X-ray experiments, only the structure factor amplitudes can be measured directly whereas the phases remain to be determined by other methods (phase problem). Methods used in macromolecular crystallography include use of anomalous dispersion (MAD), isomorphous replacement (SAD) and molecular replacement.

5.8.1 Crystal growth using the hanging drop method

The hanging drop method is based on vapour diffusion, where water diffuses from a mix of protein solution and screening solution into a solution with higher concentration. As the protein concentration in the drop increases, a precipitant in the screening solution induces formation of the protein crystal.

The protein solution was mixed with a screening solution forming a drop that is placed on a glass slide. In a usual setup, the ratio between protein solution and screening solution was 1:1. The glass slide was turned upside down and used to seal a well containing 300µl of the screening solution (hanging drop). Crystallisation trials were set up in 24-well plates (Hampton Research) using high vacuum grease as sealant. The plates were incubated at 16ºC and evaluated under the microscope for crystal growth. Annexin B1 was the only protein within this work from which a crystal could be obtained.

5.8.2 Crystal mounting and data collection

Once a crystal was produced, it was placed on a synthetic CryoLoop (fishing), soaked shortly in cryo-protectant (70µl screening solution and 30µl 75% glycerol), and shock frozen in liquid nitrogen. Crystals were mounted onto the goniometer head of the in-house diffractometer (Rigaku generator, MAR Research Image Plate) under a constant flow of liquid nitrogen, and X-rays of 1.5418nm were applied (screening). Crystals showing a protein diffraction pattern (multiple ordered spots) were dismounted, and a data set was collected at a synchrotron facility. The dataset of annexin B1 with the highest resolution was recorded at the ESRF in Grenoble at beam line BM14 with a wavelength of 0.978nm.

5.8.3 Data analysis

Datasets were analysed by Mosfilm to index the spots, predict a space group and determine the unit cell parameters.

5.9 Computational methods

5.9.1 Alignments and secondary structure prediction

Multiple sequence alignments were generated using ClustalW . The multiple sequence alignment of the PHB domains of BAP32, BAP37 and flotillin-2 was generated with MUSCLE and slightly adjusted to match conserved secondary structure elements especially in the PHB domain. The secondary structures were predicted using PSIPRED .

5.9.2 Homology modelling and refinement

PHB domains of BAP32 and BAP37 were modelled on the NMR structure of the PHB domain of mouse flotillin-2 PDB accession number **1WIN**) whereas annexin B1 was modelled to the crystal structure of annexin A5 (PDB accession number **1AVR**). Twenty independent homology models were calculated with the programme Modeller 4 , and models with the lowest energy were selected, visually inspected with O and subjected to further energy minimization using CNS . The overall geometry was scrutinized using PROCHECK . Angles Φ and Ψ of amino acids were analysed by drawing a

Ramachandran plot using PROCHECK in order to expose any tension in the protein main chain which would indicate a bad model in this area of the protein. Models of BAP32(49-194), BAP37(59-207), annexin B1(24-347) were generated. Surface properties and electrostatic characteristics were analysed using PyMol .

5.9.3 Modelling of protein:protein interactions

The modelled structures of BAP32 and BAP37 were subjected to an automated macromolecular docking calculation with the programme Hex in order to investigate potential interaction sites. Hex differs from other macromolecular docking programs in its use of polar Fourier correlations to accelerate docking calculations. Hex was run with its default settings and taking surface electrostatics into account. BAP32 was defined as protein, BAP37 was defined as ligand.

Models for BAP32:BAP37 complexes were also constructed manually by rigid body movements using the graphics programme O based on the crosslinking study by Back and colleagues . The initial model was subjected to molecular dynamics simulations in GROMACS . The simulations (50 ps, 500 ps) were carried out using a model with explicit solvation and without superimposing any user-defined distance restraints.

The dimer of the N-terminal BAP helices was constructed using α-helices generated with GARLIC which were oriented as rigid bodies in the programme O to yield a first approximation of a helix dimer. The raw model was then subjected to molecular dynamics simulations in GROMACS . No user-defined distance restraints were applied and the simulations were carried out *in vacuo* for 50ps and 500ps, respectively. The molecular dynamics simulations were analysed using the tools included in GROMACS , as well as VMD and O . Surface properties and electrostatic characteristics were analysed using PyMol .

5.9.4 Modelling of protein - ligand interactions

An automated docking approach was employed to investigate the interaction between BAP32 and its ligand melanogenin using the programme FlexX . First, the BAP32 homology model was visually inspected and potential binding sites were identified by

surface analysis. Then, the three-dimensional molecule structure of melanogenin was created and subsequently optimized by energy minimisation with Sybyl . After site point generation within the docking programmes, the ligand was fitted into the binding pockets based on chemical and shape complementation. The resulting models were analysed with Sybyl .

5.10 References:

PART D

Appendix

6 Appendix

6.1 Ramachandran Plots

Ramachandran plots of homology models of BAP32(49-194), BAP37(59-207) and annexin B1(24-347)

6.2 Publications

Winter A, Yusof AM, Gao E, Yan HL, Sun SH, Hofmann A., (2006): Biochemical characterization of annexin B1 from *Cysticercus cellulosae*. *FEBS J.* **273**(14): p. 3238-47.

Winter, A., O. Kamarainen, and A. Hofmann, (2007): Molecular modeling of prohibitin domains. *Proteins*. **68**(1): p. 353-62.

Winter, A. and A. Hofmann: Towards understanding the roles of prohibitins, multi-functional regulator proteins. *Current Chemical Biology, in press*

PROCHECK

Ramachandran Plot

bap32_1

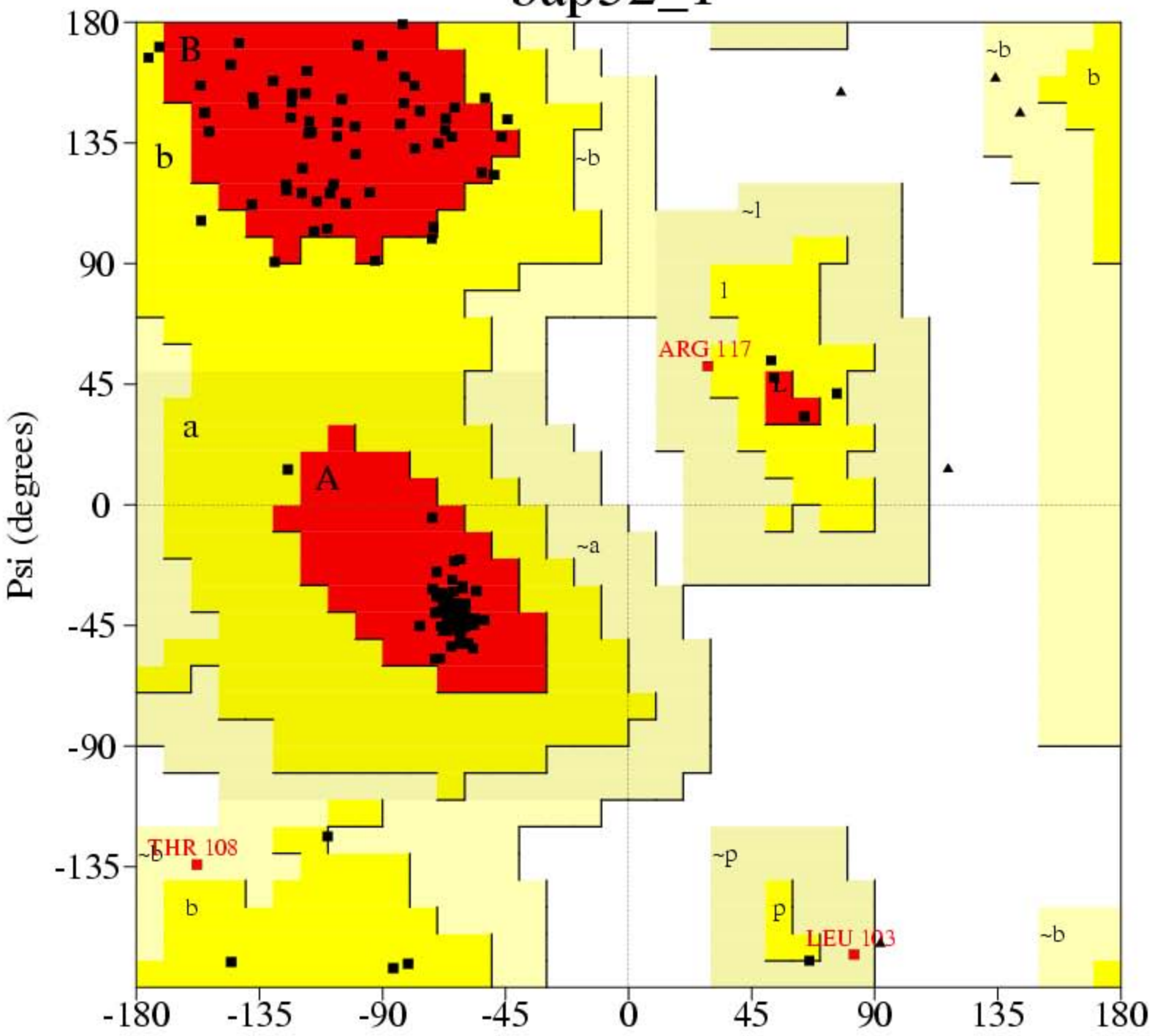

Plot statistics

Residues in most favoured regions [A,B,L]	113	86.9%
Residues in additional allowed regions [a,b,l,p]	14	10.8%
Residues in generously allowed regions [~a,~b,~l,~p]	3	2.3%
Residues in disallowed regions	**0**	**0.0%**
	----	------
Number of non-glycine and non-proline residues	130	100.0%
Number of end-residues (excl. Gly and Pro)	2	
Number of glycine residues (shown as triangles)	7	
Number of proline residues	7	

Total number of residues	146	

Based on an analysis of 118 structures of resolution of at least 2.0 Angstroms and R-factor no greater than 20%, a good quality model would be expected to have over 90% in the most favoured regions.

bap32_1_01.ps

PROCHECK

Ramachandran Plot

bap37_1

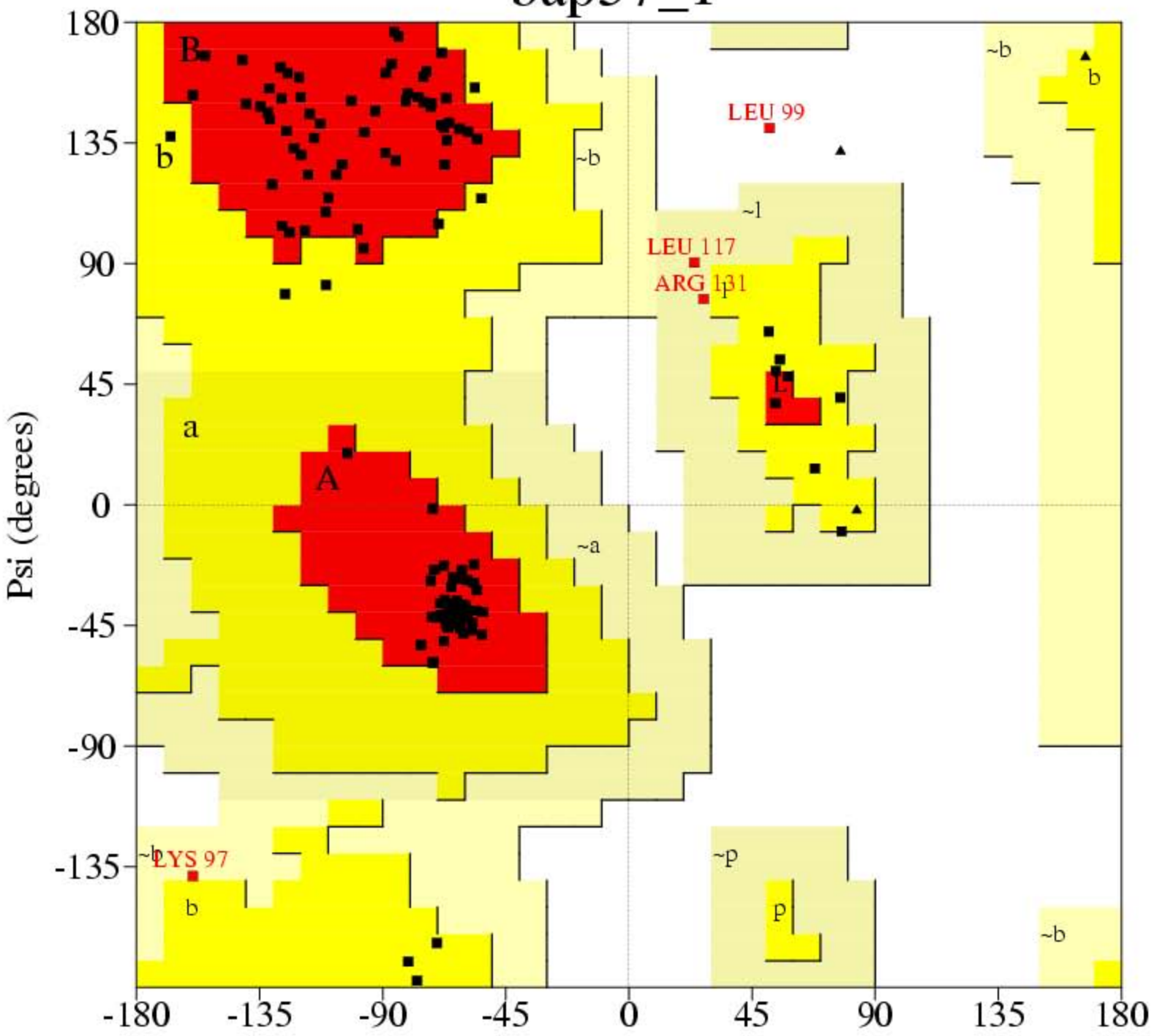

Plot statistics

Residues in most favoured regions [A,B,L]	120	87.6%
Residues in additional allowed regions [a,b,l,p]	13	9.5%
Residues in generously allowed regions [~a,~b,~l,~p]	3	2.2%
Residues in disallowed regions	1	0.7%
Number of non-glycine and non-proline residues	137	100.0%
Number of end-residues (excl. Gly and Pro)	2	
Number of glycine residues (shown as triangles)	3	
Number of proline residues	7	
Total number of residues	149	

Based on an analysis of 118 structures of resolution of at least 2.0 Angstroms and R-factor no greater than 20%, a good quality model would be expected to have over 90% in the most favoured regions.

bap37_1_01.ps

PROCHECK

Ramachandran Plot

B1-on-A8

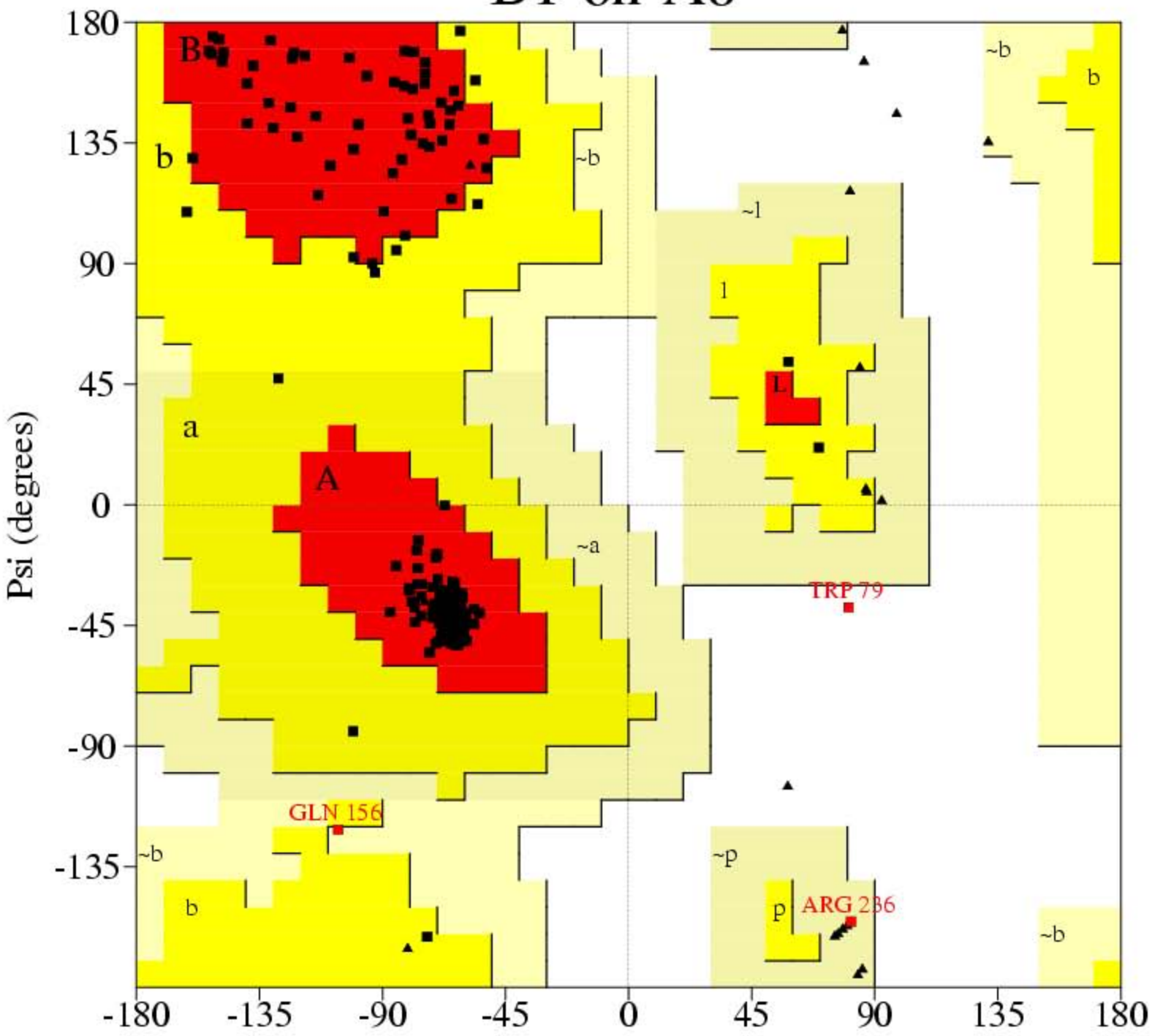

Plot statistics

Residues in most favoured regions [A,B,L]	271	95.1%
Residues in additional allowed regions [a,b,l,p]	11	3.9%
Residues in generously allowed regions [~a,~b,~l,~p]	2	0.7%
Residues in disallowed regions	1	0.4%
Number of non-glycine and non-proline residues	285	100.0%
Number of end-residues (excl. Gly and Pro)	1	
Number of glycine residues (shown as triangles)	25	
Number of proline residues	13	
Total number of residues	324	

Based on an analysis of 118 structures of resolution of at least 2.0 Angstroms and R-factor no greater than 20%, a good quality model would be expected to have over 90% in the most favoured regions.

B1-on-A8_01.ps

the FEBS Journal

Biochemical characterization of annexin B1 from *Cysticercus cellulosae*

Anja Winter[1], Adlina M. Yusof[1], Erning Gao[1], Hong-Li Yan[2] and Andreas Hofmann[1]

1 Institute of Structural & Molecular Biology, School of Biological Sciences, The University of Edinburgh, UK
2 Department of Medical Genetics, The Second Military Medical University, Shanghai, China

Keywords
annexins; calcium; heparin; protein–glycosaminoglycan interactions; protein–membrane interactions

Correspondence
A. Hofmann, Institute of Structural & Molecular Biology, School of Biological Sciences, The University of Edinburgh, The King's Buildings, Mayfield Road, Edinburgh EH9 3JR, UK
Fax: +44 131 650 8650
Tel : +44 131 650 5365
E-mail: Andreas.Hofmann@ed.ac.uk

(Received 7 March 2006, revised 7 April 2006, accepted 22 May 2006)

doi:10.1111/j.1742-4658.2006.05332.x

Annexin B1 from *Cysticercus cellulosae* has recently been identified using immunological screening in an attempt to find novel antigens for vaccine development against cysticercosis. The protein possesses anticoagulant activity and carries significant therapeutic potential due to its thrombus-targeting and thrombolytic properties. We investigated the biochemical properties of annexin B1 using liposome and heparin Sepharose copelleting assays, as well as CD spectroscopy. The calcium-dependent binding to acidic phospholipid membranes is reminiscent of other mammalian annexins with a clear preference for high phosphatidylserine content. A unique property of annexin B1 is its ability to bind to liposomes with high phosphatidylserine content in the absence of calcium, which might be due to the presence of several basic residues on the convex protein surface that harbours the membrane-binding loops. Annexin B1 demonstrates lectin properties and binds to heparin Sepharose in a cooperative, calcium-dependent manner. Although this binding is reversible to a large extent, a small fraction of the protein remains bound to the glycosaminoglycan even in the presence of high concentrations of EDTA. Analogous to annexin A5, we propose a model of heparin wrapped around the protein thereby engaging in calcium-dependent and calcium-independent interactions. Although the calcium-independent heparin-binding sites identified in annexin A5 are not conserved, we hypothesize three possible sites in annexin B1. Results from CD spectroscopy and thermal denaturation indicate that, in solution, the protein binds calcium with a low affinity that leads to a slight increase in folding stability.

Annexins are water-soluble, calcium-dependent phospholipid-binding proteins. Members of the annexin family are ubiquitously distributed in different tissues and cell types of higher and lower eukaryotes. To date, over 160 unique annexin proteins have been found in more than 65 different species ranging from fungi and plants to nonvertebrates and higher vertebrates [1]. Their abundance, as well as their calcium-regulated presence at cell membranes, makes members of this family versatile adapter and regulator proteins in membrane-associated processes. Accordingly, a role in endo- and exocytosis has been assigned to many annexin proteins [2,3]. Despite being intracellular proteins, extracellular functions have been described for several annexins. Whereas annexin A2 is known to act as a coreceptor for plasminogen and tissue plasminogen activator on the surface of endothelial cells [4], annexin A1 has been observed to bind to an extracellular domain of β_2 integrin [5]. Annexin A5 was found to bind to the intracellular part of the β_5 integrin receptor

Abbreviations
LUV, large unilamellar vesicle; PtdCho, phosphatidylcholine; PtdSer, phosphatidylserine.

subunit [6]. Annexins A2 and A5 have repeatedly been reported to act as cellular receptors for cytomegalovirus and hepatitis B virus [7–9], although this is still a matter for discussion within the community. Frequently, annexins are found to interact with cytoskeletal proteins. Annexins A1 [10] and A2 [11], as well as the plant annexins p34 and p35 from tomato [12], exhibit binding to F-actin, and others, for example plant annexins from corn [13], bell pepper [14] and cotton [15], tested negative in this context. Interactions between annexin A1 and profilin have also been demonstrated [16].

The glycosaminoglycan heparan sulfate is ubiquitously distributed on the surface of cells and acts as a regulator of ligand–receptor encounters [17], promotes protein assembly [18] and thus coordinates a variety of cellular functions. Heparan sulfate has a variable heparin-like structure but more *N*-acetylated and fewer *N*- or *O*-sulfonated groups than heparin. Heparin itself is a highly potent anticoagulant due to its ability to activate serine protease inhibitors such as antithrombin [19].

Several annexins, including annexins A1 [16], A2 [20], A4 [21], A5 [21–24], A6 [21] and Nex1 [25], are known to possess glycosaminoglycan-binding properties. The crystal structure of annexin A5 in complex with heparin-derived tetrasaccharides revealed two binding sites, a calcium-mediated one residing on the convex side and a calcium-independent one on the concave side of the protein [24]. In that study, Capila *et al*. presented a model in which the heparin chain is wrapped around the annexin molecule occupying both binding sites. Whereas binding of the carbohydrate to the site on the concave surface of the protein most likely does not interfere with the essential annexin–membrane association, the site on the convex surface would be affected by membrane binding. However, *in vitro* studies showed that heparin binding cannot compete effectively with phospholipid membrane binding to annexin A5 [21,26]. Therefore, heparin might be displaced from the binding site on the convex surface of annexin A5 upon competition by phospholipid molecules, e.g. when membrane binding occurs. In the soluble state, calcium binding contributes to the overall affinity of the annexin A5–heparin interaction. Thus, the annexin A5–heparin interaction is calcium-dependent *in vitro*, but is thought to carry less significance *in vivo* [24].

The implications of annexin proteins in health and disease are increasingly being appreciated and the term 'annexinopathies' has been put forward for annexin-related diseases. In particular, the importance of annexin A1 in inflammation [27] and annexin A2 in plasminogen-dependent fibrinolysis [28] has long been appreciated. In recent years, the role of membrane-bound annexin A5 as a protective shield has clarified the molecular mechanisms of its anticoagulant properties [29]. Altered gene regulation and/or distribution of annexins have been observed for a variety of conditions.

Cysticercosis is an infection by *Cysticercus cellulosae*, the larva of the pig tapeworm *Taenia solium*. The condition seriously affects human health and also leads to economic losses in some developing countries. Infection occurs mostly in the CNS, muscles, subcutaneous tissue and the globe of the eye [30]. In an attempt to find novel antigens for vaccine development, annexin B1 was identified by immunological screening of a *C. cellulosae* library [31]. The ability of annexin B1 to displace phospholipid-dependent coagulation factors and to prolong clotting times of human serum emphasizes its potential for antithrombotic treatments. The combination of thrombus-targeting and thrombolytic properties has also been suggested for the protein [32]. To date, there has been no systematic characterization of the molecular properties of annexin B1. All the literature reports have mainly concentrated on identification and probable functions of the protein.

Similar to other annexins, annexin B1 comprises a tetrad repeat of ~ 70 amino acids and possesses all the highly conserved residues generally found in other annexins involved in salt bridge interactions. The landmark feature of annexins is their ability to bind to acidic phospholipid membranes in the presence of calcium, which is facilitated by calcium ions coordinated within the AB and DE loop areas. Accordingly, this feature has also been observed with annexin B1 [32,33] although the primary structure (Fig. 1) suggests that the calcium-binding site in the third domain is disrupted due to a lysine (K254). This lysine occupies the position of the bidentate residue in the DE loop required for calcium coordination by the endonexin sequence [34]. Annexin B1 shares 35% amino acid identity with hydra annexin B12 and human annexin A5. Further distinct features of annexin B1 include the slightly longer N-terminal domain (~ 30 amino acids), as well as a connector region between domains II and III. The connector region of this protein comprises of 30 amino acids compared with annexins A5 and B12, which have an insertion of 14 residues.

To learn more about the molecular evolution of annexins, as well as to characterize the molecular properties of annexin B1, we set out to characterize the protein biochemically and biophysically.

In this study, we investigated the binding behaviour of annexin B1 to heparin and phospholipid vesicles in a calcium-dependent manner. Although the protein

```
AnxB1    MAYCRSLVHL YAPNGEKYKP TITPTPGFSP TADAEHLKRA MRGLGTNERA
AnxB12   ~~~~~~~~~~ ~~~~~MVVQG TVKPHASFNS REDAETLRKA MKGIGTDEKS
AnxA5    ~~~~~~~~~~ ~~~MAQVLRG TVTDFPGFDE RADAETLRKA MKGLGTDEES

AnxB1    IIDILGNRTS AERMAIRDAY PSISSKTLHD ALTSELSGKF RRFALLLIQS
AnxB12   ITHILATRSN AQRQQIKTDY TTLFGKHLED ELKSELSGNY EAAALALLRK
AnxA5    ILTLLTSRSN AQRQEISAAF KTLFGRDLLD DLKSELTGKF EKLIVALMKP

AnxB1    PWQVMAEALY DAMKGAGTKE RVLNEIIAGC SKDDIPQLKK AFEEVSGGET
AnxB12   PDEFLAEQLH AAMKGLGTDE NALIDILCTQ SNAQIHAIKA AFKLLY~KED
AnxA5    SRLYDAYELK HALKGAGTNE KVLTEIIASR TPEELRAIKQ VYEEEY~GSS

AnxB1    LDDAIKGDTS GDYREALLLA LAGQADEPQA MQLKNLTPST LSQVVNPGLA
AnxB12   LEKEIISETS GNFQRLLVSM LQGGRKEDEP ~~~~~~~~~~ ~~~~VNAAHA
AnxA5    LEDDVVGDTS GYYQRMLVVL LQANRDPDAG ~~~~~~~~~~ ~~~~IDEAQV

AnxB1    ETDAKELYAC GEGRPGTAES RFMRPIVNRS FLQLNATNEA YNRAYGHPLI
AnxB12   AEDAAAIYQA GEGQIGTDES RFNAVLATRS YPQLHQIFHE YSKISNKTIL
AnxA5    EQDAQALFQA GELKWGTDEE KFITIFGTRS VSHLRKVFDK YMTISGFQIE

AnxB1    DAIKKETSRD LEDFLITRVR YATDRASLFA ELLHFAMRGA GTKDSTLQRV
AnxB12   QAIENEFSGD IKNGLLAIVK SVENRFAYFA ERLHHAMKGL GTSDKTLIRI
AnxA5    ETIDRETSGN LEQLLLAVVK SIRSIPAYLA ETLYYAMKGA GTDDHTLIRV

AnxB1    LALRADTDLG SIKEKYAELY GETLEAAIKG DTSGDYEALC LKLIGPA~
AnxB12   LVSRSEIDLA NIKETFQAMY GKSLYEFIAD DCSGDYKDLL LQITGH~~
AnxA5    MVSRSEIDLF NIRKEFRKNF ATSLYSMIKG DTSGDYKKAL LLLCGEDD
```

Fig. 1. Amino acid alignment of annexin B1 from *C. cellulosae* (GenBank accession number AF147955), annexin B12 from *Hydra vulgaris* (GenBank accession number P2625-6) and human annexin A5 (GenBank accession number P08758). The endonexin sequence in all four domains is highlighted. The heparin binding sites HTS-1 (Arg207) and HTS-3 (Arg25) [24] are highlighted in bold. The predicted heparin binding site HTS-2 including Arg289 [45] is underlined. The potential heparin binding sites in annexin B1 are highlighted by bold italics. Alignment was calculated with the program MUSCLE [46].

shares the feature of binding membranes calcium-independently with its plant relatives, the ability to bind heparin is reminiscent of mammalian annexins. Furthermore, we developed an inexpensive purification procedure that produces protein amounts comparable with other protocols.

Results

Production of native annexin B1

Whereas recombinant annexin B1 has previously been purified either by ion-exchange chromatography [32] or liposome-affinity using proteoliposomes formed from disintegrated cell membranes [33], we explored the possibility of obtaining the protein by heparin-affinity chromatography [35]. After an initial anion-exchange chromatography step, annexin B1 was bound to heparin-Sepharose in the presence of 5 mM calcium and eluted, after extensive washing, by the application of an EDTA-containing buffer (Fig. 2). In SDS/PAGE, the protein migrates at an apparent molecular mass of 38 kDa.

This protocol yields up to 10 mg protein·L^{-1} bacterial culture with a purity of > 95%, as determined by MS. As such, this procedure results in comparable quantity and quality of protein as other methods. However, it is more convenient than the protocol based on liposome-affinity, due to utilization of re-usable affinity chromatography resin.

Protein fold and folding stability

The CD spectra of recombinant annexin B1 in the absence and presence of 5 mM calcium did not show a significant difference (Fig. 3A). Therefore, in solution, the secondary structure of the protein is not affected by calcium, an observation also seen in many other annexins.

Denaturation studies as monitored by CD indicate that there is one transition in heat-induced unfolding and that the presence of 5 mM calcium shifts the transition temperature by 6 K (Fig. 3B, Table 1). This situation is also seen in mammalian annexins such as annexin A5. Annexin B1 thus unfolds as one folding unit and the presence of calcium slightly stabilizes the protein.

Heparin binding

Calcium-dependent binding of annexin B1 to heparin was investigated using a centrifugation assay with heparin Sepharose beads. After binding the protein onto the beads in the presence of various calcium concentrations, the beads were washed once while maintaining the calcium concentrations. A washing step with calcium was performed to exclude possible artefacts from unspecific binding to the heparin matrix, and the amount of (reversibly) bound protein was determined from the EDTA eluate. As seen from Fig. 4B, the data for annexin B1 suggests a cooperative binding beha-

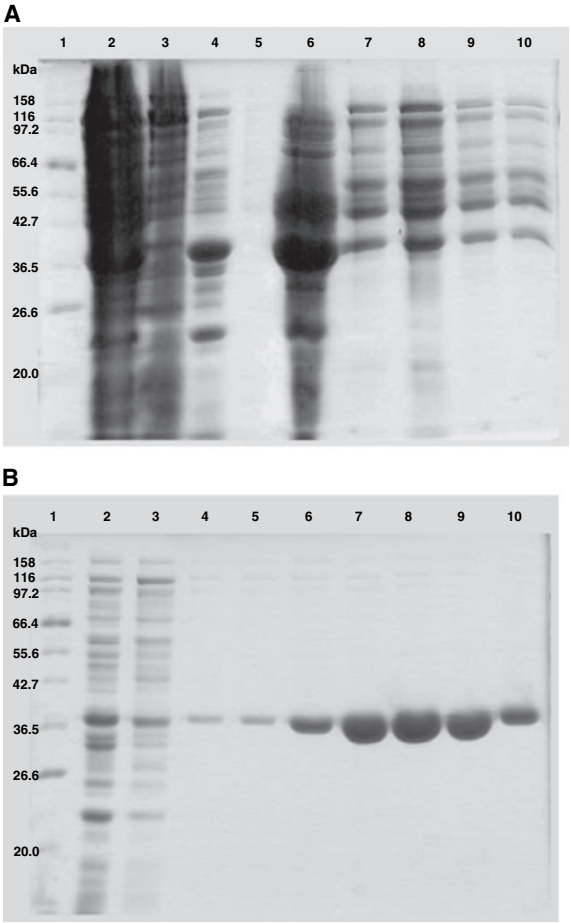

Fig. 2. Purification of native annexin B1. Fractions of the chromatography purification subjected to SDS/PAGE and stained with Coomassie Brilliant Blue. (A) After harvesting and lysing the cells, the cell lysate was applied to anion-exchange chromatography using Q-Sepharose. Shown are the molecular mass marker (lane 1), cell lysate (lane 2), flow-through (lane 3), wash (lane 4), elution fractions from 120 to 300 mM NaCl (lanes 5–10). (B) Affinity chromatography using heparin Sepharose. Protein-containing fractions from the anion-exchange chromatography were pooled, dialysed against a buffer containing 5 mM $CaCl_2$ and applied to the heparin column. Shown are the molecular mass marker (lane 1), flow-through from the loading step (lane 2), wash (lane 3), and elution fractions after applying 10 mM EDTA (lanes 4–10).

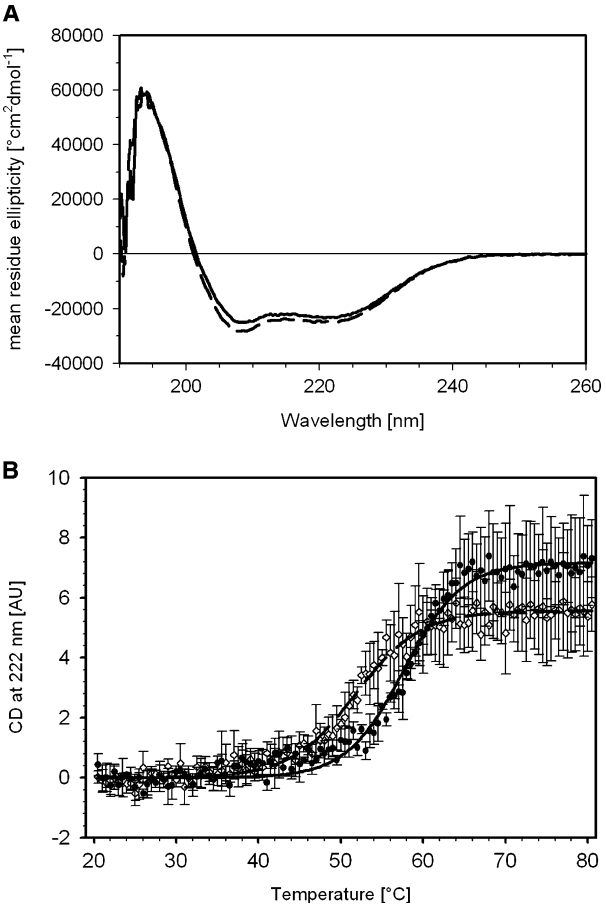

Fig. 3. Protein fold and folding stability. (A) Far-UV CD spectra of annexin B1 in the absence (dashed line) and presence (solid line) of 5 mM $CaCl_2$. (B) Thermal unfolding of annexin B1 in the absence (open circles, dashed line) and presence (closed diamonds, solid line) of 5 mM $CaCl_2$. The CD at 222 nm was monitored as described in Experimental procedures. The fit of the average of three independent experiments in the absence and presence of $CaCl_2$ is represented by the dashed and solid line, respectively.

Table 1. Thermal denaturation of annexin B1. The values for AnxA5 are given for comparison.

Protein	$T_{1/2}$ (°C) Without Ca^{2+}	$T_{1/2}$ (°C) 5 mM Ca^{2+}	$\Delta(T_{1/2})$ (K)
AnxB1	52	58	+6
AnxA5 [38]	52	59	+7

viour with respect to calcium that can be fitted with a Hill equation using a Hill coefficient of $n = 3$. For comparison, annexin A1 displays a binding behaviour with less cooperativity ($n = 1.7$; Fig. 4C). Comparing the binding curves of the two proteins, we can thus rule out the possibility that the lag phase observed with annexin B1 is due to an artefact within the assay. For both proteins, the maximal binding degree, as determined from the supernatant of the EDTA elution step, is only $\sim$ 60–70%. We therefore analysed the heparin Sepharose resin pellet in the EDTA elution step and found that not all of the protein could be released from the resin. The amount of irreversibly bound protein increases with higher calcium concentrations and reaches between 10 and 20% at 10 mM calcium for both annexins. Importantly, no annexin B1

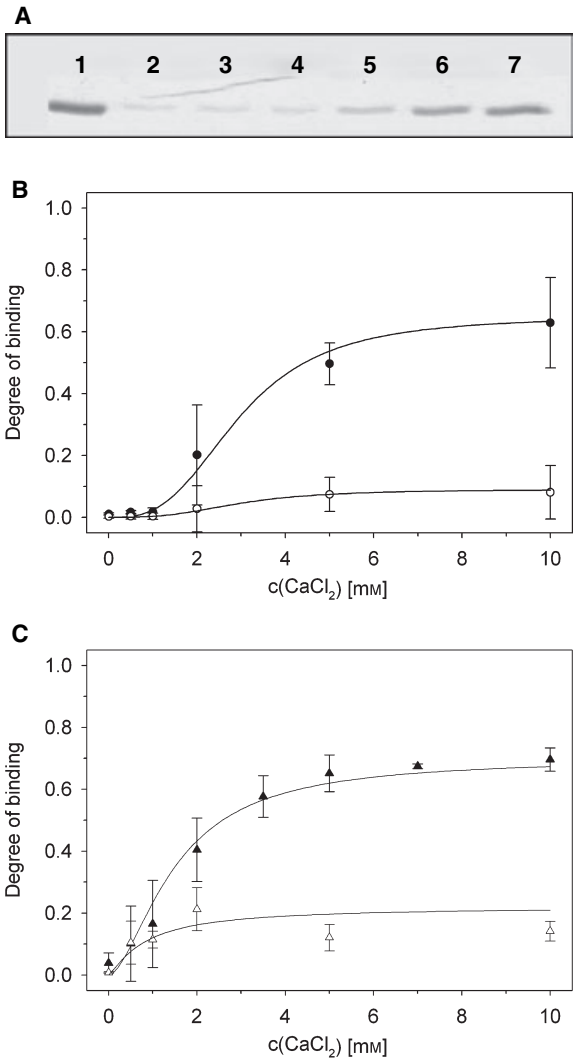

Fig. 4. Calcium-dependent binding of annexin B1 to heparin resin. (A) A representative SDS/PAGE of calcium-dependent annexin B1 binding to heparin Sepharose. Lane 1 is the amount of 100% protein ('Master sample'). Lanes 2–7 are the EDTA-elicited supernatants of samples with varying calcium concentrations (0, 0.5, 1, 2, 5, 10 mM). (B) Calcium-dependent binding of annexin B1 to heparin Sepharose displays a cooperative behaviour with respect to calcium. The degree of reversibly (closed circles) and irreversibly (open circles) bound annexin B1 was determined as outlined in Experimental procedures. Each data point represents the average of at least three independent experiments. The solid lines represent the fit of data to binding equations with a Hill coefficient of $n = 3$. (C) Annexin A1 binds to heparin Sepharose in a calcium-dependent manner with lower cooperativity ($n = 1.7$) than annexin B1. The degree of reversibly and irreversibly bound protein is shown as closed and open triangles, respectively. Each data point represents the average of at least three independent experiments. The solid lines represent the fit of data to binding equations.

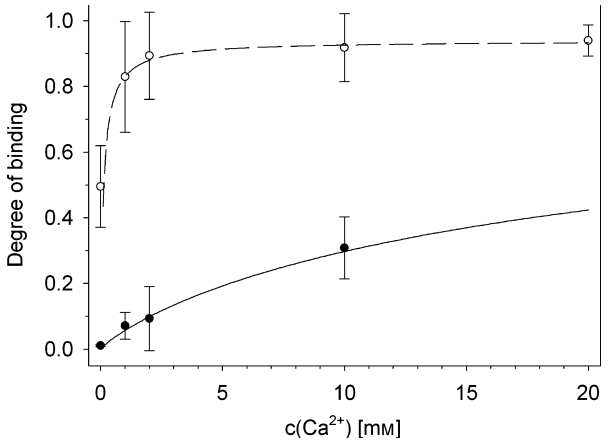

Fig. 5. Membrane binding of annexin B1 to liposomes. Membrane-binding of annexin B1 to PtdSer/PtdCho (1 : 3) (● to solid line) and PtdSer/PtdCho (3 : 1) (○ to dashed line) liposomes. The lines represent the fit of a standard binding equation to the data (one binding site). The data points are the average of at least three independent measurements.

Table 2. Calcium-dependent phospholipid binding of annexin B1.

Liposome composition	$c_{1/2}$ (Ca^{2+}) (mM)	Binding at $c(Ca^{2+})$ = 0 mM (%)	Maximum binding at $c(Ca^{2+})$ = 10 mM (%)
PtdSer/PtdCho (1 : 3)	–	0	30
PtdSer/PtdCho (3 : 1)	0.13	50	90

was found to bind to the resin at low levels of calcium (0–1 mM). Results from a precipitation assay show that only insignificant amounts of annexin B1 precipitate in the range of 0–10 mM calcium (data not shown).

Membrane binding

The calcium-dependent membrane binding of annexin B1 was assessed using large unilamellar vesicles (LUVs) with two different phosphatidylserine (PtdSer) contents (Fig. 5 and Table 2). The protein displays a calcium-dependent binding behaviour to PtdSer/phosphatidylcholine (PtdCho) (1 : 3) vesicles, albeit only to a moderate extent with a maximal binding of 30% at 10 mM calcium. In contrast, the binding is more enhanced with PtdSer/PtdCho (3 : 1) vesicles. Here, the maximal binding degree at 10 mM calcium is 90% and the half-maximal calcium concentration of 0.1 mM is at the lower end of the range observed with several plant annexins [36].

More interestingly, using PtdSer/PtdCho (3 : 1) liposomes, annexin B1 exhibits calcium-independent binding with a binding degree of $\sim 50\%$. This behaviour is

akin to that seen from bell pepper and cotton annexins, although the latter proteins have a less stringent requirement for PtdSer in this context [36].

Discussion

Denaturation studies

As seen from thermal denaturation, annexin B1 unfolds as one folding unit similar to most of its mammalian relatives. The only notable exception is annexin A3 where the N-terminal domain acts as a second unfolding unit due to the Trp5-mediated anchorage of the N-terminal tail to the core of the protein [37].

Although the calcium affinity of annexin proteins in the absence of phospholipids is rather low with micromolar and millimolar dissociation constants, a stabilization effect has been observed with mammalian annexins, in particular annexin A5, in the presence of calcium [38]. We report the same effect with annexin B1 which displays a higher folding stability in the presence of calcium as indicated by an increase of 6 K in its transition temperature. This increase is comparable with that observed with annexin A5.

Membrane binding

Annexin B1 exhibits the landmark feature of calcium-dependent binding to acidic phospholipid membranes shared by all annexins studied to date. A comparison of low and high PtdSer containing LUVs yields only poor annexin binding to PtdSer/PtdCho (1 : 3) vesicles, but enhanced binding to PtdSer/PtdCho (3 : 1) vesicles. Intriguingly, calcium-independent binding up to $\sim$50% is observed with the latter vesicles. This behaviour deviates from that of mammalian annexins which rely almost entirely on a calcium-mediated binding mode regardless of the vesicle composition. In contrast, recent results demonstrate that some plant annexins employ a second, calcium-independent mechanism that utilizes conserved exposed surface residues, including Trp35, Trp107 and Lys190 [annexin 24 (Ca32) numbering] [36]. One can therefore speculate that annexin B1 employs a similar mechanism whereby exposed residues on the convex surface engage in direct interactions with the membrane. From the three identified residues in plant annexins, only Lys190 is semiconserved in annexin B1 by Arg214. However, it is possible to identify a number of exposed basic residues on the convex surface of the protein. The involvement of these basic residues would help to explain the observation that a high PtdSer content in the membrane is required in order to bind annexin B1.

It is worth noting that, in contrast to mammalian annexins, plant annexins apparently have fewer than four canonical type II calcium binding sites. One could imagine that the calcium-independent membrane binding mechanism assists the calcium-driven membrane-binding process which might be less efficient, in case of dysfunctional calcium binding sites. The development of four canonical calcium-binding sites in certain annexins (predominantly later in evolution) might have made the calcium-independent mechanisms obsolete. The observation of calcium-independent membrane binding by annexin B1 fits well with this hypothesis, because one can anticipate a disrupted canonical calcium-binding site in domain III of this protein.

Heparin binding

Results from the heparin-binding assay show that annexin B1 possesses lectin properties. The protein binds to glycosaminoglycan in a calcium-dependent manner and displays cooperativity with respect to calcium. This latter feature is less pronounced in annexin A1, which was used as a control in this study. The binding data can be fitted assuming the presence of three binding sites which coincides with the fact that annexin B1 only has three canonical type II binding sites. It remains to be clarified whether all three binding sites engage in calcium-dependent glycosaminoglycan binding.

Interestingly, between 10 and 20% of both annexins remain bound to the glycosaminoglycan even after extraction with high concentrations of a chelating agent. Unspecific binding to the heparin matrix can be excluded due to an intermediate washing step and the fact that no protein was found to bind to the glycosaminoglycan in the absence of calcium. Based on results from precipitation assays, we can also rule out artefacts caused by calcium-mediated protein aggregation. Apparently, the protein is dependent on calcium ions to initially form interactions with heparin. Once bound, a fraction of the protein undergoes a shift in binding mode which 'irreversibly' attaches it to the glycosaminoglycan.

For annexin A5, a model of heparin binding has been put forward in which recognition and binding of heparin occurs on the concave side of the protein via the two binding sites HTS-1 (Arg207–Lys208) and HTS-2 (Arg285–Lys286–X–X–Arg289–Lys290) [24]. However, the HTS-3 (Arg25–Lys26) site on the convex surface is not involved in the recognition process but significantly increases the affinity of the interaction with heparin. Subsequent binding of annexin A5 to the membrane surface releases the glycosaminoglycan from

the HTS-3 site because its affinity for the phospholipid membrane is considerably higher [26]. In this latter state, the protein is attached to the membrane surface via its convex site and the heparin is bound with the binding sites only on the concave side. One could envision a similar mechanism with annexin B1, in which the calcium-dependent binding step occurs through the calcium-binding sites on the convex domain. Assuming the presence of further heparin-binding sites elsewhere on the protein surface, annexin B1 can remain bound to the glycosaminoglycan even in the absence of calcium ions. In this context, the amino acid sequence alignment of annexins A5 and B1 reveals that only the HTS-3 site of annexin A5 (Arg25–Lys26) is conserved in annexin B1 (Lys38–Arg39), which may thus act in the same manner as in its mammalian relative. The binding sites on the concave surface (HTS-1 and HTS-2) are not observed with annexin B1, although a K-E-K motif is present instead of the R-K-X-X-R-K motif of HTS-1. However, two other sites in annexin B1 merit attention. The motifs Arg91–Arg92 and Lys139–Lys140 on the concave sides of domains I and II, respectively, could be potential calcium-independent heparin binding sites. A further possible motif, Lys254–Lys255 is found in the DE loop of domain III, which is located in the anticipated dysfunctional canonical calcium binding site. Nevertheless, occupation of this site by heparin would compete with binding to the membrane surface. Further studies to test these hypotheses are currently under way.

Several viruses and parasites have infection strategies based on binding to proteoglycans in the extracellular matrix. Binding to the carbohydrates of proteoglycans is a crucial step in attachment, invasion and cytolysis of intestinal epithelium by parasites. Obviously, this requires the invader to have glycosaminoglycan-binding proteins. Prominent examples are microbial adhesions, including the influenza haemagglutinin, as well as the adhesins from Shiga toxin and *Entamoeba histolytica* [39]. Annexin B1 has been shown to be highly immunogenic [31], and is potentially present on the surface of *C. cellulosae*. The binding behaviour of the protein to heparin as determined in this study may therefore be a mechanism used by *C. cellulosae* to attach and invade host tissue.

Experimental procedures

Production of native annexin B1

Annexin B1 cDNA was cloned into the bacterial expression vector pRSET_6c [40] using PCR amplification to engineer *Nde*I and *Xho*I restriction sites. The construct was obtained with a P346H mutation.

The construct was expressed in *Escherichia coli* strain BL21(DE3). A total of 8 L of Luria–Bertani medium (50 mg·L^{-1} ampicillin) was inoculated with an overnight culture of 1 L. The cells were grown at 37 °C until the absorbance at 600 nm exceeded 1.0. Induction was carried out with 0.5 mM isopropyl thio-β-D-galactoside. Cell growth was then continued for 14–16 h before being harvested. The cell pellets were resuspended (100 mM NaCl, 1.5 mM EDTA, 5 mM benzamidinium chloride, 1 mM phenylmethylsulfonyl fluoride, 0.1% Triton X-100, 20 mM Tris, pH 8.0) and lysed by freeze–thaw and sonication. Cell debris was separated by centrifugation for 45 min, 60 000 ***g***, and 4 °C.

The protein was purified in two steps, anion exchange chromatography using Q-Sepharose resin, and heparin affinity chromatography. The anion-exchange column was equilibrated with 20 mM Tris, pH 9.0 and the supernatant from the centrifugation step was applied. After extensive washing with equilibration buffer, a linear NaCl gradient was applied and the protein eluted from 150 to 300 mM NaCl. The pooled fractions obtained from this step were dialysed against the equilibration buffer for heparin-affinity chromatography (5 mM $CaCl_2$, 250 mM NaCl, 50 mM Tris, pH 9.0) and loaded onto a heparin Sepharose column. After extensive washing, the protein was eluted by applying buffer containing EDTA (10 mM EDTA, 250 mM NaCl, 50 mM Tris, pH 9.0). Fractions containing annexin B1 were pooled and concentrated using 10 kDa molecular mass cut-off Vivaspin concentrators (Vivascience, Fisher Scientific, Loughborough, UK). SDS/PAGE analysis was performed throughout the purification process. The identity and purity of annexin B1 was confirmed using MALDI-TOF. The whole procedure yields ~8 mg protein·L^{-1} of cell culture.

Heparin-binding assay

Calcium-dependent binding of annexin B1 to heparin was studied by a centrifugation assay using heparin Sepharose. For the assay, 1 mL suspension of heparin Sepharose (Amersham Pharmacia Biotech, Piscataway, NJ) was equilibrated by washing three times with 3.5 mL buffer (100 mM NaCl, 20 mM Tris, pH 8.0). All centrifugation steps were carried out for 3 min, 3000 r.p.m., 4 °C. The resin was finally resuspended in 4 mL protein buffer and distributed into six aliquots. After centrifugation, the supernatant was removed and $CaCl_2$ was added to the protein buffer (total volume 390 μL) to yield varying concentrations of calcium (0, 0.5, 1, 2, 5 and 10 mM). Finally, 10 μL of annexin B1 (1–5 mg·mL^{-1}) was added to each aliquot. After 10 min incubation at room temperature, the samples were subjected to centrifugation. The pellets were then washed with 400 μL protein buffer with the appropriate calcium concentration and the samples were centrifuged again. The protein

was eluted with 400 μL of protein buffer containing 30 mM EDTA. After centrifugation, the supernatant was run on SDS/PAGE (Fig. 4A). The amount of reversibly bound annexin was determined by densitometric analysis of the Coomassie Brilliant Blue-stained gels using the program IMAGEJ [41].

Liposome-based copelleting assay

Phospholipid vesicles were prepared from 1,2-dioleoyl-*sn*-glycero-3-phosphoserine and 1,2-dioleoyl-*sn*-glycero-3-phosphocholine (Avanti Polar Lipids, Alabaster, AL, USA) according to the protocol of Reeves & Dowben [42]. The vesicles were converted into LUVs using five freeze–thaw cycles and subsequent extrusion (11 times) through 0.1 μm filter membranes using an extruder (Avanti Polar Lipids) at 37 °C. To assess the annexin–membrane binding behaviour, a copelleting assay was conducted [43]. A total of 0.2 μmol phospholipids was used for each individual sample (500 μL), composed of 0.5 nmol protein in liposome buffer and varying amounts of calcium (0, 1, 2, 10 and 20 mM). As a control, a sample of 0.1 nmol protein in 100 μL of 10% SDS was prepared at this stage. All samples were centrifuged (45 min, 13000 r.p.m., 4 °C), the pellets resuspended with 50 μL of 10% SDS and subjected to SDS/PAGE. Gels were stained with Coomassie Brilliant Blue and analysed densitometrically using the program IMAGEJ [41]. Each calcium concentration was assessed three times independently. Curve fitting was performed with SIGMAPLOT.

Calcium-dependent aggregation/precipitation assay

Calcium-induced precipitation of annexins B1 and A1 was performed as a control for the heparin binding and liposome copelleting assays. 10 μL of 2 $mg \cdot mL^{-1}$ protein in standard buffer (100 mM NaCl, 20 mM Tris, pH 8.0) or liposome buffer was added to 390 μL of standard buffer containing different concentrations of calcium (0, 0.5, 1, 2, 3.5, 7 and 10 mM) and incubated for 10 min at room temperature. After centrifugation (30 min, 16 000 ***g***, 4 °C), the supernatant were carefully removed. The tubes were washed with 20 μL of 10% SDS and the samples subjected to SDS/PAGE. Gels were stained with Coomassie Brilliant Blue and analysed densitometrically using the program IMAGEJ [41].

CD spectroscopy

CD spectra of protein samples (1.8 μM) were recorded in 50 mM NaCl, 5 mM Tris, pH 8.0 at 20 °C using a Jasco J-810 spectropolarimeter equipped with a Peltier element. Experiments in the presence of calcium were carried out with the addition of 5 mM $CaCl_2$ in the buffer. For investigation of the thermal denaturation of annexin B1, the CD signal at 222 nm was monitored from 20 to 80 °C with a heating rate of 1 $K \cdot min^{-1}$. Data were recorded at 0.5 K increments. Unfolding experiments were performed three times independently. All spectra were corrected against the baseline and the data were transformed into mean residue ellipticity using the program ACDP [44]. Changes in the mean residue ellipticity at 222 nm were used to construct an unfolding curve. Curve fitting was done with SIGMAPLOT using a sigmoidal equation.

Acknowledgements

AW gratefully acknowledges a scholarship from the Darwin Trust of Edinburgh.

References

1 Fernandez MP & Morgan RO (2003) Structure, function and evolution of the annexin gene superfamily. In *Annexins: Biological Importance and Annexin-Related Pathologies* (Bandorowicz-Pikula J, ed.), pp. 21–36. Landes Bioscience, Georgetown, TX.

2 Goldberg M, Feinberg J, Rainteau D, Lecolle S, Kaetzel MA, Dedman JR & Weinman S (1990) Annexins I–VI in secretory ameloblasts and odontoblasts of rat incisor. *J Biol Buccale* **18**, 289–298.

3 Fiedler K, Lafont F, Parton RG & Simons K (1995) Annexin XIIIb: a novel epithelial-specific annexin is implicated in vesicular traffic to the apical plasma membrane. *J Cell Biol* **128**, 1043–1053.

4 Hajjar KA, Guevara CA, Lev E, Dowling K & Chacko J (1996) Interaction of the fibrinolytic receptor, annexin II, with the endothelial cell surface. Essential role of endonexin repeat 2. *J Biol Chem* **271**, 21652–21659.

5 Liu J, Zhu X, Myo S, Lambertino AT, Xu C, Boetticher E, Munoz NM, Sano M, Cordoba M, Learoyd J *et al.* (2005) Glucocorticoid-induced surface expression of annexin 1 blocks beta2-integrin adhesion of human eosinophils to intercellular adhesion molecule 1 surrogate protein. *J Allergy Clin Immunol* **115**, 493–500.

6 Andersen MH, Berglund L, Petersen TE & Rasmussen JT (2002) Annexin V binds to the intracellular part of the beta(5) integrin receptor subunit. *Biochem Biophys Res Commun* **292**, 550–557.

7 Pietropaolo RL & Compton T (1991) Direct interaction between cytomegalovirus glycoprotein B and cellular annexin II. *J Virol* **71**, 9803–9807.

8 Neurath AR & Strick N (1994) The putative cell receptors for hepatitis B virus (HBV), annexin V, and apolipoprotein H, bind to lipid components of HBV. *Virology* **204**, 475–477.

9 Otto M, Gunther A, Fan H, Rick O & Huang RT (1994) Identification of annexin 33 kDa in cultured cells

as a binding protein of influenza viruses. *FEBS Lett* **356**, 125–129.
10 Ikebuchi NW & Waisman DM (1990) Calcium-dependent regulation of actin filament bundling by lipocortin-85. *J Biol Chem* **265**, 3392–3400.
11 Ma ASP, Bystol ME & Tranvan A (1994) *In vitro* modulation of filament bundling in F-actin and keratins by annexin II and calcium. *In Vitro Cell Dev Biol* **30A**, 329–335.
12 Calvert CM, Gant SJ & Bowles DJ (1996) Tomato annexins p34 and p35 bind to F-actin and display nucleotide phosphodiesterase activity inhibited by phospholipid binding. *Plant Cell* **8**, 333–342.
13 Blackbourn HD, Barker PJ, Huskisson NS & Battey NH (1992) Properties and partial protein sequence of plant annexins. *Plant Physiol* **99**, 864–871.
14 Hoshino T, Mizutani A, Chida M, Hidaka H & Mizutani J (1995) Plant annexins form homodimer during Ca^{2+}-dependent liposome aggregation. *Biochem Mol Biol Int* **35**, 749–755.
15 Delmer DP & Potikha TS (1997) Structures and functions of annexins in plants. *Cell Mol Life Sci* **53**, 546–553.
16 Alvarez-Martinez MT, Mani JC, Porte F, Faivre-Sarrailh C, Liautard JP & Sri Widada J (1996) Characterisation of the interaction between annexin I and profilin. *Eur J Biochem* **238**, 777–784.
17 Park PW, Reizes O & Bernfield M (2000) Cell surface heparan sulfate proteoglycans: selective regulators of ligand–receptor encounters. *J Biol Chem* **275**, 29923–29936.
18 Plotnikov AN, Hubbard SR, Schlessinger J & Mohammadi M (2000) Crystal structures of two FGF–FGFR complexes reveal the determinants of ligand–receptor specificity. *Cell* **101**, 413–424.
19 Olson ST & Bjork I (1991) Predominant contribution of surface approximation to the mechanism of heparin acceleration of the antithrombin–thrombin reaction. Elucidation from salt concentration effects. *J Biol Chem* **266**, 6353–6364.
20 Kassam G, Manro A, Braat CE, Louie P, Fitzpatrick SL & Waisman DM (1997) Characterisation of the heparin binding properties of annexin II tetramer. *J Biol Chem* **272**, 15093–15100.
21 Ishitsuka R, Kojima K, Utsumi H, Ogawa H & Matsumoto I (1998) Glycosaminoglycan binding properties of annexin IV, V, and VI. *J Biol Chem* **273**, 9935–9941.
22 Römisch J & Heimburger N (1990) Purification and characterization of six annexins from human placenta. *Biol Chem (Hoppe-Seyler)* **371**, 383–388.
23 Capila I, VanderNoot VA, Mealy TR, Seaton BA & Linhardt RJ (1999) Interaction of heparin with annexin V. *FEBS Lett* **446**, 327–330.
24 Capila I, Hernaiz MJ, Mo YD, Mealy TR, Campos B, Dedman JR, Linhardt RJ & Seaton BA (2001) Annexin V–heparin oligosaccharide complex suggests heparan sulfate-mediated assembly on cell surface. *Structure* **9**, 57–64.
25 Satoh A, Hazuki M, Kojima K, Hirabayashi J & Matsumoto I (2000) Ligand-binding properties of annexin from *Caenorhabditis elegans* (Annexin XVI, Nex-1). *J Biochem (Tokyo)* **128**, 377–381.
26 Tait JF, Gibson DF & Fujikawa K (1989) Phospholipid binding properties of the lipocortin family. *J Biol Chem* **264**, 7944–7949.
27 Kamal AM, Flower RJ & Perretti M (2005) An overview of the effects of annexin 1 on cells involved in the inflammatory process. *Mem Inst Oswaldo Cruz* **100**, 39–48.
28 Cesarman-Maus G & Hajjar KA (2005) Molecular mechanisms of fibrinolysis. *Br J Haematol* **129**, 307–321.
29 Rand JH, Wu XX, Quinn AS, Chen PP, McCrae KR, Bovill EG & Taatjes DJ (2003) Human monoclonal antiphospholipid antibodies disrupt the annexin A5 anticoagulant crystal shield on phospholipid bilayers: evidence from atomic force microscopy and functional assay. *Am J Pathol* **163**, 1193–1200.
30 Baron S (1996) *Medical Microbiology*, 4th edn. University of Texas at Galveston, Galveston.
31 Yan H, Song Y, Fan L, Chen R & Guo Y (2002) Cloning and functional identification of a novel annexin subfamily in *Cysticercus cellulosae*. *Mol Biochem Parasitol* **119**, 1–5.
32 Zhang Y, Guo YJ, Sun SH, Yan HL & He Y (2004) Non-fusion expression in *Escherichia coli*, purification, and characterization of a novel Ca^{2+}- and phospholipid-binding protein annexin B1. *Protein Expr Purif* **34**, 68–74.
33 Gao YJ, Zhang Y, Yan HL, He Y, Wang F & Sun SH (2005) Preparation and purification of recombinant annexin B1 by Ca^{2+}-triggered precipitation. *Annexins* **2**, 18–20.
34 Geisow M, Fritsche U, Hexham J, Dash B & Johnson T (1986) A consensus amino acid sequence repeat in *Torpedo* and mammalian calcium-dependent membrane binding proteins. *Nature* **320**, 636–638.
35 Alvarez-Martinez MT, Mani JC, Porte F, Faivre-Sarrailh C, Liautard JP & Sri Widada J (1996) Characterisation of the interaction between annexin I and profilin. *Eur J Biochem* **238**, 777–784.
36 Dabitz N, Hu NJ, Yusof AM, Tranter N, Winter A, Daley M, Zschörnig O, Brisson A & Hofmann A (2005) Structural determinants for plant annexin–membrane interactions. *Biochemistry* **44**, 16292–16300.
37 Hofmann A, Raguenes-Nicol C, Favier-Perron B, Mesonero J, Huber R, Russo-Marie F & Lewit-Bentley A (2000) The annexin A3–membrane interaction is modulated by an N-terminal tryptophan. *Biochemistry* **39**, 7712–7721.

38 Jatzke C (1999) Untersuchungen zur Calcium- und Phospholipid bindung von Annexin V, PhD thesis, Westfälische Wilhelms-Universität Münster, Germany.
39 Esko JD (1999) Proteins that recognise glycans. Microbial carbohydrate-binding proteins. In *Essentials of Glycobiology* (Varki A, Cummings R, Esko J, Freeze H, Hart G & Marth J, eds). Cold Spring Harbor Laboratory Press, Cold Spring Harbor, New York.
40 Schoepfer R (1993) The pRSET family of T7 promoter expression vectors for *Escherichia coli*. *Gene* **124**, 83–85.
41 Rasband W. *Imagej 1.30v*. National Institutes of Health. http://rsb.info.nih.gov/ij/.
42 Reeves JP & Dowben RM (1969) Formation and properties of thin-walled phospholipid vesicles. *J Cell Physiol* **73**, 49–60.
43 Hofmann A & Huber R (2003) Liposomes in assessment of annexin–membrane interactions. *Methods Enzymol* **372**, 186–216.
44 Hu N-J, Currid M, Daley M & Hofmann A (2005) Two new software applications for automated processing of circular dichroism and fluorescence data. *Appl Spectrosc* **59**, 68A.
45 Hileman RE, Fromm JF, Weiler JM & Linhardt RJ (1998) Glycosaminoglycan–protein interactions: definition of consensus sites in glycosaminoglycan binding proteins. *Bioessays* **20**, 156–167.
46 Edgar RC (2004) MUSCLE: multiple sequence alignment with high accuracy and high throughput. *Nucleic Acids Res* **32**, 1792–1797.

PROTEINS: Structure, Function, and Bioinformatics 68:353–362 (2007)

Molecular Modeling of Prohibitin Domains

Anja Winter,[1] Outi Kämäräinen,[1] and Andreas Hofmann[1,2]*
[1]*Institute of Structural and Molecular Biology, School of Biological Sciences, The University of Edinburgh, Scotland, United Kingdom*
[2]*Structural Chemistry Program, Eskitis Institute for Cell and Molecular Therapies, Griffith University, Brisbane, Queensland, Australia*

ABSTRACT **Prohibitins comprise a family of highly conserved ubiquitous eukaryotic proteins that mainly localize to the mitochondria. They have been implicated in important cellular processes such as cellular signaling and transcriptional control, apoptosis, cellular senescence, and mitochondrial biogenesis. Using molecular modeling techniques, we have generated structural models of human prohibitins BAP32 and BAP37, which have previously been shown to exist as large ring-like oligomers in the membrane-bound state. The middle domain of prohibitins is evolutionary conserved in the family of SPFH (PHB) domain proteins. On the basis of the known structure of flotillin-2, another member of the SPFH-domain family, we have generated homology models for BAP32 and BAP37, and elucidated the implications for formation of high molecular weight oligomers. A model for the dimeric-building block of BAP32: BAP37 for such assemblies was generated and its stability scrutinized by molecular dynamics simulations. The model of BAP32 was also analyzed as to potential ligand-binding sites and the previously identified ligand melanogenin was docked into a membrane-proximal cavity. The results are discussed in the context of prohibitin interactions with mitochondrial AAA-proteases and we suggest two possible interaction interfaces between the BAP32:BAP37 building block and the protease. Proteins 2007;68:353–362.** © 2007 Wiley-Liss, Inc.

Key words: molecular modeling; PHB domain; protein–protein interactions; *m*-AAA-protease; melanogenin

INTRODUCTION

Flotillins and prohibitins belong to a larger family of proteins that share an evolutionarily conserved stomatin/prohibitin/flotillin/HflK/C (SPFH) domain with significant homology to several eukaryotic and prokaryotic proteins. Members of this protein family are membrane-associated and implicated in cellular processes concerned with protein turnover,[1] senescence,[2] and proliferation control.[2–4] The integral membrane protein stomatin is an important component of the red blood cell membrane but can also be found in abundance in different tissues and cell lines. A possible structural role for this protein in the formation of membrane protrusions and anchorage to the actin cytoskeleton has been suggested.[5] In plants, stomatin has been implicated in ion-channel regulation and might play a role in resistance to pathogen attack via hypersensitive reactions culminating in cell death.[6] Prohibitins are thought to be involved in cell proliferation and senescence[7,8] being located both in the nucleus[9] and the mitochondrion.[10,11] Recent studies suggest that they can also act as cell surface bound receptors.[12,13] Flotillins are upregulated in the retinal ganglion cells and retinal axons of regenerating neurons.[14]

The N-terminal membrane-associating region of both mouse flotillin-1 and flotillin-2 was either identified as a conserved prohibitin homology (PHB) by the Simple Modular Architecture Research Tool (SMART)[15] or as a SPFH domain using PSI-BLAST mapping the region amino acids 4-211 of mouse flotillin-1.[1] However, it appears that regardless of the variation in boundaries described by the different data mining tools, the SPFH and PHB are essentially describing the same domain.[16] Members of the PHB domain family can be found in divergent species; they are present in higher eukaryotes (prohibitin, stomatin, and podocin), as well as in lower eukaryotes and prokaryotes (vacuolin A and vacuolin B, HflK and HflC, unc-1, unc-24, and mec-2). The PHB domain is conserved in proteins that are ubiquitously expressed like flotillin, as well as in proteins that show extremely restricted expression like the stomatin-related olfactory protein (SROP), whose expression is constrained to olfactory sensory neurons.[17] The evolutionary significance of this domain is unclear but its prokaryotic conservation suggests that it is indeed a primordial motif. As there are more than 700 nonredundant sequences containing the PHB domain throughout all kingdoms, it is clear that this domain is likely to perform an important cellular function and worthy of further examination.[16]

Grant sponsors: Darwin Trust of Edinburgh, CSO, and European League Against Rheumatism.

*Correspondence to: Andreas Hofmann, Eskitis Institute for Cell and Molecular Therapies, Griffith University, Brisbane Innovation Park, Don Young Road, Brisbane, Queensland 4111, Australia.
E-mail: a.hofmann@griffith.edu.au

Received 11 July 2006; Revised 26 September 2006; Accepted 1 December 2006

Published online 10 April 2007 in Wiley InterScience (www.interscience.wiley.com). DOI: 10.1002/prot.21355

Prohibitin, the archetypal PHB domain-containing protein, is a mitochondrial inner-membrane protein that has been proposed to act as a chaperone for the stabilization of mitochondrial proteins.[18–20]

Two homologs of the protein are known and both are membrane associated via an N-terminal membrane anchor. Bacterial overexpression leads to formation of inclusion bodies, which make structural work difficult because of a limited amount of available protein. Human prohibitin (BAP32) forms a large hetero-oligomeric complex with its closely related PHB domain-carrying homolog, B-cell receptor-associated protein (BAP37; also called prohibitone), and this complex is thought to protect non-assembled mitochondrial membrane proteins against proteolysis by the *m*-AAA protease.[19,21–23] Electron micrographs from yeast prohibitins Phb1 and Phb2 reveal large ringlike oligomers comprising 16–20 individual prohibitin molecules, and the C-terminal coiled-coil regions are thought to be involved in formation of these large oligomers.[24] Furthermore, prohibitins are thought to form a supercomplex with the *m*-AAA-protease whose catalytic domains are located in the mitochondrial matrix.[25]

Studies of the prohibitin homologs in yeast, Phb1, and Phb2, suggest that these proteins may be involved in senescence, as deletion of these genes results in a decreased replicative lifespan.[22] Interestingly, prohibitin was originally described as a tumor-suppressor gene,[7] but more recent studies suggest that this is only true for the 3′-untranslated region (3′-UTR).[26] The prohibitin proteins have been found to be localized to various compartments in the cell suggesting a multiple function in the cell. Its localization to the nucleus and its ability to prevent cell proliferation has been attributed to its interaction with E2F transcription factors in addition to Rb proteins (suppressors of E2F-mediated transcription)[9] in human cells. Despite contrary statements about whether prohibitin and BAP37 localize to the plasma membrane, there are also reports describing the presence of a surface-bound prohibitin complex,[12,13] which acts as a receptor for extracellular ligands.

In the recent years, the focus in prohibitin research has been the prohibitin-ligand interactions, including protein–protein interactions, and interactions with peptides, sugars, and organic molecules. In 1999, Wang et al. found that prohibitin could effectively interact with Rb, p107, and p130. It was also found to repress the activity of all of the five E2Fs through MAPK pathway.[9] Yeast two-hybrid screens identified α-actinin and annexin A2 as new binding partners for the prohibitin family[27] in the cell. Prohibitin was reported to be a marker of adipose tissue and found to be a target for the peptide motif CKGGRAKDC. The fusion of a proapoptotic peptide to that peptide sequence led to ablation of white fat tissue and thus reversal of obesity in a mouse model.[12] Furthermore, an interaction of cells and the Vi capsular polysaccharide, a virulent antigen of *Salmonella typhi* was shown to be mediated through a cell-surface-associated recognition complex containing prohibitins.[13]

The prohibitin complex has also been found to act as an intracellular receptor. With a chemical genetics approach searching for pigment-enhancing chemicals, melanogenin has been found to enhance melanin production in melanocytes and to bind specifically to prohibitin.[28] A sufficient pigment production in melanocytes is important to the organism, as UV irradiation can cause severe damage to the cell and finally induce apoptosis through activation of the mitochondrial permeability transition. Based on further RNA interference experiments, these authors propose that prohibitin plays a functional role in melanin induction since neither the melanin induction agent isobutylmethylxanthine nor melanogenin were able to induce melanin production when prohibitin expression was silenced.[28]

In the absence of atomic details of prohibitin structures, we present structural models for BAP32 and BAP37 based on secondary structure prediction and homology modeling using the NMR structure of the band 7 domain of mouse flotillin-2, another member of the PHB domain protein family. We also elucidate possible interactions between BAP32 and melanogenin and discuss implications for protein–protein and protein–ligand interactions.

MATERIALS AND METHODS

Secondary Structure Prediction and Homology Modeling

Multiple sequence alignment of the PHB domains of BAP32 (GenBank accession no. BC083354), BAP37 (GenBank accession no. NM_007531) and flotillin-2 (GenBank accession no. NM_008028) generated with MUSCLE.[29] The secondary structures of BAP32 and BAP37 were predicted using PSIPRED,[30] and compared to the NMR structure of the PHB domain of mouse flotillin-2 (PDB accession no. 1win). Thereafter, the multiple sequence alignment was slightly adjusted to satisfy the secondary structure elements. The flotillin-2 structure was then used as template for homology modeling. Twenty independent homology models of BAP32 and BAP37 were calculated with the programme Modeller 4[31] and those with the lowest energy were selected. The selected models were visually inspected with O[32] and subjected to further energy minimization using CNS.[33] The overall geometry was scrutinized using PROCHECK.[34] Surface properties and electrostatic characteristics were analyzed using GRASP.[35] Root mean square (rms) distances of structures were calculated using ALIGN.[36]

Modeling of Interactions Between BAP32 and BAP37

The modeled structures of BAP32 and BAP37 were subjected to an automated macromolecular docking calculation with the programme Hex[37] to investigate potential interaction sites. In the programme, one of the proteins was set as a receptor, and the other was set as a ligand. The programme was run using the default settings.

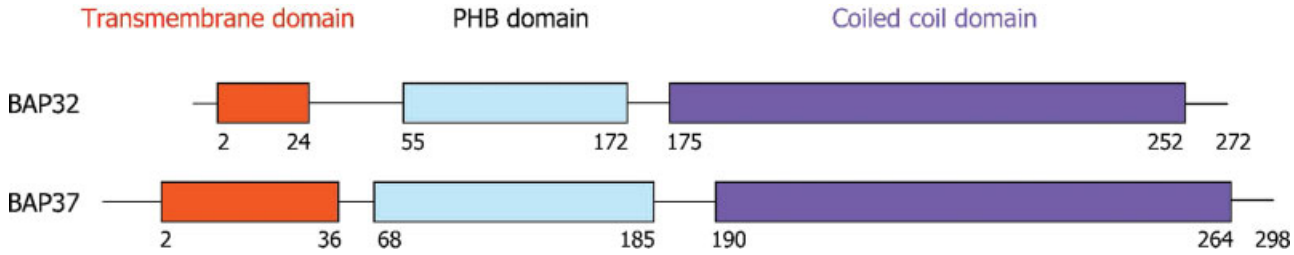

Fig. 1. Domain topology of human BAP32 and BAP37. The N-terminal transmembrane domain of BAP32 extends from residue 1 to 24, followed by the predicted PHB domain (residues 55–172) and the C-terminal coiled-coil domain (residues 175–252). BAP37 is divided into its N-terminal domain (residues 2–36), the PHB domain (residues 68–185), and the C-terminal domain from residue 190 to 264. [Color figure can be viewed in the online issue, which is available at www.interscience.wiley.com.]

Models for BAP32:BAP37 complexes were also constructed manually by rigid body movements using the graphics programme O[32] and considering a spatial vicinity of residues Pro72 (BAP32) and Arg86 (BAP37), Asp152 (BAP32) and Arg86 (BAP37), and Val149 (BAP32) and Gln159 (BAP37). The residues in those positions have been found to interact, as identified in a crosslinking study, using the yeast prohibitin complex.[38] The initial model was subjected to molecular dynamics simulations in GROMACS.[39] The simulations (50 and 500 ps) were carried out using a model with explicit solvation and without superimposing any user-defined distance restraints.

The dimer of the N-terminal BAP helices was constructed using α-helices generated with GARLIC,[40] which were oriented as rigid bodies in O to yield a first approximation of a helix dimer. The raw model was then subjected to molecular dynamics simulations in GROMACS. No user-defined distance restraints were applied and the simulations were carried out in vacuo for 50 and 500 ps, respectively.

The molecular dynamics simulations were analyzed using the tools included in GROMACS, as well as VMD[41] and O[32].

Modeling of Interactions Between BAP32 and Melanogenin

An automated docking approach was employed to investigate the interaction between BAP32 and its ligand melanogenin using the programme FlexX[42] to perform flexible ligand fitting. First, the BAP32 homology model was visually inspected and potential binding sites were identified by surface analysis. Then, the three-dimensional molecule structure of melanogenin was created and subsequently optimized by energy minimization with Sybyl (Tripos). After site point generation within the docking programme, the ligand was fitted into the binding pockets based on chemical and shape complementation. The models with highest scores were analyzed with Sybyl.

RESULTS AND DISCUSSION

Homology in the PHB Superfamily

So far, the grouping of prohibitins, flotillins, stomatins, and HflC/K into the PHB superfamily was mainly based on amino acid sequence homology with rather poor matches. Although alignment of BAP32 and BAP37 reveals a sequence similarity of 60% and an identity of 47%, the similarity of both proteins to mouse flotillin-2 is only 4 and 7%, respectively. Phylogenetic analyses of PHB domains from different proteins revealed only ambiguous relationships within this superfamily, indicating independent origins for the individual members and convergent evolution of the PHB domain.[43] Several hallmark features are shared among the members of PHB domain proteins: the association with the plasma or mitochondrial membrane is due to the hydrophobic N-terminal domain, which is fused to the PHB domain and assumed to adopt a horseshoelike structure in the case of reggies, stomatin, and podocin. Prohibitins, in contrast, possess transmembrane helices. The C-terminal region of the PHB domain contains a stretch of EA repeats. PHB domain proteins tend to form oligomers, as shown for stomatin,[44] podocin,[45] prohibitin,[24,38] and reggies.[46] In the case of stomatin, the first EA repeat was proven to be essential for oligomerization of the protein.[44] Accordingly, BAP32 and BAP37 topologically comprise an N-terminal hydrophobic transmembrane domain, followed by the well-conserved PHB domain, and a C-terminal coiled-coil region (Fig. 1).

Secondary Structure Prediction of BAP32 and BAP37

The only experimentally obtained structure for any member of the PHB superfamily is the NMR structure of the band 7 domain of mouse flotillin-2 (PDB accession no. 1win). Using fold recognition, a theoretical model for the three-dimensional structure of BAP32 has been deposited in the PDB (PDB accession no. 1lu7). However, while the theoretical model shares a very similar shape with the flotillin-2 structure, the fold differs in the position and orientation of secondary structure elements (see also Ref. 43).

Fig. 2. Alignment of BAP32 and BAP37 with the flotillin-2 PHB domain. α-Helices are displayed by cylinders and β-strands are shown as arrows. The secondary structure of flotillin-2 as seen in the NMR structure (PDB accession no. 1win) is shown by striped arrows/cylinders. The secondary structure obtained from the prohibitin fold prediction model (PDB accession no. 1lu7) is shown in light gray. Secondary structure elements for BAP32 and BAP37 are drawn in dark gray and have been obtained by prediction with PSIPRED.[30] Residues identified by an earlier crosslinking study[38] are highlighted.

We have predicted the secondary structure of BAP32 and BAP37 using the PSIPRED server[30] and compared the results to the NMR structure of flotillin-2. As seen in Figure 2, the PSIPRED-predicted secondary structure for the PHB domain of both human prohibitins is in reasonable agreement with the flotillin-2 structure. In the N-terminal region, four β-strands are predicted for BAP32 (β1, β2, β3, and β4); however, their positions are slightly different from those in the flotillin-2 structure. For BAP37, only three β-strands are predicted (β1, β2, and β4) and almost identically positioned when compared with BAP32. In the flotillin-2 structure, the β-strands are followed by two α-helices whose extents coincide nicely with the predicted three α-helices of BAP32 and BAP37 (α1, α2, and α3). The second α-helix of the flotillin-2 structure is broken into two helices (α2 and α3) of almost equal length in case of the prohibitins. The helical segment of flotillin-2 is connected to two β-strands, which are merged into one (β5) in both human prohibitins extending over almost the same area. A short α-helix in flotillin-2 marks the start of the coiled-coil region and is resembled by helix α4 in BAP32 and BAP37. As seen from Figure 2, the coiled-coil region is predicted continuously helical for BAP32, but divided into two helical segments in BAP37. However, the probability for helical geometry around residues 228/229 is less than 0.5 for BAP32 and thus it is quite likely that α4 might also be divided into two segments in BAP32. It is worth noting that neither of the two human prohibitins possesses the hepta-peptide repeat pattern $(\boldsymbol{abcdefg})_n$ characteristic for coiled-coil motifs where ***a*** and ***d*** are mostly hydrophobic residues and ***e*** and ***g*** are predominantly charged residues. Intriguingly, the N-terminal region of helix α4 already comprises EA repeat areas in both prohibitins, whereas the stretch of EA-repeats in flotillin-2 occurs only C-terminal of the PHB domain.

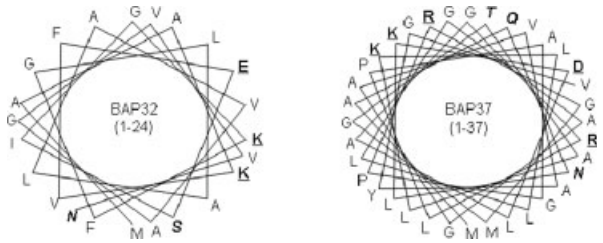

Fig. 3. Helical wheel representations for the N-terminal α-helices of human BAP32(1–24) and BAP37(1–37). Polar residues are highlighted in bold italic, basic and acidic residues are bold and underlined.

The N-Terminal Domain of BAP32 and BAP37

Results from the secondary structure predictions are well in agreement with the current state of knowledge whereby the N-terminal domains of prohibitins either form a membrane-anchoring α-helix (BAP32) or a transmembrane α-helix (BAP37). With a length of 36 Å, the N-terminal α-helix in BAP32 would just be able to span the lipid bilayer. For BAP37, the N-terminal helical segment has an expected length of 56 Å and is thus long enough to reach well into the mitochondrial interior. As seen from the helical wheel representations (Fig. 3), the helical arrangements of amino acid residue stretches 1–24 (BAP32) and 1–37 (BAP37) result in mainly hydrophobic helices with a fraction of polar and charged resi-

dues of about 20%. Intriguingly, the few polar and charged residues are all positioned on one side of the helix.

For Phb2, the yeast homolog of BAP37, the N-terminal segment shows a much higher enrichment of basic residues giving rise to a truly amphipathic α-helical segment, which is characteristic for mitochondrial sorting sequences. Mitochondrial import studies by Tatsuta et al. demonstrated that it is the bipartite feature of the N-terminal domain of Phb2, comprising the positively charged leader sequence and the hydrophobic α-helix, that is responsible for mitochondrial targeting of this protein.[24] With the yeast homolog of BAP32, Phb1, these authors have also been able to show that the presence of the N-terminal domain is required for mitochondrial targeting. Although the topology of residues on the helical wheel is very similar for Phb1 and BAP32, the characteristic bipartite feature of Phb2 is not present in BAP37. It therefore appears as if both human prohibitins utilize the same unconventional N-terminal sequence that is neither a fully hydrophobic nor a true amphipathic α-helix.

We thus investigated, whether the energetically unfavorable exposure of polar/charged residues of the membrane-inserted N-terminal helices of BAP32 and BAP37 to hydrophobic environment might be avoided by masking of the polar patches within a BAP32:BAP37 dimer. Homodimerization was not considered as there is no experimental evidence for homo-oligomers.[24] Inspection of a manually generated model of BAP32(1-24):BAP37(1-39) shows that some, but not all polar/charged residues could lie within the dimer interface (Fig. 4). The model of the helix dimer was further tested and its conformation improved by subjecting it to molecular dynamics simulations with GROMACS. Throughout the simulated time of 500 ps, the two helices stayed in contact with each other and the simulated complex equilibrated as judged by analysis of rms distances and energies. However, several polar/charged residues remained on the outside surface of the helix dimer. Lys4 and Glu7 from BAP32 and Asp3, Gln7, Lys10, Arg15, and Arg21 from BAP37 would still be in contact with the hydrophobic interior of the mitochondrial inner membrane (Fig. 4). One could therefore speculate that these residues engage in interactions with transmembrane segments of *m*-AAA protease subunits.

The C-Terminal Coiled-Coil Domain of BAP32 and BAP37

As anticipated from the predicted secondary structure, the C-terminal domain of both prohibitins presumably adopts a coiled-coil structure.[24] Further analysis with MultiCoil[49] reveals that BAP32 shows a probability of about 30% to form a two-stranded coiled coil. BAP37, in contrast, is predicted to form a three-stranded coiled coil with a probability of almost 60% (data not shown).

Generally, it is possible that the different strands of a multistranded coiled coil are provided by the same molecule or a neighboring molecule. Especially, if the coiled-coil region is divided into two segments like in BAP37, it is quite possible that the second segment adopts an antiparallel orientation with respect to the first one and thus forms the second strand of a two-stranded coiled coil. As there is no further structural information available, further predictions remain pure speculation and we have thus decided not to propose any detailed model for the C-terminal domains of prohibitins.

The Middle (PHB) Domain of BAP32 and BAP37

On the basis of the agreement between the predicted secondary structures of BAP32/BAP37 and the experimentally determined structure of flotillin-2, we generated homology models for the PHB domains of both human prohibitins using the NMR structure of flotillin-2. The domain adopts a slightly elongated globular shape where the two antiparallel helices α2 and α3 pack against the three-stranded antiparallel β-sheet formed by β1/β2, β3/β4, and β5 [Fig. 5(A,B)]. The predicted helical segment α1 at the "bottom" (N-terminal) side of the protein appears like an extended loop and probably an area of the model where the structure can be predicted with less confidence. The generated homology models have positional rms distances to the experimental flotillin-2 structure of 10.5 Å (BAP32) and 10.0 Å (BAP37). The two models among each other differ by an rms distance of 3.1 Å.

Although there are some similarities between the homology model presented in this study and the predicted BAP32 model by Khurshid and coworkers (PDB accession no. 1lu7), the latter shows a much less globular fold [Fig. 5(D)]. A β-sheet feature is present in the predicted model, but it is exclusively built by the N-terminal β-strands and there are no packing interactions to the two antiparallel helices.

A comparison of the surface properties of the prohibitin models and flotillin-2 reveal interesting differences (Fig. 6). Although the PHB domain of flotillin-2 is predominantly negatively charged with only few isolated positive areas and very little hydrophobic regions, the two prohibitins appear to have gradually more hydrophobic character. The surface of BAP32 presents a mixed arrangement of electropositive and electronegative patches all over the PHB domain. BAP37, in contrast, exposes predominantly electropositive groups and possesses only one acidic area at the "bottom" side of the protein around and the N-terminal region.

The BAP32:BAP37 Oligomer

On the basis of the finding that prohibitins exist as high molecular weight oligomers,[19,20,50] as well as results from crosslinking experiments,[38] a ringlike assembly of alternating prohibitin homologs has been proposed. This model is supported by recent electron micrographs of purified yeast prohibitin complexes revealing large ring-shaped structures consisting of about 16–20 individual prohibitin molecules.[24] So far, no experimental evidence has been obtained that would suggest formation of homo-oligomers.[24]

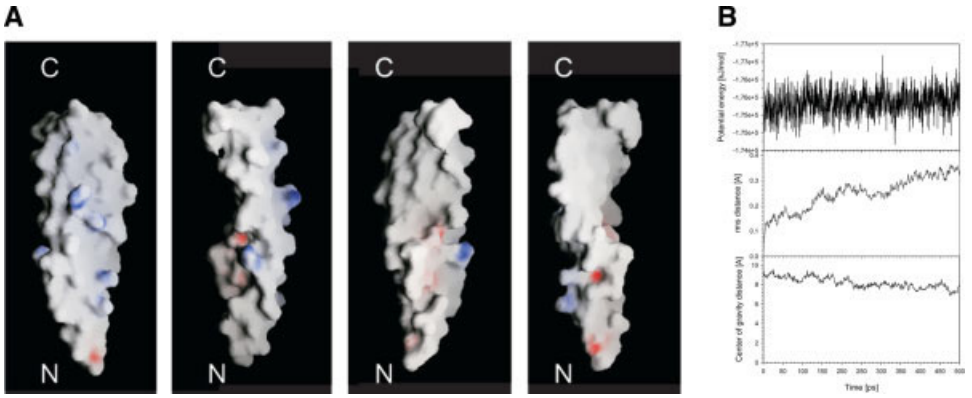

Fig. 4. Model of a putative hetero-dimer of the N-terminal membrane-anchoring helices of BAP32 and BAP37. Human prohibitins utilise unconventional N-terminal sequences as membrane-anchoring helix elements. Several polar and charged residues remain at the surface of the helical dimer and would thus be in contact with the hydrophobic interior of the mitochondrial inner membrane. **A:** A dimer model assuming parallel arrangement of N-terminal α-helical segments of human prohibitins. The manually constructed model was subjected to a molecular dynamics simulation with GROMACS.[39] The four panels show successive rotations of 90° of the simulated model around the vertical axis. The C-terminal end projects into the inter-membrane space. Figure prepared with BOBSCRIPT[47] and rendered with PovRay.[48] **B:** Analysis of the molecular dynamics simulation. The potential energy of the dimer (top panel) and the rms distance of backbone atoms (middle panel) suggests an equilibrated structure from 300 to 500 ps. The bottom panel shows the distance between both PHB domains and reveals an optimised orientation of both domains at around 500 ps.

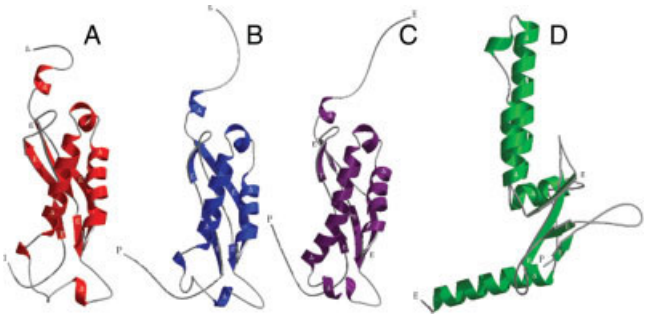

Fig. 5. Three-dimensional homology models of the PHB domains of BAP32 (red) and BAP37 (blue) based on the structure of the flotillin-2 PHB domain (purple, PDB accession no. 1win). The predicted fold by Khurshid and coworkers (PDB accession no. 1lu7) is shown in green for comparison. Figure prepared with BOBSCRIPT[47] and rendered with PovRay.[48]

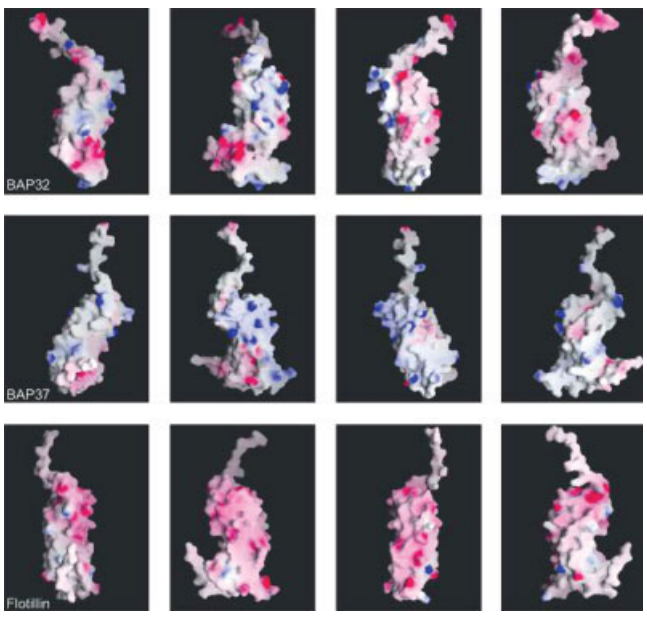

Fig. 6.

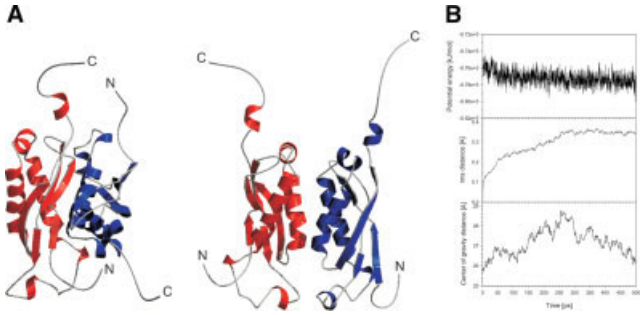

Fig. 7. The building block for ring-like prohibitin oligomers. Formation of prohibitin high-molecular weight complexes necessitates contacts between the BAP32 (red) and BAP37 (blue) PHB domains. *Left*: The dimer model as suggested by the programme HEX[37] with an almost antiparallel arrangement of the two PHB domains. *Middle*: A dimer model considering the criteria of parallel arrangement and distance restraints based on an earlier crosslinking study.[38] The manually constructed model was subjected to a molecular dynamics simulation with GROMACS.[39] *Right*: Analysis of the molecular dynamics simulation. The potential energy of the dimer (top panel) and the rms distance of backbone atoms (middle panel) suggests an equilibrated structure from 300 to 500 ps. The bottom panel shows the distance between both PHB domains and reveals an optimised orientation of both domains at around 500 ps. Left and middle panels prepared with BOBSCRIPT[47] and rendered with PovRay[48].

Protein docking calculations using the programme Hex[37] and the homology models of the middle domains of BAP32 and BAP37 resulted in a model where α2 and α3 from BAP37 pack against β1 and α2 of BAP32 [see Fig. 7(A), left]. Overall, this leads to an orientation where both molecules are positioned next to each other with a tilt angle of about 120° between their long axes. Thus, they are aligned in an almost antiparallel fashion, which is not a

Fig. 6. GRASP[35] surface representations of the BAP32 (top panel) and BAP37 (middle panel) homology models; the PHB domain of flotillin-2 is shown for comparison (bottom panel). The surfaces are colored according to electrostatic potential with blue indicating positive and red indicating negative charge. The four pictures within one panel show successive 90° rorations around the vertical axis.

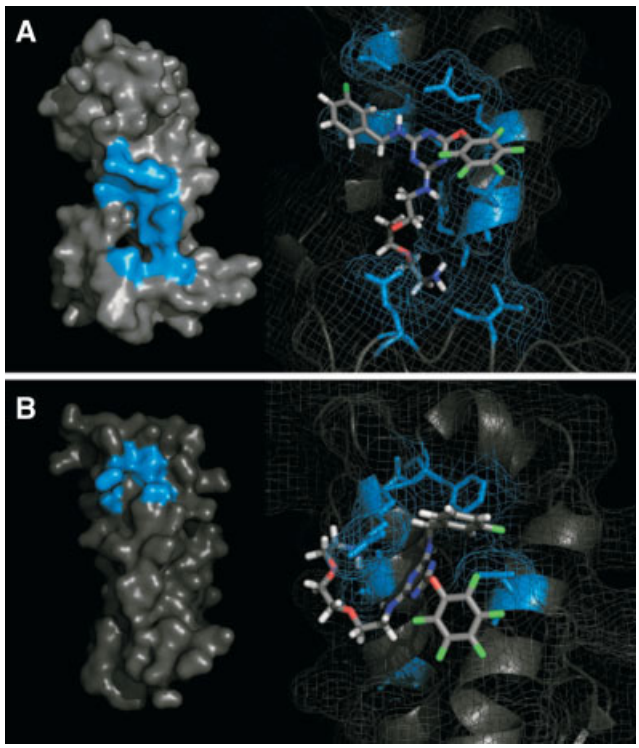

Fig. 8. Docking of melanogenin to two predicted pockets on BAP32. The melanogenin molecule was docked into pocket 1 (**A**) and pocket 2 (**B**), shown as blue areas. The potential binding pockets are displayed on the left side. The position and conformation of melanogenin in the respective pockets is shown on the right. Interacting side chains of the protein are colored in blue, the melanogenin molecule is colored by its elements. Figure prepared with PyMOL.[51]

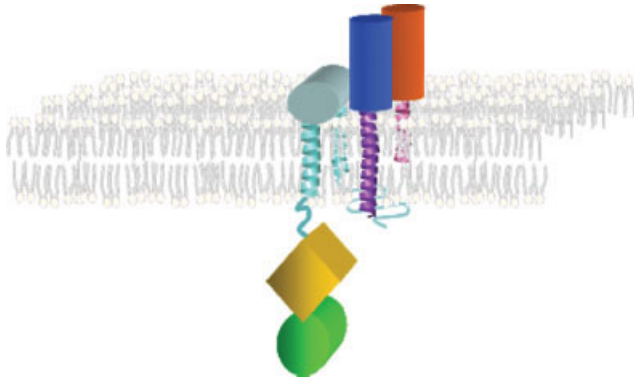

Fig. 9. Suggested model of membrane-bound prohibitin. Although BAP32 (red) and BAP37 (blue) membrane helices might interact with the m-AAA transmembrane helices (cyan), the PHB domains could interact with the m-AAA IMS region (turquoise) exposed to the intermembrane space of mitochondria. The ATPase domain and the protease domain of *m*-AAA-protease are shown in yellow and green, respectively.

preferable position considering that both N-termini carry membrane-anchoring helices and therefore should be on the same side of the prohibitin complex. The dimer is held together mainly by van der Waals interactions, and only one hydrogen bond between Thr124 (BAP32) and Glu139 (BAP37) can be identified. The buried surface area is about 2700 Å^2 corresponding to 13% of the surface of each monomer. However, the Hex-derived model does not agree with the results from the earlier crosslinking study with yeast prohibitin,[38] where residues 72 and 152 (BAP32) were found to be crosslinked with residue 86 (BAP37), and residue 149 (BAP32) was linked to residue 159 (BAP37).

To elucidate possible models fitting these criteria, we set out to manually create BAP32:BAP37 oligomers that would satisfy the anticipated parallel orientation of the two protein molecules, as well as the spatial closeness of the residues identified from crosslinking of yeast prohibitins.[38] Inevitably, this leads to a model where helices α2 and α3 from both molecules form a four-helix bundle [Fig. 7(A), right]. The starting model was subjected to a molecular dynamics simulation in order to test the stability of the complex and improve the conformations as to maximise the interactions between both monomers [Fig. 7(B)]. The interaction interface covers about 1150 Å^2 (6% surface of each individual protein molecule). Two hydrogen bonds can be identified, one between Glu90 (BAP32) and Arg174 (BAP37) and another between Asp104 (BAP32) and Ser231 (BAP37). The complex possesses pseudo-twofold symmetry, which establishes a prohibitin dimer as building block for the ring-shaped high molecular weight complex and requires a different type of protein–protein interaction with the neighboring prohibitin molecules in the ring. It is tempting to speculate that these interactions are provided by coiled-coil interactions between neighboring BAP32 and BAP37 molecules. This speculation is in agreement with the report by Tatsuta and colleagues showing that C-terminally truncated yeast Phb1 is unable to form large assemblies,[24] as well as with a number of important residues in the coiled-coil region identified in the crosslinking study by Back and coworkers.[38] Intriguingly, all previous studies in this context agree that there is no prohibitin dimer detected in physiological environment. One might therefore speculate that a cooperative effect enables BAP32-BAP37 interactions by coiled-coil strand exchange and four-helix-bundle formation, which ultimately results in the formation of large ring-shaped complexes. The fact that both proteins are membrane-bound through their N-terminal helices will most likely lower the activation energy for these interactions.

Binding of Melanogenin to BAP32

Melanogenin has been found to enhance melanin production in melanocytes and to bind specifically to prohibitin,[28] proposing a functional role for prohibitin in melanin induction. A priori, it is not clear whether the role of prohibitin in these processes involves an individual protein or the assembly of prohibitin with other proteins, especially the prohibitin high molecular weight complexes. Snyder and coworkers[28] identified prohibitin as a specific target for melanogenin by affinity chromatography with immobilized ligand. Bound proteins were identified by digestion with trypsin and subsequent sequencing using mass spectrometry. BAP32 was identified exclusively and unambiguously and we thus focused our

further analysis on BAP32. We further assume that binding of the ligand would occur at a globular domain, that is, the PHB domain of the protein.

Melanogenin possesses three substituents at the central triazine ring, a polyether/amine chain, a mono-fluoro-benzyl group, and an ether-bonded penta-fluoro-hydroxy-benzol. By visual inspection and surface analysis of our BAP32 homology model, we have identified two potential binding pockets within the PHB domain. One pocket [pocket 1; Fig. 8(A)] is located at the membrane-proximal side of BAP32 and constituted by helix α1 at the bottom, strands β5 and β4 at the side and the linker region between the N-terminal membrane helix and the PHB domain at the back. A slightly smaller pocket [pocket 2; Fig. 8(B)] is located in a groove between helices α2 and α3 in between residues Thr124 and Phe134. Both pockets are lined with hydrophobic residues in the cavities and polar/charged residues at the protein surface.

Attempts to fit the ligand into the latter pocket yielded a conformation where the two aromatic rings of the organic molecule are sticking out from the protein surface and the triazine ring, as well as the polyether/amine chain are neatly accommodated in the groove. This binding mode with a buried surface of 737 $Å^2$ is stabilized by hydrogen bonds provided by Ser129, Arg133, Gln149, and Asp153.

Docking of melanogenin into pocket 1 yields conformations with much larger buried surface areas (839 $Å^2$) when compared with pocket 2. Here, the polyether/amine branch of the ligand protrudes into the cavity at the membrane-proximal side of the protein. The side chain amine group of Gln102 provides hydrogen bonds to interact with the two ether groups and the most extreme amine group of the ligand is held in position by hydrogen bonds with the backbone carbonyl groups of Phe161, Gln102, and Val99. At the protein surface, Thr160 and Arg157 provide hydrogen bonds to two nitrogen atoms of the triazine ring system, which is further held in place by van der Waals interactions with Ile122. The fluorine of the mono-fluoro-phenyl group is hydrogen bonded by the side chains of Ser121 and Glu125, and the penta-fluoro-substituted ring system is only loosely held in place by van der Waals interactions with Thr160. An alternative binding mode where the two aromatic ring systems have switched places has also been obtained with slightly lesser scoring values. It thus remains unclear which binding mode might be preferred. For both pockets, a common observation is the fact that the penta-fluoro-substituted ring system is not fully coordinated by protein residues, sticking out of the protein surface, and available for external interactions. This is contrasted to a certain extent by a finding by Snyder and coworkers who found a melanogenin derivative with a 2,3,6-tri-fluoro-hydroxybenzol group to bind less well to prohibitin.[28]

CONCLUSIONS

In the absence of experimentally determined three-dimensional structures, the field is still far from a complete understanding of prohibitins at the molecular level. However, dissecting the proteins into the three domains allows some structural predictions. Using homology modeling, molecular dynamics simulations and the currently available information about prohibitins, one can suggest a model whereby the N-terminal transmembrane helices as well as the middle (PHB) domains are engaged in direct interactions thus constituting a dimeric-building block for the high molecular weight assemblies. Although the C-terminal coiled-coil domains will most likely be involved in intermolecular interactions as well,[52] it is not clear at this point, whether these interactions occur within the dimeric-building block or between two of these building blocks.

Given the results from an earlier crosslinking study of the yeast prohibitin complex,[38] it seems that the main interactions between the globular PHB domains of BAP32 and BAP37 occur only on one side. The formation of ringlike assemblies would require interactions between the dimeric-building blocks, most probably between either the N-terminal helices (within the membrane) or the C-terminal coiled-coil domains. Alternatively, the ringlike assembly could also be promoted by an external factor such as the *m*-AAA protease.

The *m*-AAA-protease is anchored to the inner mitochondrial membrane by the N-terminal domain of its subunits, while the C-terminal ATPase and metallopeptidase domains protrude into the mitochondrial matrix.[53] Although the X-ray structure of the ATPase domain of the *E. coli* AAA-protease FtsH has been solved,[54] only little structural information is available about the N-terminal domain. In yeast, it is thought that both subunits, Yta10 and Yta12, anchor the *m*-AAA-protease to the inner mitochondrial membrane with two transmembrane helices.[55] Both transmembrane helices are connected via a structurally well conserved N-terminal loop. Thus, interactions of the dimeric-building blocks of BAP32:BAP37 with the *m*-AAA-protease could happen at two possible interfaces (Fig. 9). The N-terminal transmembrane helices interact with each other inside the membrane, which would satisfy the need to mask the remaining exposed polar residues of the two BAP transmembrane helices. Alternatively, the N-terminal loop of *m*-AAA-protease, which is exposed at the inter-membrane space interacts with the PHB domains of the BAP32:BAP37 building blocks.

The immense difficulties in the crystallization of prohibitins and their domains (Winter and Hofmann, unpublished) might be overcome by focussing on prohibitin complexed with other proteins or ligands rather than the individual prohibitin proteins. However, interactions of prohibitins with other proteins such as Rb, p107, p130, α-actinin, and annexin A2 are complex and might involve further participants that have not yet been identified. The putative interaction with the N-terminal loop of *m*-AAA proteases concluded in this study adds a new target in this context and might well turn out to be of high interest because of its potential significance for membrane protein turnover and mitochondria-born diseases as well as its technical feasibility.

On the basis of our results from the docking studies, we believe that the larger pocket in BAP32 constituted by helix α1 and strands β5 and β4 is a likely binding pocket for melanogenin. The model obtained from our docking results does not explain the apparent discriminating effect of the fluoro-substituents in position 4 and 5 of the penta-fluoro-hydroxy-benzol group of melanogenin, but this might well be because of shortcomings of the homology model of the BAP32 PHB domain. A different conformation of amino acid residues in the area of the binding pocket might easily lead to a different conformation of the bound ligand, for example, a change of positions between the penta- and mono-fluoro-substituted ring systems.

Further experiments aiming at targeted design of lead compounds will most likely involve database-mining approaches. However, even this line of investigation put further weight on the demand for experimental structures of prohibitin proteins and their complexes.

Structural information about the prohibitin complex at atomic detail will undoubtedly be useful in understanding the molecular mechanisms of protein turnover in mitochondria as well as in structure-based lead compound discovery for novel drugs in a variety of diseases. Further efforts are currently being undertaken in our laboratory to aid in elucidation of the structural chemistry of these highly conserved proteins.

ACKNOWLEDGMENTS

We thank T. Tatsuta and T. Langer (Universität Köln) for helpful discussions.

REFERENCES

1. Tavernarakis N, Driscoll M, Kyrpides NC. The SPFH domain: implicated in regulating targeted protein turnover in stomatins and other membrane-associated proteins. Trends Biochem Sci 1999;24:425–427.
2. McClung JK, Danner DB, Stewart DA, Smith JR, Schneider EL, Lumpkin CK, Dell'Orco RT, Nuell MJ. Isolation of a cDNA that hybrid selects antiproliferative mRNA from rat liver. Biochem Biophys Res Comm 1989;164:1316–1322.
3. Nuell MJ, McClung JK, Smith JR, Danner DB. Approach to the isolation of antiproliferative genes. Exp Gerontol 1989;24:469–476.
4. Roskams AJ, Friedman V, Wood CM, Walker L, Owens GA, Stewart DA, Altus MS, Danner DB, Liu XT, McClung JK. Cell cycle activity and expression of prohibition mRNA. J Cell Physiol 1993;157:289–295.
5. Snyers L, Umlauf E, Prohaska R. Oligomeric nature of the integral membrane protein stomatin. J Biol Chem 1998;273:17221–17226.
6. Nadimpalli R, Yalpani N, Johal GS, Simmons CR. Prohibitins, stomatins, and plant disease response genes compose a protein superfamily that controls cell proliferation, ion channel regulation, and death. J Biol Chem 2000;275:29579–29586.
7. McClung JK, Danner DB, Stewart DA, Smith JR, Schneider EL, Lumpkin CK, Dell'Orco RT, Nuell MJ. Isolation of a cDNA that hybrid selects antiproliferative mRNA from rat liver. Biochem Biophys Res Commun 1989;164:1316–1322.
8. Nuell MJ, Stewart DA, Walker L, Friedmann V, Wood CM, Owens GA, Smith JR, Schneider EL, Dell'Orco RT, Lumpkin CK, Danner DB, McClung JK. Prohibitin, an evolutionarily conserved intracellular protein that blocks DNA synthesis in normal fibroblasts and HeLa cells. Mol Cell Biol 1991;11:1372–1381.
9. Wang S, Nath N, Adlam M, Chellappan S. Prohibitin, a potential tumor suppressor, interacts with RB and regulates E2F function. Oncogene 1999;18:3501–3510.
10. Ikonen E, Fiedler K, et al. Prohibitin, an antiproliferative protein, is localized to mitochondria. FEBS Lett 1995;358:273–277.
11. Ahn CS, Lee JH, Hwang RA, Kim WT, Pai HS. Prohibitin is involved in mitochondrial biogenesis in plants. Plant J 2006; 46:658–667.
12. Kolonin MG, Saha PK, Chan L, Pasqualini R, Arap W. Reversal of obesity by targeted ablation of adipose tissue. Nat Med 2004;10:625–632.
13. Sharma A, Qadri A. Vi polysaccharide of Salmonella typhi targets the prohibitin family of molecules in intestinal epithelial cells and suppresses early inflammatory responses. Proc Natl Acad Sci USA 2004;101:17492–17497.
14. Schulte T, Paschke KA, Laessing U, Lottspeich F, Stuermer CA. Reggie-1 and reggie-2, two cell surface proteins expressed by retinal ganglion cells during axon regeneration. Development 1997;124:577–587.
15. Schultz J, Milpetz F, Bork P, Ponting CP. SMART, a simple modular architecture research tool: identification of signaling domains. Proc Natl Acad Sci USA 1998;95:5857–5864.
16. Morrow IC, Parton RG. Flotillins and the PHB domain protein family: rafts, worms and anaesthetics. Traffic 2005;6:725–740.
17. Kobayakawa K, Hayashi R, Morita K, Miyamichi K, Oka Y, Tsuboi A, Sakano H. Stomatin-related olfactory protein, SRO, specifically expressed in the murine olfactory sensory neurons. J Neurosci 2002;22:5931–5937.
18. Ikonen E, Fiedler K, Parton RG, Simons K. Prohibitin, an antiproliferative protein, is localized to mitochondria. FEBS Lett 1995;358:273–277.
19. Steglich G, Neupert W, Langer T. Prohibitins regulate membrane protein degradation by the m-AAA protease in mitochondria. Mol Cell Biol 1999;19:3435–3442.
20. Nijtmans LG, de Jong L, Artal Sanz M, Coates PJ, Berden JA, Back JW, Muijsers AO, van der Spek H, Grivell LA. Prohibitins act as a membrane-bound chaperone for the stabilization of mitochondrial proteins. EMBO J 2000;19:2444–2451.
21. Artal-Sanz M, Tsang WY, Willems EM, Grivell LA, Lemire BD, van der Spek H, Nijtmans LG. The mitochondrial prohibitin complex is essential for embryonic viability and germline function in Caenorhabditis elegans. J Biol Chem 2003;278:32091–32099.
22. Coates PJ, Jamieson DJ, Smart K, Prescott AR, Hall PA. The prohibitin family of mitochondrial proteins regulate replicative lifespan. Curr Biol 1997;7:607–610.
23. Terashima M, Kim KM, Adachi T, Nielsen PJ, Reth M, Kohler G, Lamers MC. The IgM antigen receptor of B lymphocytes is associated with prohibitin and a prohibitin-related protein. EMBO J 1994;13:3782–3792.
24. Tatsuta T, Model K, Langer T. Formation of membrane-bound ring complexes by prohibitins in mitochondria. Mol Biol Cell 2005; 16:248–259.
25. Steglich G, Neupert W, Langer T. Prohibitins regulate membrane protein degradation by the *m*-AAA protease in mitochondria. Mol Cell Biol 1999;19:3435–3442.
26. Jupe ER, Liu XT, Kiehlbauch JL, McClung JK, Dell'Orco RT. The 3′ untranslated region of prohibitin and cellular immortalization. Exp. Cell Res 1996;224:128–135.
27. Bacher S, Achatz G, Schmitz ML, Lamers MC. Prohibitin and prohibitone are contained in high molecular weight complexes and interact with α-actinin and annexin A2. Biochimie 2002;84: 1207–1220.
28. Snyder JR, Hall A, Ni-Komatsu L, Khersonsky SM, Chang YT, Orlow SJ. Dissection of melanogenesis with small molecules identifies prohibitin as a regulator. Chem Biol 2005;12:477–484.
29. Edgar RC. MUSCLE: multiple sequence alignment with high accuracy and high throughput. Nucleic Acids Res 2004;32:1792–1797.
30. Bryson K, McGuffin LJ, Marsden RL, Ward JJ, Sodhi JS, Jones DT. Protein structure prediction servers at University College London. Nucl Acids Res 2005;33 (Web Server issue):W36–W38.
31. Sali A, Blundell TL. Comparative protein modelling by satisfaction of spatial restraints. J Mol Biol 1993;234:779–815.
32. Jones T, Zou J, Cowan S, Kjeldgaard M. Improved methods for building protein models in electron density maps and location of errors in these models. Acta Crystallogr A 1991;47:110–119.
33. Brünger A, Adams P, Clore G, Delano W, Gros P, Grosse-Kunstleve R, Jiang J, Kuszewski J, Nilges N, Pannu N, Read R, Rice L, Simonson T, Warren G. Crystallography and NMR system

(CNS): a new software system for macromolecular structure determination. Acta Crystallogr 1998;D54:905–921.
34. Laskowski RA, MacArthur MW, Moss DS, Thornton JM. PROCHECK: a program to check the stereochemical quality of protein structures. J Appl Cryst 1993;26:283–291.
35. Nicholls A, Bharadwaj R, Honig B. GRASP: graphical representation and analysis of surface properties. Biophys J 1993;64: A166.
36. Hofmann A, Wlodawer A. PCSB—a program collection for structural biology and biophysical chemistry. Bioinformatics 2002;18: 209–210.
37. Richie GJL, Kemp DW. Protein docking using spherical polar fourier correlations. Proteins: Struct Funct Genet 2000;39:178–194.
38. Back JW, Sanz MA, De Jong L, De Koning LJ, Nijtmans LG, De Koster CG, Grivell LA, Van Der Spek H, Muijsers AO. A structure for the yeast prohibitin complex: structure prediction and evidence from chemical crosslinking and mass spectrometry. Protein Sci 2002;11:2471–2478.
39. Lindahl E, Hess B, van der Spoel D. GROMACS 3.0: a package for molecular simulation and trajectory analysis. J Mol Mod 2001;7:306–317.
40. Zucic D, Juretic D. Precise annotation of transmembrane segments with garlic—a free molecular visualization program. Croatica Chem Acta 2004;77:397–401.
41. Humphrey W, Dalke A, Schulten K. VMD—visual molecular dynamics. J Mol Graph 1996;14.1:33–38.
42. Rarey M, Kramer B, Lengauer T, Klebe GJ. A fast flexible docking method using and incremental docking algorithm. Mol Biol 1996;261:470–489.
43. Rivera-Milla E, Stuermer CA, Malaga-Trillo E. Ancient origin of reggie (flotillin), reggie-like, and other lipid-raft proteins: convergent evolution of the SPFH domain. Cell Mol Life Sci 2006;63:343–357.
44. Snyers L, Umlauf E, Prohaska R. Oligomeric nature of the integral membrane protein stomatin. J Biol Chem 1998;273:17221–17226.
45. Huber TB, Simons M, Hartleben B, Sernetz L, Schmidts M, Gundlach E, Saleem MA, Walz G, Benzing T. Molecular basis of the functional podocin-nephrin complex: mutations in the NPHS2 gene disrupt nephrin targeting to lipid raft microdomains. Hum Mol Genet 2003;12:3397–3405.
46. Neumann-Giesen C, Falkenbach B, Beicht P, Claasen S, Luers G, Stuermer CA, Herzog V, Tikkanen R. Membrane and raft association of reggie-1/flotillin-2: role of myristoylation, palmitoylation and oligomerization and induction of filopodia by overexpression. Biochem J 2004;378:509–518.
47. Esnouf RM. Further additions to MolScript version 1.4, including reading and contouring of electron-density maps. Acta Crystallogr D Biol Crystallogr 1999;55:938–940.
48. Persistence of Vision Development Team. POVRay—The Persistence of Vision Raytracer, version 3.5. 2002. Available at http://www.povray.org/.
49. Wolf E, Kim PS, Berger B. MultiCoil: a program for predicting two- and three-stranded coiled coils. Protein Sci 1997;6:1179–1189.
50. Snedden WA, Fromm H. Characterisation of the plant homologue of prohibitin, a gene associated with antiproliferative activity in mammalian cells. Plant Mol Biol 1997;33:753–756.
51. DeLano WL. The PyMOL Molecular Graphics System. 2002. Available at http://www.pymol.org/.
52. Wienke D, Drengk A, Schmauch C, Jenne N, Maniak M. Vacuolin, a flotillin/reggie-related protein from *Dictyostelium* oligomerizes for endosome association. Eur J Cell Biol 2006;85:991–1000.
53. Ogura T, Wilkinson AJ. AAA+ superfamily ATPases: common structure—diverse function. Genes Cells 2001;6:575–597.
54. Krzywda S, Brzozowski AM, Verma C, Karata K, Ogura T, Wilkinson AJ. The crystal structure of the AAA domain of the ATP-dependent protease FtsH of Escherichia coli at 1.5 Å resolution. Structure 2002;10:1073–1083.
55. Langer T. AAA proteases: cellular machines for degrading membrane proteins. Trends Biochem Sci 2000;25:247–251.

Towards understanding the roles of prohibitins, multi-functional regulator proteins

Anja Winter[1,2] & Andreas Hofmann[2*]

[1]ISMB, School of Biological Sciences, The University of Edinburgh, Scotland, UK

[2]Structural Chemistry Program, Eskitis Institute for Cell & Molecular Therapies, Griffith University, Brisbane, Australia

*Correspondence to Andreas Hofmann, Structural Chemistry Program, Eskitis Institute for Cell & Molecular Therapies, Griffith University, Brisbane Innovation Park, Don Young Road, Brisbane, Qld 4111, Australia.
Tel.: +61-7-3735-6086, Fax: +61-7-3735-6001
Email: a.hofmann@griffith.edu.au

Keywords: Molecular modelling, PHB domain, protein-protein interactions, *m*-AAA-protease, melanogenin

Revised version, 25.05.07

Abstract

Prohibitins comprise a family of highly conserved ubiquitous eukaryotic proteins that localise to different compartments of the cell. They have been implicated in important cellular processes such as cellular signalling and transcriptional control, apoptosis, cellular senescence, early development of *Caenorhabditis elegans* and mitochondrial biogenesis.

In yeast, mammals and *C. elegans* there exist at least two homologous prohibitin proteins (yeast: PHB1, PHB2; human: BAP32, BAP37), which assemble into high molecular weight complexes of about 1.2 MDa in the inner mitochondrial membrane. Experimentally determined structural information about these proteins has been elusive for a long time. Recently, however, the biogenesis and architecture of the yeast prohibitin complex has been analysed and yielded ring-shaped structures as visualised by single particle electron microscopy.
Structural details at atomic level remain to be determined, but a first step into this direction is provided by modelling approaches. Prohibitins consist of three domains, an N-terminal transmembrane helix, a middle (PHB) domain and a C-terminal coiled coil domain. The PHB domain is the landmark feature within the super-family of SPFH (stomatin / prohibitin / flotillin / HflK/C) domain proteins. The recently determined NMR structure of mouse flotillin-2 provides a first access to structural details of prohibitins.

While the first functional role attributed to prohibitins was the regulation of cellular senescence, DNA transcription and tumour cell growth, there is recent evidence that they also can act as markers for adipose tissue. In a mouse model, an apoptotic peptide targeted at prohibitin was successful in reversing obesity. An extracellular complex containing both BAP32 and BAP37 was found to bind to the Vi capsular polysaccharide, first identified as a virulence antigen of *Salmonella typhi*, suggesting a key role for both proteins in infection with *S. typhi*. Furthermore, the interaction of prohibitin with compounds activating melanin production has placed these proteins at a central position in melanogenesis, and further implicates mitochondria in signalling pathways of the pigmentation process. Accumulating evidence suggests that prohibitins are implicated in mitochondrial, age and oxidative stress -related diseases, as well as in immunity and inflammation, cancer and cancer-like diseases, obesity, and drug resistance.

The complementary interplay between structural and chemical biology will provide important insights into the molecular mechanisms of prohibitins and, more generally, the functions of mitochondria in living cells.
This review discusses the current state of knowledge about prohibitins, and provides a vision for further developments in the field of these eminently important proteins.

Introduction

Prohibitins comprise a family of conserved ubiquitous eukaryotic proteins [1]. They have been implicated in important cellular processes and have been found in different cellular compartments, including mitochondria. Prohibitin 1 cDNA was first isolated by hybridisation to RNA in rat liver and the protein was proposed to be an inhibitor of cellular proliferation [2]. Inhibition of DNA synthesis was observed upon microinjection of prohibitin 1 mRNA into human fibroblasts [3], an effect that was subsequently found to be a feature of the 3'-untranslated region of prohibitin 1 [4].

While prohibitin 1 is usually referred to as Phb1, its human orthologue is known as B-cell receptor associated protein 32 (BAP32). The related protein prohibitin 2 (Phb2) is also known as prohibitone [5], and the human orthologue is known as BAP37 which is identical to a protein earlier identified as repressor of estrogen receptor action (REA) [6]. Prohibitin orthologues have also been identified in other mammals, *Drosophila*, plants and yeast. In yeast, prohibitin 1 is referred to as PHB1, whereas prohibitone is called PHB2.

Prohibitins belong to a larger super family of proteins, called the stomatin/prohibitin/flotillin/HflK/C (SPFH) super family, that share an evolutionary conserved domain, the SPFH, or PHB domain. Members of this protein family are membrane-associated and implicated in cellular processes concerned with protein turnover [7], senescence [2] and proliferation control [2, 8, 9]. They can be found in higher eukaryotes (prohibitin, stomatin, podocin), as well as in lower eukaryotes and prokaryotes (vacuolin A, vacuolin B, HflK, HflC, unc-1, unc-24, mec-2). The PHB domain is conserved in proteins that are ubiquitously expressed such as flotillin, as well as in proteins that show extremely restricted expression like the stomatin-related olfactory protein (SROP) whose expression is constrained to olfactory sensory neurons [10]. The evolutionary significance of this domain is unclear but its prokaryotic conservation suggests that it is indeed a primordial motif likely to perform an important cellular function.

Cellular localisation of prohibitins

Prohibitins have been found in several intra- as well as extra-cellular locations. In early studies, prohibitins were nearly exclusively found to localise to mitochondria, but later studies reported prohibitins to be localised also in the nucleus and the cytosol, as well as at the cell surface. While it has been suggested that the N-terminal sequences of PHB-domain containing proteins are responsible for subcellular targeting [11], it remains unclear which mechanisms and what signals are used to transport prohibitins to different cell compartments.

With immunohistochemical methods and subcellular fractionation, prohibitins have been found most abundantly in mitochondria [12-15], where they form ring-shaped high molecular weight complexes in the inner mitochondrial membrane [16].

Using differential immunisation, BAP32 and BAP37 have been detected in the human circulation system, with considerably higher levels in cancer patients [17]. The implications of extra-cellular

prohibitins remain to be elucidated, but BAP32 has recently been linked to complement activation since it interacts with complement component C3 [18]. Most likely, the externalisation of prohibitins happens by release from lipid vesicles rather than protein translocation using signal peptides [19] which might also be the mechanism of prohibitin transport to the endothelium.

Using mouse and human tissues, an immunohistochemical study revealed that prohibitin 1/BAP32 is present in the vasculature of white adipose tissue [20], and may therefore be used as a target for apoptosis inducing drugs to fight obesity. Cell surface –associated BAP32 and BAP37 have also been shown to interact with Vi capsular polysaccharide of *Salmonella typhi* [21] in the intestinal epithelium.

Phb1/BAP32 [22-25] and Phb2/BAP37 [26, 27] were repeatedly shown to be present in the nucleus. BAP32 possesses a nuclear export signal and, in breast cancer cells, translocates to the cytoplasm upon apoptotic stimulation [24, 28, 29]. Recently, prohibitin 2 has been shown to translocate from the mitochondria to the nucleus in the presence of estrogen receptor alpha and estradiol, suggesting a role of this protein in coupling of mitochondrial-nuclear interactions [30].

Both proteins were also found to be associated with cytoskeletal proteins [31], and the association with annexin A2 provides a link of prohibitins to lipid rafts. This notion is further supported by the discovery of the PHB-domain containing proteins erlin-1 and erlin-2 in lipid rafts of the endoplasmic reticulum [11], and the association of lipid rafts with BAP32 and BAP37 on the cell surface [21]. Notably, for podocin and mec-2, the palmitoylated PHB domains have been proven to be essential for the ability to bind cholesterol [32].

Topology and structure of prohibitins

Topologically, prohibitins can be dissected into three domains: an N-terminal membrane-anchoring α-helix, the middle or prohibitin homology (PHB) domain, and the C-terminal coiled coil region. In the absence of atomic details of prohibitin structures, homology models for the PHB domains of both human prohibitins have been generated [33] based on the NMR structure of the related flotillin-2 (PDB accession number 1win). The domain adopts a slightly elongated globular shape where the two anti-parallel α-helices pack against a three-stranded anti-parallel β-sheet. A comparison of the surface properties of the prohibitin models and flotillin-2 reveals interesting differences with the PHB domain of flotillin-2 being predominantly negatively charged. The surface of BAP32, in contrast, presents a mixed arrangement of electropositive and electronegative patches all over the PHB domain, and with BAP37 an almost exclusively electropositive surface potential is observed in the PHB domain. Figure 1 shows representations of the secondary structure elements and surfaces of the modelled PHB domains of BAP32 and BAP37 in combination with their modelled N-terminal helices [33] embedded in the inner mitochondrial membrane.

Prohibitins show a limited sequence similarity to chaperonins of the GroEL/Hsp60-class. Since prohibitins were found to interact with newly synthesised mitochondrial translation products such as cytochrome c oxidase, they have been proposed to function as a chaperoning "holdase" during the assembly of the respiratory chain [12]. Incidentally, the architecture of the membrane-bound yeast prohibitin complex that has been analysed recently by single particle electron microscopy yielded ring-shaped structures with outer dimensions of about 270 x 200 Å [16] and is thus reminiscent of chaperonins that provide a sequestered environment within cylindrical structures. However, compared to GroEL with a diameter of 150 Å, the prohibitin ring is substantially larger. This prompted Langer and colleagues to suggest a scaffolding function of the prohibitin complex that may ensure the organisation and integrity of the inner mitochondrial membrane. This role would also agree with the functional interaction of prohibitins with various mitochondrial proteins reflecting the proposed role of prohibitins for the maintenance of mitochondrial morphology [16].

The ring-like structures of membrane-bound prohibitins imply a topology where prohibitin 1 and 2 associate by an interaction interface that may be formed by the PHB domain. A model of the PHB domain dimer of BAP32:BAP37 has been constructed based on earlier crosslinking experiments [33, 34]. While molecular details remain to be clarified, the ring-like structures of both prohibitins confirm earlier findings of both proteins forming a tight complex and thus stabilising each other [12, 35, 36].

In contrast, Bacher and coworkers reported that both isolated prohibitins, BAP32 and BAP37, preferably form homotetramers as well as calcium-independent heteromeric complexes with affinities of 10^{-7} M [31]. Potentially, BAP32 could form dithioether-based dimers via its cysteine residue in position 69 (see Figure 2) and, intriguingly, is substrate of the transglutaminase 2, a disulphide isomerase [37]. This finding also poses the question of the importance of prohibitin disulphide RedOx chemistry and fold stability for its function. However, since BAP37 does not have any cysteine residue, the BAP32:BAP37 interactions cannot involve dithioether functionalities.

Apart from their oligomeric species, prohibitins 1 and 2 have also been found to interact with target proteins in their monomeric states. In the nucleus, for instance, prohibitin 1 (BAP32) was found to interact with p53 [24], Rb [23, 38], and E2F [39]. Prohibitin 2 (BAP37) was reported to bind to estrogen receptor (ER) [6, 30] and Akt [27]. It remains to be clarified under which circumstances the proteins exist in the respective oligomeric states. Most likely, occurrence of the monomeric state in non-membrane-bound states would require binding of stabilising proteins to mask the hydrophobic N-terminal domains [33].

The wide range of interactions of prohibitins with other proteins might not only result from different quaternary structures, but also post-translational modifications of the proteins enabling them to carry out various functions in the cell. Phosphorylated species of prohibitins were found in 2D-gel

electrophoresis experiments in plants [40], and it was also shown that purified JNK1 successfully phosphorylates prohibitin *in vitro* [39]. While phosphorylation of yeast prohibitin 2 by Akt could not be confirmed despite the presence of a consensus Akt phosphorylation site in prohibitin 2 (86-RPRKIS-91), an interaction of both proteins could be verified in co-immunoprecipitation assays and yeast two-hybrid screens [27]. Residues 120-232 on prohibitin 2 were identified as interaction interface (see figure 2), indicating that it might belong to the class of Akt-binding proteins that are not substrates for the kinase (see next section).

Examination of our proposed PHB domain dimer model of BAP32 and BAP37 [33] shows that most of the three predicted phosphorylation sites (ExPASy proteomics server, www.expasy.ch) in BAP32 (T108, S109, T141) and BAP37 (T194, S190, S110) are surface-accessible (Figure 2). Importantly, some phosphorylation sites are positioned in interaction interfaces to other proteins and might thus be involved in modulation of binding properties to target proteins.

Another post-translational modification might happen by lipo-conjugation of the PHB domain as observed with podocin and mec-2, two PHB domain -containing proteins [32]. As palmitoylation occurs at accessible cysteine residues, only BAP32 (one cysteine at position 69; see Figure 2), but not BAP37 (no cysteine) is anticipated to possess this feature. Based on a preliminary secondary structure alignment of BAP32 with podocin and mec-2, Cys69 seems to be located in a similar position like the conjugated cysteine in podocin/mec-2.

Prohibitins as regulators of gene expression

Several studies have identified prohibitins as cell cycle regulators, although the detailed mechanisms remain to be clarified [18, 41]. There is accumulative evidence of prohibitins acting as transcription regulators. Prohibitin 1 interacts with checkpoint molecules of the cell cycle, such as p53 [24] and Rb [23, 38], and with the transcription factor E2F [39]. The reported interaction sites of Rb and E2F with prohibitin 1/BAP32 can be mapped on the modelled BAP32:BAP37 dimer unit as illustrated in Figure 2. The region on prohibitin 1 C-terminal to the PHB domain (residues 185 to 214) is required for repression of E2F activity in addition to the Rb-binding domain [39]. The transcription of multiple genes has been found to be modulated by increased cellular levels of prohibitin in transfection experiments, and, accordingly, prohibitin has been implicated in cell cycle regulation [23, 24, 39].

The repressor function of BAP32 with respect to E2F-mediated transcription appears to utilise molecular mediators and signalling pathways different from the Rb pathway [41]. BAP32 recruits co-repressors HP1γ and Brg1/Brm to repress E2F-mediated transcriptional activity [42-44]. Breast cancer cells treated with estrogen antagonist showed an enhanced association between Brg1/Brm and prohibitin [43, 44].

A similar observation has been reported for the anti-proliferative actions of vitamin D [45]. Cellular levels of BAP32 were found to be increased by vitamin D treatment of breast cancer cell lines subsequently leading to growth inhibition. While a binding site for the vitamin D receptor/retinoid X

receptor has been predicted in the promoter region of BAP32, direct interactions at protein level remain to be clarified.

The Rb binding region on BAP32 spans residues 74-116, where three of four point mutations of prohibitin are found in sporadic breast cancer cells [38, 46, 47]. Interestingly, those residues span the anti-parallel β-sheet of BAP32, which is proposed not to interact with its homologue, BAP37, and would thus be potentially available for interactions with other target proteins. Further research in this area might give clues to the nature of this interaction and thus provide insights in the mechanism responsible for E2F repression.

BAP37, originally known as REA, is a repressor of estradiol-dependent transcription [6, 30] and binds directly to the estrogen receptor (ER) in the presence of its ligand estradiol. While BAP37 possesses the common ER-binding motif L-X-X-L-L N-terminal of its PHB domain, residues 175-198 are required for binding to ER [48] (see Figure 2). The L-X-X-L-L motif is suggested to be required for its repressive activity due to inhibiting ER co-activation by SRC-1.

Interestingly, BAP32 was also shown to have a repressive effect on androgen receptor (AR)–mediated transcription and androgen-dependent cell growth without an apparent direct interaction with AR [49].

In the nucleus, Akt has been shown to stimulate the transcription factor families of MyoD and MEF2 indirectly during muscle differentiation. This action was specifically repressed by prohibitin 2, possibly with the help of co-activators such as histone deacetylases. Prohibitin 2 might thus act as a miogenic repressor by competing with Akt to prevent its interaction with MyoD and MEF2 [27].

One can thus speculate that a complex consisting of both prohibitins acts as a mediator between Rb and E2F (interacting with BAP32) on the one hand, and ER receptor (interacting with BAP37) on the other. Furthermore, these functions might be activated by phosphorylation since some phosphorylation sites are situated in the proposed binding sites of Rb/E2F (see Figure 2).

Prohibitins in cancer

Early work on BAP32 suggested that the protein is a tumour suppressor, because a growth arrest was found in HeLa cells after microinjection of prohibitin transcripts [3]. It was shown later that this property actually resides in the 3'-UTR of BAP32 mRNA and the ability to inhibit cell cycle activity is restricted to normal cells and cells of the so-called group B immortal complementation group [12]. A polymorphism in the 3'-UTR of BAP32 has been identified as a risk modifier in breast cancer in the presence of BRCA1 mutation [12]. In a screening for somatic mutations in 23 breast cancers, four mutations leading to amino acid changes at positions 88 (Val→Ala) and 105 (Arg→His), as well as a frame shift mutation leading to a truncation at position 53 [46]. Within an intron, a C→T change was observed which may interfere with the splicing process. Interestingly, almost all mutations reported in sporadic breast cancer lie within the Rb-binding domain of prohibitin [46].

BAP32 has also been localised to the nuclei of breast cancer cells [24] and the cellular expression of the non-mutated protein is generally up-regulated in tumour cells as compared to normal cells [12, 50-53]. BAP32/BAP37 was also found at the cell surface of cultured colorectal tumour cells, and, notably, significant levels of both proteins were found in the serum [17]. It is not entirely clear whether BAP32/BAP37 are intentionally released into the blood or whether this is a direct consequence of the necrosis of tumour cells. In any case, these observations support a probable usability of prohibitins as tumour markers (see also [50]).

The involvement of BAP32 in repression of estrogen-dependent transcription has brought the prohibitin proteins back into focus as potential targets for breast cancer therapy. Estrogen antagonists are the commonly used endocrine therapy in breast cancer, but application is limited due to development of cellular resistance [44]. Further investigation of the prohibitin-E2F interactions and the involvement of estrogen antagonists at the molecular level might lead to development of new drugs in breast cancer therapy. The re-gained attention as potential cancer targets is further deserved because BAP32 was identified as a novel target gene of vitamin D, leading to downregulation of proliferation by activation of the vitamin D receptor. The clinical use of vitamin D in cancer therapy and prevention is restricted by its toxic effects at higher concentrations. Recently, BAP32 has been shown to enhance the anti-proliferative effects of vitamin D in breast cancer cells [45].

The re-gained interest in prohibitin for cancer treatment is also supported by the observation that interaction of BAP32 with the signalling kinase cRaf is crucial for Ras-mediated activation, as well as membrane targeting of cRaf [54]. BAP32 directly interacts with the kinase and is indispensable for the replacement of 14-3-3 from cRaf by Ras-GTP. Because Ras mutants activating Raf kinases are frequently found in tumours, and BAP32 is a crucial facilitator of this signalling pathway, prohibitin has again become a possible target for therapeutic applications.

Interestingly, a recent study elucidating the mechanisms for occurrence of multidrug resistance in a *Caenorhabditis elegans* model identified the E130K mutation in prohibitin 2 to be responsible for drug resistance of drugs binding to tubulin and camptothecin [55]. The location of Glu130 in the region of prohibitin 2 binding to Akt, MyoD and α-actinin (see table 1) might indicate the direction of further studies to elucidate the molecular mechanism.

The role of prohibitins in apoptosis

Very early on, the implications of prohibitins for cellular senescence have been emphasised by a number of studies, mainly fuelled by the observation of a shortened replicative life span of an yeast phenotype with disrupted prohibitin [35, 36]. While disruption of prohibitin genes in *S. cerevisiae* does not result in a lethal phenotype [35], the deletion of a prohibitin homologue in *D. melanogaster* [56] and *C. elegans* [57] is lethal during larval development. In a quest for finding drug-regulated genes in osteosarcoma cells, the cytotoxic chemicals cis-platin, methotrexate and doxorubicin were found to

increase cellular expression of eight genes mainly coding for electron transfer proteins, but to significantly decrease the expression of prohibitin and α-actinin [58]. The role of prohibitin in modulation of drug-induced apoptosis was further confirmed by the finding that its overexpression reduced chemosensitivity of the cells by about 50%.

Similar observations have been made with granulosa cells [59] and plant prohibitins. After inducing defense responses with the protein phosphatase inhibitor calyculin A, rice prohibitin 1 becomes hyper-phosphorylated in a lesion-mimic mutant that exhibits spontaneous cell death in the leaf [40, 60]. The down-regulation of expression of petunia prohibitin 1 by virus-induced gene silencing resulted in an acceleration of senescence of the flower [61]. While the same observation was made for prohibitin 1 in tobacco, the suppression of prohibitin 2 resulted in even more severe growth inhibition and apoptosis [62].

The senescent and apoptotic effects of prohibitin downregulation have always been observed to be accompanied by mitochondrial effects. In normal prostate epithelium, the transforming growth factor-β (TGF-β) acts as a tumor suppressor via induction of apoptosis and inhibition of cell proliferation. However, in advanced cancer, TGF-β signaling is deregulated which leads to promotion of tumor progression and metastasis acquiring anti-apoptotic pathways. Upon treatment with TGF-β, prohibitin translocates from the nucleus to the cell cytosol and was found strongly associated with the mitochondrial apoptosis-suppressor Bcl-2 [29]. In the yeast phenotype, a defect of the mitochondrial membrane potential has been observed [35], and the mitochondrial segregation from the mother to the daughter cells seems to be the reason for the shortened lifespan [63]. A disruption of mitochondrial biogenesis has also been found in *C. elegans* mutants [57]. Recent studies in tobacco show that a depletion of both prohibitins leads to a loss of mitochondrial integrity, excessive production of reactive oxygen species, and, subsequently, over-sensitivity to various stresses [62].

As for possible mechanisms, it has been suggested that the downregulation of prohibitin increases E2F acitvity, and thus E2F-mediated transcription which then triggers the apoptotic processes during the cell cycle at the entry into the S-phase [41]. Very recently, BAP37 has been reported to interact with the anti-apoptotic protein Hax-1 [30], an integral membrane protein of the outer mitochondrial membrane that is exposed to the intermembrane space. A model has been postulated where Hax-1 is being protected from proteolytic degradation through association with BAP37. Notably, the authors report indications that the interaction of BAP37 with Hax-1 is stronger than the BAP32-BAP37 interaction [30]. It will be interesting to see in future experiments whether specific, individual target proteins exist for both prohibitins.

Implications for mitochondrial functions

Different stimuli such as UV irradiation, reactive oxygen species, hormones and growth factors can induce apoptosis which is a well-characterised form of programmed cell death [64] that requires the

action of caspases. Mitochondria play a pivotal role in the signal transduction of apoptosis, since they trigger the activation of caspases by release of cytochrome c, apoptosis-inducing factor and Smac/Diablo in a process called mitochondrial permeability transition which is the main pathway of programmed cell death in animal cells [65-68].

To date, it is known that prohibitin 1 and 2 assemble into hetero-oligomers to yield high-molecular weight complexes of about 1.2 MDa as shown for yeast [69], mammals [12] and *C. elegans* [57]. For most interactions with prohibitin target proteins, it is not clear whether this requires reorganisation or indeed disassembly of the prohibitin hetero-oligomers. However, prohibitins seem to be able to interact with several target proteins simultaneously [31].

Further weight was put on the notion that high-molecular weight prohibitin complexes play an important role for the integrity of mitochondrial membranes [36] by the finding that prohibitin mutations in yeast are lethal when combined with disruption of the phosphatidylethanolamine (a major component of mitochondrial membranes) biosynthetic pathway [70]. This hypothesis is further supported by the first structural characterisation of membrane-bound prohibitin ring complexes. The findings by Langer's group indicate a direct effect of the complexes on the ultrastructure of the inner mitochondrial membrane, since the ring-like structures have a similar diameter to cristae junctions [16]. In tobacco, prohibitin depletion causes abnormal mitochondria that lack inner cristae and contain fibre-like structures that probably represent disintegrated inner membrane [62]. The phenotype is further characterised by disrupted mitochondrial biogenesis or stimulated mitochondrial degeneration, and a reduction in number and mass of mitochondria in the cell. Aberrant mitochondria lacking the mitochondrial genome were found to accumulate in *S. cerevisae* when the function of either prohibitin was lost [36, 63]. A lack of prohibitins was shown to affect mitochondrial distribution and morphology during development of body wall muscle cells of *C. elegans* [57]. In this context, RNAi-mediated elimination of prohibitin 2 was found to lead to mitochondrial fragmentation in HeLa cells [30].

The importance of prohibitins for programmed cell death might thus be due to their crucial role for mitochondrial integrity as suggested by recent studies in plants [40, 60]. Since prohibitins seem to protect inner membrane proteins, modifications such as phosphorylation (of BAP32) might change their functional properties or interactions with other proteins and finally lead to cell death. Accordingly, the high-molecular weight complexes of prohibitins with *m*-AAA protease are of particular interest. AAA protease, as well as the bacterial orthologue FtsH and other FtsH-like proteases from plants [71, 72], degrades membrane proteins in mitochondria [73] and seems to be regulated by prohibitins. Recently, the PHB domain –containing protein QmcA was identified in *E. coli* as a factor involved in membrane protein quality control [74]. As concluded from pulldown assays, QmcA interacts with FtsH to form oligomers. Based on findings from proteolytic accessibility experiments, these authors also suggested that PHB domains might be present on both sides of the membrane.

Generally, mitochondrial disorders can give rise to a broad spectrum of diseases such as myopathies, loss of hearing and optic neuropathy [75]. Mitochondrial dysfunction has also been implied in inflammatory diseases such as ulcerative colitis, a disorder characterised by chronic inflammation of the colon mucosa [76]. With a proteomics approach, several mitochondrial proteins have been found to be down-regulated in colon mucosa from patients with ulcerative colitis. This phenomenon is accompanied by pathological alterations of the mitochondrial ultrastructure [76].

Metabolic stress caused by imbalances of mitochondrial and nuclear encoded proteins leads to up-regulation of BAP32 and BAP37 expression levels [75]. The mitochondrial prohibitin complex was found to bind to mitochondrial translation products of the respiratory chain such as cytochrome c oxidase (COX). Here, it acts as a chaperone to assemble the COX complex [12], thus exerting important functions in maintaining a healthy protein population in mitochondria.

Disturbances in mitochondrial function might be common in aged population and probably contribute to age-related diseases, such as Type 2 Diabetes [41]. In ageing mitochondria, oxidative stress leads to accumulation of superoxide, which could lead to the promotion of type 2 diabetes [77]. One might speculate that prohibitins could play a role in this process, especially when considering that prohibitin depletion leads to an excessive production of reactive oxygen species in plants [62]. Furthermore, overexpression of prohibitin increases the expression of glutathione-S-transferase π and protects from accumulation of reactive oxygen metabolites, as well as increased permeability induced by oxidative stress in intestinal epithelial cells. As such, prohibitin might act as a cellular defense against oxidant injury and thus be an interesting target for tissue injury and inflammatory diseases such as bowel and Crohn's disease [78].

This link deserves further attention, since the addition of BAP32 to cultured adipocytes has been reported to result in inhibition of mitochondrial pyruvate carboxylase and subsequent suppression of glucose and fatty acid oxidation [79].

With a chemical genetics approach searching for pigment-enhancing chemicals, melanogenin has been found to enhance melanin production in melanocytes and to bind specifically to prohibitin [80]. A sufficient pigment production in melanocytes is important for the organism, since UV irradiation can cause severe damage to the cell and finally induce apoptosis through activation of the mitochondrial permeability transition. The damage is possibly caused by favouring the opening of the mitochondrial permeability transition pore. Based on further RNA interference experiments, it has been proposed that prohibitin plays a functional role in melanin induction, since neither the melanin induction agent isobutylmethylxanthine nor melanogenin were able to induce melanin production when prohibitin expression was silenced [80]. Not only opens this finding another avenue for potential therapeutic applications of compounds targeting prohibitin, but it also demonstrates the possibilities of chemical biology approaches to probe organelle functions.

Prohibitin interactions with cytoskeletal proteins

Employing an yeast two-hybrid screen, annexin A2 and α-actinin have been identified as binding partners for BAP32 and BAP37 [31]. Both proteins are able to bind to various target proteins in a calcium-dependent or a calcium-independent fashion. Annexin A2 is also able to bind to acidic phospholipid membranes in a calcium-regulated fashion.

Truncation experiments by Bacher and colleagues [31] show that for binding to annexin A2, full-length BAP32 or BAP37 is required. The first 100 N-terminal residues of BAP32 displayed a strong binding to α-actinin, but in BAP37 the binding site for α-actinin seems to reside in the C-terminal domain. While each prohibitin was able to bind to each target protein, the stronger affinities were observed between BAP32 and annexin A2, and BAP37 and α-actinin, respectively [31]. The fact that these interactions are calcium-mediated does not automatically suggest a 'sandwich' role for the metal ion, since both target proteins are known to possess calcium-dependent allosteric mechanisms [81].

Notably, prohibitins can interact with several target proteins simultaneously which might also explain the rather moderate *in vitro* binding affinities determined so far. Homo- and hetero-oligomerisation, as well as ligand interactions probably stabilise the overall complex and thus would increase the affinity constants.

Extra-cellular functions of prohibitins

In an attempt to find peptide motifs that specifically target white tissue, the motif CKGGRAKDC was specifically localised to and internalised by blood vessels of subcutaneous and peritoneal white fat in mice [20]. The peptide interacts with prohibitin 1 at the protein level which further supports the notion that prohibitins, probably as part of higher order complexes, are present as surface receptors of certain cell types, specifically in endothelial white adipose tissue. The study by these authors [20] went even further in showing that conjugation of a pro-apoptotic peptide to the CKGGRAKDC motif was successful in reversing obesity in the mouse model.

Salmonella typhi is a pathogen that enters the human body by intake of contaminated food or water causing typhoid fever [82]. After intake, the bacterium is translocated to the intestine and subsequently distributed through the reticuloendothelial system. To date, the host-pathogen interactions of *Salmonella* remain incompletely characterised, but the Vi capsular polysaccharide had been identified as a major virulence factor [83]. Vi is currently one of the most efficient available vaccines for use in humans [84]. Using a human model intestinal epithelium cell line, the polysaccharide has been shown to interact with a specific cell surface -associated recognition complex that contains BAP32 and BAP37 [21]. Possibly by activating the MAP kinase pathway through the BAP32/BAP37 cell surface complex, Vi reduces an early

inflammatory response of the host organism [39, 85]. The role of prohibitins in this context could go beyond extra-cellular recognition, and include a possible participation in intracellular signalling.

Recently, BAP32, but not BAP37, has been shown to circulate in the serum and to exist in a complex with C3, thus being able to enhance complement activation [86]. This ability assigns a potential role to prohibitin in innate immunity which is in agreement with the findings that prohibitins localise to the plasma membrane of human intestinal epithelial cells [21] and lymphocytes [87]. Intriguingly, during infection with *S. typhi*, serum complement activation is inhibited, if the strains carry the Vi antigen [88]. A link between both findings could be provided by prohibitins, circulating in the serum on the one hand and residing in a cell-surface complex on the other.

Conclusion: Chemical biology of prohibitins

Prohibitins have first been characterised about 18 years ago, but research on these highly conserved and important proteins has been intensified only in the last six to seven years. By now, the initial focus of prohibitins as new tumour suppressors has been shifted towards detecting intra- and extra-cellular interaction partners, which also diversified the significance of these proteins. The wide range of interaction partners shows that the anticipated fundamental role of prohibitins within the cell has not only been confirmed, but broadened. The involvement in pivotal cellular processes places prohibitins in the context of mitochondrial, age and oxidative stress -related diseases, as well as in immunity and inflammation, cancer and cancer-like diseases, obesity, and drug resistance. While a wealth of information on prohibitin implications in cellular processes has become available, structurally, these proteins are poorly understood. A major breakthrough in this context was achieved by Langer and colleagues who obtained the first visualisation of a low-resolution structure of membrane-bound prohibitins.

Further efforts will now have to be undertaken to obtain more detailed, atomic structure information about the various molecular states of prohibitins. Structural information and their correlation with available functional data will lead to a deeper understanding of the molecular mechanisms of this protein system and reveal their roles in cellular processes.

Chemical biology and structural chemistry will be able to provide this information. The use of small molecules or protein ligands in these studies will not only lend aid in stabilising this protein system *in vitro*, but will also allow insights into protein-ligand binding. Moreover, this approach will yield valuable data for evaluation of drug interference with the functions of these proteins. Since prohibitins are implicated in a variety of disorders, this will certainly be a highly beneficial undertaking for finding new drugs to fight those diseases.

Acknowledgements

Work in the laboratory of AH is funded by the European League Against Rheumatism (EULAR), Griffith University, and the Parkinson's Disease Society (UK). AW is the recipient of a scholarship of the Darwin Trust of Edinburgh.

Figure legends

Figure 1

Model of a putative membrane-anchored hetero-dimer of BAP32 and BAP37 [33]. The hetero-dimer would be part of a larger oligomer forming ring-like structures in the mitochondrial inner membrane as observed by Langer and colleagues [16]. The dimer model of the N-terminal and PHB domains of BAP32 (orange) and BAP37 (blue) assumes a parallel arrangement of both proteins in the membrane-bound state. Figure prepared with PyMOL [89].

Figure 2

Visualisation of functionally important sites on prohibitins. Interaction and modification sites are mapped onto the putative hetero-dimer of BAP32 (orange) and BAP37 (blue). Putative phosphorylation sites are indicated by explicitly drawn residues: T108, S109, T141 (BAP32); S110, S190, T194 (BAP37). The interaction site of BAP32 with Rb is shown in green, the interaction site with E2F is shown in cyan. The putative palmitoylation site at Cys69 is indicated explicitly. The BAP37 interaction site with Akt is coloured in yellow, which also includes the binding site for estrogen receptor (purple). Figure prepared with PyMOL [89].

Figure 1

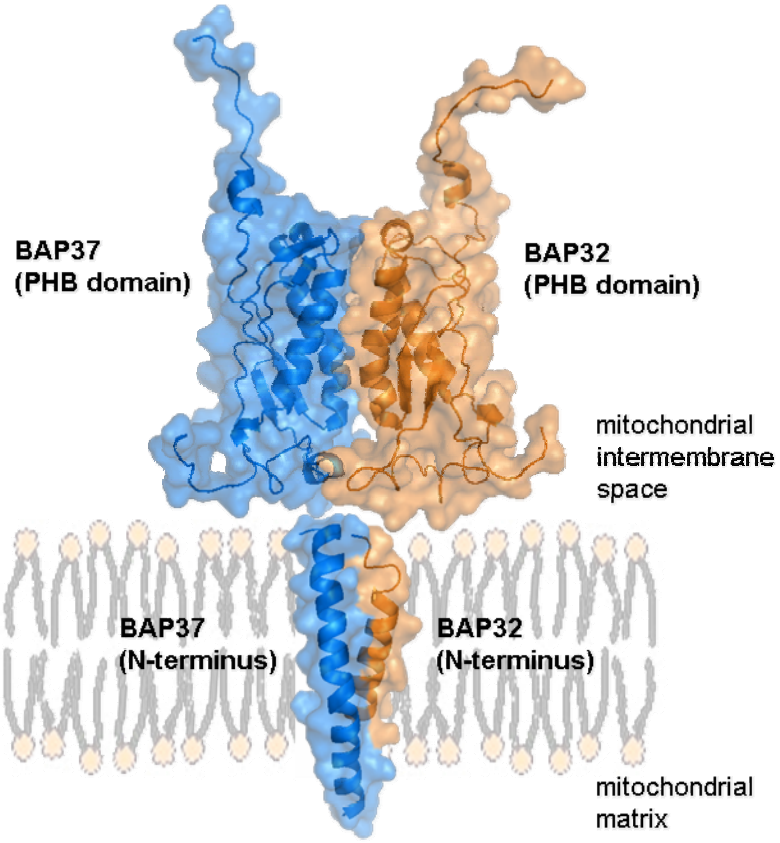
BAP37
(PHB domain)
BAP32
(PHB domain)
mitochondrial
intermembrane
space
BAP37
(N-terminus)
BAP32
(N-terminus)
mitochondrial
matrix

Figure 2

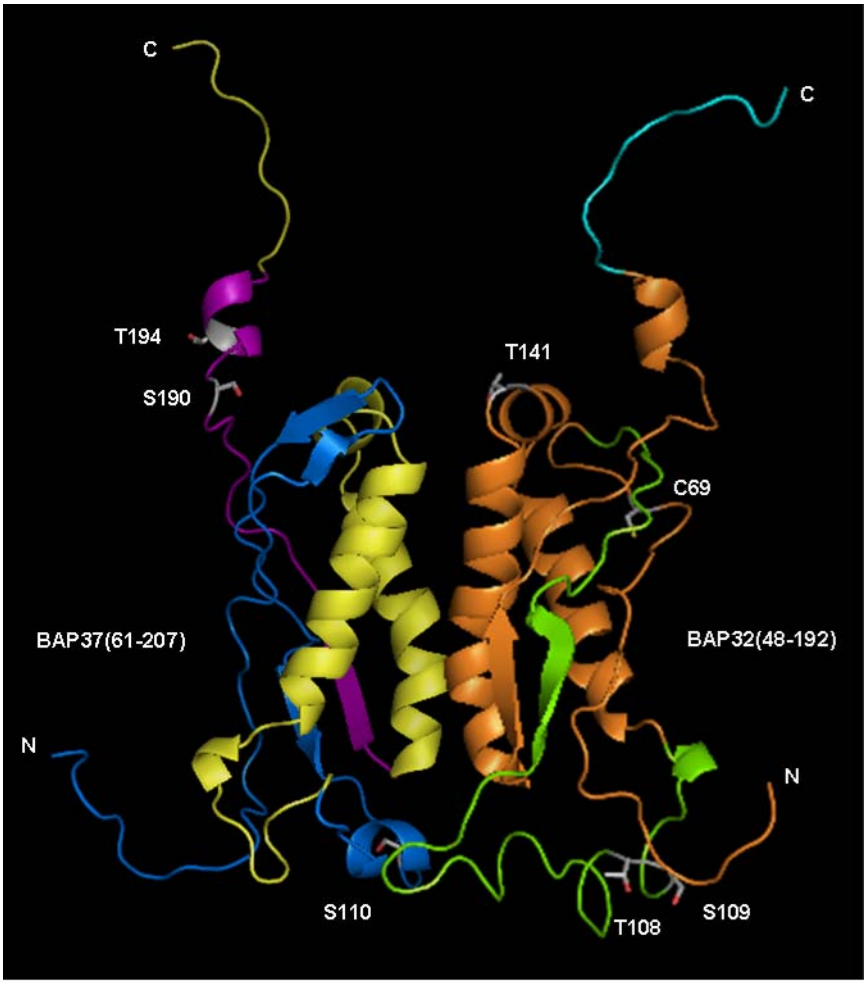
C
C
T194
T141
S190
C69
BAP37(61-207)
BAP32(48-192)
N
N
S110
T108
S109

Table 1: **Prohibitin-protein interactions**

Target protein	Prohibitin	Context	Binding sites	Reference
Akt	BAP37	The protein kinase Akt competitively binds to BAP37 to inhibit binding to transcription factors (MyoD, MEF2).	BAP37: 120-232 Akt: 413-480	[27]
MyoD	BAP37	The transcription factor MyoD belongs to the myogenic regulatory factors that are important for establishing the myogenic fate of muscle precursor cells.	BAP37: 57-299	[27]
MEF2	BAP37	MEF2 transcription factors increase the transcription of many muscle-specific genes.	No direct binding (yeast two-hybrid)	[27]
HDAC1	BAP32 BAP37	BAP32 and BAP37 represses transcription by recruiting the repressor histone deacetylase 1.	Co-immunoprecipation of BAP32 and BAP37 and HDAC1	[23, 27]
Rb	BAP32	Binding to Rb is necessary for prohibitin to execute its anti-proliferative action via E2F.	BAP32: 74-116	[6, 23, 38, 39, 48]
E2F	BAP32	Repression of E2F caused by prohibitin leads to abolished transcription of cell-cycle genes like cyclin E and A .	BAP32: 185-214	[38, 39, 48]
Estrogen receptor (ER)	BAP37	BAP37 dampens response of ER to extra-cellular estradiol stimulation.	BAP37: 175-198	[30, 38, 39, 48]
cRaf-1	BAP32	The signalling kinase cRaf-1 could effectively reverse prohibitin-mediated repression of E2F activity.	BAP32: 243-275	[39]
		BAP32 is needed for Ras-mediated activation and membrane targeting of cRaf.		[54]
Annexin A2	BAP32 BAP37	Interaction negatively regulated by calcium, association with lipid rafts, plasma membrane, possible presence in nucleus.	Full-length BAP32 Full-length BAP37	[31]
α-actinin	BAP32 BAP37	Interaction negatively regulated by calcium, association with plasma membrane, interaction with other cytoskeletal proteins, possible translocation to the nucleus.	BAP32: 1-99 BAP37: 118-299	[31]
VDAC-2, ANT 2	BAP37	No data available.		[30]
Hax-1	BAP37	BAP37 is involved in the regulation and stability of the anti-apoptotic Hax-1.	Co-immunoprecipation of BAP37 and Hax-1	[30]

References

[1] Dell'Orco RT, McClung JK, Jupe ER, et al. Prohibitin and the senescent phenotype. Exp Gerontol 1996; 31:245-52.

[2] McClung JK, Danner DB, Stewart DA, et al. Isolation of a cDNA that hybrid selects antiproliferative mRNA from rat liver. Biochem Biophys Res Comm 1989; 164:1316-22.

[3] Nuell MJ, Stewart DA, Walker L, et al. Prohibitin, an evolutionarily conserved intracellular protein that blocks DNA synthesis in normal fibroblasts and HeLa cells. Mol Cell Biol 1991; 11:1372-81.

[4] Manjeshwar S, Lerner MR, Zang XP, et al. Expression of prohibitin 3' untranslated region suppressor RNA alters morphology and inhibits motility of breast cancer cells. J Mol Histol 2004; 35:639-46.

[5] Lamers MC, Bacher S. Prohibitin and prohibitone, ubiquitous and abundant proteins that are reluctant to reveal their real identity. Int Arch Allergy Immunol 1997; 113:146-9.

[6] Montano MM, Ekena K, Delage-Mourroux R, et al. An estrogen receptor-selective coregulator that potentiates the effectiveness of antiestrogens and represses the activity of estrogens. Proc Natl Acad Sci USA 1999; 96:6947-52.

[7] Tavernarakis N, Driscoll M, Kyrpides NC. The SPFH domain: implicated in regulating targeted protein turnover in stomatins and other membrane-associated proteins. Trends Biochem Sci 1999; 24:425-7.

[8] Nuell MJ, McClung JK, Smith JR, et al. Approach to the isolation of antiproliferative genes. Exp Gerontol 1989; 24:469-76.

[9] Roskams AJ, Friedman V, Wood CM, et al. Cell cycle activity and expression of prohibitin mRNA. J Cell Physiol 1993; 157:289-95.

[10] Kobayakawa K, Hayashi R, Morita K, et al. Stomatin-related olfactory protein, SRO, specifically expressed in the murine olfactory sensory neurons. J Neurosci 2002; 22:5931-7.

[11] Browman DT, Resek ME, Zajchowski LD, et al. Erlin-1 and erlin-2 are novel members of the prohibitin family of proteins that define lipid-raft-like domains of the ER. J Cell Sci 2006; 119:3149-60.

[12] Nijtmans LG, de Jong L, Artal Sanz M, et al. Prohibitins act as a membrane-bound chaperone for the stabilization of mitochondrial proteins. EMBO J 2000; 19:2444-51.

[13] Santamaria E, Avila MA, Latasa MU, et al. Functional proteomics of nonalcoholic steatohepatitis: mitochondrial proteins as targets of S-adenosylmethionine. Proc Natl Acad Sci 2003; 100:3065-70.

[14] Matsuyama S, Kubo K, Ohashi F, et al. Partial cloning of prohibitin cDNA from canine, feline, bovine, equine, and rabbit liver mRNA by RT-PCR. J Vet Med Sci 1997; 59:201-3.

[15] McClung JK, Jupe ER, Liu XT, et al. Prohibitin: Potential role in senescence, development, and tumor suppression. Exp Gerontol 1995; 30:99-124.

[16] Tatsuta T, Model K, Langer T. Formation of Membrane-bound Ring Complexes by Prohibitins in Mitochondria. Mol Biol Cell 2005; 16:248-59.

[17] Mengwasser J, Piau A, Schlag P, et al. Differential immunization identifies PHB1/PHB2 as blood-borne tumor antigens. Oncogene 2004; 23:7430-5.

[18] Mishra S, Murphy LC, Murphy LJ. The Prohibitins: emerging roles in diverse functions. J Cell Mol Med 2006; 10:353-63.

[19] Brasaemle DL, Dolios G, Shapiro L, et al. Proteomic analysis of proteins associated with lipid droplets of basal and lipolytically-stimulated 3T3-L1 adipocytes. J Biol Chem 2004; 279:46835-42.

[20] Kolonin MG, Saha PK, Chan L, et al. Reversal of obesity by targeted ablation of adipose tissue. Nat Med 2004; 10:625-32.

[21] Sharma A, Qadri A. Vi polysaccharide of Salmonella typhi targets the prohibitin family of molecules in intestinal epithelial cells and suppresses early inflammatory responses. Proc Natl Acad Sci 2004; 101:17492-7.

[22] Thompson WE, Branch A, Whittaker JA, et al. Characterisation of prohibitin in a newly established rat ovarian granulosa cell line. Endocrinol 2001; 142:4076-85.

[23] Wang S, Fusaro G, Padmanabhan J, et al. Prohibitin co-localizes with Rb in the nucleus and recruits N-CoR and HDAC1 for transcriptional repression. Oncogene 2002; 21:8388-96.
[24] Fusaro G, Dasgupta P, Rastogi S, et al. Prohibitin induces the transcriptional activity of p53 and is exported from the nucleus upon apoptotic signaling. J Biol Chem 2003; 278:47853-61.
[25] Gamble SC, Odontiadis M, Waxman J, et al. Androgens target prohibitin to regulate proliferation of prostate cancer cells. Oncogene 2004; 23:2996-3004.
[26] Kurtev V, Margueron R, Kroboth K, et al. Transcriptional regulation by the repressor of estrogen receptor activity via recruitment of histone deacetylases. J Biol Chem 2004; 279:24834-43.
[27] Sun L, Liu L, Yang XJ, et al. Akt binds prohibitin 2 and relieves its repression of MyoD and muscle differentiation. J Cell Sci 2004; 117:3021-9.
[28] Rastogi S, Joshi B, Fusaro G, et al. Camptothecin induces nuclear export of prohibitin preferentially in transformed cells through a CRM-1 dependent mechanism. J Biol Chem 2005.
[29] Zhu B, Fukada K, Zhu H, et al. Prohibitin and Cofilin Are Intracellular Effectors of Transforming Growth Factor β Signaling in Human Prostate Cancer Cells. Cancer Res 2006; 66:8640-7.
[30] Kasashima K, Ohta E, Kagawa Y, et al. Mitochondrial functions and estrogen receptor-dependent nuclear translocation of pleiotropic human prohibitin 2. J Biol Chem 2006; 281:36401-10.
[31] Bacher S, Achatz G, Schmitz ML, et al. Prohibitin and prohibitone are contained in high molecular weight complexes and interact with alpha-actinin and annexin A2. Biochimie 2002; 84:1207-20.
[32] Huber TB, Schermer B, Muller RU, et al. Podocin and MEC-2 bind cholesterol to regulate the activity of associated ion channels. Proc Natl Acad Sci 2006; 103:17079-86.
[33] Winter A, Kamarainen O, Hofmann A. Molecular modeling of prohibitin domains. Proteins 2007.
[34] Back JW, Sanz MA, De Jong L, et al. A structure for the yeast prohibitin complex: Structure prediction and evidence from chemical crosslinking and mass spectrometry. Prot Sci 2002; 11:2471-8.
[35] Coates PJ, Jamieson DJ, Smart K, et al. The prohibitin family of mitochondrial proteins regulate replicative lifespan. Curr Biol 1997; 7:607-10.
[36] Berger KH, Yaffe MP. Prohibitin family members interact genetically with mitochondrial inheritance components in *Saccharomyces cerevisiae*. Mol Cell Biol 1998; 18:4043-52.
[37] Mastroberardino PG, Farrace MG, Viti I, et al. "Tissue" transglutaminase contributes to the formation of disulphide bridges in proteins of mitochondrial respiratory complexes. Biochim Biophys Acta 2006; 1757:1357-65.
[38] Wang S, Nath N, Adlam M, et al. Prohibitin, a potential tumor suppressor, interacts with RB and regulates E2F function. Oncogene 1999; 18:3501-10.
[39] Wang S, Nath N, Fusaro G, et al. Rb and prohibitin target distinct regions of E2F1 for repression and respond to different upstream signals. Mol Cell Biol 1999; 19:7447-60.
[40] Takahashi A, Kawasaki T, Wong HL, et al. Hyperphosphorylation of a mitochondrial protein, prohibitin, is induced by calyculin A in a rice lesion-mimic mutant cdr1. Plant Physiol 2003; 132:1861-9.
[41] Mishra S, Murphy LC, Nyomba BL, et al. Prohibitin: a potential target for new therapeutics. Trends Mol Med 2005; 11:192-7.
[42] Rastogi S, Joshi B, Dasgupta P, et al. Prohibitin facilitates cellular senescence by recruiting specific corepressors to inhibit E2F target genes. Mol Cell Biol 2006; 26:4161-71.
[43] Wang S, Zhang B, Faller DV. Prohibitin requires Brg-1 and Brm for the repression of E2F and cell growth. EMBO J 2002; 21:3019-28.
[44] Wang S, Zhang B, Faller DV. BRG1/BRM and prohibitin are required for growth suppression by estrogen antagonists. EMBO J 2004; 23:2293-303.
[45] Peng X, Mehta R, Wang S, et al. Prohibitin is a novel target gene of vitamin d involved in its antiproliferative action in breast cancer cells. Cancer Res 2006; 66:7361-9.
[46] Sato T, Saito H, Swensen J, et al. The human prohibitin gene located on chromosome 17q21 is mutated in sporadic breast cancer. Cancer Res 1992; 52:1643-6.

[47] Sato T, Sakamoto T, Takita K, et al. The human prohibitin (PHB) gene family and its somatic mutations in human tumors. Genomics 1993; 17:762-4.
[48] Delage-Mourroux R, Martini PG, Choi I, et al. Analysis of estrogen receptor interaction with a repressor of estrogen receptor activity (REA) and the regulation of estrogen receptor transcriptional activity by REA. J Biol Chem 2000; 275:35848-56.
[49] Gamble SC, Chotai D, Odontiadis M, et al. Prohibitin, a protein downregulated by androgens, represses androgen receptor activity. Oncogene 2007; 26:1757-68.
[50] Wang KJ, Wang RT, Zhang JZ. Identification of tumor markers using two-dimensional electrophoresis in gastric carcinoma. World J Gastroenterol 2004; 10:2179-83.
[51] Asamoto M, Cohen SM. Prohibitin gene is overexpressed but not mutated in rat bladder carcinomas and cell lines. Cancer Lett 1994; 83:201-7.
[52] Shan L. cDNA microarray profiling of rat mammary gland carcinomas induced by 2-amino-1-methyl-6-phenylimidazo-4,5-β-pyridine and 7,12-dimethyl-benz-α-anthracene. Carcinogenesis 2002; 23:1561-8.
[53] Dowling P, Meleady P, Dowd A, et al. Proteomic analysis of isolated membrane fractions from superinvasive cancer cells. Biochim Biophys Acta 2007; 1774:93-101.
[54] Rajalingam K, Wunder C, Brinkmann V, et al. Prohibitin is required for Ras-induced Raf-MEK-ERK activation and epithelial cell migration. Nat Cell Biol 2005; 7:837-43.
[55] Zubovych I, Doundoulakis T, Harran PG, et al. A missense mutation in *Caenorhabditis elegans* prohibitin 2 confers an atypical multidrug resistance. Proc Natl Acad Sci 2006; 103:15523-8.
[56] Eveleth DDJ, Marsh JL. Sequence and expression of the Cc gene, a member of the dopa decarboxylase gene cluster of *Drosophila*: possible translational regulation. Nucleic Acids Res 1986; 14:6169-83.
[57] Artal-Sanz M, Tsang WY, Willems EM, et al. The mitochondrial prohibitin complex is essential for embryonic viability and germline function in *Caenorhabditis elegans*. J Biol Chem 2003; 278:32091-9.
[58] Fellenberg J, Dechant MJ, Ewerbeck V, et al. Identification of drug-regulated genes in osteosarcoma cells. Int J Cancer 2003; 105:636-43.
[59] Chowdhury I, Xu W, Stiles JK, et al. Apoptosis of Rat Granulosa Cells After Staurosporine And Serum Withdrawal Is Suppressed by Adenovirus Directed Overexpression of Prohibitin. Endocrinology 2007; 148:206-17.
[60] Takahashi A, Kawasaki T, Henmi K, et al. Lesion mimic mutants of rice with alterations in early signaling events of defense. Plant J 1999; 17:535-45.
[61] Chen JC, Jiang CZ, Reid MS. Silencing a prohibitin alters plant development and senescence. Plant J 2005; 44:16-24.
[62] Ahn CS, Lee JH, Reum Hwang A, et al. Prohibitin is involved in mitochondrial biogenesis in plants. Plant J 2006; 46:658-67.
[63] Piper PW, Jones GW, Bringloe D, et al. The shortened replicative life span of prohibitin mutants of yeast appears to be due to defective mitochondrial segregation in old mother cells. Aging Cell 2002; 1:149-57.
[64] Jacobson MD, Weil M, Raff MC. Programmed cell death in animal development. Cell 1997; 88:347-54.
[65] Green DR, Reed JC. Mitochondria and apoptosis. Science 1998; 281:1309-12.
[66] Susin SA, Lorenzo HK, Zamzami N, et al. Molecular characterisation of mitochondrial apoptosis-inducing factor. Nature 1999; 397:441-6.
[67] Verhagen AM, Ekeert PG, Pakusch M, et al. Identification of DIABLO, a mammalian protein that promotes apoptosis by binding to and antagonising IAP proteins. Cell 2000; 102:43-53.
[68] Lam E, Kato N, Lawton M. Programmed cell death, mitochondria and the plant hypersensitive response. Nature 2001; 411:848-53.
[69] Steglich G, Neupert W, Langer T. Prohibitins regulate membrane protein degradation by the *m*-AAA protease in mitochondria. Mol Cell Biol 1999; 19:3435-42.

[70] Birner R, Nebauer R, Schneiter R, et al. Synthetic Lethal Interaction of the Mitochondrial Phosphatidylethanolamine Biosynthetic Machinery with the Prohibitin Complex of *Saccharomyces cerevisiae*. Mol Biol Cell 2003; 14:370-83.
[71] Adam Z, Adamska I, Nakabayashi K, et al. Chloroplast and mitochondrial proteases in *Arabidopsis*: a proposed nomenclature. Plant Physiol 2001; 125:1912-8.
[72] Seo S, Okamoto M, Iwai T, et al. Reduced levels of chloroplast FtsH protein in tobacco mosaic virus-infected tobacco leaves accelerate the hypersensitive reaction. Plant Cell 2000; 12:917-32.
[73] Leonhard K, Guiard B, Pellecchia G, et al. Membrane protein degradation by AAA proteases in mitochondria: extraction of substrates from either membrane surface. Mol Cell Biol 2000; 5:629-38.
[74] Chiba S, Ito K, Akiyama Y. The *Escherichia coli* plasma membrane contains two PHB (prohibitin homology) domain protein complexes of opposite orientations. Mol Microbiol 2006; 60:448-57.
[75] Nijtmans LG, Artal SM, Grivell LA, et al. The mitochondrial PHB complex: roles in mitochondrial respiratory complex assembly, ageing and degenerative disease. Cell Mol Life Sci 2002; 59:143-55.
[76] Hsieh SY, Shih TC, Yeh CY, et al. Comparative proteomic studies on the pathogenesis of human ulcerative colitis. Proteomics 2006; 6:5322-31.
[77] Lowell BB, Shulman GI. Mitochondrial dysfunction and type 2 diabetes. Science 2005; 307:384-7.
[78] Theiss AL, Idell RD, Srinivasan S, et al. Prohibitin protects against oxidative stress in intestinal epithelial cells. FASEB J 2007; 21:197-206.
[79] Vessal M, Mishra S, Moulik S, et al. Prohibitin attenuates insulin-stimulated glucose and fatty acid oxidation in adipose tissue by inhibition of pyruvate carboxylase. FEBS J 2006; 273:568-76.
[80] Snyder JR, Hall A, Ni-Komatsu L, et al. Dissection of melanogenesis with small molecules identifies prohibitin as a regulator. Chem Biol 2005; 12:477-84.
[81] Hofmann A, Huber R. Structural conservation and functional versatility: Allostery as a common annexin feature. In: Bandorowicz-Pikula J, ed. *Annexins: Biological importance and annexin-related pathologies*. Georgetown, TX: Landes Bioscience 2003:38-60.
[82] Keusch GT. In: Wilson JD, Braunwald E, Isselbacher KJ, Petersdorf RG, Martin JB, Fauci AS, et al., eds. *Harrison's Principal of Internal Medicine*. New York: McGraw-Hill 1991:609-13.
[83] Szu SC, Bystricky S. Physical, chemical, antigenic, and immunologic characterization of polygalacturonan, its derivatives, and Vi antigen from *Salmonella typhi*. Methods Enzymol 2003; 363:552-67.
[84] Lin FY, Ho VA, Khiem HB, et al. The efficacy of a *Salmonella typhi* Vi conjugate vaccine in two-to-five-year-old children. N Engl J Med 2001; 344:1263-9.
[85] Hobbie S, Chen LM, Davis RJ, et al. Involvement of mitogen-activated protein kinase pathways in the nuclear responses and cytokine production induced by *Salmonella typhimurium* in cultured intestinal epithelial cells. J Immunol 1997; 159:5550-9.
[86] Mishra S, Moulik S, Murphy LJ. Prohibitin binds to C3 and enhances complement activation. Mol Immunol 2007; 44:1907-12.
[87] Terashima M, Kim K-M, Adachi T, et al. The IgM antigen receptor of B lymphocytes is associated with prohibitin and a prohibitin-related protein. EMBO J 1994; 13:3782-92.
[88] Hornick RB, Greisman SE, Woodward TE, et al. Typhoid fever: pathogenesis and immunologic control. N Engl J Med 1970; 283:686-91.
[89] DeLano WL. The PyMOL Molecular Graphics System. http://wwwpymolorg 2002.